SYNTHESIS OF NOVEL POLYFLUORENES

FOR BIOSENSOR APPLICATIONS

THESIS SUBMITTED TO THE

SAVITRIBAI PHULE PUNE UNIVERSITY

FOR THE DEGREE OF

DOCTOR OF PHILOSOPHY

IN CHEMISTRY

BY

T. SENTHILKUMAR

RESEARCH SUPERVISOR

Dr. S. K. ASHA

POLYMER SCIENCE AND ENGINEERING DIVISION

CSIR-NATIONAL CHEMICAL LABORATORY

PUNE 411 008

JULY 2015

Dedicated to My Family

For their Love and Support

DECLARATION

I hereby declare that the thesis entitled **"Synthesis of Novel Polyfluorenes for Biosensor Applications"** submitted for the award of degree of Doctor of Philosophy in chemistry to the Savitribai Phule Pune University has been carried out by me. This work was carried out at the Polymer Science and Engineering Division of CSIR-National Chemical Laboratory, Pune under the supervision of Dr. S. K. Asha. I also affirm that this work is original and has not been submitted in part or full, for any other degree or diploma to this or any other University or Institution.

T. Senthilkumar   **July 2015**

Polymer Science and Engineering Division,

CSIR-National Chemical Laboratory,

Pune 411008,

Maharashtra, India.

CERTIFICATE

This is to certify that the work presented in the thesis entitled **"Synthesis of Novel Polyfluorenes for Biosensor Applications"** has been carried out by **Mr. T. Senthilkumar** under my supervision at the Polymer Science and Engineering Division of CSIR-National Chemical Laboratory, Pune and the same has not been submitted elsewhere for any other degree. Such materials as obtained from other sources have been duly acknowledged in the thesis.

Dr. S. K. Asha   **July 2015**

(Research Supervisor)

Polymer Science and Engineering Division

CSIR-National Chemical Laboratory

Pune 411008,

Maharashtra, India.

ACKNOWLEDGEMENTS

Table of Contents

Chapter 3

Water-Soluble Polyfluorenes for Selective Sensing of Free Bilirubin in Human Blood Serum

Chapter 4

Orientation Effects Induced Selective Chelation of Fe^{2+} to Glutamic acid Appended Polyfluorenes for Sensing and Live Cell Imaging

List of Abbreviations

AFM   Atomic Force Microscopy

B_c Conjugated Bilirubin

BT   Benzothiazole

CD   Circular Dichroism

CIE   International Commission on Illumination (*Comission*

Internationale de l'Eclairage)

CPs   Conjugated Polymers

CPE   Conjugated Polyelectrolyte

DLS   Dynamic Light Scattering

DSC   Differential Scanning Calorimetry

ee   Enantiomeric Excess

FRET   Fluorescence Resonance Energy Transfer

FTIR   Fourier Transform Infrared Spectroscopy

GPC   Gas Permeation Chromatography

HES   Heterogeneous Enantioselective Separation

HeLa   A type of Cell named after Henrietta Lacks'

HPLC   High Performance Liquid Column Chromatography

HRMS   High Resolution Mass Spectroscopy

HSA   Human Serum Albumin

ITC   Isothermal Titration Calorimetry

LOD   Limit of Detection

LED   Light Emitting Diode

MALDI	Matrix-Assisted Laser Desorption/Ionization
MIP	Molecular Imprinted Polymer
MOF	Metal Organic Framework
MTT	Methylthiazoletetrazolimium Dye
M_n	Number Average Molecular Weight
M_w	Weight Average Molecular Weight
$Ð_m$	Poly Dispersity Index
NMR	Nuclear Magnetic Resonance
OFET	Organic Field Effect Transistors
OLED	Organic Light Emitting Diodes
PDAF	Poly Dialkyl fluorenes
PFs	Polyfluorenes
PPE	Polyphenylene Ethynylene
QD	Quantum Dots
SEM	Scanning Electron Microscopy
SEC	Size Exclusion Chromatography
SLS	Static Light Scattering
R_H	Hydrodynamic Radius
R_g	Radius of Gyration
TCSPC	Time Correlated Single Photon Counting
TEM	Transmission Electron Microscopy
TGA	Thermo gravimetric Analysis
TMS	Tetramethyl Silane

ABSTRACT

Biosensors are highly essential prerequisites in clinical diagnosis of the diseased state in physiological functions. To save human life from the pathological threats and to control the death rate during epidemic periods, early detection of diseases is of high importance. Material design which have the potential for selective sensing of trace amount of analytes, can make early detection possible even in case of complex biofluids like blood serum, saliva and urine. Conjugated polymers are good candidate for such applications since the electronic structure of their conjugated backbone can function as 'molecular wires' that exhibit amplified sensitivity even for minute amount of analytes. Speed of sensing, visual response and accuracy are the additional attractions of conjugated polymers based sensors. Among various conjugated polymers, the polyfluorene class of conjugated polymers is widely explored for its brilliant blue emission and tunable emission covering the entire visible region. According to literature, visual sensing of heparin in water was successfully accomplished using polyfluorene based design. In another example, concanavalin-A protein was fluorimetrically identified using mannose appended polyfluorene.

In this thesis, selective detection of biologically important biomolecules is targeted by making use of polyfluorene backbone appended with biocompatible moieties in a cost effective manner. The importance of bio-inspired approaches and also morphological control of polymer architectures in selective sensing of analytes is highlighted through the demonstration of sensing studies in water, the competitive environment of complex biofluids like human blood serum and imaging studies in living cells.

The **first chapter** describes a critical review on conjugate polymer based fluorimetric sensors and advancement of polyfluorene in biosensing applications. The chapter describes the significances of sensing bioanalytes like Bilirubin, Enantioselective sensing of $_L$-enantiomers including Camptothecin, an anti-cancer drug and selective sensing of labile Fe^{2+} pools in living cells.

The **second chapter** describes the design of tailor made polyfluorenes appended with the bulky group pentadecyl phenol. Investigation on the morphology

of the polymers in solid state as well as solution state indicated formation of self-assembled nanostructures like vesicles and porous spheres. Taking advantage of spectral overlap between polyfluorenes and bilirubin, sensing of bilirubin was targeted. Highly selective sensing of free bilirubin with visual colour change from blue to green was demonstrated.

The **third chapter** deals with the real world application of sensing of free bilirubin in complex human blood serum containing crucial interferences. Inspired by the biological glucuronidation process, $_D$-Glucuronic acid was appended to polyfluorene, which facilitated non-covalent interactions with bilirubin. This in conjunction with favourable spectral overlap between the polymers and bilirubin favoured efficient FRET process in water and in serum. Selective sensing of free bilirubin in the clinically relevant range of < 25 µmol/L to > 50 µmol/L in human blood serum was successfully accomplished.

In the **Fourth Chapter**, homochiral conjugated polyfluorene (PF-GAP) with protected $_L$-glutamic acid appendage was designed for the first time. The polymer exhibited biomimetic conformation and porous helical morphology. The chiral recognition property assisted in enantioselective uptake of a wide variety of substrates such as amino acids, amino alcohols, hydroxyl acids, sugars and aromatic drug from aqueous racemic mixtures through the pores on the wall of the polymer. The entrapped substrates involved in self assembly along with the polymer backbone resulting in chiral amplification as directed by 'Sergeant and Soldier' principle.

The **Fifth Chapter** enumerates the idea of intracellular Iron(II) ion detection and imaging in living cells using glutamic acid appended polyfluorene. Orientation effects of the polymer induced selective chelation of Fe^{2+} to glutamic acid moiety leading to quenching of polymer fluorescence. The appendage afforded significant biocompatibility to the polymer, which was evident from MTT assay demonstrating >90 % of cell viability even at 300 µg/ml of polymer loading. The polymer exhibited supreme selectivity for Fe^{2+} ion with immediate sensitive response for 0.1 µmol concentration of intracellular Fe^{2+} which was verified by conducting the same experiment with various metal ions including bioavailable alkali metal ion, transition metal ions particularly Fe^{3+}, Zn^{2+}, Co^{2+}, Hg^{2+} metal ions.

CHAPTER - 1

INTRODUCTION

1.1 General Background

To introduce the topic of sensors, our sensory organs stand out as typical examples that bestow us with the natural ability to perceive the world around us. The exciting phenomenon of responses of these sensory organs towards external stimuli such as light, smell, taste, sound and touch is made possible by our nerve impulses through the transportation of ions. Besides empowerment of life by perception of external stimuli some special sensory organs present in plants and animals afford innovative functions to compensate for their deficiencies as well as to compete for the survival of the fittest. Bats and marine mammals are able to use ultra-high frequency sounds (Echolocation) for the purpose of navigation and the distance of the prey.[1] The returning echoes deliver the information or an 'image' about its environment to the animal that alleviate their problems of eye blindness. Notably, the action of self-defense is performed in sensitive leaves of *Mimosa pudica* that folds inward and droop when it is touched or shaken.[2]

These natural sensors have given us the insight to develop generations of sensing devices that have improved our standards of living. Figure 1.1 illustrates the advancement of sensors in various activities of day-to-day life.

Figure 1.1 Representation on the utility of sensors in various fields.

The significance of sensor devices is constantly growing to detect or predict, natural calamities (earthquakes, tsunami, volcanic eruptions and flood), war related alarms to safeguard the life on earth and diagnosing the biomedical problems in order to control the epidemic diseases and to increase the life expectancy as well. There is compulsive need to develop new sensors for increasing the speed of detection, accuracy, sensing powers that are cost effective for all economic classes of people.

Generally sensors are classified into many types based on the applications and lists of some sensors are as follows:

- Acceleration/Vibration
- Acoustic/Ultrasonic

- Chemical/Bio/Gas
- Electric/Magnetic

- flow
- Force/Load/Torque/Strain

- Humidity/Moisture
- leak level

- Machine level
- Optical

- Motion/Velocity/Displacement
- pressure

- Position/Presence/Proximity
- Temperature

The description on the terminologies which are routinely used in the context of sensors is given below so as to understand the concept in a better way.

i) Sensors:

Sensor is a device (also called as transducer) used to detect the nearby surroundings to provide information about the environment in a readable signal. In other words it can be described as a device that receives and responds to a stimulus or signal.[3]

Sensor devices majorly contain 3 working parts. They are 1) Receptor 2) Transducer 3) Processor unit (signal processor and amplifiers).

1) Receptor is the molecular recognition unit of the sensor that interacts with the environment.

2) Transducer/Transduction is a device or process that converts from one type (energy/signal) to another.

3) Processor unit is used to amplify the response in a readable signal output.

ii) Stimulus:

It is a matter or analyte that can elicit or evoke a response. For example heat is an external stimulus for the human body.

Among the various sensor types, the present thesis focuses on chemo and biosensors and the corresponding definitions are referred below for easy understanding.

Biosensor is any analytical device that detects biomolecules such as proteins, nucleic acids, enzymes, antibodies, carbohydrates, and analytes in blood serum, in water or in complex biofluids. Chemical sensor is a device that specifically detects the presence of one particular chemical compound in a system and provides an indicative signal.

The detection processes include the following methods depending on the mode of conversion of the responses.

a) **Electrochemical sensors** convert chemical or biochemical responses into current/potential/conductivity signals between the electrodes and thus the transducers are called as amperometric/potentiometric/conductometric sensor respectively.

b) **Optical Sensors** transform chemo and biochemical signal into absorption/emission and they are referred as colorimetric and fluorimetric sensor respectively. A detail description of the fluorimetric sensors and different classes of materials that can be utilized for it etc is provided in the following section.

c) **Piezoelectric sensors** play a relatively small role in chemo and biosensors. Piezoelectric sensors measure changes in pressure, temperature, stress etc and convert into electric charge. Piezoelectric sensors are used as humidity gauges, thin film monitors and gas sensors.

d) **Thermo chemical sensors** generates heat signal during a chemical transformation and amount of heat is quantified to realize the sensing activity.

1.2 Fluorimetric Sensors

Fluorometric sensors are one type of optical sensors that operate on the principle of change in the emission (or fluorescence) intensity of the probe in

response to the analyte. Fluorescence is the phenomenon of emission of photons from the lowest singlet excited state to the ground state of a matter which is a spin allowed process; typically with the rate of fluorescence of 10^8 s^{-1}.[4] The absorption and emission processes are illustrated in Jablonski diagram as shown in Figure 1.2. The initiating process is the absorption of light by the ground state (S_0) that is excited to singlet excited state denoted as S_1, S_2 etc. When the fluorophores return back to the ground state from the S_1 lowest singlet state with an emission of photons, the emission is called as fluorescence. The fluorophores which are commonly used in the sensing processes are rhodamine, pyrene, anthracene, perylene, fluorescein, dansyl chloride, etc.
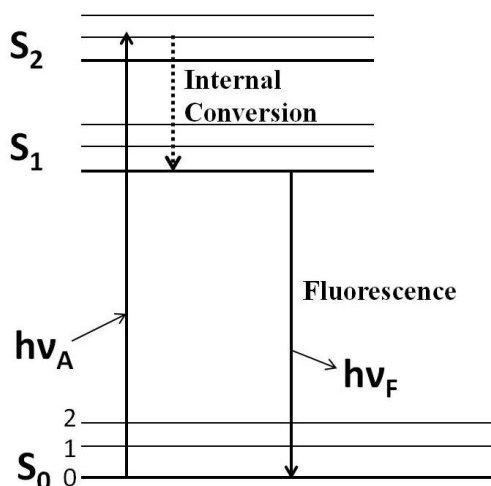
Figure 1.2 Schematic representation of Fluorescence process. (Figure was adapted from Ref. 4)

The fluorimetric sensors are categorised based on transduction mechanisms as follows 1) Quenching of fluorescence intensity (Turn-off sensor): two modes namely static quenching and dynamic quenching can take place depending on the system. 2) Increase in fluorescence intensity (Turn-on sensor): When the probe is prequenched followed by the addition of analyte an enhancement of emission occurs. 3) Energy transfer (FRET): emission energy of the probe is absorbed by the quencher staying in the ground state and that energy is exploited to excite the quencher to the excited state, resulting in emission from the quencher as the signal response.

Fluorescent sensors are widely used for chemical sensing due to their inherent sensitivity of detection with proportional change in the fluorescence intensity of the probe as a function of concentration of the analyte.[5] Fluorometric sensors are advantageous over other types of sensors because of the following reasons: 1) Operation in wide window of analyte concentration from moles to single molecules. 2) Fast response of sensing of samples belonging to various sectors such as clinical, bioprocess and environment. 3) The sensitivity of fluorimetric methods is about 1000 fold greater than other spectrophotometric methods and the lower detection limit of the analyte in picomolar regime can be achieved.[6]

Based on the chemical nature of the fluorescent probes, the sensors can be classified as follows. (1) Small molecules (2) Polymers (3) Metals and metal complexes (4) Quantum dots (5) Metal organic frameworks.

1) **Small Molecules:**

Small molecules like rhodamine, pyrene etc that can act as fluorophores, are functionalized with suitable functional groups targeting for specific analyte. Small molecule based sensors require stoichiometric amount of analyte in order to realize their sensing activity.[7] From the plot of the fluorescence response against their intensity, the concentration of the analyte can be directly quantified. For example, pyrene functionalized with cationic indolene moiety could selectively sense mercury ions in water and the resulting complex is presented in Figure 1.3.[8]
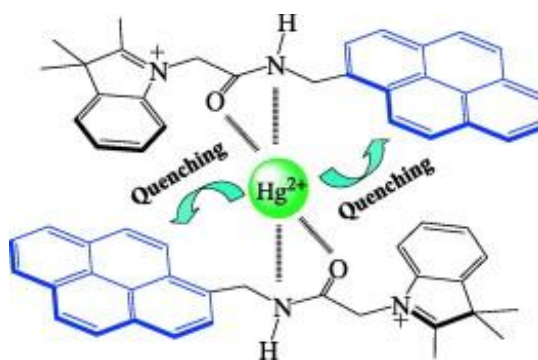
Figure 1.3 Pyrene based probe for sensing of Hg ions in water. (Adapted from ref. 8)

Rhodamine based small molecular probe could selectively sense the fluoride ions in water resulting in enhancement of fluorescence whereas other anions could not perform the same reaction to give fluorescent product as shown in Figure 1.4.[9]
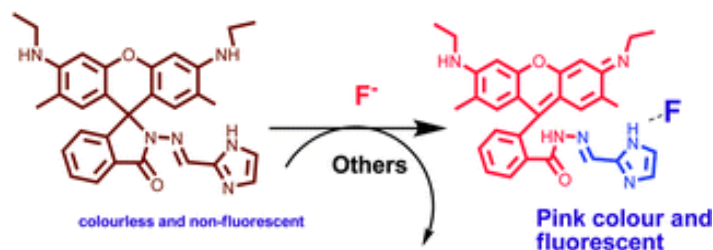
Figure 1.4 Rhodamine based probe for sensing of F⁻ ions. (Adapted from Ref. 9)

2) Polymers:

Polymers are the most commonly used fluorescent chemo-sensors for availing the advantage of easy processability into thin films, and are deposited on optical fibres and wave guides for sensor device fabrication.[10] Based on the structure of the polymers, they are classified into three types such as (i) Polymer particles (ii) Molecularly imprinted polymers (iii) Conjugated polymers (CPs).

(i) Polymer Particles:

Fluorescent polymer particles are prepared by physical entrapment or covalent linking of dyes into the polymer matrix. The covalent linking can be performed by copolymerizing with fluorescent polymerizable monomer or by the post-modification of the fluorescent polymer if it is constituted with the reactive functional group. The monomer, 2-allyl-1, 3-dioxo-2, 3-dihydro-1*H*-benzo[de]isoquinoline-6-sulfonyl azide (AISA) was designed and copolymerized with styrene to produce a polymeric fluorescent sensor material. Poly(styrene-*co*-AISA) (PSAISA) showed a turn-on fluorescence response and high selectivity for hydrogen sulfide (H_2S) over other related species including HSO_3^-, SO_4^{2-}, $S_2O_3^{2-}$ and cysteine.[11] Polymers such as polystryrene,[12] PMMA,[13] cellulose,[14] and luminescent dendrimers[15] can also act as fluorescent sensors by functionalizing with suitable fluorophores. These fluorescent polymer contain a receptor unit that interacts with the targeted analyte, and the fluorescent dye responds to the binding between the polymer and the analyte.

(ii) Molecularly Imprinted Polymers (MIPs):

MIPs are a special class of fluorescent polymer based probe, where the imprint analyte creates a 3-D cavity in the polymer scaffold during polymerization of monomers. After the polymerization the imprinted molecule is removed by solvent

extraction and the complementary cavity it leaves behind, helps in the selective uptake of the same analyte molecule. In fact, MIPs are selective for the analytes without containing a receptor for selective binding. The imprinting process involves the co-polymerization of functional monomers and a cross-linker in the presence of target analytes which act as a molecular template (imprint molecule). The following example describes the sensing of cyclobarbital using molecularly imprinted polymer. Co-polymerization of 2-acrylamidoquinoline as the functional monomer and ethylene glycol dimethylacrylate as cross-linker in the presence of cyclobarbital yielded a fluorescent hydrogen-bonded MIP that was able to bind selectively to cyclobarbital as shown in Figure 1.5.[16] Cyclobarbital showed high binding affinity towards the imprinted polymer than its structurally similar analytes with same functional groups. The main advantages of the MIPs are easy synthesis, high affinity and selectivity for the template analyte.
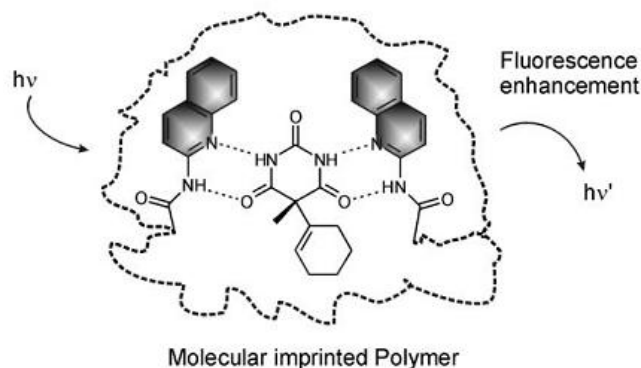
Figure 1.5 The design represents MIP sensor for sensing cyclobarbital. (Figure was adapted from Ref. 16)

(iii) Conjugated Polymers (CPs):

Fluorescent conjugated polymers based on 2, 2'-bipyridyl-phenylene-vinylene,[17] terpyridine-based poly(p-phenylene-ethynylene)-alt-(thienylene-ethylene) polymers,[18] and poly(p-phenylene-ethynylene)[19] have been reported as sensitive probes for the detection of metal ions in aqueous solution. Further details are discussed in later sections.

3) Metals and Metal Complexes:

Fluorescent metal nanoparticle and metal complexes are used as fluorescent probe for chemical and gas sensing. Metal complexes of Co(II), Fe(II), Ru(II), Rh(II), and Cu(II) act as a turn-on fluorescent probe for nitric oxide.[20] Similarly ruthenium bipyridyl complex $[Ru(bpy)_2(pip)]^{2+}$ that could function as switch-on fluorescent sensor for Hg^{2+} and switch-off fluorescent probe for biothiols were developed.[21]

4) Quantum Dots (QDs):

Semiconductor quantum dots have recently emerged as fluorescent probes due to their high photoluminescence quantum yield, narrow emission spectra, surface functionalization, energy transfer efficiency and high photostability.[22] The orientation and the structure of the Escherichia coli maltose-binding protein (MBP) was determined using CdSe-ZnS core–shell QDs. For performing the analysis, different amounts of rhodamine red dye-labelled MBP protein was attached on surface of CdSe-ZnS core–shell QDs.[23] FRET occurring between the QDs (donor) and the dye (acceptor) helped in determining the distance between the rhodamine red (RR) dye and the QD centre. From the aforementioned study, the orientations of the MBP protein on the QD surface were revealed.

5) Metal Organic Frameworks (MOFs):

MOFs are one type of porous materials finding applications in gas storage, separation, catalysis and recently as chemo sensors.[24] The recognition of the analyte takes place by simple physisorption or by the receptors introduced on the surface of the MOF leading to fluorescence response of the ligands attached in MOF. There is an exciting review covering the application of chemo sensors using MOF as probe.[25] Luminescent micro-porous cadmium–organic framework {[Cd(l2-Cl)(l4-5MT)]n (5MT = 5-methyl-1H-tetrazole)} exhibited highly sensitive sensing activity toward nitrite ion in both DMF and water.[26] Figure 1.6 shows the structure and sensing activity of the Cd based MOF.
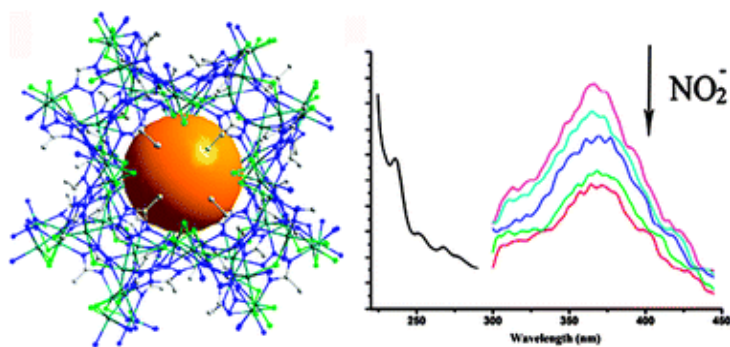
Figure 1.6 Structure of Cd- MOF and sensing of nitrite ion. (Taken from Ref. 26)

1.3 Conjugated Polymers (CPs) as Biosensors

Conjugated polymers are organic macromolecules containing alternating double and single bonds extended in a long backbone structure. Conjugated polymers find applications in the field of organic light emitting diodes (OLEDs),[27] organic field effect transistors (OFETs),[28] solar cells,[29] super capacitors,[30] drug delivery,[31] logic gates,[32] chemo[33] and biosensors.[34] The advancement of CPs in diverse fields became possible due to the ability to combine the electronic and light harvesting properties.[35] Generally, the attachment of receptor to the conjugated backbone increases the sensitivity of the fluorescent sensor for that particular analyte. Scheme 1.1 shows the backbone structures of some representative CPs, including polyacetylenes (PAs), poly(arylene vinylene)s (PAVs), poly(para-phenylene)s (PPPs), polyfluorenes (PFs), poly(arylene ethynylene)s (PAEs), polyanilines (PANIs), polypyrroles (PPys) and polythiophenes (PTs).
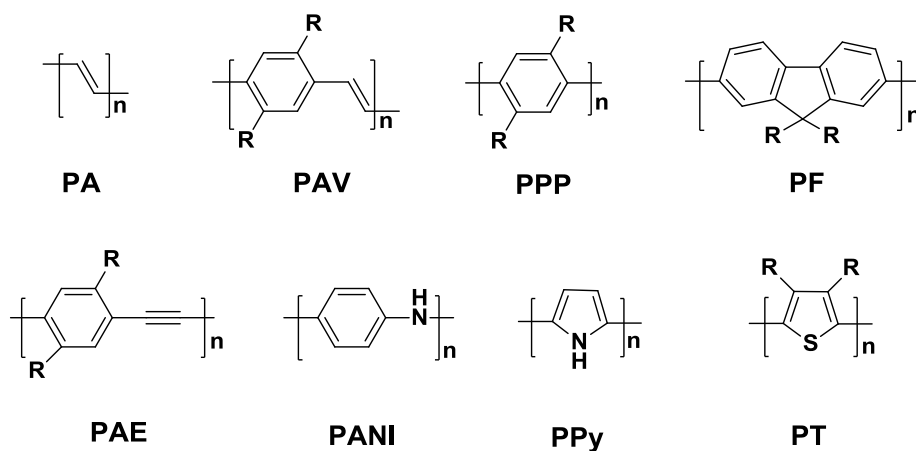
Scheme 1.1 The chemical structure of various conjugated polymers.

Research on the development of CP based biosensors has steadily increased over the past decade. The main attractive feature of the conjugated polymer probe is the amplified fluorescent signals with addition of very small quantity of analyte.[36] Small molecule based fluorescent sensors need stoichiometric amounts of the analytes to realize their sensing activity and the sensitivity of detection depends on the equilibrium constant upon binding. CPs can be explored for specific sensing of an analyte by tuning the structure property relationship of the probe design. The collective system response of CPs[37] as shown in Figure 1.7 provides the platform for amplified sensitivity. The delocalized π-electronic conjugation between each repeat unit creates the molecular wire self-assembly that involve in the migration of the charges across large distances along the conjugated backbone.[38]
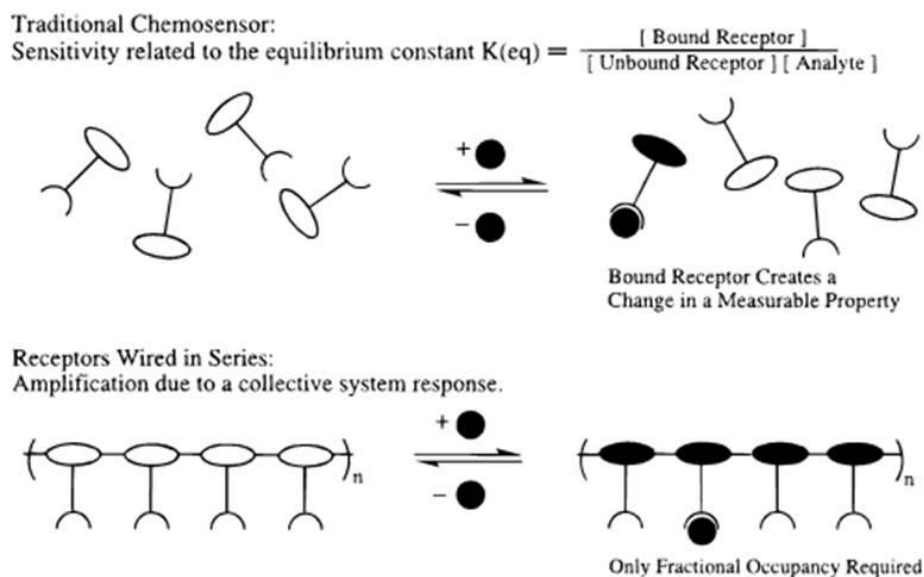
Figure 1.7 Schematic representation of amplified response of a conjugated polymer. (Figure was taken from Ref. 37)

In order to prove the concept of molecular wire assembly, Swager et.al.,[39] demonstrated a fluorescence experiment using conjugated polymer. The different molecular weight of the same structural polymer was numbered 6-8 in the increasing trend of molecular weight. The conjugated polymers were attached with receptor on each repeat unit, and its similar monomer analogue (2; figure 1.8 b) also contained the receptor unit. Addition of paraquat [PQ^{2+}] molecule, a known electron transfer and quenching agent for cyclophane based CPs was carried out. They monitored the

fluorescence quenching for 6-8 and 2 from the emission spectrum by plotting $F_0/F = 1 - K[PQ^{2+}]$. A linear Stern-Volmer plot was obtained for all the polymers and monomer analogue.

Careful observation of the stern-volmer plots in Figure 1.8c revealed the large difference between the polymers (6-8) and their monomeric analogue (2) in the slope parameters. For the addition of 0.002 M of PQ^{2+} ions the association constant calculated for the monomer was 1600 M^{-1}, whereas for polymer it was very high ranging from 75000 M^{-1} to 105000 M^{-1} depending upon their molecular weight and approximately 44-66 times higher for polymers compared to the monomer clearly indicating the amplified quenching.
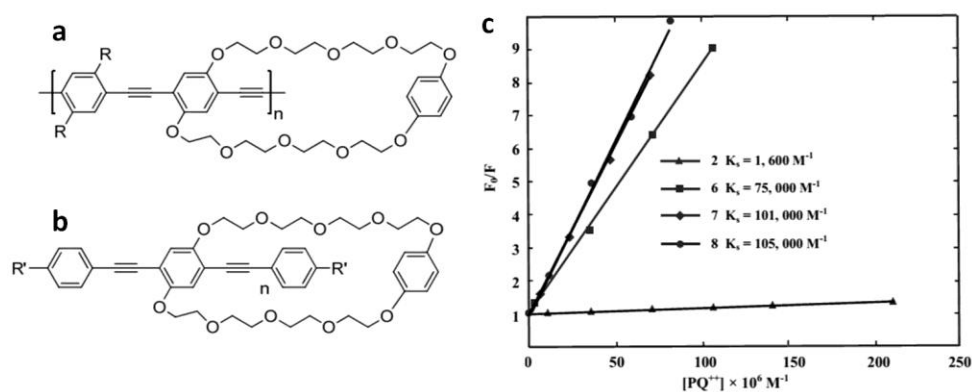
Figure 1.8 The Chemical structure of **(a)** the polymers (6-8) and **(b)** small molecule **(c)** The Stern-Volmer plot for the sensing of PQ^{2+} by the polymers and small molecule which is denoted as (2). (Figure was taken from Ref. 39)

The amplified sensitivity toward the quencher is explained from the band structure of the conjugated polymers (Figure 1.9).[40] Excitation of the conjugated polymer creates electron-hole pairs which migrate throughout the entire polymer backbone due to the extended electronic communication and transport property. The quencher binds with one of the receptor and the exciton senses the resistive element in the wire resulting in the quenching of the exciton. All the charge carriers (or electrons) that flow in the molecular wire experience an impediment leading to an electron transfer from polymer to the quencher. Thus the single binding event reduces the transport of many of the conducting electrons resulting in signal enhancement of the conjugated polymers. Binding constants of all the receptors also remains an additive factor for

signal amplification. Therefore, the polyreceptor system in polymer shows very high effective binding constant compared to small molecular counter parts.
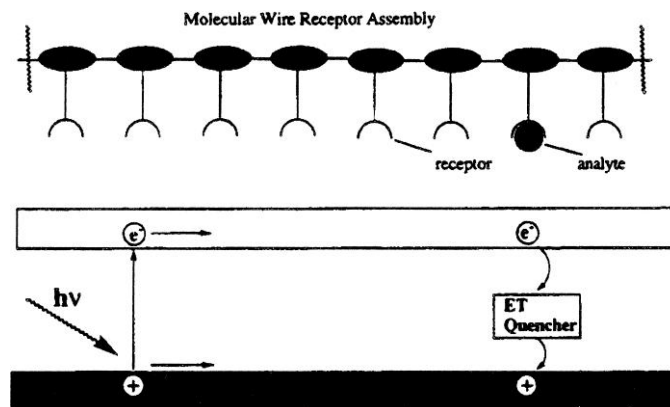
Figure 1.9 Band structure diagram of the conjugated polymer illustrating the amplified sensitivity. Figure was taken from Ref. 40)

The water-solubility is a fundamental requirement for any conjugated polymer to act as biosensor is and also to couple the analyte-receptor interactions into an observable signal.[41] Water-dispersible or water-soluble conjugated polymers are synthesized using the strategy of introducing different polar groups as side pendants. Based on the nature of polar functional groups, water-soluble CPs can be categorized into four types: Cationic CPs (CCPs), anionic CPs (ACPs), zwitterionic CPs (ZCPs), and nonionic CPs (NCPs). Detailed discussion on the side pendants will be given in the coming sections. However, significant quenching of polymer fluorescence due to self aggregation of the rigid rod backbones of CPs by hydrophobic and π-π stacking interactions is a major drawback.[42]

Major sensing mechanisms of the CPs are described using suitable examples.

Fluorescence quenching, CP self-aggregation induced aggregate emission and Förster resonance energy transfer (FRET) from donor CPs to acceptor fluorophores.

1) Fluorescence Quenching (Turn-off):

Fluorescence quenching is a process of decrement in the fluorescence intensity of the probe resulting from various molecular interactions such as excited state reactions, molecular rearrangements, energy transfer, ground-state complex formation, and collisional quenching due to the interaction with the analyte.[4] It can be sub-categorized as (i) Static quenching (ii) dynamic or collisional quenching. In the case

of static quenching a ground state complex is formed between the probe and analyte and this complex is non-fluorescent. On the other hand, dynamic quenching the analyte interacts with the excited-state of the probe hindering the emission of photons from the probe during relaxation to ground state.[4] In the collisional quenching process there is neither change in the chemical behavior nor in the photochemical change of the probe. Static quenching can be confirmed by recording lifetime measurements of the probe wherein the lifetime of the probe should not show any change because of the fact that the uncomplexed probe should give the same lifetime. In 2002, Heeger and coworkers[43] demonstrated that cytochrome c (Cyt C) could quench the fluorescence of PPV-SO$_3^-$ with an extremely high quenching constant ($K_{sv} = 10^8$ M^{-1}). Cyt C is a hemoglobin containing protein. At neutral pH, Cyt C is cationic and can bind with polyanions and adopt a conformation ready for rapid electron transfer. In contrast, a control protein such as myoglobin which is another heme protein did not have any electron transfer center. The nonspecific interactions between multiple proteins and carboxylate substituted anionic PPE were reported by Bunz and coworkers.[44] They stated that proteins without quenching centers (such as histone and lysozyme) could also induce indirect CP fluorescence quenching through analyte induced CP aggregation via nonspecific electrostatic and hydrophobic interactions.

2) Fluorescence Enhancement (Turn-on):

Fluorescence enhancement is a process of increment in the fluorescence intensity of the probe upon interaction with the analyte. The classic examples from the literature for the turn-on sensing analyte is based on enhancement of CP emission or prequenched CP emission that is retrieved upon addition of analyte. In 2006, Swager et. al.,[45] demonstrated a turn-on sensing mechanism for the trace detection of hydrazine. The turn-on response of the conjugated polymer based sensor (Figure 1.10) was active even at 1 ppm and a minimum of 100 ppb concentration of the hydrazine molecule. Addition of hydrazine molecules to conjugated polymer film resulted in an increase in the emission of the polymer without any change in the shape of excitation or emission spectrum. A possible explanation for the increase in emission of CP was that hydrazine eliminated a non-radiative decay pathway of the

conjugated polymer, resulting in a higher solid-state quantum yield of the conjugated polymer.
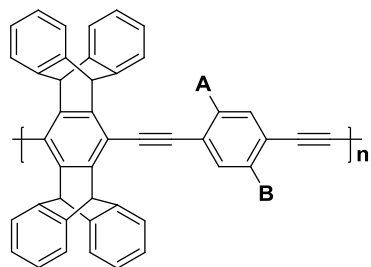
Figure 1.10 The chemical structure of the conjugated polymer for sensing hydrazine. (Figure was adapted from Ref. 45)

P1: A=B=O(n-C$_{10}$H$_{21}$)
P2: A=N(n-C$_8$H$_{17}$)$_2$; B=H
P3: A=B=N(n-C$_8$H$_{17}$)$_2$

The second type of turn-on fluorescent sensor uses the principle of pre-quenching CP emission and retrieving it with the addition of analyte to visualize the turn-on response. For example, the neutral CP (P1) was pre-quenched using the Cu complex (c) as shown in the left and middle photographs in Figure 1.11.
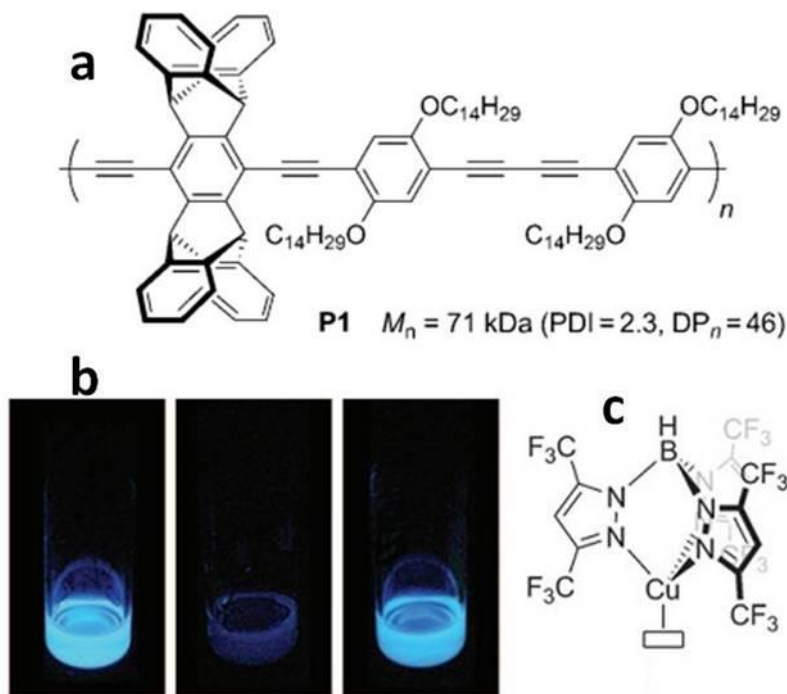
Figure 1.11 (a) The chemical structure of sensing probe **P1**, (b) Photographs denoting **P1** (left) with Cu-complex added (middle) and ethylene gas treated (right) and (c) The structure of Cu-complex. (Figure was taken from the Ref. 46)

The triple bonds in the **P1** polymer assisted in coordination with the Cu(I) complex resulting in the amplified quenching. This pre-quenched polymer solution was purged with ethylene gas to restore 95 % of the polymer fluorescence to its original intensity shown in right side photograph.[46]

3) Fluorescence Resonance Energy Transfer (FRET):

FRET is the process by which excited state donor transfers energy to a ground state acceptor through dipole-dipole interactions resulting in the fluorescence quenching of donor and fluorescence enhancement of acceptor.[4] FRET depends on two factors (i) Spectral overlap between the donor and acceptor and (ii) the distance between donor and the acceptor. FRET has become a popular technique demonstrated in fluorescence analysis of proteins, DNA, fluorescence imaging and membranes.

Bazan and coworkers[47] reported the first conjugated polymer based FRET sensing for DNA sequence identification. The assay contained cationic conjugated polymer (PFP-NMe$_3^+$) (shown in blue) and dye linked peptide nucleic acid (PNA-C*, shown in black). Cationic CP and the dye C* had good spectral overlap favoring FRET in the close proximal distance. Addition of complementary ss-DNA, specifically hybridized with PNA-C* to form ss-DNA/PNA-C* complex with multiplex negative charges. Electrostatic interaction between ss-DNA/PNA-C* and cationic CP brought them in close vicinity and efficient FRET occurred with 25 times enhanced emission for C* under optimized conditions. As non- complementary DNA could not hybridize with PNA-C*, there was no observation of FRET between cationic CP and non-complementary ss-DNA. Thus, this protocol could be used to generate sensing array for DNA and the corresponding cartoon representation is given in Figure 1.12.

Bin Liu et. al,[48] studied the analyte induced aggregation of cationic conjugated polymer resulting in FRET for generating light-up probes as shown in Figure 1.13. The anionic analyte, heparin formed an electrostatic complex with cationic CP that induced aggregation of polymer chains. Polymer aggregation enhanced the energy transfer from fluorene units to benzathiadiazole units resulting in color tuning from blue to orange. The emission spectrum of the polymer showed decrease in the emission of polyfluorene units and increase in the emission of BT units with low detection limit of 30 nM of heparin. Moreover, the distinguishable solution

fluorescence color at different heparin concentrations made naked-eye heparin detection and quantification feasible.
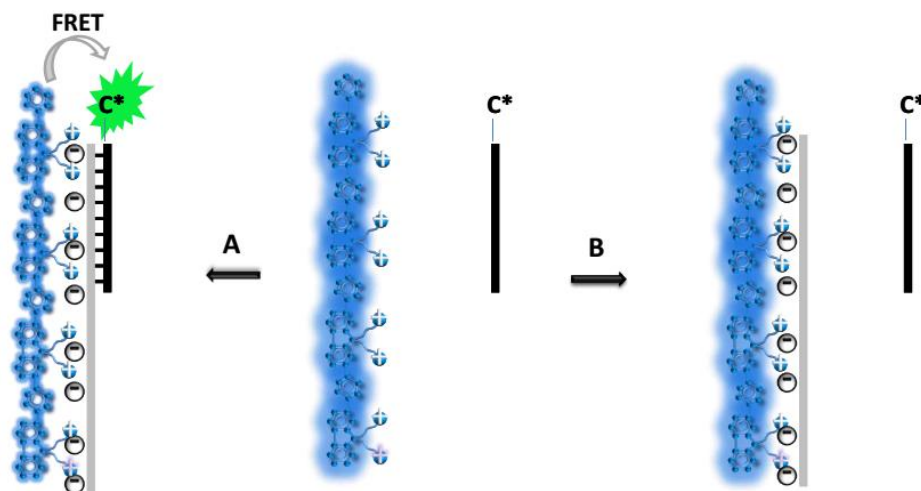
Figure 1.12 FRET based sensing of DNA sequence using CPE. (Figure was taken from the Ref. 47)
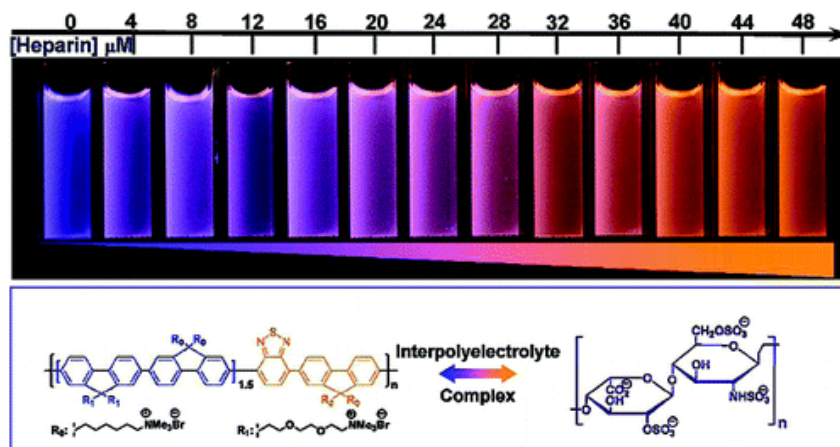
Figure 1.13 Conjugated polymer as light-up probe for heparin sensing. (Figure was taken from the Ref. 48)

1.4 Polyfluorenes – Our Choice

Polyfluorenes are one of the conducting polymers belonging to the class of rigid-rod polymers obtained from coal tar. The backbone of polyfluorene consists of a planar biphenyl unit connected by carbon atom at the 9 position, ensuring high degree of conjugation. The carbon atom at the 9 position is substituted with functional

groups to bring the processability for the polymer chains and also play an important role in inter-chain interactions without modifying the optical and electronic structure of the polyfluorenes.[49] Polyfluorenes find potential application in organic light emitting diodes, field effect transistor, solar cells, chemo and biosensors. Polyfluorenes are connected with aromatic rings in the backbone resulting in high thermal stability and its decomposition temperature exceeds above 400 ^{0}C. Polyfluorenes exhibit thermotropic liquid crystalline property which allows the polymers to align on rubbed polyimide layers.[49] The chemical structure of polyfluorene is shown in Figure 1.14.
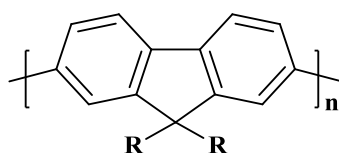
Figure 1.14 Representation of the chemical structure of polyfluorene.

1.4.1 Optical Properties of Polyfluorenes:

Polyfluorene contains chromophoric aromatic backbone enabling natural tendency to absorb and emit light. Generally polyfluorene class of polymers absorb strongly at about 387 nm due to π-π* transition with a single peak maxima indicating the broad distribution of chains.[50] In contrast to absorption spectrum, emission spectra of the polyfluorenes are well defined with three vibronic transitions corresponding to 0-0, 0-1 and 0-2 intrachain singlet transition, with the 0-0 fundamental transition being the most intense peak.[50] Polyfluorenes exhibit bright sky blue color under uv light. The fluorescence quantum yield of the polyfluorenes is higher than 50 % both in solution and in solid state.

1.4.2 Synthesis of Polyfluorenes:

Polyfluorene can be designed and synthesized with tunable photophysical properties exercising synthetic control over the electron donating or withdrawing character of the substituent's on fluorene or the comonomers in polyfluorene. The aspect of solubility of the polymers is an important factor because solution state processing approach is very common. Since conjugated polymers tend to aggregate due to their planar structure, side chains are added (to the 9 position of fluorene) so as to increase

the solubility of the polymer. The functionalized dialkylfluorene monomers laid a strong platform for the extensive development of various derivatives of poly(dialkylfluorene)s PDAFs. Few of the main methods practiced for the synthesis of the polymers are described below. PDAFs can be made by oxidative coupling of the monomer with iron(III) chloride. Poly(9,9-dihexyl-2,7-fluorene) with a molecular mass of 5000 was made in this way by Yoshino and co-workers (**Scheme 1.2**) and used to make low-efficiency blue-emitting devices.[50]
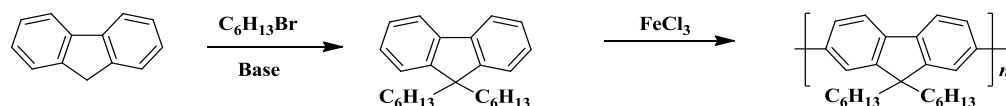
Scheme 1.2 Synthesis of polydialkylfluorene through oxidative coupling.

The disadvantages of this method are the low degree of polymerization and the high level of defects that are produced due to coupling other than at the 2nd and 7th positions. Therefore, this method is generally not practiced to make PDAFs. Most of the synthetic methods for polyfluorene employ Suzuki polycondensations of dibromomonomers (**Scheme 1.3**).
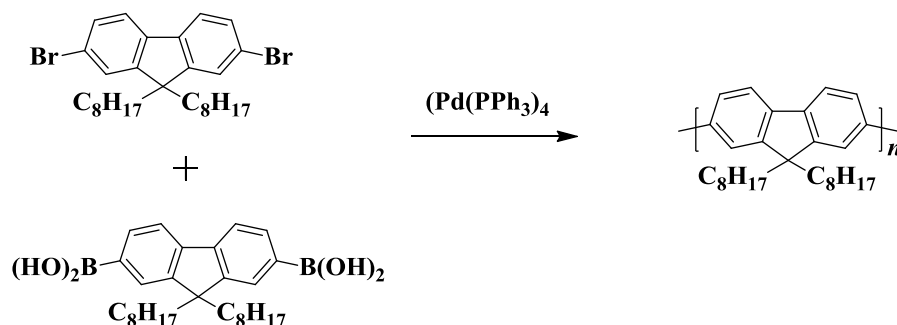
Scheme 1.3 Synthesis of Polydialkylfluorene through Suzuki polycondenzation.

Poly(9,9-dioctylfluorene) with a $M_n > 100,000$ g/mol was obtained after less than 24 h of reaction time.[50] Copolymers of polyfluorenes are also synthesized by Heck, Sonogarshira and Stille coupling routes[50] and such synthesized polyfluorenes are obtained as solid powders with blue fluorescence and good thermal stability. Other methods such as Yamamoto or Kumada coupling using Ni(0) catalyst is reported for the preparation of homo-polyfluorenes.[50]

1.4.3 Structure-Property Relationship:

The chemical and optical properties of the polyfluorenes mainly depend on their structure and the nature of the appended pendant groups. Depending upon the functionalization, polyfluorenes find application in solar cells, light emitting diodes, and color tuning, chemo and biosensors which will be discussed in detail in the next section.

1.5 Effect of Appendages on Polyfluorenes:

Appendages play a crucial role in determining the properties of polyfluorenes because they are able to tune the optical, electrical and conducting properties of the polyfluorenes.[49] Generally, the pendants are broadly classified into 3 categories: (i) Alkyl chains and aromatic groups as pendants, (ii) Polar pendants and (iii) Chiral pendants.

(i) Alkyl Chains and Aromatic Groups as Pendants:

Alkyl chains such as hexyl, octyl, decyl and dodecyl chain appended polyfluorenes exhibit hairy-rod morphological feature wherein polyfluorene backbone behave as rod segment and the alkyl chains behave as hairy functional chains. Among various alkyl chain system, hexyl and octyl chain appendage have received great attention. Alkyl chains usually do not alter the optical properties of the polyfluorenes in good solvents. In poor solvents (cyclo hexane and methyl cyclohexane) polydioctyl fluorenes tend to aggregate to form β-phase.[51] In solid state or in thin film the optical properties vary depending upon their interchain interactions. Alkyl substituted polyfluorenes exhibit nematic liquid crystalline behaviour and is favoured in light emitting diodes (for blue LEDs) and electronic applications.[52] Bradley and co-workers reported that octyl chain appended polyfluorene showed the hole mobility in the range of 3×10^{-4} to 4.2×10^{-4} cm^2 V^{-1} s^{-1} which could be enhanced upto 5×10^{-3} to 9.2×10^{-3} cm^2 V^{-1} s^{-1}.[53]

(ii) Polar Pendants:

Polar pendants are the interesting pendants from the last decade because they find application in OLED, OFET, chemo and biosensors. Polar pendants are classified into two categories (a) Polar ionic pendants (b) Polar neutral pendants.

(a) Polar Ionic Pendants:

Polyfluorenes functionalized with ionic pendants such as cationic, anionic and zwitterionic pendants are termed as conjugated polyelectrolytes (CPE) (Figure 1.15) which are highly water soluble or dispersible in nature.[54] The charged side chains of CPEs interact with other molecules through electrostatic and hydrophobic interactions. During the sensing processes, these two interactions drive CPEs toward targeted analyte in the close proximity that induces changes in the optical properties of CPE. In 2002, Huang and co-workers reported cationic, water-soluble CPE which was synthesized through a post polymerization methodology.[55] There are numerous reasons to develop CPEs and tailor their phase behaviour, structure, and self-assembly in water.
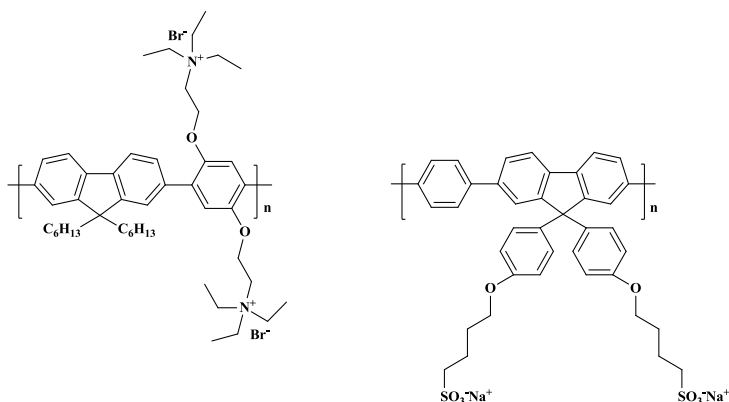
Figure 1.15 Examples of polar ionic conjugated polyelectrolyte system.

In particular, attention was paid to the aqueous solubility and supramolecular organization of a water–polyfluorene–surfactant (amphiphile) system composed of polyelectrolyte (PBS-PFP). The photophysical properties of CPEs have been extensively investigated, both from the fundamental viewpoint and applications oriented in chemo- and biosensors and organic optoelectronic devices. Owing to their inherently amphiphilic structures (hydrophobic backbone and hydrophilic side groups), CPEs have a tendency to self-aggregate in aqueous solution or polar organic solvents, and as a result their photophysical properties strongly depends on the solvent. A cationic polyfluorene-*alt*-phenylene (PFP) derivative (blue emitter) containing 5 mol % of 2, 1, 3-benzothiadiazole (BT) units was first synthesized for multicolor DNA sensing and DNA quantification. Electrostatic interaction between

the CPE chains and negatively charged DNA molecules induced polymer aggregation, leading to enhanced interchain contacts between optical partners. Under these specific conditions, interchain FRET occurred from the fluorene segments (donor) to the BT units (acceptor) which was more efficient than intrachain FRET process and consequently green emission dominated the solution fluorescence. Such an aggregation-enhanced FRET allowed B1 to effectively quantify ds-DNA ranging from 0.6 nM to 0.15 μM in terms of base pairs.[56]

(b) Neutral Pendants:

Polyfluorenes functionalized with neutral pendants such as sugar units and ethylene glycol units are called neutral water soluble polyfluorenes. The key advantage of neutral polyfluorene in biosensor applications is the specificity in recognition or binding of targeted analyte.[57] For example mannose substituted polyfluorene selectively binds with Concanavalin-A protein resulting in the energy transfer from fluorene units to BT units.[58] Similarly polyethylene glycol grafted densely on the surface of cationic polyfluorene suppresses the non-specific interactions between the polymer and protein[59] leading to quenching of polymer fluorescence. PEG grafted CPE has been shown to act as fluorescence markers for the cancer cells.

(iii) Chiral Pendants:

Polyfluorenes functionalized with chiral pendants such as chiral alkyl chains, chiral binapthol units and amino acids impart helicity in the whole polymer chains. The chirality of the side chains transfers its chirality to the backbone conferring three dimensional structures.[60] Chiral polyfluorenes find application in the field of electronic devices because they are defect free materials with high crystallinity. The helical packing supports high charge transport through their helically ordered backbones. Polyfluorene functionalized with triphenyl amine groups having chiral C-9 carbon exhibited blue emission with maximum external quantum efficiency. The single-layer device using this copolymer as the emitting layer showed efficiency of 1.21 % (at a brightness of 354 cd/m^2 with driving voltage of 7.6 V).[61] Other advantages of chiral polymers are in the field of photonics, chiral catalyst, enantioselective sensing and separation. As an example, chiral poly(fluorene-alt-

benzothiadiazole) (PF-BT) formed a nanocomposite with gold nanoparticle and it could act as a chiral metamaterial. This polymer-gold nanocomposite demonstrated the plasmonic enhancement of the chiro optical activity of PF-BT.[62]

1.6 Overview of Appendages and Applications in the Thesis:

In this thesis, four different appendages were employed for demonstrating biosensing applications. The selection of appendages was based on aspects of biocompatibility factor, morphological control and amphiphilic structure.

A. Appendages Explored in the Thesis

Appendage I: 3-pentadecyl Phenol:

3-Pentadecyl phenol is the chemical product obtained from catalytic hydrogenation of cardanol which is naturally available from cashew-nut shell liquid. It possesses a pentadecyl alkyl chain with a phenolic group and the corresponding structure is given in Figure 1.16.
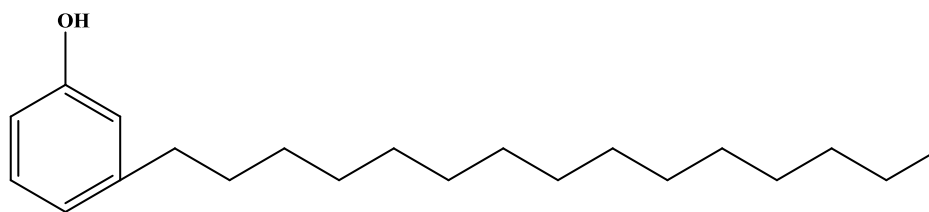
Figure 1.16 The chemical structure of 3-pentadecyl phenol.

The attractive feature of this molecular structure is that it combines the properties of an aromatic moiety, polar moiety and long alkyl chain. Recently, it gained importance in research field in designing bilayer morphological structures. The molecule is known for its interdigitating property which can exhibit spherical curvature design. On appending to a conjugated backbone, the self-assembly of the system is driven by the interdigitating property forming vesicular,[63] tubular[64] and spherical morphologies[65] that can serve as delivery vehicles of biomolecules. In chapter 2, this molecule was used as appendage to polyfluorene to bring morphological control.

Appendage II: D-glucuronic Acid:

Glucuronic acid belongs to the chemical class of carbohydrates with structure analogous to that of Glucose. When the primary alcohol group of the glucose is oxidised, it is converted into Glucuronic acid and its structure is depicted in Figure1.17. This bio-available carbohydrate is commonly found in the chains of proteoglacans, mucuous secretions, and a precursor to ascorbic acid and in intercellular matrix.[66]
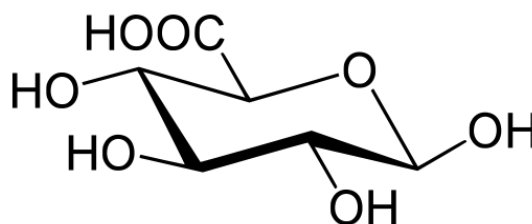
Figure 1.17 The chemical structure of D-glucuronic acid.

Glucuronic acid is highly soluble in water due to the possibilities of hydrogen bonding between polar carboxylic, alcoholic groups and water molecules. The presence of two different chemical groups affords versatile functionalization ability. This carbohydrate is the key substance in the biological process of enzyme mediated glucuronidation that is one of the important stages in drug metabolism mostly taking place in liver, pancreas, spleen and also lungs.[67] The accumulation of insoluble substances, drugs, free bilirubin, androgens, fatty acids and retinoid is highly toxic to physiological functions. The glucuronidation process involves the formation of water soluble gluoronides through conjugating insoluble substances to glucuronic acid via esterification process thereby facilitating their excretion. The appendage of hydrophilic glucuronic acid to the hydrophobic conjugated backbone brings amphiphilic structure with water solubility and biocompatibility. It can also provide interacting site for bilirubin that can be exploited in sensing applications.

Appendage III: L-glutamic Acid:

L-Glutamic acid is one of the proteogenic amino acid which is frequently found in the sequencing of proteins. It is a negatively charged amino acid because of the additional side chain carboxylic acid group along with amino acid moiety. Figure 1.18 shows the structure of the L-glutamic acid. Glutamic acid is a vital

neurotransmitter and it also takes part in other biological activities namely cellular metabolism, enhancing flavors, brain signaling circuit, GABA precursor (GABA-gamma-aminobutyric acid synthesized from L-glutamic acid using the enzyme L-glutamic acid decarboxylase) and is an important protein nutrient. Since it is an amino acid, biocompatibility and zwitterionic nature can be expected for the amino acid appended polyfluorene.
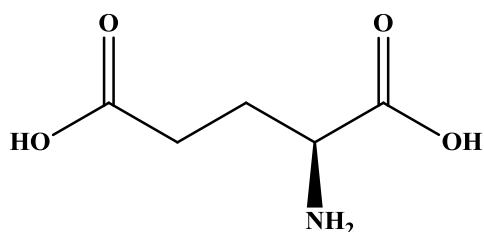
Figure 1.18 The chemical structure of L-glutamic acid.

By appending amino acid to polyfluorene, it is possible to meet all the concerned aspects of biocompatibility, amphiphilic structure and water solubility due to zwitterionic amino acid pendants. α-Amino acid moiety can serve as coordinating or chelating site to metal ions. It is well known that all the amino acids are natural chiral substituent's participating in the building blocks of proteins. Homochirality can be conferred to the conjugated backbone by appending an amino acid. The appendage of amino acid can enable the self-assembly of three dimensional morphological structures.

B. Biosensing Applications Explored in the Thesis

a. Sensing of Biomolecule:

Detection of biomolecules is an essential prerequisite to understand the functioning of biological process and to diagnose the diseased state of a body. Dioxy ribo nucleic acid (DNA), proteins, heparin, bilirubin and Glucose are some of the important biomolecules receiving research interest in biosensing applications. In this context, sensing a biomolecule in biofluids such as urine, saliva, and blood serum is highly challenging due to the complexity of the system.[68] The biofluids constitutes similar structured, charged interferences that complicate or challenge the sensitivity of the probe. Therefore, the design of the probe should meet high levels of selective

interaction with the analyte and sensitivity in nanomolar regime so as to identify early stage of a disease. The probe is expected to be water soluble so as to be miscible in the body fluids and also with robust structure and photophysical activities with respect to pH changes relevant to body fluids.

b. Sensing of Labile Metal ion Pools in Living Cells:

Bio-available metal ions play important roles such as gas transportation, ion carriers, energy generation and structural and functional unit in metalloproteins. The most typical example is hemoglobin in which the metal center performs the transport of oxygen. The changes in the levels of metal ions will affect homeostatis of the cellular environment leading to cell damage.[69] To monitor their levels, fluorescent imaging of the metal ion pools inside living cells is the most necessary requisite. The polymer probes which are designed for this intracellular application should be cell viable even at maximum uptake levels and also should have the potential to identify the changes in the metal ion in rapid time.

c. Chiral Sensing:

Chirality takes indispensible part in the molecular design of most of the naturally occurring biomolecules such as proteins, DNA, amino acids and sugars.[70] Most of the biologically active drugs exhibits chiral selective activity. For example only S enantiomer of Camptothecin shows anticancer activity whereas activity for R enantiomer is almost negligible. Enantiopurity of such chiral molecules is in great demand. Chiral sensing and enantioselective separation of racemic mixtures via simple and viable method is highly challenging. The foremost requirements desired in a probe are the homochirality and chiral selective interacting nature.

1.7 Characterization Methods adopted in the thesis

Polyfluorenes are characterized by relevant techniques such as NMR and GPC. The NMR shows broadness of peaks in the monomer repeat unit region indicative of polymer formation and gel permeation chromatography (GPC) helps to determine the molecular weight of the polymer such as Mn, Mw and polydispersity index. Some of the techniques used in the thesis for demonstrating the sensing studies are described below.

i) Fluorescence Sensing:

Fluorescence sensing reveals the photophysical changes of the probe polyfluorenes and the targeted analyte. This experiment provides valuable information of sensing activity of the probe. The interaction between the probe and the analyte changes the fluorescence intensity of the probe. The change in the fluorescence intensity is directly proportional to the concentration of the analyte. FRET based sensors provide information in determining the distance between the probe and the targeted analyte with change in the fluorescence color of the solution for easy identification.

ii) Fluorescence Lifetime:

Time correlated single photon counting (TCSPC) or florescence lifetime technique helps in identifying the transduction mechanism for the fluorescence sensing process. Decrease in the lifetime of the probe upon addition of analyte indicates the fluorescence quenching process. FRET based responses can be easily identified from the lifetime studies by observing the decrease in the lifetime of the donor and the increase in the lifetime of the acceptor.

iii) Isothermal Titration Calorimetry (ITC):

ITC provide information regarding the nature of interaction between the analyte and the polymer probe depending upon the heat changes. ITC experiment directly provides parameters such as change in enthalpy (ΔH), change in entropy (ΔS) stoichiometry (N), binding constant (K), and the Gibbs free energy (ΔG). The addition of analyte to the polymer produces or absorbs the heat depending upon the nature of interaction. The type of heat change (exothermic or endothermic) of the overall system can be distinguished and fitted to obtain the thermodynamic parameters.

iv) Circular Dichroism (CD):

CD spectroscopy is an excellent tool to determine the secondary structure and folding properties of the proteins and polymers. CD provides information regarding the helicity of the polymers, sheet type of self-assembled three dimensional structures etc. Chiral pendants groups attached to the polyfluorene backbone transfer their

chirality to the backbone resulting in the helical assembly of the polyfluorenes that can be analyzed only through CD spectroscopy.

1.8 Objective of the Thesis

The discussion on the literature reports and the versatile applications of sensors enumerate the applicability of sensors in day-to-day life. The advantages of conjugated polymers over small molecule counterpart emphasize the importance of conjugated polymer based sensors for highly sensitive, rapid and accurate detection of biomolecules. The outline on the properties of polyfluorene and aspects of appendages for achieving desired features has brought insight into the designing of polyfluorene based biosensors. In this thesis, we have attempted designing new polyfluorenes that are targeted for sensing biomolecule, intracellular labile metal ion and chiral molecules. The objectives of the thesis along with the respective motivation of the work are described as follows.

Detection of bilirubin levels could serve as potential route for diagnosing jaundice and liver disorders. There is need of a sensor for immediate and accurate sensing in the presence of structurally similar biological interferences. A polymer probe for detecting bilirubin is unprecedented so far.

The specific objectives presented in this thesis are:

➢ Design of new polyfluorenes for selective visual sensing of bilirubin.

➢ Understanding the mechanism of sensing of bilirubin and the relationship of self-assembly (or morphology) with the sensing efficiency.

➢ Design of new water-soluble polyfluorenes for selective sensing of bilirubin in complex human blood serum to realize real world sensing applications.

➢ Sensing and imaging of intracellular labile iron (II) in living cells using new polymer probe with high selectivity, cell viability and sensitivity. To synthesize new biocompatible polyfluorene with high cell viability.

➢ Demonstrating selective sensing and intracellular imaging of Fe(II).

➢ Enantioselective sensing and separation of particular enantiomer from a racemic mixture in aqueous medium using polymer probe. This is highly challenging and very essential for obtaining enantiopure drugs, nutrients, chemical intermediates.

➢ Developing new homochiral polyfluorene probe.

➢ Executing chiral sensing and enantioselective separation of racemic mixtures in a wide range of chemical classes.

1.9 Outline of the Thesis

This section will give a brief outline on the content of each chapters of the thesis. The **first chapter** describes the concepts, types and mechanistic aspects of fluorimetric sensors and provides a review of the advancement of π-conjugated polymer based fluorimetric sensors in biosensing applications using suitable examples from literature. The chapter enumerates the potential of polyfluorene and structure-property relationship of different types of appendages targeted toward selective biosensing application. The chapter presents the overview of the appendages, biosensing applications, synthesis and characterization methods used in the thesis. It also highlights the objectives of thesis with motivation for sensing of biologically significant biomolecules: Bilirubin, Labile Fe^{2+} pools in living cells and enantioselective sensing of $_L$-enantiomers.

The **second chapter** demonstrates the design of new polyfluorenes for sensing of bilirubin. Two new polyfluorenes appended with bulky 3-pentadecylphenoxy group were synthesized. Investigation on the solid state and solution state morphology of the polymers using relevant techniques like TEM, AFM, DLS and SLS in THF are discussed. FRET based sensing of free bilirubin (BR) in THF was carried out using the new polyfluorenes as probe. The mechanism of sensing was probed using fluorimetric lifetime experiments. Selectivity and sensitivity of the probe toward bilirubin was also verified.

The **third chapter** deals with the real world application of sensing of bilirubin in complex biofluids namely human blood serum. Two new polyfluorenes with D-glucuronic acid appendage that is a non-receptor for any serum protein was utilized for this purpose. The structural, photophysical properties and morphological features of the new polymers studied using relevant techniques are described. Sensing studies of free bilirubin in the clinically relevant range of < 25 μmol/L to > 50 μmol/L in water and in human blood serum containing crucial interferences was successfully

demonstrated. The stability of the polymer and sensing studies with respect to pH changes was also explored. The mechanism of sensing was evidenced from photophysical changes of the probe and analyte.

The **fourth chapter** describes intracellular metal ion detection and sensing in living cells using amino acid appended polyfluorene. Glutamic acid appended polyfluorene was designed, synthesized and characterized using relevant techniques. Sensing of the polymer for Fe(II) ion in water was studied and selectivity over other competitive bio-available metal ions, transition metal ions was confirmed. The cell viability of the new water-soluble polyfluorene as fluorescent probe was analyzed in living HeLa cells and intracellular imaging of Fe(II) was also successfully accomplished.

The **fifth chapter** presents the design of homochiral polyfluorene probe with biomimetic conformation and morphology. The probe was exploited for enantioselective separation and sensing of particular type of enantiomer from respective racemic mixture in water. Using solid state and solution state CD technique, chiral sensing was explained. Applicability of the probe for a wide variety of chemical classes highlighted the efficacy of the probe design.

The **sixth chapter** summarizes the contents of each chapter and compiles the conclusions derived from each chapter.

1.10 References

1. Teeling, E. C.; Scally, M.; Kao, D. J.; Romagnoli, M. L.; Springer, M. S.; Stanhope M. J. *Nature* **2000**, *403*, 188-192.

2. Ahmad, H.; Sehgal, S.; Mishra, A.; Gupta, R. *Pharmacogn Rev.* **2012**, *6*, 115–124.

3. Fraden, J. *Handbook of modern sensors*, Springer, 4th edition, **2010**.

4. Lakowicz, J. *Principles of fluorescence spectroscopy*, Springer, 3rd edition, **2006**.

5. Basabe.-Desmonts, L.; Reinhoudt, D. N.; Crego.-Calama, M. *Chem. Soc. Rev.* **2007**, *36*, 993–1017.

6. Demchenko, A. P. *Introduction to fluorescence sensing*, Springer, **2009**.

7. Lee, M. H.; Kim, J. S.; Sessler, J. L. *Chem. Soc. Rev.* **2015**, *44*, 4185-4191.

8. Yang, Y.; Gou, X.; Blecha, J.; Cao, H. *Tetrahedron Lett.* **2010**, *51*, 3422–3425.

9. Sivaraman, G.; Chellappa, D. *J. Mater.Chem. B* **2013**, *1*, 5768–5772.

10. Li, J.; Wu, Y.; Song, F.; Wei, G.; Cheng, Y.; Zhu, C. *J. Mater. Chem.* **2012**, *22*, 478 - 482.

11. Sun, K.; Liu, X.; Wang, Y.; Wu, Z. *RSC Adv.* **2013**, *3*, 14543-14548.

12. Huang, Y.; Liu, X.; Shi, M.; Zhao, S.; Hu, K.; Chen, Z. F.; Liang, H. *Chem. Asian. J*. **2014**, *10*, 2755-60.

13. Baldini, F.; Carloni, A.; Giannetti, A.; Porro, G.; Trono, C. *Sensors Actuat. B-Chem* **2009**, *139*, 64–68.

14. Wang, X.; Guo, Y.; Dong, L.; Chen, H.; Sun, R. C. *Chem. Commun.* **2012**, *48***, 5569-5571.

15. Pugh, V. J.; Hu, Q.-S.; Pu, L. *Angew. Chem. Int. Ed.* **2000**, *39*, 3638–3641.

16. Kubo, H.; Yoshioka, N.; Takeuchi, T. *Org. Lett*. **2005**, *7*, 359–362.

17. Wang, B.; Wasielewski, M. R. *J. Am. Chem. Soc*. **1997**, *119*, 12–21.

18. Zhang, Y.; Murphy, C. B.; Jones, W. E. *Macromolecules* **2002**, *35*, 630–636.

19. Chen, Z.; Xue, C. H.; Shi, W.; Luo, F. T.; Green, S.; Chen, J.; Liu, H. Y. *Anal. Chem.* **2004**, *76*, 6513–6518.

20. Lim, M. H.; Lippard, S. J. *Acc. Chem. Res.* **2007**, *40*, 41–51.

21. Wang, L.; Yao, T.; Shi, S.; Cao, Y.; Sun, W. *Sci. Rep.* **2010**, *4*, 5320.

22. Michalet, X.; Pinaud, F. F.; Bentolila, L. A.; Tsay, J. M.; Doose, S.; Li, J. J.; Sundaresan, G.; Wu, A. M.; Gambhir, S. S.; Weiss. S. *Science* **2005**, *307*, 538–544.

23. Medintz, I. L.; Konnert, J. H.; Clapp, A. R.; Stanish, I.; Twigg, M. E.; Mattoussi, H.; Mauro, J. M.; Deschamps, J. R. *Proc. Nat. Acad. Sci. USA*. **2004**, *101,* 9612-9617.

24. Ferey, G. *Chem. Soc. Rev.* **2008**, *37*, 191-214.

25. Kreno, L. E.; Leong, K.; Farha, O. K.; Allendorf, M.; Van Duyne, R. P.; Hupp, J. T. *Chem. Rev.* **2012**, *112,* 1105–1125.

26. Qiu, Y.; Deng, H.; Mou, J.; Yang, S.; Zeller, M.; Batten, S. R.; Wu, H.; Li, J. *Chem. Commun.* **2009**, 5415-5417.

27. Burroughes, J. H.; Bradley, D. D. C.; Brown, A. R.; Marks, R. N.; Mackay, K.; Friend, R. H.; Burns, P. L.; Holmes, A. B. *Nature* **1990**, *347*, 539–541.

28. Facchetti, A. *Chem. Mater.* **2011**, *23,* 733–758.

29. Cheng, Y. J.; Yang, S. H.; Hsu, C. S. *Chem. Rev*. **2009**, *109*, 5868–5923.

30. Marchioni, F.; Yang, J.; Walker, W.; Wudl, F. *J. Phys. Chem. B*, **2006**, *110,* 22202–22206.

31. Tang, H. W.; Duan, X. R.; Feng, X. L.; Liu, L. B.; Wang, S.; Li, Y. L.; Zhu, D. B. *Chem. Commun*. **2009**, *6*, 641-643

32. Tang, Y.; He, F.; Wang, S.; Li, Y.; Zhu, D.; Bazan, G. C. *Adv. Mater*. **2006**, *18*, 2105-2110.

33. Qin, C.; Cheng, Y.; Wang, L.; Jing, X.; Wang, F. *Macromolecules* **2008**, *41*, 7798-7804.

34. Feng, X.; Liu, L.; Wang, S.; Zhu, D. *Chem. Soc. Rev.* **2010**, *39*, 2411–2419.

35. Rose, A.; Tovar, J. D.; Yamaguchi, S.; Nesterov, E. E.; Zhu, Z.; Swager, T. M. *Phil. Trans. R. Soc. A*. **2007**, *365*, 1589–1606.

36. Zhu, C.; Liu, L.; Yang, Q.; Lv, F.; Wang, S. *Chem. Rev*. **2012**, *112*, 4687−4735.

37. Chen, L.; McBranch, D. W.; Wang, H. L.; Helgeson, R.; Wudl, F.; Whitten, D. G. *Proc. Natl. Acad. Sci. USA*. **1999**, *96*, 12287–12292.

38. Zhou, Q.; Swager, T. M. *J. Am. Chem. Soc*. **1995**, *117*, 12593-12602.

39. Zhou, Q.; Swager, T. M. *J. Am. Chem. Soc*. **1995**, *117*, 7017-7018.

40. Swager, T. M. *Acc. Chem. Res.***1998**, *31*, 201-207.

41. Rochat, S.; Swager, T. M. *ACS Appl. Mater. Interfaces*. **2013**, *5,* 4488–4502.

42. Attar, H. A. A.; Monkman, A. P. *J. Phys. Chem. B* **2007**, *111*, 12418-12426.

43. Fan, C. H.; Plaxco, K. W.; Heeger, A. J. *J. Am. Chem. Soc*. **2002**, *124*, 5642-5643.

44. Kim, I. B.; Dunkhorst, A.; Bunz, U. H. F. *Langmuir* **2005**, *21*, 7985-7989.

45. Thomas III, S. W.; Swager, T. M. *Adv. Mater*. **2006,** *18,* 1047–1050.

46. Esser, B.; Swager, T. M. *Angew. Chem. Int. Ed. Engl*. **2010,** *49*, 8872-8875.

47. Gaylord, B. S.; Heeger, A. J.; Bazan, G. C. *Proc. Natl. Acad. Sci. USA* **2002**, 99, 10954-10957.

48. Pu, K. Y.; Liu, B. *Macromolecules* **2008**, *41*, 6636-6640.

49. Neher, D. *Macromol. Rap. Commun.* **2001**, *22*, 1365–1385**.**

50. Ullrich, S.; Dieter, N. *Polyfluorene*, Springer series, **2008**.

51. Bright, D. W.; Dias, F. B.; Galbrecht, F.; Scherf, U.; Monkman, A. P. *Adv. Funct. Mater*. **2009**, *19*, 67–73.

52. Gong, X.; Iyer, P. K.; Moses, D.; Bazan, G. C.; Heeger, A. J.; Xiao, S. S. *Adv. Funct. Mater*. **2003**, *13,* 325–330.

53. Grell, M.; Bradley, D. D. C.; Inbasekarkan, M.; Woo, E. P. *Adv. Mater.* **1997**, *9*, 798-802.

54. Duarte, A.; Pu, K. Y.; Liu, B.; Bazan, G. C. *Chem. Mater.* **2011**, *23*, 501–515.

55. Liu, B.; Yu, W.; Lai, Y.; Huang, W. *Macromolecules* **2002**, *35*, 4975 – 4982

56. Hong, J. W.; Hemme, W. L.; Keller, G. E.; Rinke, M. T.; Bazan, G. C. *Adv. Mater*. **2006**, *18*, 878–882.

57. Jiang, H.; Taranekar, P.; Reynolds, J. R.; Schanze, K. S. *Angew. Chem. Int. Ed*. **2009**, *48*, 4300 – 4316.

58. Pu, K. Y.; Shi, J.; Wang, L.; Cai, L.; Wang, G.; Liu, B. *Macromolecules* **2010**, *43*, 9690–9697.

59. Pu, K. Y.; Li, K.; Liu, B. *Adv. Funct. Mater*. **2010**, *20*, 2770–2777.

60. Oda, M.; Nothofer, H. G.; Lieser, G.; Scherf, U.; Meskers, S. C. J.; Neher, D. *Adv. Mater*. **2000**, *12*, 362-365.

61. Shu, C. F.; Dodda, R.; Wu, F. I. *Macromolecules* **2003**, *36*, 6698-6703.

62. Oh, H. S.; Liu, S.; Jee, H. S.; Baev, A.; Swihart, M. T.; Prasad, P. N. *J. Am. Chem. Soc*. **2010**, *132*, 17346–17348.

63. Pramod, P. S.; Takamura, K.; Chaphekar, S.; Balasubramanian, N.; Jayakannan, M. *Biomacromolecules* **2012**, *13,* 3627–3640.

64. Rekha, N.; Asha, S. K. *J. Polym. Sci. Part A: Polym. Chem*. **2009**, *47*, 2996-3009.

65. Kaushlendra, K.; Asha, S. K. *Langmuir* **2012**, *28*, 12731-12743.

66. Bock, K.; Köhle, C. *Methods enzymol.* **2005**, *400*, 57–75.

---

67. Zheng, Z.; Fang, J. L.; Lazarus, P. *Drug Metab. Disp*. **2002**, *30*, 397–403.

68. Senthilkumar, T.; Asha, S. K. *Macromolecules* **2015**, *48*, 3449-3461.

69. Maton, A; Hopkins, J; Johnson, S; Warner, M. Q.; McLaughlin, D. L. C. W.; Warner, M. Q.; Wright, J. D. *Human Biology and Health*, Englewood Cliffs, New Jersey, USA: Prentice Hall, **1994**.

70. Avalos, M.; Babiano, R.; Cintas, P.; Jimenez, J. L.; Palacios, J. C. *Chem. Commun*. **2000**, 887-892.

CHAPTER - 2

Tailor- Made Polyfluorenes for Visual FRET Sensing of Bilirubin: A Model Sensor

Free bilirubin is an important bile pigment which if found in higher than normal level in blood/body fluids indicates the diseased state of liver. Thus, detection of free bilirubin could serve as a potential route for diagnosing Jaundice and other various liver disorders. In this chapter, we have developed a new fluorimetric model sensor based on polyfluorenes appended with pentadecyl appendages for highly selective, nanomolar sensitive and immediate visual detection of free bilirubin.

2.1 Introduction

Bilirubin is the breakdown product of hemoglobin and contains a tetrapyrrole moiety with six intramolecular hydrogen bonds existing in ridge tile conformation.[1] Under normal physiological conditions bilirubin is mostly present as the conjugated form which is bound with human serum albumin (direct/bound bilirubin), which makes it water soluble. The unconjugated or free fraction which is potentially toxic is usually present in small amounts and is excreted after enzymatic esterification with glucuronic acid.[2] Abnormal levels of bilirubin – either conjugated or unconjugated, detected in serum samples is an indicator for disturbed bilirubin metabolism. For instance, increased levels of conjugated bilirubin in serum could signal disturbance of bile drainage as in obstructive jaundice or increased levels of unconjugated bilirubin could be due to abnormally high breakdown of hemoglobin (haemolysis).[2,3] Therefore, monitoring the bilirubin concentration in body fluids is a vital step in diagnosing liver disorders and jaundice. Clinically, the levels of bilirubin (conjugated and unconjugated bilirubin) is determined by the color change from yellow to red produced by the diazotization reaction of bilirubin and sulphanilic acid using spectrophotometer (total van den Bergh reaction, 1914).[2,4] The major disadvantage of the assay is that it overestimates conjugated bilirubin and is time-consuming (30 minutes to develop the maximum color).[5] There are only very few reports on fluorimetric bilirubin sensing; till date there are no reports on bilirubin sensing using conjugated polymer as the fluorescent sensor.

The combination of amplified response and sensitivity in conjugated polymer based sensors makes them superior compared to their small molecule counterparts.[6] By taking advantage of overlapping photophysical properties of bilirubin and polyfluorenes we have developed a model polyfluorene sensor to detect unconjugated bilirubin via fluorescence resonance energy transfer (FRET) process for the first time. In the scenario of FRET based enhanced acceptor emission, self-assembly of the donor polymer plays a major role as desirable morphologies like vesicles, porous assemblies etc enable close interaction of the donor and acceptor units.[7] Vesicular morphology is very promising as drug delivery vehicles as they help encapsulate hydrophilic/hydrophobic drug molecules in their interior cavity depending on their

structural constitution.[8] In general, researchers have sought the help of amphiphilic (hydrophilic/ hydrophobic combinations) structural modifications in polymers to explore self-assembled architectures like vesicles.[9] There have been reports where oligo/polyfluorenes modified with hydrophilic units were used for sensing application based on the characteristic optical properties of the self-assembled nanoparticles.[10] Reports on the application of conjugated homopolymers or conjugated polymers without the required amphiphilic structure for self-assembly for florescence based sensing are very rare.

In our molecular design we incorporated bulky pentadecyl phenol (PDP) units, (which are well-known to have the ability to self-organize by way of alkyl chain interdigitation as well as aromatic π stacking interactions),[11] at the 9, 9'position of fluorene with the anticipation that the structurally modified polyfluorene would be able to self-assemble into desired morphologies resulting in close interaction with bilirubin. The self-assembled structures of the PDP substituted polyfluorenes were studied in solution state using static and dynamic light scattering (SLS and DLS), and in solid state using microscopic techniques like TEM and AFM. Steady state as well as time-resolved fluorescence analysis was conducted to study the donor-acceptor interaction parameters. Although simple dialkyl polyfluorenes like 9, 9'-dioctylpolyfluorenes also exhibited complimentary photophysical characteristics to bilirubin, its sensing efficiency was very low. The selectivity and sensitivity of the bilirubin sensing by the new polyfluorene was verified with structurally analogous molecules like porphyrin which had very similar absorption spectra with that of bilirubin. The tailor-made polyfluorene structure presented here illustrates the importance of self-assembling building blocks like the PDP unit which helps induce self organization even in the homopolymer, without having to design amphiphilic block copolymers or polymers incorporated with hydrophilic units like the oligooxyethylene to induce phase separation.

2.2 Experimental Section

Materials: 2, 7-Dibromo-9-[H]-fluorene, 3-pentadecyl phenol, bilirubin, biliverdin, rhodamine, 5, 10, 15, 20-tetrapyridyl-20H, 25H-porphine (TPY), Pd(PPh$_3$)$_4$, 1, 4-

benzene diboronic acid, sodium hydride, 1, 6-dibromo hexane, 2-isopropoxy-4, 4, 5, 5-tetramethy-[1, 3, 2]-dioxaborolane, t-BuLi and 1-bromo octane were purchased from Aldrich company Ltd and were used as such. Potassium hydroxide, potassium carbonate and ethanol were purchased from Merck chemicals Ltd. Tetrahydrofuran (THF), acetone and methanol were purchased locally and were purified using standard procedures.

Measurements: ^1H & $^{13}CNMR$ were recorded on a Bruker-AVENS 200 MHz spectrometer. Chemical shifts are reported in ppm at 25°C using CDCl$_3$ as solvent containing small amount of tetramethylsilane (TMS) as internal standard. The purity of the compounds was determined by elemental analysis and MALDI-TOF. Elemental analysis was done by Thermofinnigan flash EA 1112 series CHNS analyser. The MALDI-TOF analysis was done on Voyager-De-STR MALDI-TOF (Applied Biosystems, Framingham, MA, USA) equipped with 337-nm pulsed Nitrogen laser used for desorption and ionization. 1 µM solution of sample was premixed with DHB (2, 5 dihydroxy benzoic acid) matrix in CHCl$_3$ and mixed well before spotting on 96-well stainless steel MALDI plate by dried droplet method for MALDI analysis. For small molecules SEC was performed using polystyrene standards for the calibration in CHCl$_3$ as eluent. The flow rate of CHCl$_3$ was maintained as 1 µL/min throughout the experiments and the sample solutions at concentrations 3-4 mg/ml were filtered and injected for recording the chromatograms at 30°C. The molecular weights of the polymers were determined by Size exclusion Chromatography (SEC), which was performed using a Viscotek VE 1122 pump, Viscotek VE 3580 RI detector and Viscotek VE 3210 UV/vis detector in THF using polystyrene as standards.

Photophysical Studies:

Absorption spectra were recorded using Perkin-Elmer Lambda 35 UV-spectrophotometer. Steady-state fluorescence studies and time-resolved fluorescence lifetime measurements were performed using Horiba Jobin Yvon Fluorolog 3 spectrophotometer having a 450 W xenon lamp for steady-state fluorescence. Fluorescence lifetime decays were collected by a time-correlated single photon counting (TCSPC) setup from IBH Horiba Jobin Yvon (U.S.) using a 375 nm diode

laser (IBH, U.K., NanoLED-375 L, with a λ max = 375 nm) having a fwhm of 89 ps as a sample excitation source. The emission and excitation slit width was maintained at 1 nm throughout the experiments, and the data was obtained in "S1c/R1" mode (to account for the variations in lamp intensity).

Transmission Electron Microscopy:

For TEM measurements, the samples in THF were deposited directly on a carbon coated copper grid. No staining treatment was performed for the measurement. A JEOL JEM-3010 electron microscope operating at 300 kV (Cs = 0.6 mm, resolution 1.7 Å) was used for HR-TEM sample observation. A Gatan digital camera (model 794, Gatan 1024 × 1024 pixels, pixel size 24 × 24 μm) at 15000 − 80000× magnifications was used to record micrographs.

Atomic Force Microscopy:

AFM images were taken by using a multimode scanning probe microscope equipped with a Nanoscope IV controller from Veeco Instruments, Inc. in the tapping mode using a SiN probe, with a maximum scan size of 10 mm × 10 mm and with a vertical range of 2.5 mm. For the AFM studies, samples were prepared by drop-casting THF solution of the polymers onto the silicon wafer and allowed to dry at ambient temperature before being subjected to AFM analysis.

Dynamic and Static Light Scattering (DLS and SLS):

DLS measurements were carried out on Zetasizer ZS-90 apparatus, utilizing 633 nm red laser (at 90 ° angle) from Malvern instruments. The reproducibility of the data was checked at least three times using independent polymer solutions. The static light scattering experiment (SLS) was carried out using 3D-DLS spectrometer, from LS instruments, Switzerland. The instrument consisted of a He Ne laser having wavelength of 632.8 nm attached to computer using Lab view interface utilizing toluene as reference. The measurement was performed in autocorrelation mode from 20 ° to 134 ° in steps of 2 °.

Synthesis of 1-(6-bromohexyloxy)-3-pentadecylbenzene (1):

3-Pentadecylphenol (10 g, 3.29 mmol), KOH (9.21 g, 16.4 mmol) were dissolved in ethanol (50 ml) and stirred for 30 minutes to obtain a reddish black precipitate. 1, 6-

dibromohexane (25 ml, 16.4 mmol) in dry acetone (25 ml) was added very slowly to this reaction mixture and heated to reflux for 24 h. After cooling to room temperature, the solvent and excess 1, 6-dibromohexane was distilled off and the product extracted with dichloromethane. The organic layer was washed with water, brine and dried with Na_2SO_4. The solvent was removed under vacuum. The crude product was purified by silica gel column chromatography using pet ether/ethyl acetate (v/v, 97/3) as eluent to yield the product. Yield (18 g, 78 %). ^{1}H NMR (CDCl$_3$, 200 MHz): δ = 7.17 (t, 1H), 6.72 (t, 3H), 3.94 (t, 2H), 3.42 (t, 2H), 2.56 (t, 2H), 1.9-1.7 (m, 4H), 1.50 (m, 6H), 1.35-1.15 (m, 24H), 0.87 (t, 3H).

Synthesis of 2, 7-dibromo-9, 9-bis(6-(3-pentadecylphenoxy)hexyl)-9H-fluorene (2):

2, 7-Dibromofluorene (3 g, 9.26 mmol) and NaH (2.22 g, 92.6 mmol) were taken in a two necked round bottom flask and purged with Nitrogen. Dry THF (60 ml) was added to this to obtain a dark red precipitate. 1-((6-bromohexyl)oxy)-3-pentadecylbenzene (17.32 g, 37.04 mmol) was added very slowly to this reaction mixture and heated to reflux for 12 h. The reaction mixture was poured into water and the product was extracted with ethyl acetate. The organic layer was washed with water, brine and dried over Na_2SO_4. The solvent was removed under vacuum. The crude product was purified by silica gel column chromatography using pet ether/ethyl acetate (v/v, 95/5). Yield (6.4 g, 64 %). ^{1}H NMR (CDCl$_3$, 200 MHz): δ = 7.55-7.4 (m, 6H), 7.15 (t, 3H), 6.8-6.6 (m, 6H), 3.83 (t, 3H), 2.55 (t, 3H), 1.98-1.90 (m, 4H), 0.89 (t, 6H), 0.62 (m, 4H). MALDI (calculated (M+Na) = 1120.21; observed (M+Na) = 1119.67). Elemental analysis, Calculated = C (59.71 %), H (7.23 %); Observed = C (59.53%), H (7.31).

Synthesis of 2, 2'-(9, 9-bis(6-(3-pentadecylphenoxy)hexyl)-9H-fluorene-2, 7-diyl)bis(4, 4, 5, 5-tetramethyl-1, 3, 2-dioxaborolane) (3):

2, 7-Dibromo-9, 9-bis(6-(3-pentadecylphenoxy)hexyl)-9H-fluorene (1.35 g, 1.24 mmol) was dissolved in dry THF (20 ml) and cooled to -78 [0]C. n-BuLi (1.5 ml, 2M in hexane) was added drop wise over a period of 45 minutes to the above THF solution and the reaction mixture was stirred for 1 h. At the same temperature 2-isopropoxy-4,

4, 5, 5-tetramethyl-1, 3, 2-dioxaborolane (0.7 ml, 4.93 mmol) was added over a period of 30 minutes and stirred for further 2 h. The reaction mixture was then slowly warmed to room temperature and stirred for 12 h. For workup, the reaction was quenched with water (10 ml), and the reaction mixture was poured into water and extracted with dichloromethane. The organic layer was washed with water and brine and dried over Na_2SO_4. The solvent was removed under reduced pressure. The crude product was purified by silica gel column chromatography using pet ether/ethyl acetate (v/v, 90/10). Yield (0.75 g, 51 %). ^{1}H NMR (CDCl$_3$, 200 MHz) δ = 7.7-7.2 (m, 6H), 7.15 (t, 2H), 6.67 (m, 6H), 3.81 (t, 4H), 2.55 (t, 4H), 1.95 (m, 4H), 1.58 (m, 10H), 1.38 (s, 24H), 1.25 (m, 50H), 0.89 (t, 6H), 0.64 (m, 4H). MALDI (calculated (M+Na) = 1214.41; observed (M+Na) = 1214.22).

Synthesis of 2, 7-dibromo-9, 9-dioctylfluorene (4):

2, 7-Dibromofluorene (3 g, 9.26 mmol) and NaH (2.22 g, 92.6 mmol) were taken in a two necked round bottom flask and purged with Nitrogen. Dry THF (60 ml) was added to this to obtain a dark red precipitate. 1-bromo octane (5.6 ml, 32.41 mmol) was added very slowly to this reaction mixture and heated to reflux for 12 h. The reaction mixture was poured into water and the product was extracted with ethyl acetate. The organic layer was washed with water, brine and dried over Na_2SO_4. The solvent was removed under vacuum. The crude product was purified by silica gel column chromatography using pet ether/ethyl acetate (v/v, 98/2). Yield (80 %). ^{1}H NMR (CDCl$_3$, 200 MHz δ 7.52 (d, 2 H), 7.43- 7.47 (4 H, m), 1.88- 1.93 (m, 4H), 1.04- 1.28 (m, 20H), 0.83 (t, 6H), 0.54-0.64 (m, 4H). MALDI (calculated (M+Na) = 548.146; observed (M+Na) = 548.147).

Synthesis of 2, 2'-(9, 9-dioctyl-9H-fluorene-2, 7-diyl)bis(4, 4, 5, 5-tetramethyl-1, 3, 2-dioxaborolane) (5):

2, 7-Dibromo-9, 9-dioctylfluorene (1.5 g, 2.7 mmol) was dissolved in dry THF (40 ml) and cooled to -78 ^{0}C. n-BuLi (2.2 ml, 2M in hexane) was added drop wise over a period of 45 minutes to the above THF solution and the reaction mixture was stirred for 1 h. At the same temperature 2-isopropoxy-4, 4, 5, 5-tetramethyl-1, 3, 2-dioxaborolane (2 ml, 9.8 mmol) was added over a period of 30 minutes and stirred for

further 2 h. The reaction mixture was then slowly warmed to room temperature and stirred for 12 h. For workup, the reaction was quenched with water (15 ml), and the reaction mixture was poured into water and extracted with dichloromethane. The organic layer was washed with water and brine and dried over Na_2SO_4. The solvent was removed under reduced pressure. The crude product was purified by silica gel column chromatography using pet ether/ethyl acetate (v/v, 93/7). Yield (0.75 g, 51 %). ^{1}H NMR ($CDCl_3$, 200 MHz) δ = 7.81 (dd, 2H), 7.75 (s, 2H), 7.72 (d, 2H), 1.95-2.05 (m, 4H), 1.39 (s, 24H), 0.96- 1.23 (m, 20H), 0.81 (t, 6H), 0.50-0.60 (m, 4H). MALDI (calculated (M+Na) = 642.562; observed (M+Na) = 642.566).

Polymerization:

2, 7-Dibromo-9, 9-bis(6-(3-pentadecylphenoxy)hexyl)-9H-fluorene (300 mg, 0.27 mmol), 2, 2'-(9, 9-bis(6-(3-pentadecylphenoxy)hexyl)-9H-fluorene-2, 7-diyl)bis(4, 4, 5, 5-tetramethyl-1, 3, 2-dioxaborolane) (diboronic ester) (325 mg, 0.27 mmol) and tetrakis(triphenylphosphine) palladium (20 mg, 0.04 mmol) were taken in a two necked round bottom flask under Nitrogen atmosphere. Dry THF (8 ml) was added to the mixture. K_2CO_3 dissolved in water (2 ml) was added to the reaction medium. The reaction mixture was heated to reflux for 36 h under Nitrogen atmosphere. The mixture was cooled down to room temperature and added drop-wise into a stirred solution of methanol (100 ml) in an open vessel. The precipitate was isolated and dissolved in dichloromethane and filtered to remove the catalyst. The collected dichloromethane solution was concentrated under reduced pressure and purified by repeated precipitation from methanol (100 ml). The precipitate was filtered, washed with methanol (50 ml) and dried under high vacuum.

Poly[2, 7-(9, 9-bis(6-(3-pentadecylphenoxy)hexyl)-9H-fluorene)] (PDP-PF):

^{1}H NMR ($CDCl_3$, 200 MHz): δ (ppm) 7.66 (4H, m), 7.48 (2H, m), 7.11 (2H, q), 6.65 (6H, m), 3.80 (4H, m), 2.51 (4H, m), 2.10 (4H, m), 1.58 (8H, m), 1.23 (60H, m), 0.87 (6H, m). (Yield: 75 %). ^{13}C NMR ($CDCl_3$, 200 MHz): δ (ppm) 158.63, 139.53, 129.14, 127.29, 121.66, 120.72, 114.82, 111.18, 107.61, 82.62, 67.69, 56.17, 35.91, 31.69, 29.24, 28.82, 22.16, 14.03.

Poly[(1, 4-phenylene)-2, 7-(9, 9-bis(6-(3-pentadecylphenoxy)hexyl)-9H-fluorene)] (PDPPF-co-Ph):

The copolymer PDPPF-co-Ph was prepared by following the same procedure but using 1, 4-bis(4, 4, 5, 5-tetramethyl-1, 3, 2-dioxaborolan-2-yl)benzene as the co monomer. (Yield: 78 %). ^{1}H NMR (CDCl$_3$, 200MHz): δ (ppm) 7.77 (4H, m), 7.64 (4H, m), 7.48 (2H, m), 7.12 (2H, q), 6.65 (6H, m), 3.79 (4H, m), 2.52 (4H, m), 2.0 (4H, m), 1.58 (8H, m), 1.23 (60H, m), 0.87 (6H, m). ^{13}C NMR (CDCl$_3$, 200 MHz): δ (ppm) 159.03, 144.50, 139.83, 129.03, 127.55, 121.36, 120.60, 114.73, 111.21, 107.79, 82.59, 67.62, 56.06, 36.01, 31.92, 29.68, 29.36, 22.69, 14.13.

Poly[2, 7-(9, 9-dioctylfluorene)] (POF):

POF was synthesized by the coupling 4 & 5 and followed the same polymerization procedure described earlier. (Yield: 80 %). ^{1}H NMR (CDCl$_3$, 200 MHz): δ (ppm) 7.85 (2H, d), 7.68 (4H, m), 2.15 (4H, m), 1.2 (24H, m), 0.8 (6H, t). ^{13}C NMR (CDCl$_3$, 200 MHz): δ (ppm) 150.69, 141.11, 126.97, 122.85, 119.63, 55.02, 40.38, 31.80, 29.23, 23.74, 22.61, 14.09.

Poly[(1, 4-phenylene)-2, 7-(9, 9-dioctylfluorene)] (POF-co-Ph):

The copolymer POF-co-Ph was prepared by following the same procedure but using 4, 4-bis(4, 4, 5, 5-tetramethyl-1, 3, 2-dioxaborolan-2-yl)benzene as the co monomer. (Yield: 75 %). ^{1}H NMR (CDCl$_3$, 200 MHz): δ (ppm) 7.85 (4H, d), 7.65-7.5 (2H, m), 2.1 (4H, m), 1.15 (24H, m), 0.85 (6H, t). ^{13}C NMR (CDCl$_3$, 200 MHz): δ (ppm) 151.79, 140.46, 140.14, 127.55, 125.95, 121.43, 120.09, 55.29, 31.89, 29.80, 29.32, 23.92, 22.67, 14.11.

2.3 Results and Discussion

2.3.1 Synthesis and characterization:

The synthesis of PDP-PF and PDPPF-co-Ph are shown in Scheme 2.1. The dibromo monomer 2, 7-dibromo-9, 9-bis(6-(3-pentadecylphenoxy)hexyl)-9H-fluorene (**2**) and the dioxaborolane monomer, 2, 2'-(9, 9-bis(6-(3-pentadecylphenoxy)hexyl)-9H-fluorene-2, 7-diyl)bis(4, 4, 5, 5-tetramethyl-[1, 3, 2]-dioxaborolane) (**3**), were synthesized in 50-64 % yield and the details of synthesis are given in the experimental section. The structure and purity of the monomers were confirmed by

^{1}H NMR, MALDI and elemental analysis. Scheme 2.2 shows the synthesis of 2, 7-dibromo-9, 9-dioctylfluorene (**4**), its boronic ester (**5**), and its homo and copolymer POF and POF-co-Ph respectively. The detailed synthetic procedure is described in the experimental section. The Suzuki polymerization of the monomers 2 and 3 in the presence of Pd(PPh$_3$)$_4$ catalyst afforded poly (2, 7-dimethyl-9, 9-bis (6-(3-pentadecylphenoxy) hexyl)-9H-fluorene) (PDP-PF) in 75% yield. The monomer 2 was coupled with 1, 4-bis(4, 4, 5, 5-tetramethyl-1, 3, 2-dioxaborolan-2-yl)benzene to obtain the copolymer (PDPPF-co-Ph).
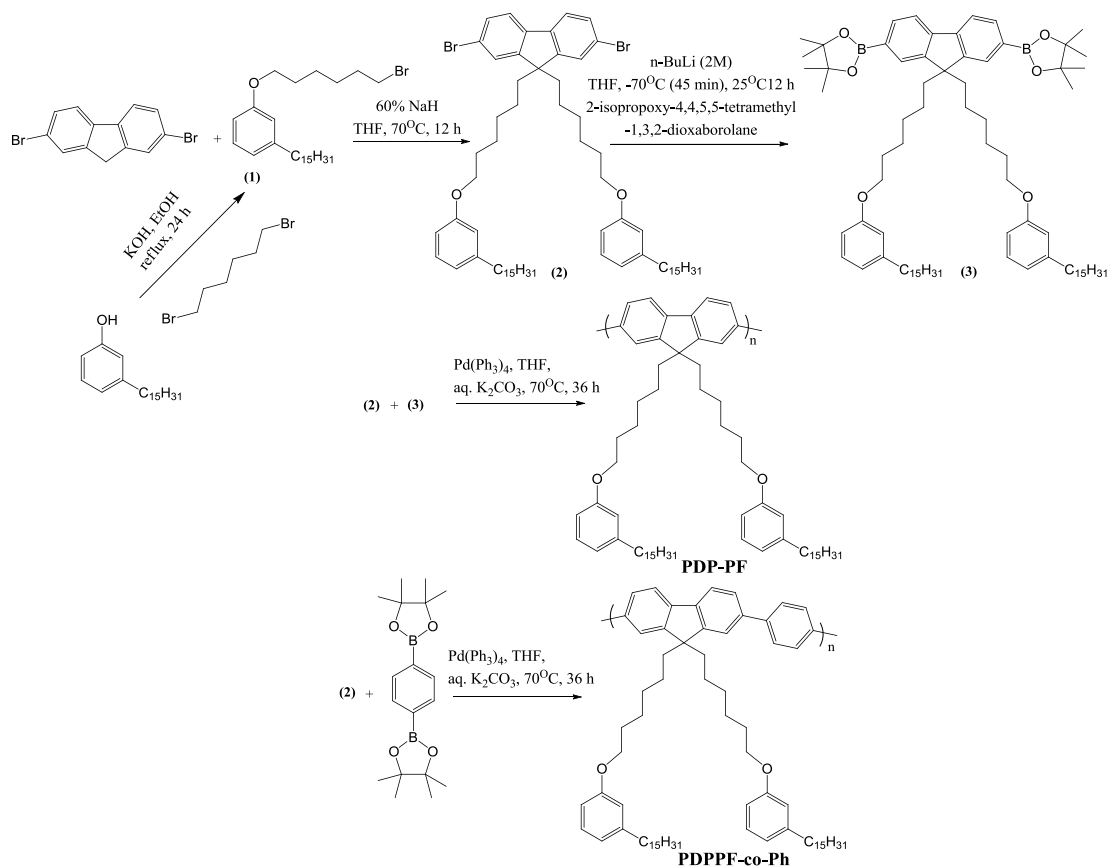
Scheme 2.1 Synthesis of monomers and Polymers (PDP-PF, PDPPF-co-Ph)

Poly[2, 7- diyl- (9, 9- dioctyl fluorene)] (POF) and its copolymer with phenyl group, Poly[(1, 4-phenylene)-2, 7-diyl-(9, 9-dioctylfluorene)] (POF-co-Ph) were synthesized as benchmark polymers to compare the photophysical and sensing properties. Scheme 2.3 shows the structure of all the polymers that were used in the present study along with the gross structure of Bilirubin.
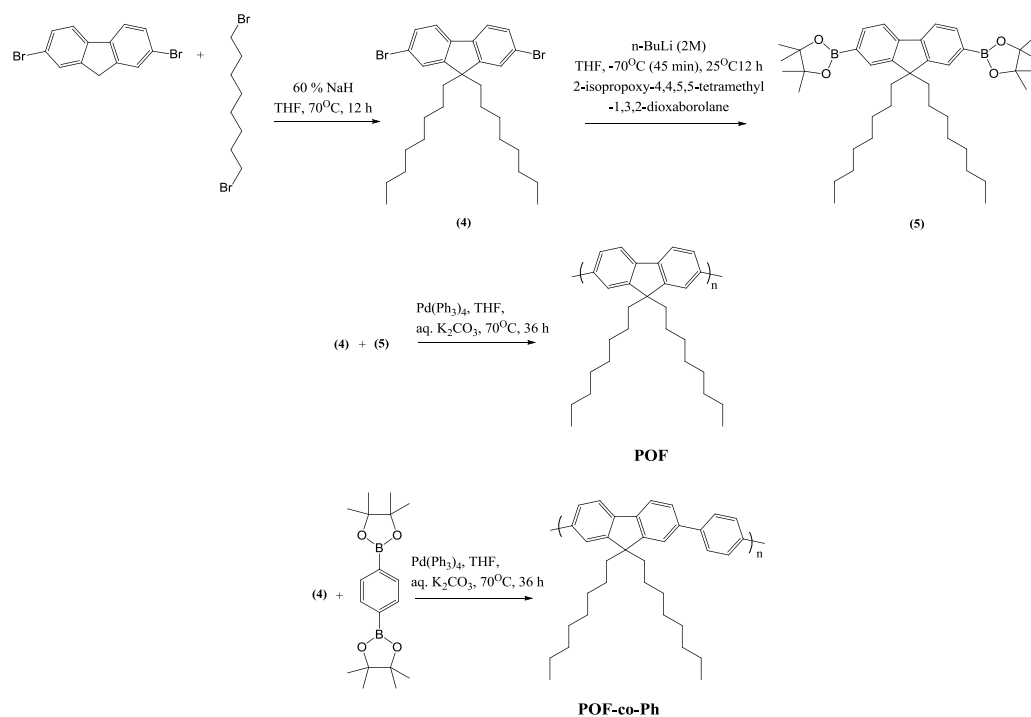
Scheme 2.2 Synthesis of monomers and Polymers (POF, POF-co-Ph)
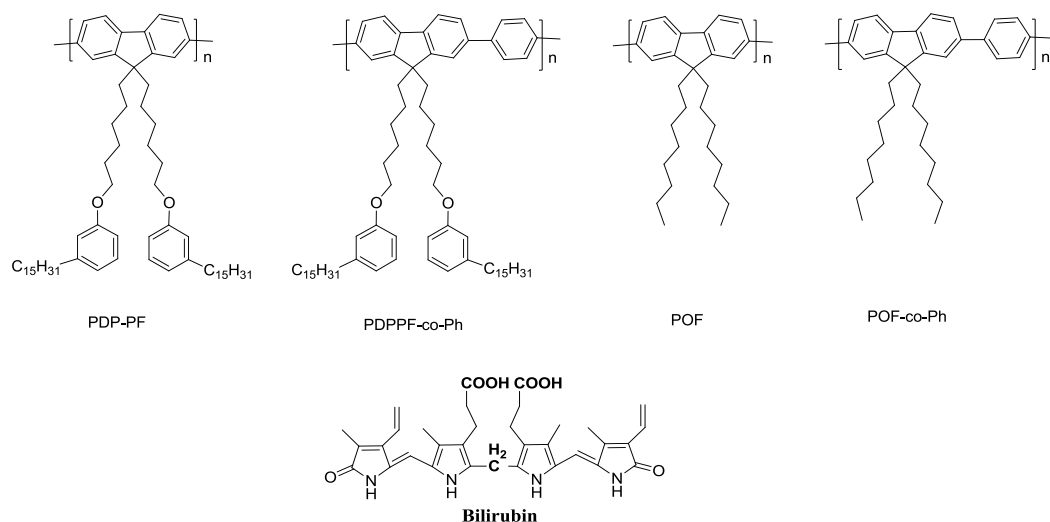
Scheme 2.3 Structure of the Polyfluorenes and Bilirubin used in the study.

Figure 2.1 compares the labeled proton NMR spectra of PDP-PF and copolymer PDPPF-co-Ph. The broadening of the peaks in ^{1}H NMR indicated reasonably high molecular weights.
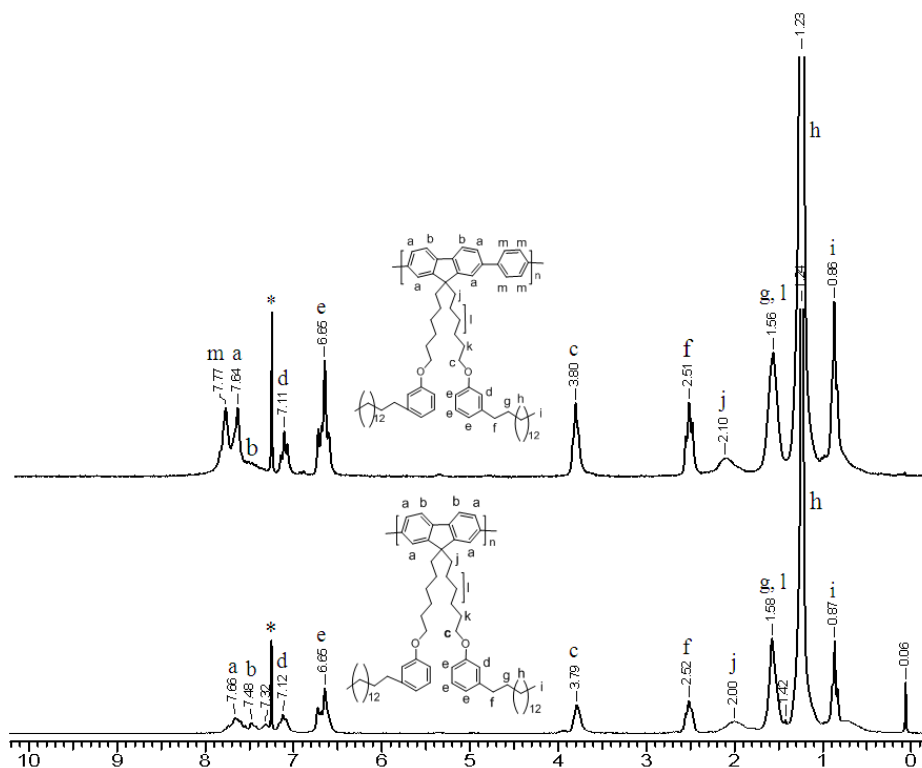
Figure 2.1 ^{1}H NMR spectra of PDPPF-co-Ph and PDP-PF recorded in CDCl$_3$.

Table 2.1 Sample designations, number and weight average molar mass, polydispersity indices, Yield and 10 Weight % loss temperature of the polyfluorenes.

Polymer	Number average molecular weight (Mn)[a]	Weight average molecular weight (Mw)[a]	Poly dispersity index (Đ$_M$)	Yield (%)	10 % weight loss Temperature (°C)
PDP-PF	19600	53000	3.5	75	370
PDPPF-co-Ph	18600	46000	2.4	78	408
POF	9000	22000	2.4	80	420
POF-co-Ph	20300	36100	1.7	75	411

a. Measured by size exclusion chromatography (SEC) in THF, calibrated with linear, narrow molecular weight distribution polystyrene standards.
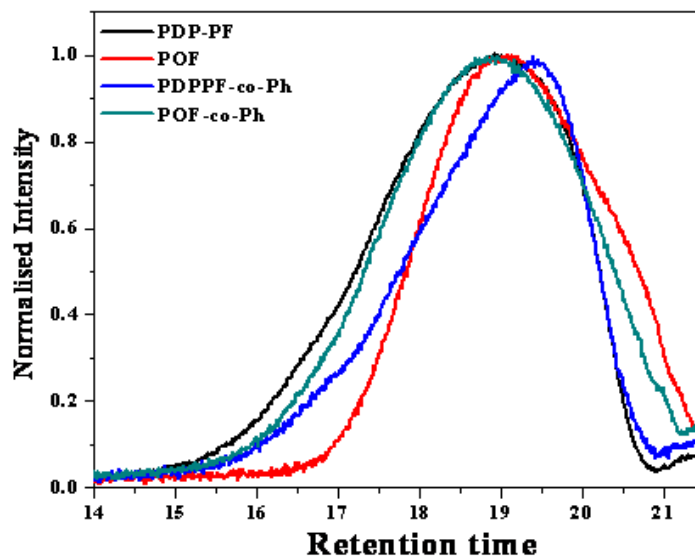
Figure 2.2 Size exclusion chromatogram of all the polymers.

The number average molecular weight (M_n) and polydispersity of the polymers were determined by gel permeation chromatography (GPC) using THF as solvent was shown in Figure 2.2. The number and weight average molecular weight (M_n, M_w), polydispersity index, yield and 10 % weight loss temperature of the different polymers are given in Table 2.1. PDP-PF had a M_w of 53, 000 with a polydispersity index $Đ_M$ of 3.5 and PDPPF-co-Ph had a M_w of 46, 000 with a $Đ_M$ of 2.4.The molecular weight and polydispersity values were comparable with the polyfluorenes reported in literature.[12]

2.3.2 Self-Assembly:

The PDP substituted polyfluorene has a rod-coil structure with the rigid polyfluorene backbone forming the rod segment and the hexyloxy appended PDP unit forming the coil segment. In general, rod-coil structures modified with hydrophilic and hydrophobic groups have been shown to exhibit nanophase separation into various morphologies. Dialkyl substituted polyfluorene particularly 9, 9-dioctylfluorene has been shown to self-assemble into hairy rod structures,[13] whereas polyfluorene with poly(ethylene oxide) side chains have been shown to form fluorescent micellar structures in aqueous solution.[10] The self-assembly behavior of the two polymers PDP-PF and PDPPF-co-Ph was studied in THF as solvent. Both polymers had good solubility in THF and a 1x 10^{-5} M solution in THF was drop cast

onto TEM grids and the solvent was allowed to evaporate at room temperature. PDP-PF formed vesicles with an average diameter of 300-500 nm as shown in Figure 2.3.a top where a thin wall could be clearly differentiated by the dark contrast. AFM was also recorded by casting the sample in THF onto silicon wafers. Figure 2.3.b shows the tapping-mode AFM height profile clearly showing spheres with a small crater-like depression characteristic of vesicles. The average diameter observed from AFM was around 400 nm. In sharp contrast, the PDPPF-co-Ph formed soap bubble-like porous spherical structures with average diameter of 300-700 nm (Figure 2.3.c). The AFM height profile (Figure 2.3.d) also clearly distinguished them as spheres and not vesicles. Energy minimization was carried out for one repeat unit of PDP-PF & PDPPF-co-Ph using DFT,[14,15] which showed that the PDP unit in PDP-PF with the C15 alkyl chain was extended outwards resulting in a torsion angle of ~62 ° with the plane of the fluorene ring. The presence of two hexyloxy pentadecyl phenyl units on each repeating unit could be expected to put a strain on the polyfluorene backbone resulting in reduced conjugation of the backbone. This was proved by the blue shift in the absorption spectra of PDP-PF compared to POF, as discussed later on. Figure 2.3.e shows a schematic diagram representing the self-assembly of PDP-PF into vesicles. Bilayer structures are formed by the interdigitation of the C15 alkyl chains of the PDP units, which would further transform into vesicles due to the curvature formed by twisting of the strained polyfluorene backbone. The extra phenyl ring on each repeating unit of the polyfluorene backbone in the case of PDPPF-co-Ph could be expected to lessen the strain felt by the backbone leading to a more open porous structure with accessible interior volumes. Figure 2.3.f shows the schematic representation of self-assembly in PDPPF-co-Ph resulting in formation of open and interconnected porous spheres. Small structural changes in fluorene oligomers have been shown to result in differences in torsion angles between neighboring units and different molecular shapes eventually resulting in strong differences in aggregation behavior.[16,17] The differences in the extent of twisting/torsion angle of the polyfluorene backbone is expected to be the driving force causing strong differences in the mode of self-assembly in the two polymers PDP-PF and PDPPF-co-Ph.
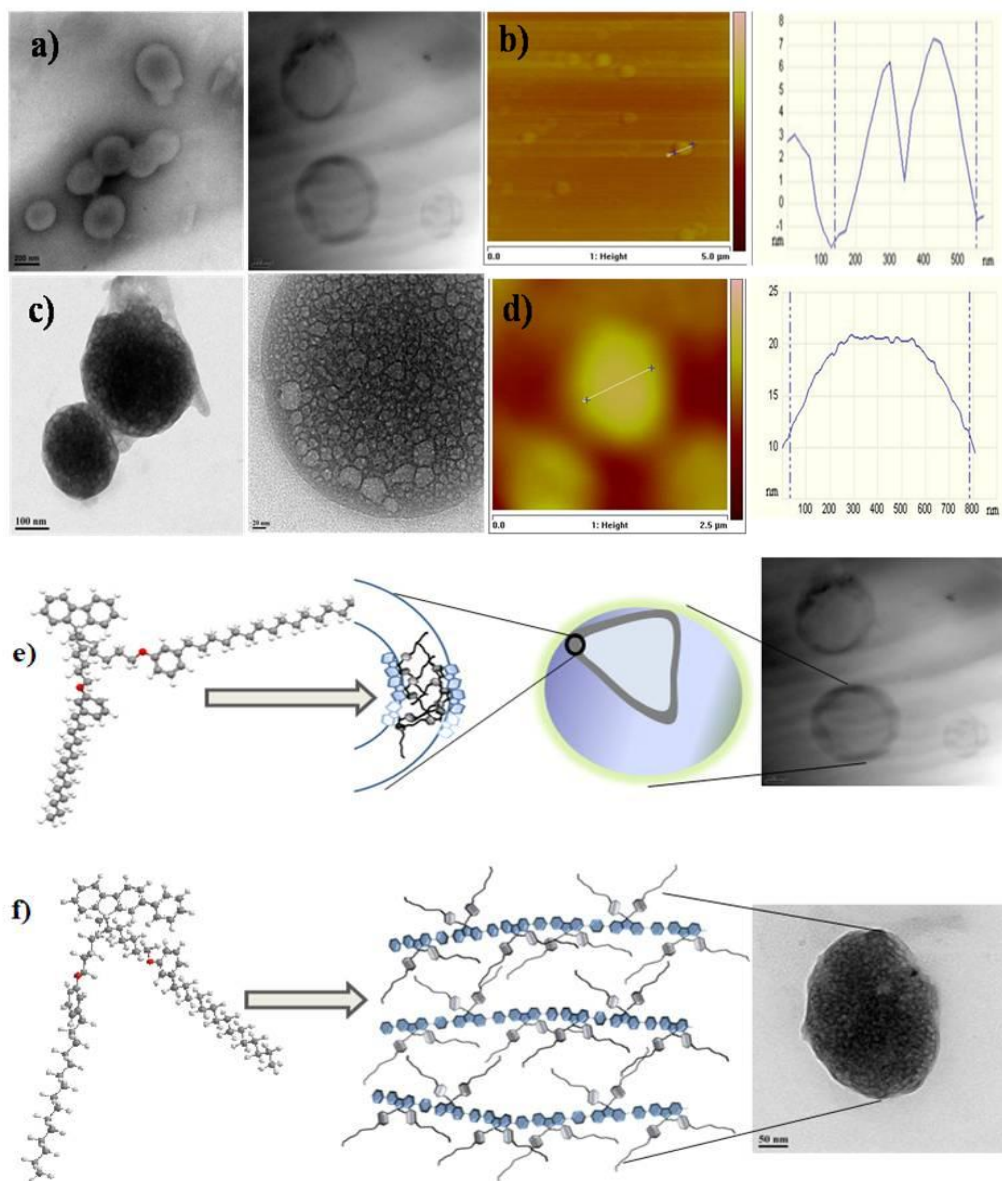
Figure 2.3 (a, c) TEM images of PDP-PF (top) and PDPPF-co-Ph (bottom) at 1×10^{-5} M concentration drop cast on carbon coated copper grids. (b, d) Tapping mode AFM images of PDP-PF (top) and PDPPF-co-Ph (bottom) at 1×10^{-5} M concentration coated on silicon wafers. The corresponding height section analysis is also shown. (e, f) Schematic diagrams show the self-assembly of PDP-PF and PDPPF-co-Ph into vesicles and porous spherical aggregates.

Rod-coil polymers are known to exist in self-assembled vesicles and micelles in solution, which are retained in film form upon evaporation of solvent.[18] Information regarding the size and morphology of the particles in solution can be

obtained from dynamic and static light scattering experiments (DLS and SLS).[19] DLS analysis in THF showed a good auto-correlation and indicated presence of particles with average diameter ~ 200 nm & 260 nm for PDP-PF & PDPPF-co-Ph polymers as shown in Figure 2.4.a which was in good correlation with the size obtained from TEM and AFM measurements. The slight increase in size of the self-assembled structures in film is probably due to aggregation upon solvent evaporation. The hydrodynamic radius (R_H) of 96 nm and 99 nm was extracted from the dynamic light scattering experiments for PDPPF-co-Ph and PDP-PF respectively. In the static light scattering experiment, the intensity of the scattered light measured at different angles is plotted against q^2, where q is the magnitude of the scattering vector. This plot known as the Guinier plot is shown in Figure 2.4.b for PDPPF-co-Ph and PDP-PF. A radius of gyration (R_g) value of 73 nm and 95 nm were obtained for PDPPF-co-Ph and PDP-PF respectively. The ratio between R_g/R_H obtained from the static and dynamic light scattering experiments respectively, called shape factor (ρ) is a well-known indicator for the morphology of the assemblies in solution (ρ ~ 0.77 for hard sphere, ρ ~ 1 for vesicles, and ρ ~ 1.7 for the coil conformation).[20]
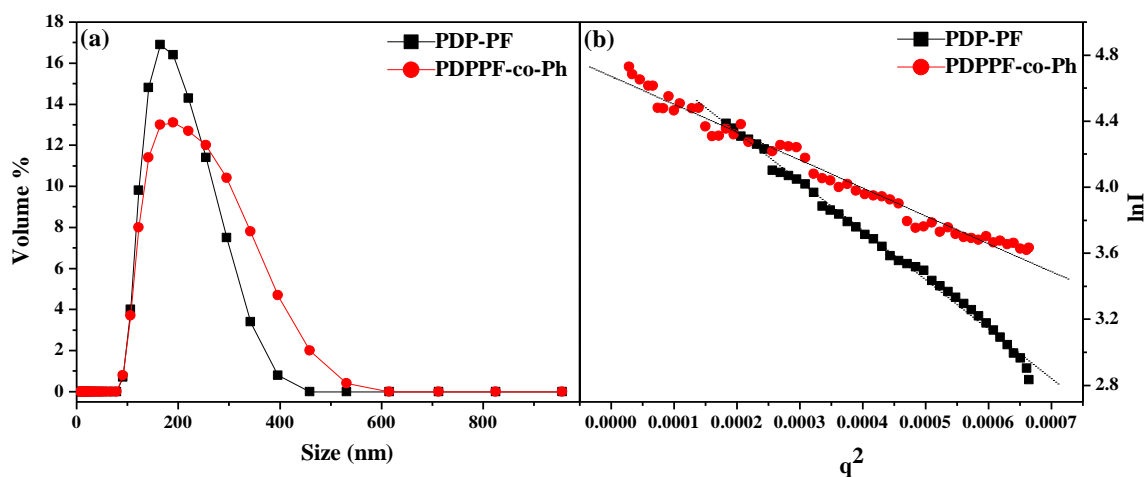
Figure 2.4 (a) Volume – average size distribution of the two polymers PDP-PF and PDPPF-co-Ph in THF (5 x 10^{-6} M) obtained by dynamic light scattering (DLS) analysis. (b) Static light scattering (Guinier plot) for PDP-PF and PDPPF-co-Ph (5 x 10^{-6} M) in THF.

The ratio Rg/R_H was obtained as 0.76 for PDPPF-co-Ph and 0.96 for PDP-PF confirming the existence of spherical particles for the former and vesicles for the latter in solution. Thus the observations from the light scattering experiments strongly supported the morphology observed using the various microscopic techniques.

2.3.3 Photophysical properties:

Figure 2.5 depicts the absorption and emission characteristics of all the polymers used in the present study in THF solvent along with that of the absorption spectrum of bilirubin (pink line). The characteristic broad featureless absorption of the polymers with absorption maxima at 350 nm and 366 nm for PDP-PF and PDPPF-co-Ph respectively is assigned to the π-π* transition of the polyfluorene backbone. Compared to the absorption of dialkyl substituted polyfluorenes like 9, 9'-dioctyl polyfluorene which has absorption wavelength maxima at 383 nm, the absorption maximum of PDP-PF was blue shifted by 33 nm. The introduction of bulky hexyloxy pentadecyl phenol unit twisted the polyfluorene backbone resulting in reduced conjugation length as indicated by the DFT energy minimized structure discussed earlier. The degree of backbone twisting was lessened in the case of copolymer PDPPF-co- Ph because of the presence of the rigid phenyl unit. Figure 2.5 also compares the normalized emission spectra (dotted lines) of the polymers in THF upon excitation at their absorption wavelength maxima. The polymers exhibited emission spectra with clear vibronic transitions at 409, 432, and 462 nm for PDPPF-co-Ph and at 404, 422 and 456 nm for PDP-PF corresponding to 0-0, 0-1, and 0-2 transitions respectively from the lowest singlet excited state. The fluorescence quantum yield of the two polymers PDP-Ph and PDPPF-co-Ph along with that of POF and POF-co-Ph polymers were determined using 0.1 OD solutions in THF relative to quinine sulphate (Φ_{fl}=0.546) as the reference. The PDPPF-co-Ph exhibited the highest quantum yield of 78 %, whereas PDP-PF had a quantum yield of ~61 % only. Although bulky groups are known to enhance the quantum yield significantly by retarding detrimental polymeric aggregation,[21] if the bulky groups result in considerable twisting of the conjugated polymer backbone the result would be a reduction in emission efficiency and quantum yield.[22]
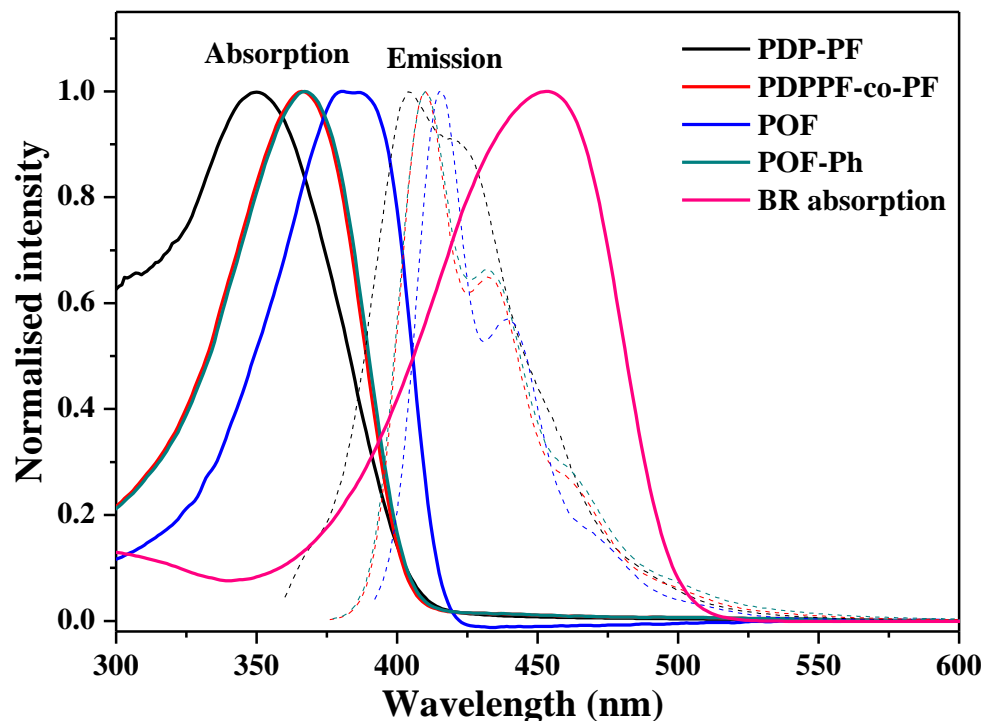
Figure 2.5 Stack plot of normalized absorption and emission spectra of all polymers along with the absorption spectrum of Bilirubin in THF. Polymers were excited at the respective absorption wavelength maxima.

2.3.4 Fluorescence sensing of Bilirubin:

The targeted analyte molecule Bilirubin (gross structure shown in scheme 2.2) undergoes structural isomerization into another isomer (lumirubin) upon prolonged exposure to light.[23] Hence all the photophysical studies with bilirubin in THF were carried out in dim light and bilirubin stock solutions were kept away from light and stored below room temperature (~10 ^{0}C). The emission spectra of PDP-PF and PDPPF-co-Ph showed good overlap with the absorption spectra of bilirubin (shown in Figure 2.5) indicating the possibility of FRET from polymer to bilirubin. Figure 2.6a shows the effect of addition of varying concentrations of bilirubin (0.1×10^{-6} to 10×10^{-6} M) on the absorption spectra of PDPPF-co-Ph (5×10^{-6} M). No change was observed in the absorption spectra of polyfluorene upon addition of bilirubin, but a new peak at 453 nm corresponding to bilirubin absorption became more prominent at higher concentrations of bilirubin. Figure 2.6.b shows the corresponding emission spectra, upon excitation at 367 nm. On addition of bilirubin, there was a drastic

reduction in the characteristic emission of polymer at 410 nm. The inset in Figure 2.6b shows the same figure with the unquenched emission of PDPPF-co-Ph removed for better clarity. Figure 2.6.c shows the same spectra after normalizing at polyfluorene emission maxima highlighting the FRET induced bilirubin emission at 502 nm. Bilirubin is known to emit at 502 nm with low quantum efficiency ($<$ 0.00002 at 25^0C in (CHCl$_3$).[24] The bilirubin emission at 502 nm increased in intensity with obvious color change in solution from blue to green. The inset in Figure 2.6c shows photographs taken under a hand held UV lamp highlighting the visual color change at various intervals of addition of bilirubin. The gradual evolution of color change upon addition of bilirubin to PDPPF-co-Ph is also explained using the CIE diagram where the emission at various concentrations was plotted in the CIE graphical representation in Figure 2.7. This visual color change makes quick and easy monitoring of bilirubin levels a reality. The gradual color change with varying concentration of bilirubin signals the corresponding change from normal to abnormal levels of bilirubin. Similar fluorescence quenching experiments were conducted for PDP-PF and also for the dioctyl substituted benchmark polymers POF and POF-co-Ph and are given in Figure 2.8.
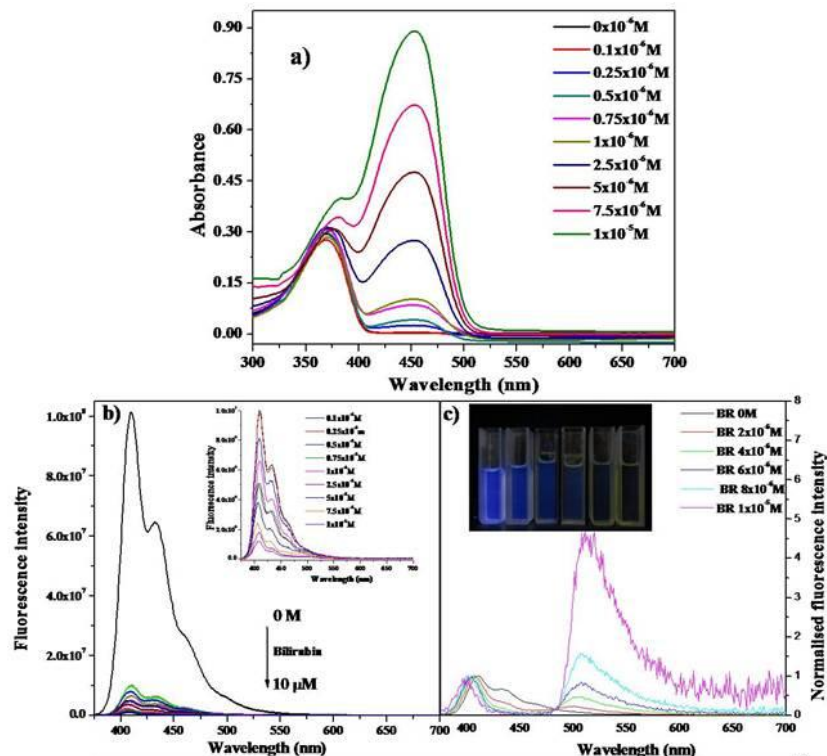
Figure 2.6 (a) Absorption spectra of PDPPF-co-Ph ($5x10^{-6}$ M) upon addition of various concentrations of Bilirubin ($0.1x10^{-6}$ M to $1x10^{-5}$ M) in THF. (b) Fluorescence spectra of PDPPF-co-Ph ($5x10^{-6}$ M) upon addition of various concentrations of Bilirubin ($0.1x10^{-6}$ to $1x10^{-5}$ M) in THF. Inset shows the same figure without the initial unquenched emission of PDPPF-co-Ph. Excitation wavelength was 367 nm. (c) Normalized (~ 410 nm) emission spectra highlighting the FRET induced bilirubin emission at 502 nm. Inset shows the photograph of the emission observed under a hand-held UV lamp.
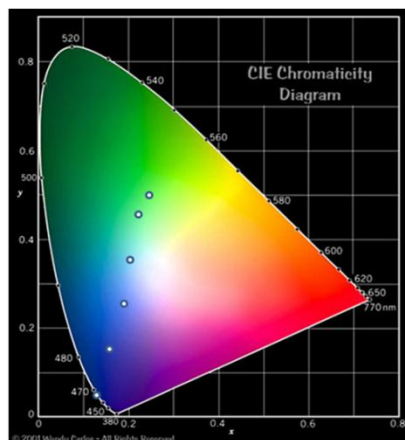
Figure 2.7 CIE color coordinate diagram for the change of color from blue to green upon addition of bilirubin to PDPPF-co-Ph in THF.
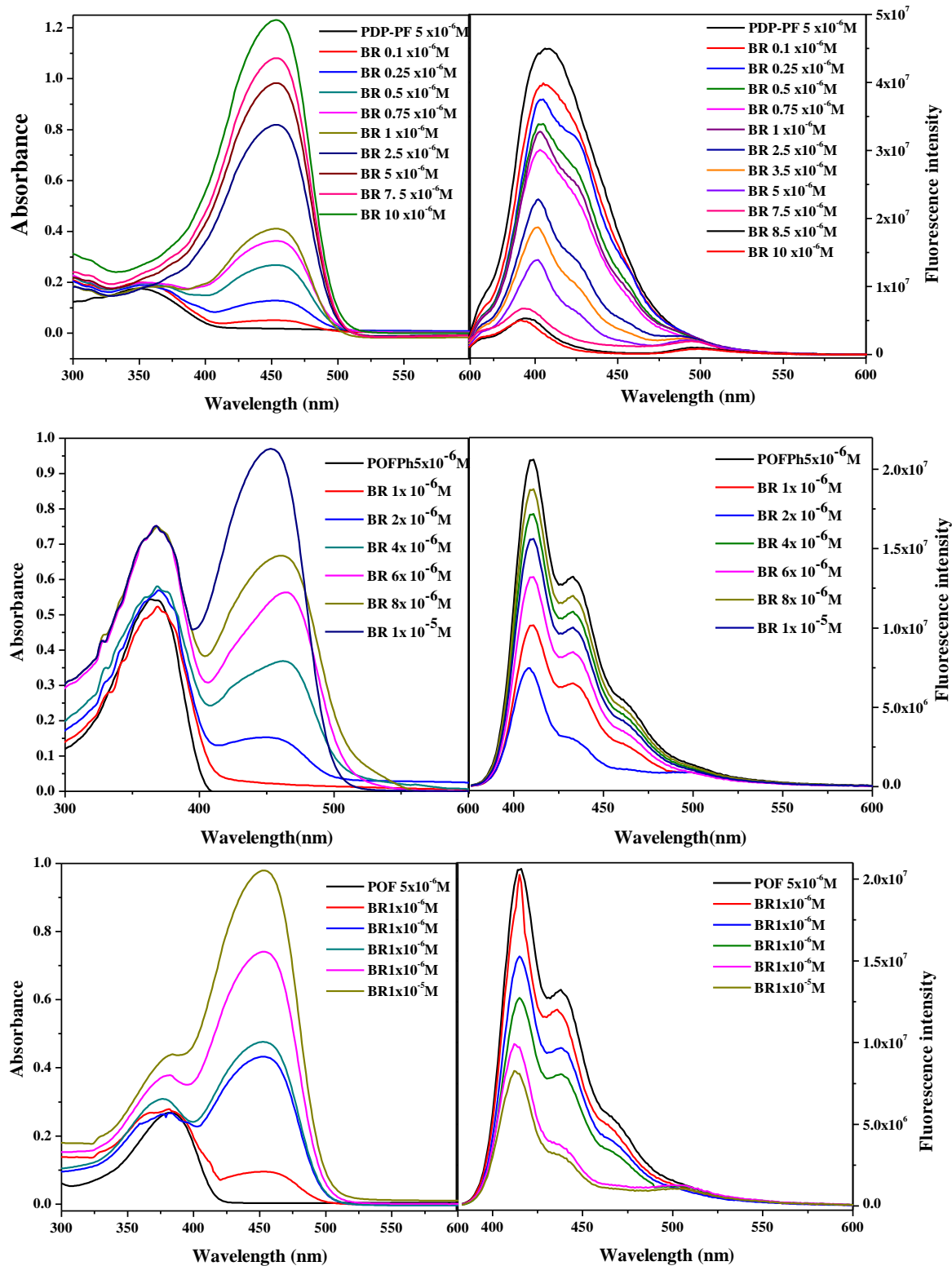
Figure 2.8 Absorption (left) and emission (right) spectra of PDP-PF, POF-co-Ph and POF in THF upon addition of bilirubin (0 μM - 10 μM).

Figure 2.9.a compares the change in fluorescence intensity for the four polymers as a function of varying bilirubin to polymer concentration. There was a 10 fold reduction in the emission of PDPPF-co-Ph for 0.1 mol % addition of bilirubin. The homopolymer PDPD-PF also showed a reduction in emission intensity upon addition of bilirubin although the reduction was gradual and not drastic as in the case of the phenyl copolymer PDPPF-co-Ph. Compared to the PDP substituted polyfluorenes, the performance of the POF and copolymer (POF-co-Ph) were very poor with marginal decrease in emission intensity. The quenching of polymer fluorescence upon addition of bilirubin was not accompanied by changes in the polymer absorption spectra which ruled out charge transfer between polymer and bilirubin. The good overlap in the emission spectra of polymer and absorption spectra of bilirubin suggested energy transfer as the most plausible reason for the quenching of polymer fluorescence. The FRET ratio calculated as the ratio of integrated area of bilirubin emission from 482 nm to 700 nm to that of polyfluorene emission in the range 360 nm to 482 nm for the four polymers as a function of increasing bilirubin concentration was compared in Figure2.9.b.
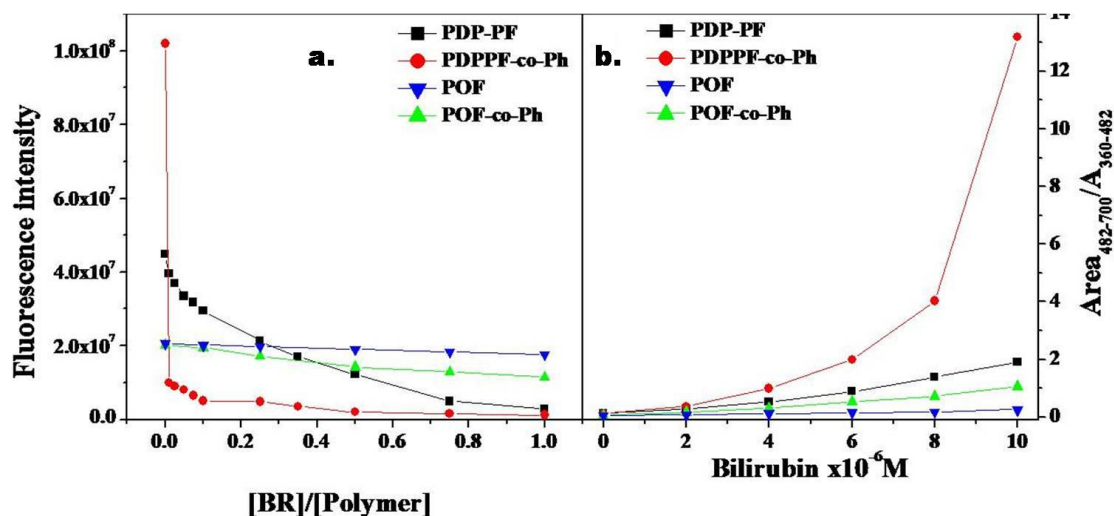
Figure 2.9 (a) Fluorescence intensity of polymers at 410 nm as a function of [Bilirubin]/[Polymer] ratio. (b). FRET ratio (Integrated area of bilirubin emission to that of polyfluorene emission; $A_{BR(482-700)}/A_{PF(360-482)}$) of the polymers at various concentration of Bilirubin.

At all bilirubin concentrations, PDPPF-co-Ph exhibited the highest FRET efficiency compared to the other polymers. The FRET efficiency at higher bilirubin concentrations was ~ 7 times higher for PDPPF-co-Ph compared to the PDP-PF.

Since FRET is a distance-dependant radiationless transfer of energy from a donor to acceptor molecule it can be used to investigate molecular interactions between the donor and acceptor. The FRET efficiency is good for donor-acceptor distances in the range of ~ 10-100 Å and it depends on the spectral overlap of the donor emission and the acceptor absorption (spectral overlap integral 'J') and the relative orientation of the donor and acceptor transition dipole moments (orientation factor 'k') must be approximately parallel. The various parameters for calculating donor – acceptor distance (r) like the spectral overlap integral $J(\lambda)$, forster distance (R^0), and Energy transfer efficiency (E) were calculated following standard procedure for 0.1 OD solutions of the polyfluorenes in the absence and presence of bilirubin (1×10^{-5} M) in THF. The energy transfer was highest for the PDP-co-Ph polymer with a maximum value of 86 % followed by the PDP-PF homo polymer (52 %). POF and POF-co-Ph gave efficiency values of 43 % and 33 % respectively. The energy transfer efficiency is related to the Förster distance by the equation (1). The Förster distances for the four polymers were similar and in the range of 46-50 Å, which was within the maximum separation distance (20-60 Å) between donor and acceptor over which resonance energy transfer can occur.[25] From the known values of E and R_0, the actual distance between the donor and acceptor – 'r' was determined. Comparing the values of the donor-acceptor distances of the four polymers it was observed that PDPPF-co-Ph had the shortest distance of ~ 36 Å, whereas the other polymers had larger D-A distances (> 45 Å).

$$E = 1 - (F_{DA}/F_D) \text{ --- (1)}$$

The spectral overlap of the Polyfluorene emission with bilirubin absorption was in the similar range for all the polymers used in the present study. The physical proximity of the analyte to the polymer is a major deciding factor in these energy transfer processes. The open porous spherical self-assembled aggregates of PDPPD-co-Ph allowed easy access to the bilirubin molecules whose diameter ranges < 5 nm,[26] into the interior of the spherical assembly (r_{PF-BR} ~36 Å). This resulted in a more

efficient transfer of energy from PF to BR upon excitation of PF. On the other hand, the closed vesicular assembly of PDP-PF allowed interaction of BR only on the periphery, limiting their proximity to $r_{PF-BR} > 45$ Å. The synergistic effect of morphology and efficient energy transfer thus acted in favor of PDPPD-co-Ph enabling naked eye detection of bilirubin using hand-held UV lamp.

2.3.5 Fluorescence lifetime Studies:

Fluorescence lifetime of the polyfluorenes was obtained by picosecond time-correlated single photon counting (TCSPC) technique. Time resolved fluorescence decays were collected at 410 nm (polyfluorene emission) with excitation at 375 nm in THF as solvent at 25 ^{0}C. The lifetime decay analysis of bilirubin could not be carried out due to the very weak nature of its fluorescence. Polyfluorenes are known to exhibit complex fluorescence decay behavior in solution which is both solvent and temperature dependent.[27] The fluorescence decay of PDPPF-co-Ph could be fitted to a biexponential fit with lifetimes of 211 ps (0.35 %) and 495 ps (0.65 %) (χ^2=1.005).
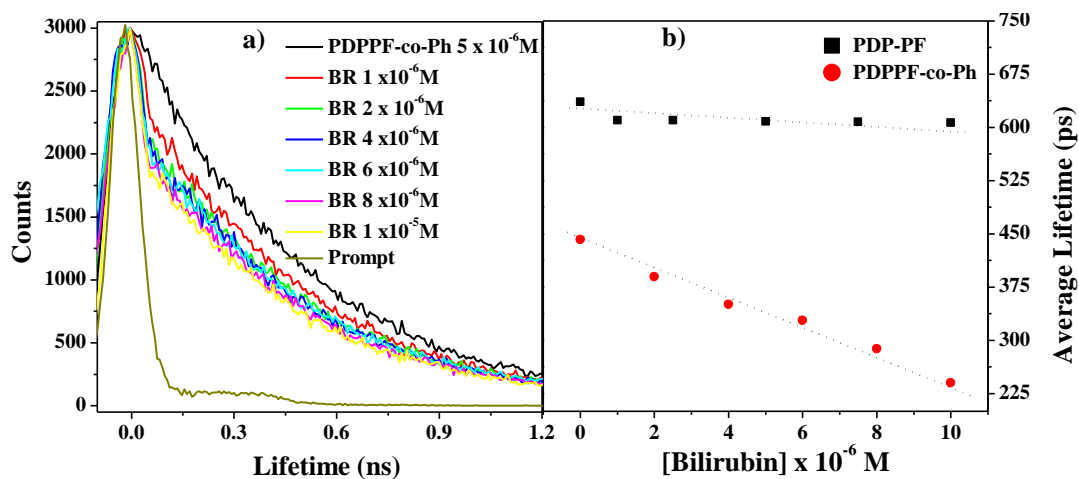
Figure 2.10 (a) Fluorescence lifetime measurement for the polymer [PDPPF-co-Ph] = 5x10^{-6} M at various Bilirubin concentration (1x10^{-6} M to 1x10^{-5} M) collected at 410 nm by using nanoLED of 375 nm. (b) Plot of the average lifetime of PDP-PF and PDPPF-co-Ph as a function of bilirubin concentration.

The lifetime reduced sharply with increasing bilirubin concentration reaching biexponential fit values of 38 ps (0.30 %) and 253 ps (0.70 %) (χ^2=1.06) for the highest bilirubin content of 1x10^{-5} M. Figure 2.10.a shows the time-resolved

fluorescence decay of PDPPF-co-Ph upon addition of varying concentrations of bilirubin. The decay of the polymer alone in the absence of bilirubin is also given for comparison. A sharp change in the decay pattern identifiable as two distinct regions – one where the slope was similar to that of the polymer alone (> 0.2 ps) and the other where the slope changed with the different bilirubin concentration (< 0.2 ps) was clearly discernible in the PDPPF-co-Ph bilirubin system. The average lifetime $<\tau>$ calculated as $<\tau> = \Sigma a_i \tau_i^2 / \Sigma a_i \tau_I$,[28] (where 'a' is the amplitude (normalized contribution)), was plotted as a function of bilirubin concentration for the two PDP substituted polyfluorenes and given in Figure 2.10.b. Similar time-resolved fluorescence decay was collected for all the other polymers also upon addition of bilirubin (10^{-5} M) (given in Table 2.2).

Table 2.2. Time resolved fluorescence decay parameters.

Sample	τ_1 (ps)	τ_2 (ps)	a_1	a_2	Average lifetime $<\tau>$ (ps)	χ^2
PDP-PF	536	675	0.23	0.77	636	1.063
PDP-PF + BR	102	609	0.02	0.98	606	1.05
PDPPF-co-Ph	211	495	0.35	0.65	441	1.008
PDPPF-co-Ph + BR	38	253	0.3	0.7	239	1.05
POF	134	422	0.15	1.0	408	1.04
POF + BR	377	515	0.67	0.33	432	1.08
POF-co-Ph	119	436	0.18	0.82	433	1.03
POF-co-Ph + BR	67	419	0.15	0.85	409	1.07

From the table it was clearly observed that the average fluorescence lifetime of the homopolymer PDP-PF did not decrease much upon bilirubin addition; in fact, after the first addition of bilirubin the lifetime remained constant indicating very low energy transfer. On the other hand, the drastic reduction in the average fluorescence lifetime in the case of PDPPF-co-Ph upon addition of bilirubin clearly gave evidence for efficient fluorescence energy transfer from polymer to bilirubin.

2.3.6 Sensitivity and Selectivity:

The sensitivity of the bilirubin sensing was determined by adding nanomolar ($1x10^{-9}$ M) solution of bilirubin to the polymers PDP-PF, PDPPF-co-Ph, POF and POF-co-Ph (concentration of the polymers: $1x10^{-5}$ M), followed by excitation at the respective absorption wavelength maximum. Figure 2.11.a compares the fluorescence spectra of the four polymers before and after addition of nanomolar concentration of bilirubin. Among all the polymers PDPPF-co-Ph showed the highest fluorescence quenching of 11 % for nanomolar concentrations of bilirubin ($1x10^{-9}$ M) where as no fluorescence quenching was observed at this low level of bilirubin in the case of the other polymers.

The selectivity of PDPPF-co-Ph towards bilirubin was investigated by analyzing sensing activity with structural analogues of bilirubin like biliverdin, dyes like TPY and Rhodamine-B. Biliverdin, which is also a haeme residue co exists with bilirubin in plasma and bile and is the structural analogue of bilirubin with a double bond at the C10 position.[29] The electronic absorption spectrum of biliverdin has two peak maxima at 376 and 666 nm and it is a non-fluorescent molecule. The spectral overlap for the polyfluorene emission and the biliverdin absorption is almost negligible. TPY is another structurally similar molecule, which can be considered as the closed ring analogue of bilirubin. All the analytes absorption spectra were plotted together with the emission of the PDPPF-co-Ph given in Figure 2.12 and the structures of the analytes are shown in Figure 2.13. Figure 2.11.b compares the percentage reduction of polymer (0.1 OD) fluorescence upon addition of $1x10^{-5}$ M of various analytes such as bilirubin, biliverdin, TPY and rhodamine B dye. Pronounced selectivity was observed only for bilirubin as analyte compared to the other structural analogues.
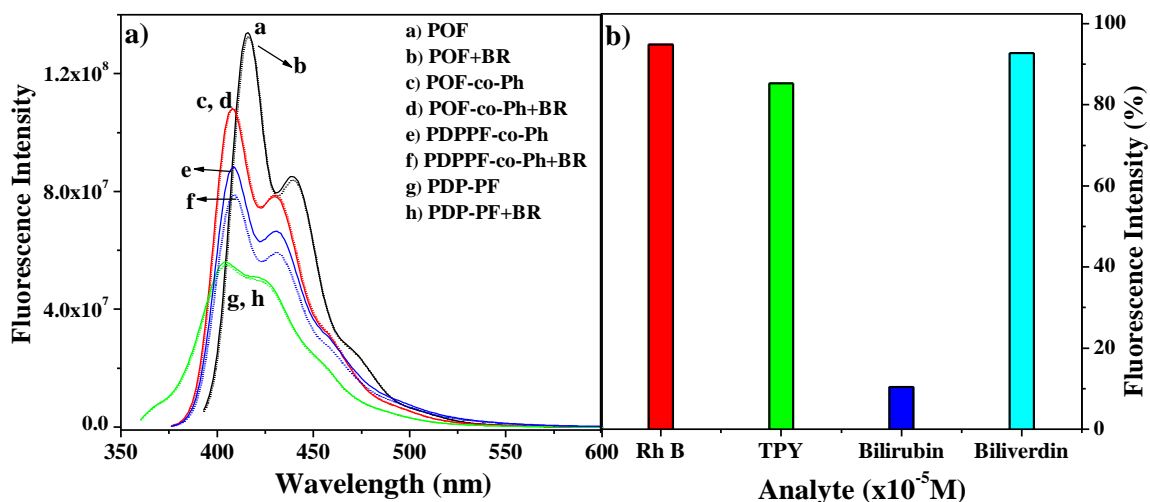
Figure **2.11** (a) Nanomolar sensing of all polymers. [polymer] = 1×10^{-5} M and [Bilirubin] = 1×10^{-9} M. (b) Bar graph denoting fluorescence emission response profiles of PDPPF-co-Ph on addition of various analytes. [PDPPF-co-Ph] = 2×10^{-6} M, [Analyte] = 1×10^{-5} M.
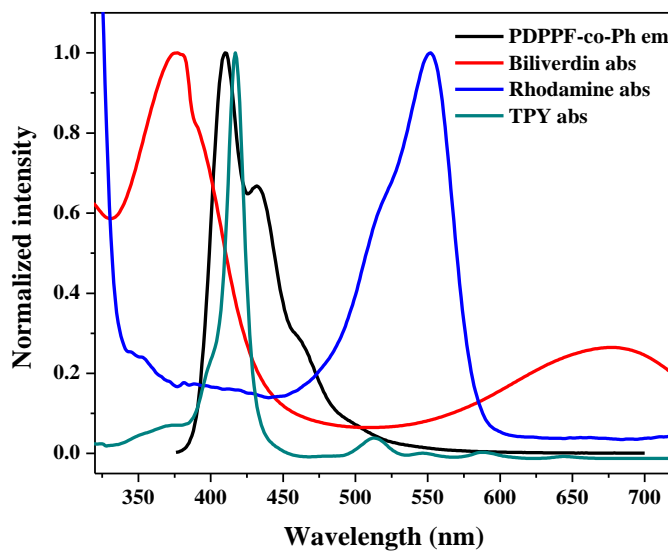
Figure 2.12 Absorption spectra of Biliverdin, Rhodamine and 5, 10, 15, 20-tetra(4-pyridyl)-21H, 23H- porphine (TPY) along with the emission of PDPPF-co-Ph.
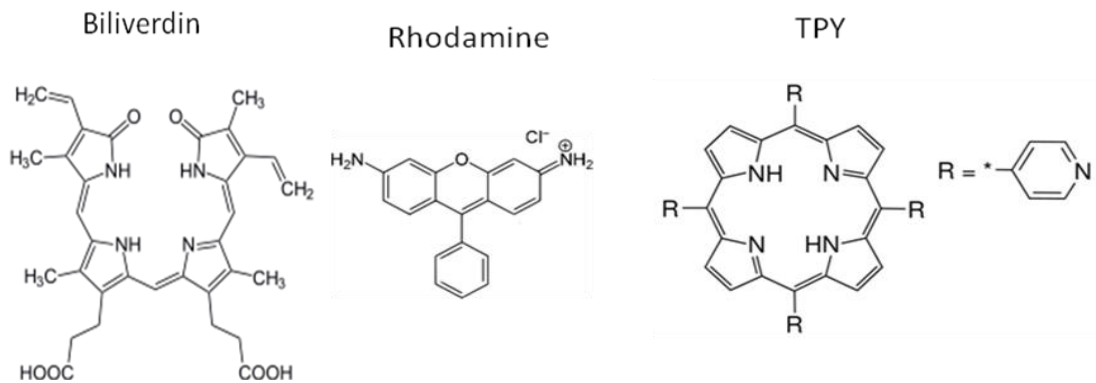
Figure 2.13 Structure of Biliverdin, Rhodamine and 5, 10, 15, 20-tetra(4-pyridyl)-21H, 23H- porphine (TPY).

This confirmed that the polymer PDPPF-co-Ph had pronounced selectivity for bilirubin. Biliverdin, the important structural analogue of bilirubin was unable to quench the polymer fluorescence even at higher concentrations.

2.4 Summary

In summary, pentadecyl phenol appended polyfluorene homo (PDP-PF) and phenyl co polymer (PDPPF-co-Ph) were synthesized and characterized. The sensing efficiency of both polymers towards the biologically important analyte bilirubin was demonstrated by the quenching of polymer fluorescence and FRET based bilirubin emission. Although both polymers showed good overlap of their respective emission spectra with the absorption spectra of bilirubin, higher extent of quenching of polyfluorene emission at 410 nm (86 %) together with increased bilirubin emission at 502 nm (5 times) was observed only in the case of PDPPF-co-Ph. The change in emission color from blue to green upon addition of bilirubin could be easily detected using a hand-held UV lamp. The differential self-assembling tendency of the polymers – open porous interconnected spherical assembly of PDPPF-co-Ph versus vesicles for PDP-PF proved to play a crucial role in their energy transfer efficiencies. A short donor (polyfluorene) - acceptor (bilirubin) distance of 36 Å was obtained for PDPPF-co-Ph in contrast to 46 Å for PDP-PF using steady state fluorescence based calculations.

Fluorescence lifetime decay measurements also showed a significant reduction in the average lifetimes of PDPPF-co-Ph upon addition of bilirubin. The sensitivity of bilirubin detection by PDPPF-co-Ph polymer was tested using nanomolar concentrations of bilirubin. PDPPF-co-Ph exhibited a 11 % quenching of its fluorescence upon addition of a 1×10^{-9} M solution of bilirubin, whereas PDP-PF and dioctyl substituted bench mark polyfluorene polymers did not exhibit any sensitivity to the presence of bilirubin at such low concentrations. The selectivity of detection was also investigated using structural analogues of bilirubin like biliverdin, TPY and Rhodamine-B. Pronounced selectivity was observed only for bilirubin as analyte compared to the other structural analogues. Thus this chapter highlighted the successful application of tailor-made highly fluorescent conjugated polymer based on polyfluorene for the sensitive and selective sensing of bilirubin using handheld UV lamp or a laboratory fluorimeter.

2.5 References

1. Bonnett, R.; Davies, J. E.; Hursthouse, M. B. *Nature* **1976**, *262*, 326-328.

2. Fevery, J. *Liver International* **2008**, 592-605.

3. Koolman, J.; Roehm, K. H. *Color atlas of Biochemistry*. Thieme Stuttgart. New york. 2nd edition, **2005**

4. Van den Bergh, A. A. H.; Snapper, J. *Deutsh. Arch. Klin. Med.* **1913**, *110*, 540-561.

5. Rand, R. N.; di Pasqua, A. *Clin. Chem*. **1962**, *8,* 570-578.

6. Zhou, Q.; Swager, T. M. *J. Am. Chem. Soc.* **1995**, *117*, 12593-12602.

7. Kaeser, A.; Fischer, I.; Abbel, R.; Besenius, P.; Dasgupta, D.; Gillisen, M. A. J.; Portale, G.; Stevens, A. L.; Herz, L. M.; Schenning, A. P. H. J. *ACS Nano* **2013,** *7*, 408-416.

8. Discher, D. E.; Eisenberg, A. *Science* **2002**, *297*, 967-973.

9. Jianzhong, Du.; O'Reilly, R. K. *Soft matter* **2009**, *5*, 3544-3561.

10. Yao, J. H.; Mya, K. Y.; Shen, L.; He, B. P.; Li, L.; Li, Z. H.; Chen, Zhi-Kuan.; Li, X.; Loh, K. P. *Macromolecules* **2008,** *41***,** 1438-1443.

11. Pramod, P. S.; Takamura, K.; Chaphekar, S.; Balasubramanian, N.; Jayakannan, M. *Biomacromolecules* **2012**, *13*, 3627-3640.

12. Ranger, M.; Rondeau, D.; Leclerc, M. *Macromolecules* **1997**, *30*, 7686−7691.

13. Knaapila, M.; Hase, T. P. A.; Torkkeli, M.; Stepanyan, R.; Bouchenoire, L.; Cheun, Hyeun-Seok.; Winokur, M. J.; Monkman, A. P. *Cryst. Growth Des.* **2007**, *7,* 1706-1711.

14. Ahlrichs, R.; Bär, M.; Baron, H. P.; Bauernschmitt, R.; Böcker, S.; Ehrig, M.; Eichkorn, K.; Elliott, S.; Furche, F.; Haase, F.; Häser, M.; Horn, H.; Huber, C.; Huniar, U.; Kattannek, M.; Kölmel, C.; Kollwitz, M.; May, K.; Ochsenfeld, C.; Öhm, H.; Schäfer, A.; Schneider, U.; Treutler, O.; von Arnim, M.; Weigend, F.; Weis, P.; Weiss, H. TURBOMOLE (Version 6.2); Universität Karlsruhe, Karlruhe, Germany, **2000**.

15. Becke, A. D. *Phys. Rev. A.* **1988***, 38,* 3098-3100.

16. Abbel, R.; van der Weegen, R.; Pisula, W.; Surin, M.; Leclère, P.; Lazzaroni, R.; Meijer, E. W.; Schenning, A. P. H. J. *Chem. -Eur. J.* **2009**, *15*, 9737–9746.

17. Stevens, A. L.; Kaeser, A.; Schenning, A. P. H. J.; Herz, L. M. *ACS Nano* **2012**, *6*, 4777-4787.

18. Knaapila, M.; Evans, R. C.; Gutacker, A.; Garamus, V. M.; Torkkeli, M.; Adamczyk, S.; Forster, M.; Scherf, U.; Burrows, H. D. *Langmuir* **2010**, *26*, 5056-5066.

19. Hotz, J.; Meier, W. *Langmuir* **1998**, *14*, 1031-1036.

20. Houga, C.; Giermanska, J.; Lecommandoux, S.; Borsali, R.; Taton, D.; Gnanou, Y.; Francois Le Meins, J. *Biomacromolecules* **2009,** *10,* 32-40.

21. Lee, J.; Cho, H. J.; Jung, B. J.; Cho, N. S.; Shim, H. K. *Macromolecules* **2004**, *37*, 8523– 8529.

22. Li, Y.; Vamvounis, G.; Holdcroft, S. *Macromolecules* **2002**, *35*, 6900-6906.

23. Rodes, J.; Benhamou, Jean-Pierre.; Blei, A.; Reichen, J.; Rizzetto, M. *The Textbook of Hepatology: From Basic Science to Clinical Practice*, Wiley-Blackwell, 3rd Edition, **2007**. Chapter-2.

24. Zietz, B.; Gillbro, T. *J. Phys. Chem. B*. **2007**, *111*, 11997-12003.

25. Corry, B.; Jayatilaka, D.; Rigby, P. *Biophys. J.* **2005**, *89*, 3822-3836.

26. Baydemir, G.; Andac, M.; Bereli, N.; Say, R.; Denizli, A. *Ind. Eng. Chem. Res*. **2007**, *46*, 2843-2852.

27. Scherf, U.; Neher, D. *Polyfluorene*, Springer-Verlag: Berlin and Heidelberg, Germany, **2008**.

28. Al Attar, H. A.; Monkman, A. P. *Biomacromolecules* **2009**, *10*, 1077-1083.

29. Mcdonagh, A. F.; Palma, L. A. *Biochem. J.* **1980**, *189*, 193-208.

Water-Soluble Polyfluorene for Selective Sensing of Free Bilirubin in Human Blood Serum

Selective sensing of a biomolecule in a competitive medium like complex biofluids is highly challenging. To meet the challenge of finding real world applications, water solubility and non- adherence to serum proteins are the necessary prerequisites expected in a probe. In this chapter, we have appended $_D$-glucuronic acid to the Polyfluorene that afforded dual advantages such as water solubility and selective interactive site for free bilirubin. Selective sensing of free bilirubin in water and in human blood serum in the clinically relevant levels was successfully demonstrated.

3.1 Introduction

Selective sensing of a biomolecule in complex biofluids like saliva, urine and human blood serum is highly essential for realizing real world biosensing applications. Solubility in aqueous medium is the prime pre-requisite for a conjugated polymer to find desired potential in biosensing applications. Generally, the rigid conjugated polymers are functionalized with either charged side chains or nonionic neutral side chains with high polarity to achieve solubility in aqueous medium. The hydrophilic pendant groups aid in compensating the hydrophobic nature of the polymer backbone, thereby enhancing water solubility and also facilitate interactions with specific targeted analytes.[1] Functionalization of ionic pendants[2-4] induces remarkable water solubility but selectivity is compromised in presence of multiple interferences from biological substances such as proteins,[5] nucleic acids,[6] due to nonspecific electrostatic interactions.[7] Conjugated polymers with charged pendants are known to show differential binding towards serum proteins that are used to develop sensing array for proteins.[8] Substitution of neutral side chains of sugar units such as glucose, mannose etc also act as receptors toward proteins.[9,10] Consequently, selective sensing of small biomolecules like free bilirubin in presence of serum proteins poses significant challenges to a conjugate polymer based probe.

The detection of free bilirubin in human blood serum is considered as one of the potential routes for diagnosing liver disorders.[11] Liver disorders result in increment of free bilirubin concentration from normal level of < 25 µmol (< 1.2 mg/dL) to > 50 µmol/L (> 2.5 mg) in blood indicative of jaundice condition.[12] Excess level of free bilirubin is severely toxic to human body because it can accumulate in body organs and causes brain hemorrhage by crossing the blood brain barrier.[13] Considering the drawbacks in the currently practiced diazo test method for free bilirubin estimation,[14] fluorometric biosensors offering amplified sensitivity, selectivity with a wide window of analyte concentration range are highly desirable. Reports on fluorometric detection of bilirubin in human blood serum are very sparse. In this chapter, a Förster resonance energy transfer (FRET) based visual fluorescence color change (from blue to light green) method of detection of free bilirubin in human blood serum sample is presented. In the previous chapter, pentadecyl phenol (PDP) functionalized

polyfluorenes were employed as a model for fluorimetric detection of bilirubin in organic (THF) medium.[15] Our preliminary work highlighted the potential of developing a water soluble polyfluorene which could take advantage of the favorable photophysical properties of polyfluorene-bilirubin combination for the detection of bilirubin. The advantage is expected to be twofold if the moiety incorporated into polyfluorene backbone could also additionally act as an interaction site for bilirubin.

$_D$-Glucuronic acid is a vital water soluble carbohydrate that performs the key function of removing several insoluble toxic substances through glucuronidation and subsequent urinal excretion as glucuronides in human metabolism.[16] In the liver, glucuronidation of bilirubin (insoluble in water) plays a vital role in forming bilirubin glucuronides (soluble in water) to avoid accumulation of toxic unconjugated (free) bilirubin in body fluids.[17] In addition; $_D$-Glucuronic acid is also a non-receptor carbohydrate for the serum proteins, thereby providing a platform for receptor-free selective biosensing applications. Thus incorporation of $_D$-glucuronic acid into polyfluorenes is expected to serve the dual purpose of imparting water solubility to the otherwise fully hydrophobic polyfluorenes while additionally acting as an interacting site for bilirubin. As the competitive interference of proteins can be eliminated via $_D$-glucuronic acid appendage, selective sensing of bilirubin in serum is expected to be feasible. A polymer appended with the sugar unit $_D$-Glucose was also designed as a non-bilirubin interacting reference polymer.

This is the first successful report of water soluble conjugated polyfluorene appended with $_D$-Glucuronic acid and $_D$-Glucose for biosensing application in human blood serum. The structure as well as photophysical properties of the polymers were characterized by relevant techniques. The appendage of glucuronic acid imparted water solubility and amphiphilic nature that could aid in the self-organization of the polymers. Unfortunately, the water solubility of the glucose appended polyfluorene was not very good. The polymers exhibited good spectral overlap with bilirubin; thus fulfilling the criteria for energy transfer process. Fluorescence sensing experiments were carried out in human serum which contained hemoglobin, proteins, cholesterol, glucose and metal ions as crucial interferences. The glucuronic acid appended polymer exhibited high degree of selectivity towards bilirubin that was verified from

the poor quenching efficiencies of competing interferences such as biliverdin, cholesterol, sugars and metal ions.

3.2 Experimental Section

Materials: 2, 7-Dibromo-9-[H]-fluorene, $_D$-glucuronic acid, $_D$-glucose pentaacetate, Trifluoroacetic acid (TFA), bilirubin, biliverdin, phosphate buffered saline (PBS), Azido trimethylsilane, $SnCl_4$, propargyl alcohol, $Pd(PPh_3)_4$, 1, 4-benzene diboronic bis(pinacol ester), sodium methoxide, sodium hydride, $Pd_2(dba)_3$, CsF, quinine sulphate, tetra butyl ammonium bromide, 1, 6-dibromohexane, Human blood serum (Heat Inactivated from male AB clotted whole blood, USA origin and sterile-filtered, CAS no-H5667) used as such without any further treatment, uridine diphosphate glucuronic acid sodium salt and bis(pinacolato)diboron were purchased from Aldrich company Ltd and were used as such. Liver homogenate was purchased from MP biomedicals, Inc. Copper sulfate, sodium ascorbate, HCl, acetic anhydride, iodine, sodium thiosulfate, potassium hydroxide, glucose, sucrose, sodium bicarbonate, K_2CO_3, and ethanol were purchased from Merck chemicals Ltd. Tetrahydrofuran, acetone, pet ether, ethyl acetate, DCM and methanol were purchased locally and were purified using standard procedures.

Methods: ^{1}H, and ^{13}C NMR spectra were analyzed using Bruker-AVENS 200 and 400 MHz spectrometer. Chemical shifts are reported in ppm at 25 ^{0}C using $CDCl_3$ and MeOH-d_4 as solvents containing trace quantity of tetramethylsilane (TMS) as internal standard. The purity of the compounds was determined by HR-MS or MALDI-TOF in combination with elemental analysis. The MALDI-TOF analysis was done on Voyager-De-STR MALDI-TOF (Applied Biosystems, Framingham, MA, USA) equipped with 337-nm pulsed Nitrogen laser for the purpose of desorption and ionization. A 2 μM solution of sample was premixed with DHB (2,5 dihydroxy benzoic acid) matrix in THF and mixed well before spotting on 96-well stainless steel MALDI plate through dried droplet method for the analysis. Mass spectra were measured with ESI ionization in MSQ LCMS mass spectrometer. Elemental analysis was done by Thermofinniganflash EA 1112 series CHN analyzer. HRMS (ESI) were recorded on ORBITRAP mass analyzer (Thermo Scientific, Q Executive). The

molecular weights of the polymers were determined by size exclusion Chromatography (SEC), which was performed using a Viscotek VE 1122 pump, a Viscotek VE 3580 RI detector and a Viscotek VE 3210 UV/vis detector in DMF using polystyrene as standards. DLS measurements were carried out on a Zetasizer ZS-90 apparatus, utilizing 633 nm red laser (at 90° angle) from Malvern Instruments. The reproducibility of the data was checked at least three times using independent polymer solutions.

Photophysical Studies:

Absorption spectra were measured using Perkin-Elmer Lambda 35 UV-Visible spectrophotometer. Steady-state fluorescence studies and time-resolved fluorescence lifetime measurements were recorded using Horiba Jobin Yvon Fluorolog 3 spectrophotometer having a 450 W xenon lamp for steady-state fluorescence and Fluorescence lifetime decays were collected by a time-correlated single photon counting (TCSPC) setup from IBH Horiba Jobin Yvon (U.S.) using a diode laser (IBH, U.K., NanoLED-320 and 375 L, with a λ max = 320 and 375 nm) having a full width half maximum of 89 ps as a sample excitation source. All the absorption and emission studies were conducted in dim light at a temperature of 15 ^{0}C in order to avoid structural isomerization of bilirubin and the stock solutions were stored below of 10 ^{0}C. Due to the insolubility of bilirubin in water at pH = 7.4, all the bilirubin stock solutions were prepared at pH=10 using PBS buffer.

Isothermal Titration Calorimeter Experiment:

ITC experiments were carried out in Micro cal iTC-200 instrument. The titration was carried out in PBS buffer in alkaline medium at 25 ^{0}C using an isothermal titration calorimeter (Microcal iTC-200) with stirring at 1000 rpm. 200 μL of polymer at a concentration of 2 mM was taken in the sample cell and bilirubin (~ 20 mM) was taken in the syringe. A typical titration experiment consisting of 19 consecutive injections each of 2 μl volume in the duration of 20 s at an interval of 180 s was conducted. Heat of dilution (T) upon addition of bilirubin in solvent was determined by performing a blank titration by injecting the bilirubin solution into the solvent. To obtain the heat of binding between polymer and bilirubin, the value of heat of dilution

was subtracted from the total value of heat of binding. A single set of binding model was fitted with the binding isotherm which was used to extract binding constant (K), binding stoichiometry (N), change of enthalpy (ΔH) and the change of entropy (ΔS) for the binding.

Sensing of Free Bilirubin in Water:

The stock solutions of the polymers were prepared at 1 μM in water at pH=10 using PBS buffer. Bilirubin solutions of concentrations ranging from 1×10^{-6} M to 1×10^{-4} M in PBS buffer at pH=10 were prepared and kept in dark at 15 ^{0}C. The bilirubin solution was added to the 1 μM solution of polymer in water (pH=10). The changes in the absorption and emission of the polymer on addition of different concentrations of bilirubin were recorded at 15 ^{0}C.

Sensing of Free Bilirubin in Human Serum:

Human serum is the preferred part of blood containing vital components such as hemoglobin ($\leq$ 25 mg/dl), total proteins (4-9 g/dl), iron (40 UG %), cholesterol (80-200 mg/dl), glucose (50-180 mg/dl), sodium (100-160 mg/dl) etc. The absorption and fluorescence measurements were conducted using a fixed amount of 100 μL of human blood serum. The analyte, free bilirubin was added directly to serum in the concentration range of 1×10^{-6} M to 1×10^{-4} M and this mixture was added to the 1 μM solution of polymer in water (pH=10). The final volume of test solution was adjusted to the fixed volume of 2.5 ml by using PBS buffer at pH=10. A control experiment was performed in the same volume of serum and polymer without the addition of bilirubin. The changes in the absorption and emission of the polymer on addition of different concentrations of bilirubin in presence of serum were recorded at 15 ^{0}C.

Preparation of Conjugated Bilirubin (B_c):

An aliquot of the freshly prepared liver homogenate was mixed thoroughly but gently with stock solutions of free bilirubin and uridine diphosphateglucuronide (UDPG1cUA) to achieve final concentrations of 50-500 mg/L (0.86 to 8.6 mol/L) bilirubin and 10 to 50 mol/L UDPGIcUA. The acceptable pH range for the incubation mixture was 7.0-7.8. For routine incubations, 10-15 g/liter Triton X-100 surfactant and 10 mol/L $MgCl_2$ were also present in the medium. The entire reaction mixture

was kept in a Nitrogen-rich atmosphere, shielded from strong light, and at 37 ^{0}C (with constant, gentle swirling) during the 3-4 h incubation. After incubation the content was extracted with chilled chloroform to remove unconjugated bilirubin from the medium. The contents were then centrifuged to remove the solid materials. The aqueous layer was separated and the isolation of conjugated bilirubin was done using the lucassen procedure.[18]

Detailed Synthetic Procedure for Monomers and Polymers:

a. Synthesis of 2, 7 dibromo-9, 9-(6-bromohexyl)fluorene (2):

2, 7-diromofluorene (10 g, 30.86 mmol) and NaH (3.71 g, 0.154 mol) were taken in RB along with stir bar after evacuating air followed by purging N_2 gas. Dry THF (200 ml) was transferred through cannula to this reaction mixture. After a dark red colored precipitate was observed, 1, 6-dibromohexane (19 ml, 0.124 mol) was added and the reaction mixture was heated to reflux for 12 h. The entire amount of reactant mixture was poured into water and extracted with ethyl acetate and washed with water, brine and finally solvent was evaporated under vacuum. The excess of 1, 6-dibromohexane was distilled off and the crude compound was purified by column chromatography using pet ether as eluent. The product was obtained as yellow solid. Yield of the product: 85 %. ^{1}H NMR (200 MHz, CDCl$_3$): δ in ppm 7.54-7.42 (m, 6H), 3.28 (t, 4H), 1.96-1.87 (m, 4H), 1.73-1.64 (m, 4H), 1.26-1.03 (m, 8H), 0.65-0.57 (m, 4H). MALDI (calculated (M+Na) = 673.12; Observed (M+Na) = 673.2).

b. Synthesis of 2, 7-dibromo-9,9-bis(6-(prop-2-yn-1-yloxy)hexyl)-9H-fluorene (3):

To a solution of NaH (1.85 g, 0.077 mol) in dry THF, Propargyl alcohol (9 ml, 0.154 mol) was added drop wise and stirred for 30 minutes at room temperature. Then the 2, 7 dibromo-9, 9-(6-bromohexyl)fluorene (**2**) (10 g, 15.38 mmol) was added slowly to the reaction mixture and the content was refluxed for 15 h. The reaction mixture was allowed to cool to room temperature and methanol was added to quench NaH. The solvent was removed by evaporation and the crude product was extracted with DCM; the organic layer was washed with water, brine and further purified by column chromatography using 97:3 pet ether: ethyl acetate as eluent. Yield: 60 %. ^{1}H NMR (200 MHz, CDCl$_3$): δ in ppm 7.54-7.36 (m, 6H), 4.06 (d, 4H), 3.38 (t, 4H), 2.37 (t,

2H), 1.96-1.87 (m, 4H), 1.45-1.33 (m, 4H), 1.26-1.03 (m, 8H), 0.65-0.57 (m, 4H). IR spectrum: υ in cm^{-1} 3308, 2978, 2865, 1648, 1500, 1250, 1135, 770. MALDI:(Calculated (M$^+$) = 600.42; observed (M$^+$) = 600.43).

c. Acylation of _Dglucuronic acid:

_DGlucuroinc acid (5 g) was dispersed in acetic anhydride (75 ml) and stirred at 0 ^{0}C. I_2 (350 mg) was added, upon which it developed red color. This solution was stirred for 2 h in ice and further 3 h at room temperature. Excess acetic anhydride was removed by fractional distillation and the remaining mixture was extracted with DCM. The organic layer was then washed twice with $Na_2S_2O_3$, dried with sodium sulphate, filtered and concentrated to afford acetic (2S, 3S, 4S, 5R, 6S)-3, 4, 5, 6-tetraacetoxytetrahydro-2H-pyran-2-carboxylic anhydride as white solid. The product was recrystallized from DCM/petether. Yield: 75 %. ^{1}H NMR (200 MHz, CDCl$_3$): δ in ppm 6.39 (d, 1H), 5.51 (s, 1H), 5.25 (t, 1H), 5.09 (dd, 1H), 4.46 (dd, 1H), 2.18 (s, 3H), 2.09 (s, 3H), 2.05 (s, 3H), 2.03 (s, 3H), 2.01 (s, 3H). LC-MS (Calculated (M+Na) = 427.52; Observed (M+Na) = 427.54).

d. Synthesis of (2S, 3R, 4S, 5S, 6S)-6-(methoxycarbonyl)tetrahydro-2H-pyran-2, 3, 4, 5-tetrayl tetraacetate:

The pentacetate product was refluxed in dry methanol for 24 h. The excess methanol was distilled off and dried under vacuum. The product was purified by column chromatography using pet ether:ethyl acetate (4:6), and further recrystallized from methanol. Yield: 65 %. ^{1}H NMR (200 MHz, CDCl$_3$): δ in ppm 5.76 (d, 1H), 5.25 (q, 2H), 5.11 (t, 1H), 4.18 (d, 1H), 3.72 (s, 3H), 2.09 (s, 3H), 2.07 (s, 3H), 2.03 (s, 3H), 2.01(s, 3H).

e. Synthesis of (2R, 3R, 4S, 5S, 6S)-2-azido-6-(methoxycarbonyl)tetrahydro-2H-pyran-3, 4, 5-triyl triacetate (4):

(2S, 3R, 4S, 5S, 6S)-6-(methoxycarbonyl)tetrahydro-2H-pyran-2, 3, 4, 5-tetrayl tetraacetate (5 g, 13.3 mmol) was dissolved in anhydrous DCM (0.1 g/ml) under Argon atmosphere and TMS-N$_3$ (4.4 ml, 33.3 mmol) and SnCl$_4$ (0.8 ml, 6.65 mmol) were added to it. The reaction mixture was stirred for 15 h. The mixture was diluted with DCM, saturated sodium bicarbonate solution was added to it and vigorously

stirred for 30 min. The mixture was poured into water and twice extracted with DCM. The combined organic layer was washed with 10 % K_2CO_3, brine and finally with water. The final product was purified by column chromatography. (EtOAc/MeOH = 95/5).Yield: 90 %.^{1}H NMR (200 MHz, CDCl$_3$): δ in ppm 5.24 (t, 2H), 4.95 (t, 1H), 4.72 (d, 1H), 4.13 (d, 1H), 3.77 (s, 3H), 2.07 (s, 3H), 2.03 (s, 3H), 2.01 (s, 3H). IR spectrum: υ in cm^{-1} 3308, 2978, 2865, 1648, 1500, 1250, 1135,770. LC-MS: (Calculated (M+Na) = 382.29; Observed (M+Na) = 382.35).

f. Click Reaction to Obtain (5):

To a solution of (2R, 3R, 4S, 5S, 6S)-2-azido-6-(methoxycarbonyl)tetrahydro-2H-pyran-3, 4, 5-triyl triacetate (**4**) (0.66 g, 1.83 mmol) in THF/MeOH/water (2:0.5:0.2) was added propargyl functionalized fluorene (**3**) (0.5 g, 0.83 mmol) and the resultant reaction mixture was degassed 3 times by freeze-thaw cycles. CuSO$_4$ (0.33 g, 0.83 mmol) & sodium ascorbate (0.1 g, 0.42 mmol) was then added one after the other and the reaction was allowed to proceed for 24 h in Argon atmosphere. The progress of the reaction was monitored by IR. After completion of the reaction, reaction mixture was filtered to remove solid mass and solvent was removed by rotary evaporator. The reaction mixture was purified by column chromatography using (pet ether/ethyl acetate = 40/60) to get 2-(5-((((6-(2, 7-dibromo-9-(6-((1-((2R, 3S, 4S, 5R, 6S)-3, 4, 5-triacetoxy-6-(methoxycarbonyl)tetrahydro-2H-pyran-2-yl)-1H-1, 2, 3-triazol-4-yl)methoxy)hexyl)-9H-fluoren-9-yl)hexyl)oxy)methyl)-1H-1, 2, 3-triazol-1-yl)-6-(methoxycarbonyl)tetrahydro-2H-pyran-3, 4, 5-triyl triacetate (**5**). Yield: 65 %. ^{1}H NMR (200 MHz, CDCl$_3$): δ in ppm 7.41 (m, 6H), 5.45-5.30 (m, 8H), 4.53 (d, 2H), 4.25 (dd, 2H), 3.73 (s, 6H), 3.35 (t, 8H), 2.07, 2.05, 2.02 (s, 18H), 1.87-1.83 (m, 8H), 1.39 (m, 4H), 1.09 (m, 8H), 0.54 (m, 4H). HR-MS: Calculated (M+Na) = 1341.2888; Observed (M+Na) = 1341.2881. Elemental analysis: Calculated- C, 51.90; H, 5.35; N, 6.37; Observed- C, 52.27; H, 5.49; N, 6.85.

g. Synthesis of poly[(1, 4-phenylene)-2, 7(9, 9bis(6-((1-((2R, 3S, 4S, 5R, 6S)-3, 4, 5-triacetoxy-6-(methoxycarbonyl)tetrahydro-2H-pyran-2-yl)-1H-1, 2, 3-triazol-4-yl)methoxy)hexyl)-9H-fluoren-9-yl)hexyl)oxy)methyl)-1H-1, 2, 3-triazol-1-yl)-6-(methoxycarbonyl)tetrahydro-2H-pyran-3, 4, 5-triyltriacetate. (PF-Ph-GlcA(OAc)):

2-(5-(((6-(2,7-dibromo-9-(6-((1-((2R, 3S, 4S, 5R, 6S)-3, 4, 5-triacetoxy-6-(methoxycarbonyl)tetrahydro-2H-pyran-2-yl)-1H-1, 2, 3-triazol-4-yl)methoxy)hexyl)-9H-fluoren-9-yl)hexyl)oxy)methyl)-1H-1, 2, 3-triazol-1-yl)-6-(methoxycarbonyl)tetrahydro-2H-pyran-3, 4, 5-triyl triacetate (**5**) (300 mg, 0.23 mmol), 1, 4-bis(4, 4, 5, 5-tetramethyl-1,3,2-dioxaborolan-2-yl)benzene (75 mg, 0.23 mmol) and tetrakis(triphenylphosphine) palladium (30 mg, 0.03 mmol) were taken in a two necked round bottom flask under Nitrogen atmosphere. Dry THF (8 ml) was added to the mixture. K_2CO_3 (0.127 g, 0.92 mmol) was dissolved in degassed water (2 ml) and added to the reaction medium. The reaction mixture was heated to reflux for 36 h under Nitrogen atmosphere. The mixture was cooled down to room temperature and added drop-wise into a stirred solution of acetone (100 ml) in an open vessel. The precipitate was isolated and dissolved in dichloromethane and filtered to remove the catalyst. The collected dichloromethane solution was concentrated under reduced pressure and purified by repeated precipitation from acetone (100 ml). The precipitate was filtered, washed with methanol (50 ml) and dried under high vacuum. Yield: 75 %. ^{1}H NMR (200 MHz, CDCl$_3$): δ in ppm 7.7-7.61 (dd, 4H) 7.51-7.44 (m, 6H), 5.65 (d, 2H), 5.31 (d, 2H), 5.0 (s, 2H), 4.55 (s, 4H), 3.82 (s, 6H), 3.37-3.10 (d, 8H), 2.0, 1.98, 1.93 (s, 18H), 1.42-1.21 (m, 8H), 0.84 (t, 8H), 0.59 (b, 4H). ^{13}C NMR (400 MHz, CDCl$_3$): δ in ppm 184.85, 162.41, 152.21, 138.85, 136.38, 131.84, 128.43, 128.32, 125.88, 61.28, 55.41, 48.59, 36.35, 31.66, 31.46, 28.84, 28.46, 26.06, 22.05, 13.91.

h. Homopolymerization of glucuronic acid monomer (PF-GlcA(OAc)):

To a 50 ml round bottom flask, 2-(5-(((6-(2, 7-dibromo-9-(6-((1-((2R, 3S, 4S, 5R, 6S)-3, 4, 5-triacetoxy-6-(methoxycarbonyl)tetrahydro-2H-pyran-2-yl)-1H-1, 2, 3-triazol-4-yl)methoxy)hexyl)-9H-fluoren-9-yl)hexyl)oxy)methyl)-1H-1, 2, 3-triazol-1-yl)-6-(methoxycarbonyl)tetrahydro-2H-pyran-3, 4, 5-triyl triacetate (**5**) (500 mg, 0.379 mmol), was added along with bis(pinacolato)diboron (96 mg, 0.379 mmol), Pd$_2$(dba)$_3$ (6.87 mg, 7.5 µmol), tricyclohexylphosphonium tetrafluoroborate (8.36 mg, 22.7 µmol), and CsF (400 mg, 2.6 mmol). The RB was attached to a reflux condenser fitted with Argon atmosphere. The flask was evacuated and backfilled with Argon, after which degassed dioxane (35 ml) was transferred to the reaction mixture via

syringe. Polymerization was started by heating at 90 ^{0}C and stirred for 24 h at the same temperature. Tetrabutylammonium bromide (24.4 mg, 75 µmol) dissolved in dry dioxane was added to the reaction mixture via syringe, and the reaction was stirred for 24 h. The reaction was cooled to room temperature, solvent removed in vacuum, and the contents redissolved in minimal amount of THF and precipitated in water. The solid was isolated by filtration, dissolved in THF and precipitated into acetone. Yield: 90 %. ^{1}H NMR (200 MHz, CDCl$_3$): δ in ppm 7.37-7.19 (m, 6H), 5.76 (d, 2H), 5.28-5.16 (m, 4H), 4.5 (dd, 2H), 4.16 (dd, 2H), 3.57 (s, 6H), 3.22 (t, 8H), 1.92, 1.89, 1.87 (s, 18H), 1.78-1.65 (m, 16H), 0.91 (b, 8H), 0.4 (b, 4H). ^{13}C NMR (400 MHz, CDCl$_3$): δ in ppm 184.85, 162.41, 152.21, 138.85, 136.38, 131.84, 128.43, 128.32, 61.28, 55.41, 48.59, 36.35, 31.66, 31.46, 28.84, 28.46, 26.06, 22.05, 13.91.

(i) Synthesis of (2R, 3R, 4S, 5R, 6R)-2-(acetoxymethyl)-6-azidotetrahydro-2H-pyran-3, 4, 5-triyl triacetate (6):

TMS-N$_3$ (2.5 eq, 3.8 ml) and SnCl$_4$ (0.5 eq, 0.13 ml) were added to a solution of (2.0 g, 5.12 mmol) (2S, 3R,4S, 5R, 6R)-6-(acetoxymethyl)tetrahydro-2H-pyran-2, 3, 4, 5-tetrayl tetraacetate in dry DCM (20 ml) under N$_2$ atmosphere and the reaction mixture was stirred for 15 h. The mixture was diluted with DCM and the solution was vigorously stirred for 30 – 40 minutes in presence of equal volume of saturated NaHCO$_3$ in water. A white emulsion was formed, from which the organic and aqueous layers could be separated after filtering through whatmann filter paper. The product was purified by column chromatography using pet ether:ethyl acetate (40:60). ^{1}H NMR (200 MHz, CDCl$_3$): δ in ppm 5.25-5.05 (q, 2H), 4.94 (t, 1H), 4.65 (d, 1H), 4.28-4.11 (q, 2H), 3.82-3.74 (dt, 1H), 2.09, 2.06, 2.01, 1.99 (s, 12H).

(j) 'Click' Reaction to obtain (7):

To a solution of (2R, 3R, 4S, 5R, 6R)-2-(acetoxymethyl)-6-azidotetrahydro-2H-pyran-3, 4, 5-triyl triacetate (6) (0.8 g, 2.14 mmol) in THF was added 2, 7-dibromo-9, 9-bis(6-(prop-2-yn-1-yloxy)hexyl)-9H-fluorene (3) (0.576 g, 0.9 mmol), CuSO$_4$ (0.39 g, 2.14 mmol) and the resultant reaction mixture was degassed. Sodium ascorbate (0.212 g, 1.07 mmol) was added and the reaction mixture was stirred for 24 h in Argon atmosphere. The progress of the reaction was monitored by FT-IR

spectroscopy. After completion of the reaction solvent was evaporated and monomer was column purified using pet ether:ethyl acetate (40:60) to give glucose functionalized monomer (**7**). ^{1}H NMR (200 MHz, CDCl$_3$): δ in ppm 7.71 (s, 2H), 7.52-7.40 (m, 6H), 5.42 (2H), 5.21 (t 2H), 5.09 (t, 1H), 4.94 (q, 1H), 4.8 (d, 2H), 4.53 (d, 2H), 4.22 (d, 2H), 4.14 (dt, 4H), 4.01-3.94 (m, 2H), 3.36 (t, 4H), 2.09, 2.06, 2.01, 1.99 (s, 24H), 1.83 (m, 8H), 1.41 (m, 4H), 1.07 (m, 8H), 0.57 (m, 4H). HR-MS: (Calculated (M+Na) = 1367.3222; Observed (M+Na) = 1367.3217).

(k) Polymerization to obtain PF-Ph-Glu(OAc):

To a 50 ml round bottom flask, (2S, 3S, 4R, 5S)-2-(acetoxymethyl)-6-(4-(((6-(2, 7-dibromo-9-(6-((1-((3R, 4S, 5R, 6R)-3,4,5-triacetoxy-6-(acetoxymethyl)tetrahydro-2H-pyran-2-yl)-1H-1, 2, 3-triazol-4-yl)methoxy)hexyl)-9H-fluoren-9-yl)hexyl)oxy)methyl)-1H-1, 2, 3-triazol-1-yl)tetrahydro-2H-pyran-3, 4, 5-triyl triacetate (**7**) (350 mg, 0.26 mmol), was added along with 1, 4-bis(4, 4, 5, 5-tetramethyl-1,3,2-dioxaborolan-2-yl)benzene (86 mg, 0.26 mmol), tetrakis(triphenylphosphine) palladium (35 mg, 0.048 mmol). The RB was attached to a reflux condenser fitted with Argon atmosphere. The flask was evacuated and backfilled with Argon, after which degassed THF (20 ml) was transferred to the reaction mixture via syringe. Polymerization was started by heating to 70 ^{0}C and stirring for 48 h at the same temperature. The reaction was cooled to room temperature, solvent removed in vacuum, and the contents dissolved in minimal amount of THF and precipitated in water. The solid was isolated by filtration, dissolved in THF and precipitated into acetone. Yield: 87 %. ^{1}H NMR (400 MHz, CDCl$_3$): δ in ppm 7.85-7.41 (m, 10H), 5.83 (b, 2H), 5.41 (d, 4H), 5.21 (t, 2H), 4.83 (m, 2H), 4.54 (m, 4H), 4.26 (d, 2H), 4.15 (m, 2H), 3.96 (m, 2H), 3.38 (t, 4H), 2.10, 2.05, 2.03, 2.0 (s, 24H), 1.84 (m, 4H), 1.60 (m, 8H), 1.10 (m, 4H), 0.67 (m, 4H). ^{13}C NMR (400 MHz, CDCl$_3$): 162.73, 152.52, 139.17, 136.7, 132.5, 132.16, 130.37, 128.74, 126.2, 121.63, 61.59, 55.73, 48.9, 40.13, 36.67, 31.78, 29.19, 26.37, 25.0, 22.72, 14.26.

(l) Deprotection of Glucuronic acid appended Polymers:

The glucuronic acid appended polyfluorenes (40.0 mg) were dissolved in the mixture of methanol (6 mL) and dichloromethane (10 mL), to which CH_3ONa in methanol solution (4 mL, 1 M) was added. The mixture was stirred at room temperature for 8 h for deacetylation. After rotary evaporation of the solvents, the residue was washed with acetone, and dissolved in THF and water (1:1). Dilute HCl (0.5 M, 3ml) was added and stirred for 24 h to hydrolyze the methyl ester. Excess acid was neutralized with NaOH. After removal of the solvents, the polymer was washed with DCM to remove unhydrolyzed polymer and then acetone was added. The precipitate was filtered and then dried under vacuum. Powder was redissolved in distilled water and dialyzed against Mill-Q water using 2 KDa molecular weight cut-off dialysis membrane for 2 days, changing the Mill-Q water every 6 hours. After freeze drying, pure polymer was obtained as powder (yield = 80 %). Final polymers were named as PF-Ph-GlcA and PF-GlcA respectively.

^{1}H NMR of PF-GlcA Polymer: ^{1}H NMR (200 MHz, MeOH-d4): δ in ppm 7.47-7.19 (m, 6H), 5.76 (d, 2H), 5.28-5.16 (m, 4H), 4.5 (dd, 2H), 4.16 (dd, 2H), 3.22 (t, 8H), 1.78-1.65 (m, 16H), 0.91 (b, 8H), 0.4 (b, 4H).

^{1}H NMR of PF-Ph-GlcA polymer: ^{1}H NMR (200 MHz, MeOH-d4): δ in ppm 7.92-7.15 (m, 10H), 5.76 (d, 2H), 5.28-5.16 (m, 4H), 4.5 (dd, 2H), 4.16 (dd, 2H), 3.22 (t, 8H), 1.78-1.65 (m, 16H), 0.91 (b, 8H), 0.4 (b, 4H).

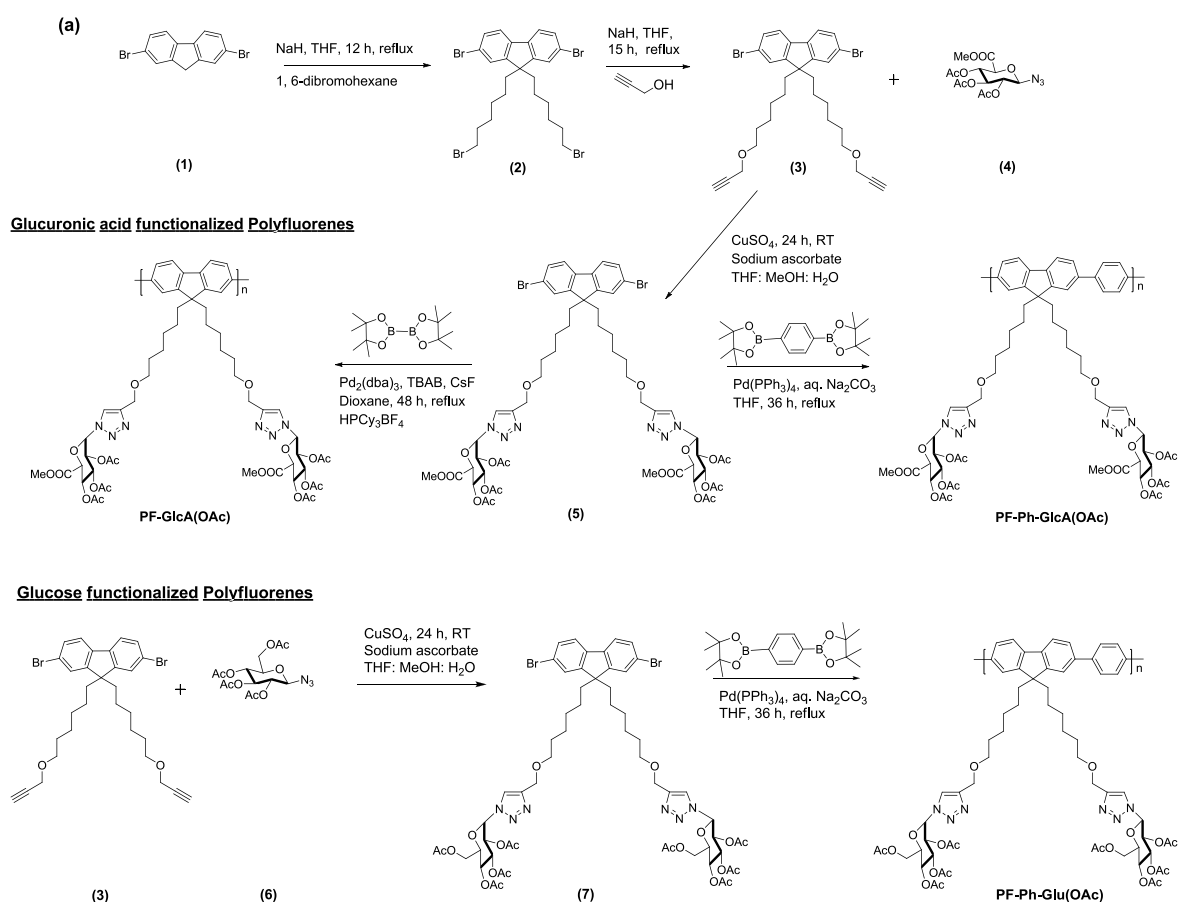**(m) Deprotection of Glucose appended Polymer (PF-Ph-Glu):**

Polymer (40.0 mg) was dissolved in a mixture of methanol (5 ml) and dichloromethane (5 ml). To this mixture trifluoroacetic acid was added and stirred at room temperature for 12 h for deacetylation. After rotary evaporation of the solvents, the residue was washed with DCM 3 times. Powder was redissolved in distilled water and dialyzed against Mill-Q water using 2 KDa molecular weight cut-off dialysis membrane for 2 days, changing the Mill-Q water every 6 hours. After freeze drying, pure polymer was obtained as powder (yield = 85 %). Final polymer was named as PF-Ph-Glu. ^{1}H NMR (400 MHz, MeOH-d4): δ in ppm 7.59-7.25 (m, 10H), 5.24 (b, 2H), 5.04 (d, 4H), 4.93 (t, 2H), 4.78 (m, 2H), 4.76 (m, 4H), 4.38 (d, 2H), 4.37 (m,

2H), 4.09 (m, 2H), 3.98 (t, 4H), 3.96 (m, 2H), 3.2 (t, 4H), 1.67 (m, 4H), 1.43 (m, 8H), 0.93 (m, 4H), 0.50 (m, 4H).

3.3 Results and Discussion

3.3.1 Synthesis and structural characterization:

Water soluble polyfluorenes functionalized with glucuronic acid (GlcA) and glucose (Glu) side chains were synthesized via click chemistry followed by Palladium catalyzed cross coupling which is shown in Scheme 3.1a-b. 2, 7-dibromofluorene (1) was reacted with 1, 6-dibromohexane in presence of NaH to obtain 2, 7-dibromo-9, 9-bis(6-bromohexyl)-9H-fluorene (2).
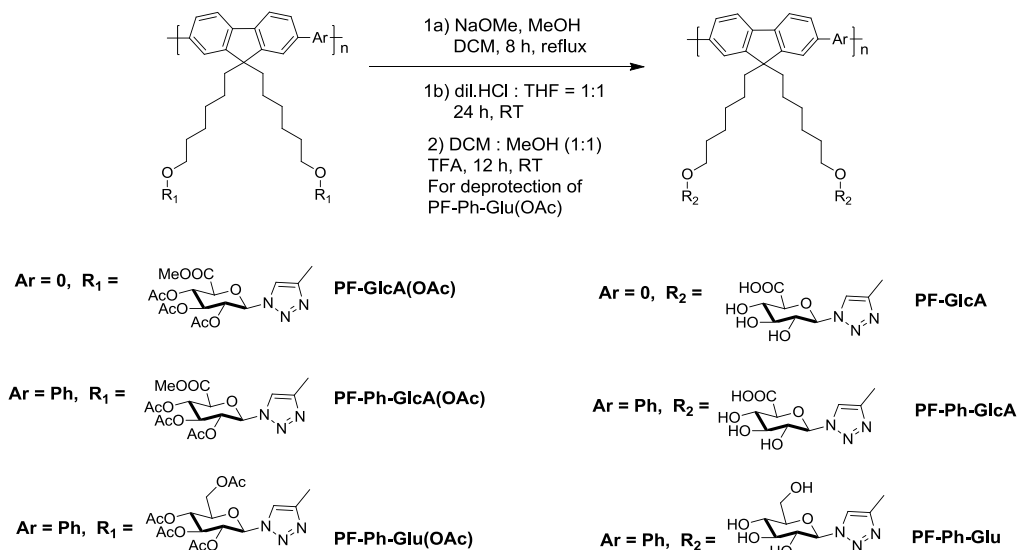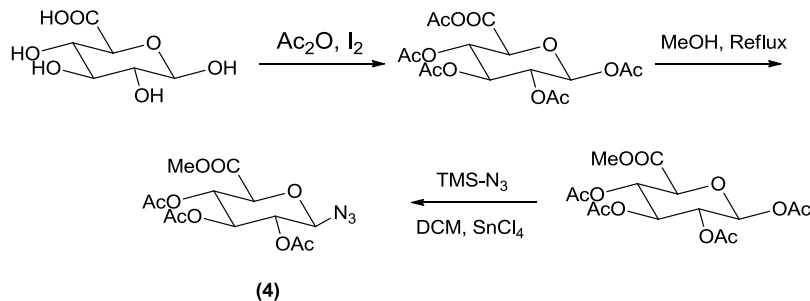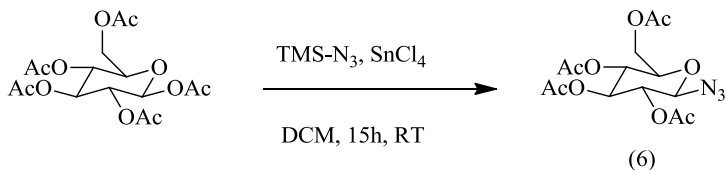
Scheme 3.1 (a) Synthesis of Glucuronic acid and glucose functionalized Polyfluorenes and (b) deprotection of polymers.

a. Synthesis of azide functionalized glucuronic acid methyl ester (4)

b. Synthesis of azide functionalized glucose ester (6)

Scheme 3.2. Synthesis of azides (4) and (6)

Compound (2) was etherified with propargyl alcohol to obtain 2, 7-dibromo-9, 9-bis(6-(prop-2-yn-1-yloxy)hexyl)-9H-fluorene (3). The synthesis of azide functionalized glucuronic acid and glucose was followed from literature report and shown in scheme 3.2.[19] In short, D-Glucuronic acid/ D-Glucose was initially protected with acetic anhydride in presence of iodine to give the penta acetylated product. In

the case of D-Glucuronic acid an additional step involving conversion of the acetylated ester (COOAc) to its methyl ester derivative (COOMe) was also carried out by refluxing the penta acetylated product in dry methanol for 24 h. The esters were further reacted with TMS-N$_3$ and SnCl$_4$ to obtain the corresponding azido derivatives (4) and (6) respectively as the major product which were purified by column chromatography.

Click reaction between the azide functionalized glucuronic acid/ glucose and propargyl functionalized fluorene was carried out using copper catalyzed azide-alkyne chemistry to get the desired glucuronic acid and glucose functionalized fluorene monomer (5) and (7) respectively. The monomers were copolymerized with 1, 4-benzene diboronic bis(pinacol ester) via Suzuki coupling reaction to obtain the glucuronic acid functionalized fluorene copolymer PF-Ph-GlcA(OAc) and glucose functionalized fluorene copolymer PF-Ph-Glu(OAc) respectively. A homopolymer of the glucuronic acid functionalized polyfluorene – PF-GlcA(OAc) was also synthesized by using bis(pinacolato)diboron as the coupling reagent. The polymers were deprotected using NaOMe in MeOH:DCM (1:1) and further treated with dilute HCl or TFA (trifluoroacetic acid) to produce PF-Ph-Glu, PF-Ph-GlcA, and PF-GlcA. The polymers were purified by repeated washing in CHCl$_3$ and dialyzing the powdered sample against mill-Q water using 2KDa molecular weight cut-off dialysis membrane for two days. The deprotected glucuronic acid functionalized polymers were readily soluble in water, DMF, DMSO and MeOH compared to its precursor protected polymer which was insoluble in water. The glucose functionalized polyfluorene had poor water solubility compared to the glucuronic acid functionalized counterpart. The detailed synthetic procedure for the monomers and polymers are given in the experimental section.

Both protected and deprotected polymers were characterized by NMR spectroscopy for chemical structure analysis and size exclusion chromatography (SEC) (using DMF as solvent) for molecular weight analysis. Broadening of proton NMR peaks and broad distribution in SEC indicated high molecular weight for the polymers. All the monomers and polymers including the glucose functionalized polymer PF-Ph-Glu were characterized by ^{1}H and ^{13}C NMR spectra. The proton NMR

spectra of deprotected polymers (PF-GlcA, PF-Ph-GlcA and PF-Ph-Glu) are shown in Figure 3.1. The peaks observed at δ 3.7 ppm for methyl ester and δ 2.15-2.0 for acetyl protons in the NMR spectra for the protected polymers were completely absent in case of deprotected polymers represented in Figure 3.1. The molecular weights (M_n and M_w) and polydispersity index ($Đ_M$) of the protected and deprotected polymers were determined by size exclusion chromatography (SEC) using DMF as solvent (Figure 3.2) and the corresponding values are tabulated in Table 3.1. The molecular weights of the new polymers were comparable with that of polyfluorenes functionalized with mannose reported in literature.[20] As expected, the observed molecular weights of the protected polymers were larger compared to that of the deprotected polymers due to the elimination of protecting functional groups during deprotection. The yield of the deprotected polymers is not 100 % because there was a little amount of protected polymers were present removed during the repeated washing with $CHCl_3$.

Table 3.1 Polymer designation, molecular weight, polydispersity index and yield of polymers before and after deprotection.

Name	M_n[a]	M_w[a]	Poly dispersity index $(Đ_M)$[a]	Yield (%)
PF-GlcA(OAc)	16800	25800	1.54	90
PF-Ph-GlcA(OAc)	20200	38300	1.89	85
PF-Ph-Glu(OAc)	17300	35800	2.07	87
PF-GlcA	15500	24200	1.56	78
PF-Ph-GlcA	17900	35900	1.94	80
PF-Ph-Glu	14200	25600	1.8	85

a. Molecular weights as determined by size exclusion chromatography using DMF as eluent at 30 °C and polystyrene standards for calibration.
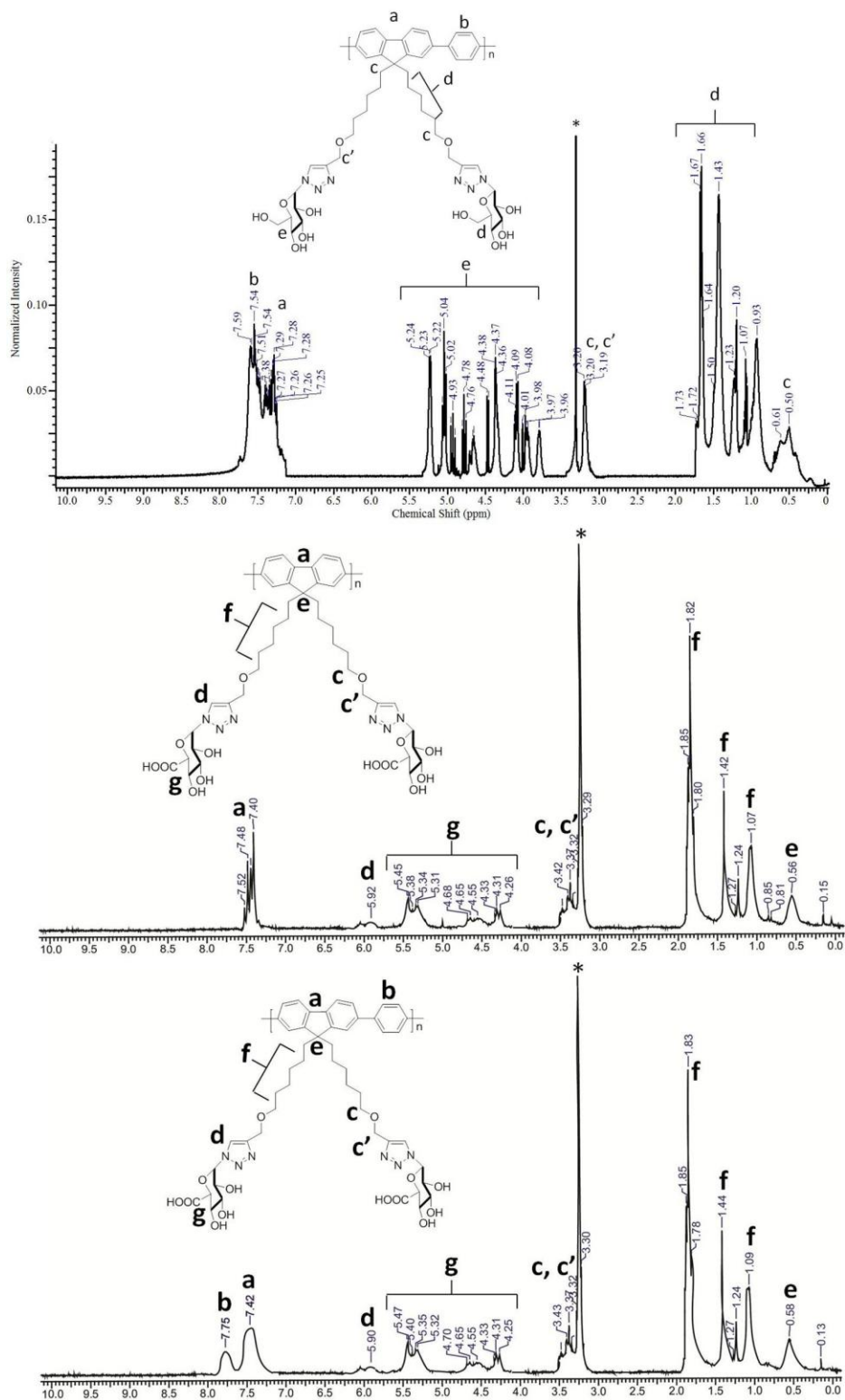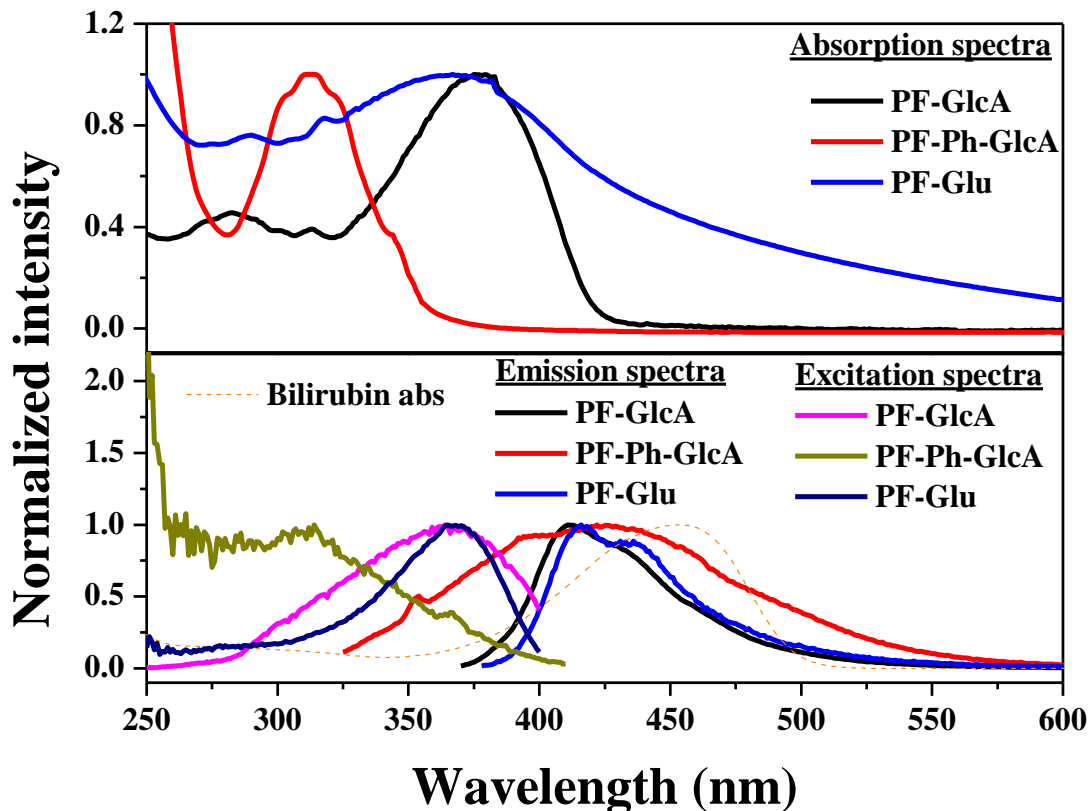
Figure 3.1 ^{1}H NMR spectra of PF-Ph-GlcA, PF-GlcA and PF-Ph-Glu in MeOH-D4.
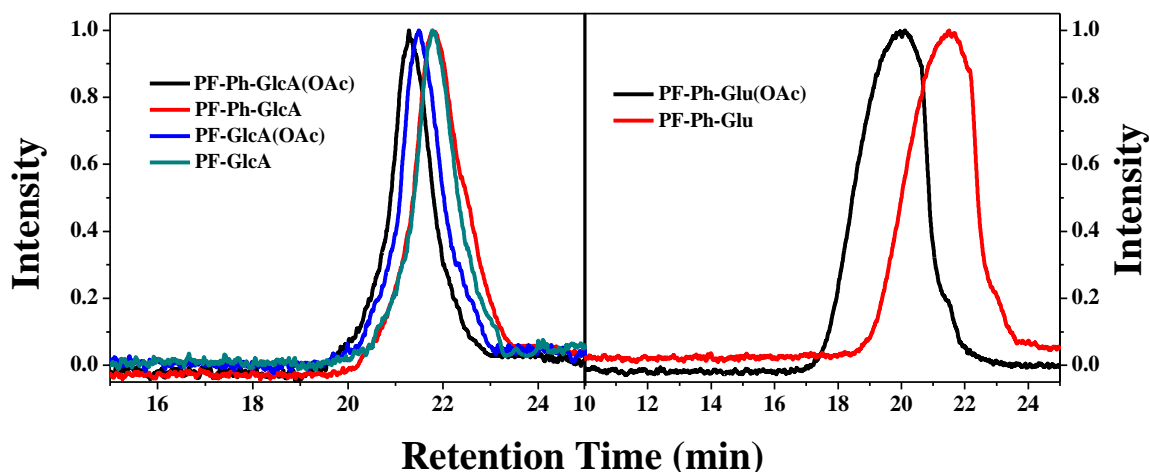
Figure 3.2 Size exclusion chromatogram of the polymers in DMF solvent.

3.3.2 Photophysical properties of the water soluble Polyfluorenes:

The normalized absorption and emission spectra of the synthesized polymers were recorded in PBS buffer at pH= 10. The normalized emission and excitation spectra at pH=10 are compared for the three polymers. It should be mentioned here that due to poor solubility of the glucose functionalized reference polymer in water at both the pH studied, its solution remained turbid. The excitation spectra were comparable with that of the absorption spectra of the polymers shown in Figure 3.3. The sensing studies to be discussed later on were all carried out at pH=10, therefore the photophysical studies carried out at pH=10 is discussed in detail here. Figure 3.3 compares the absorption (top) and emission, excitation (bottom) spectra of the three polymers in PBS buffer at pH=10. PF-Ph-GlcA copolymer and PF-GlcA homopolymer showed absorption centered at 315 nm and 360 nm respectively. The absorption spectrum of PF-Ph-Glu was broad (maximum ~ 360 nm) and the baseline was high due to scattering. The emission maximum of 0.1 OD aqueous solutions of the polymers PF-Ph-Glu excited at 315 nm, PF-Ph-GlcA, and PF-GlcA excited at 360 nm was observed around 410-420 nm. The peak appearing at 350 nm in the emission spectra of PF-Ph-GlcA corresponded to the water Raman peak.[21] The emission spectrum of the polymers overlapped with the absorption maximum of bilirubin (target analyte) at 455 nm (denoted in dotted line), thereby favoring energy transfer from polymer to bilirubin.

Figure 3.3 Absorption (top) and emission, excitation spectra (bottom) of PF-Ph-Glu, PF-Ph-GlcA and PF-GlcA polymers along with absorption of bilirubin (dotted line, bottom Figure) in PBS buffer at pH=10.

The fluorescence quantum yield of the polymers were determined in water at neutral pH using quinine sulfate (Φ_{fl} = 0.546 in 0.1 M H_2SO_4) as reference. The calculated quantum yield for PF-Ph-GlcA polymer was 0.43 and for PF-GlcA was 0.48. The quantum yield of the homopolymer (PF-GlcA) was slightly higher than PF-Ph-GlcA because the solubility of PF-GlcA (5 mg/ml) was better in water compared to that of PF-Ph-GlcA (2 mg/ml). The quantum yield of PF-Ph-Glu was not determined due to the turbid nature of the solution.

3.3.3 Fluorescence Sensing of Free Bilirubin in Water:

Sensing of free bilirubin in water was targeted taking the key advantage of spectral overlap between emission of polymers and absorption of bilirubin which is the necessary condition for feasible FRET to occur.[22] The glucuronic acid functionalization imparted water solubility to the polymer, facilitating sensing studies

to be carried out in water. The bilirubin molecule is a tetrapyrrole moiety, which exists in the ridge tile conformation due to several intramolecular hydrogen bonds. It has been variously reported in literature as a porphyrin-like-structure or linear representation. Single crystal X-ray structure of bilirubin has confirmed the *Z* configuration at the C4-C5 and C15-C16 position.[23] The gross structure of bilirubin is shown in Scheme 3.3 in its linear representation. Bilirubin is reported to have a very low solubility of ~7 nanomoles in water at pH = 7.4.[24] A pH of ~10 is required to induce solubility in water by breaking the hydrogen bonding in bilirubin. Therefore, studies involving bilirubin are usually reported at pH = 10 in the literature.[25]
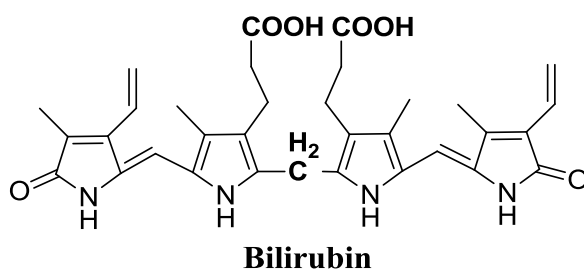
Bilirubin

**Scheme 3.3** Gross structure of bilirubin in its linear representation.

Thus stock solutions of bilirubin and polyfluorene were prepared at pH=10. Figure 3.4a shows the absorption spectrum of the homopolymer PF-GlcA upon addition of various concentration of bilirubin ranging from 1×10^{-6} M to 1×10^{-4} M in water at pH=10. The concentration of the polymer was kept constant at 1×10^{-6} M (1 μM). When the concentration of bilirubin was increased, an increase in the absorption of bilirubin at 455 nm was observed. Figure 3.4b shows the corresponding emission spectra upon excitation at 360 nm. Similar sensing experiments were conducted for the copolymers (PF-Ph-GlcA and PF-Ph-Glu) in water as shown in Figure 3.4c-f. Similar conditions of addition of bilirubin to polymer in water were followed and fluorescence quenching of the polymer was monitored. The notable observation was the quenching of polymer fluorescence with concurrent increase in the emission of bilirubin at 520 nm. Figure 3.5 shows emission spectra of PF-GlcA, normalized at polymer emission maxima highlighting the FRET induced bilirubin emission. A clear visual color change from blue fluorescence to light green was observed at higher concentrations of bilirubin, which is shown in the inset image of Figure 3.5. Bilirubin

does not emit in any solvent (including water) due to inherent property of poor quantum yield. However, upon interaction with the polymer, mediated by the glucuronic acid moiety, enhanced green emission of bilirubin was observed. The intensity of the bilirubin emission observed in this PF-bilirubin system was much higher compared to that of bilirubin complexed with HSA protein reported in literature.[25]
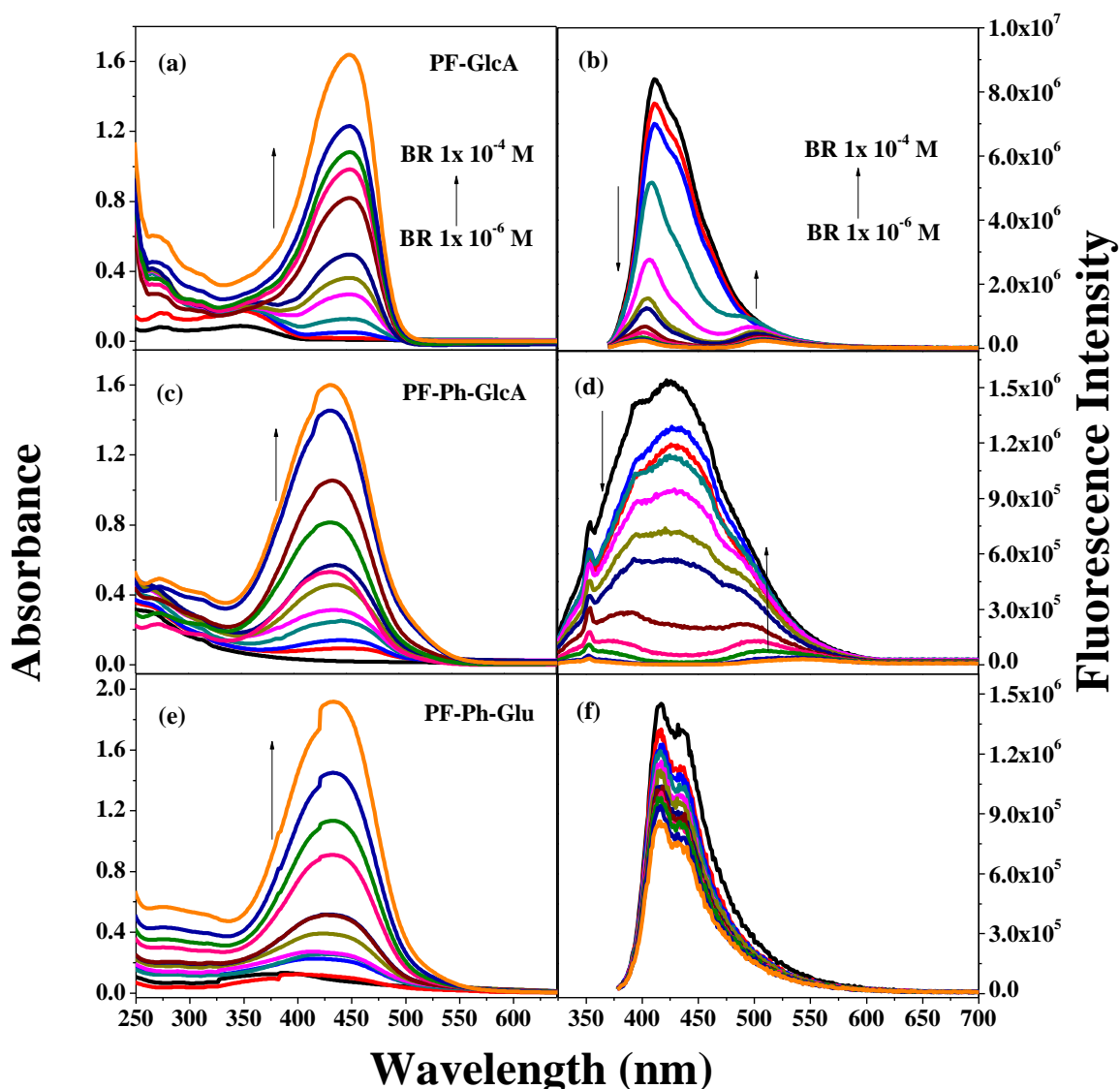

Figure 3.4 (a, c, e) Absorption and (b, d, f) Emission spectra of PF-GlcA, PF-Ph-GlcA and PF-Ph-Glu (1µM) respectively in water at pH=10 upon addition of various concentrations of Bilirubin from 1×10^{-6} M to 1×10^{-4} M.

Direct excitation at the bilirubin absorption maxima at 455 nm showed a steady increase in the bilirubin emission intensity with increase in the concentration of bilirubin as shown in Figure 3.6. FRET induced bilirubin emission at 520 nm that was observed upon excitation of the polymer in water highlighted the potential of the polymer as a biosensor.
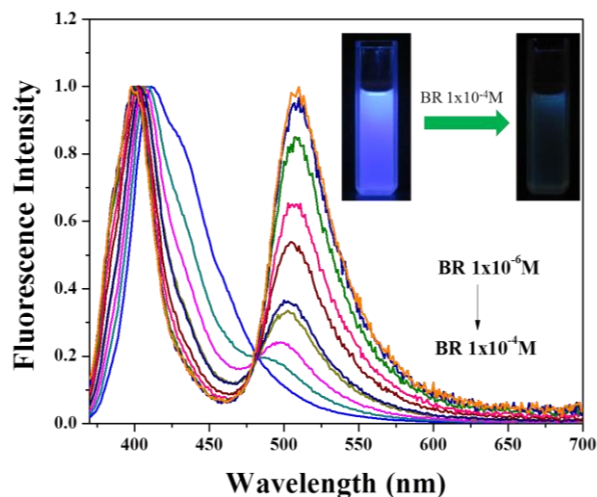
Figure 3.5 Normalized emission spectra of PF-GlcA in water upon addition of various concentration of bilirubin ranging from $1x10^{-6}M$ to $1x10^{-4}M$ (excitation λ=360 nm; normalized at 410 nm)
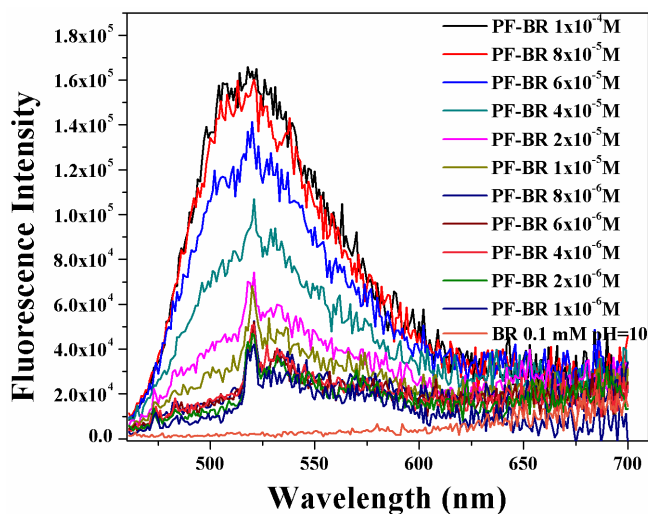

Figure 3.6 Emission spectra of bilirubin in water (excitation λ=455 nm) for the polymer- bilirubin complex in PF-GlcA polymer upon addition of various concentration of bilirubin.

The changes in the fluorescence intensity of the polymers in the plot of Figure 3.4 upon addition of bilirubin were plotted against the concentration of bilirubin and the result is given in Figure 3.7a. From the plot it could be seen that the homopolymer PF-GlcA exhibited a sharper drop in the polyfluorene emission upon addition of bilirubin with almost complete quenching of the blue polymer fluorescence at 20 μM concentration of bilirubin. The copolymer exhibited complete quenching of the polymer fluorescence at 40 μM concentration of bilirubin. On the other hand, the glucose appended polymer PF-Ph-Glu exhibited very poor quenching of polymer fluorescence with only 40 % quenching observed even for the highest addition of bilirubin ($1x10^{-4}$ M). In fact, beyond 10 μM of bilirubin, the polymer fluorescence remained unaffected. Figure 3.7b compares the intensity of FRET induced bilirubin emission upon excitation of polymers at the polymer absorption maximum, which also showed that the homopolymer exhibited higher FRET induced bilirubin emission compared to the copolymers at higher bilirubin concentrations in water. The emission from bilirubin was almost non-observable in the case of the glucose appended polymer PF-Ph-Glu. The better sensing efficiency of the homopolymer compared to the copolymers could be attributed to the greater number of glucuronic acid appendage per repeat unit present in the former compared to the latter, which facilitated better polymer-analyte interaction. Isothermal titration calorimetric (ITC) experiments (to be discussed later on) pointed towards a higher binding constant for the homopolymer with bilirubin, which also supported this observation of better sensing efficiency for the homopolymer. Thus the above experiment stressed the importance of interaction between the polyfluorene and free bilirubin in facilitating the biosensing property of the polymers.

### 3.3.4 Sensing of Bilirubin in Human Serum Samples:

To understand the reliability of the new polymers for biosensing applications, sensing studies were proposed to be carried out in human serum containing interferences such as hemoglobin, proteins, triglyceride, cholesterol, glucose and metal ions.
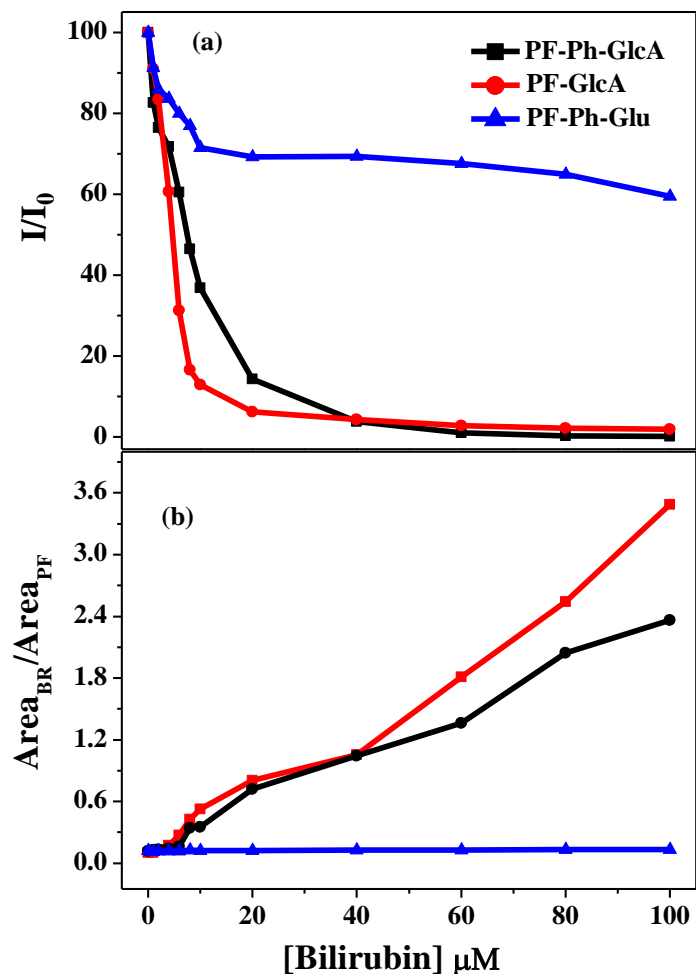
Figure 3.7 (a) Ratio of fluorescence Intensity of polymers observed at emission maximum to that of the initial emission intensity and (b) extent of FRET emission of bilirubin (Integrated area of bilirubin emission / Integrated area of polymer emission) as a function of bilirubin concentration.

Although the homopolymer (PF-GlcA) showed better sensing activity in water, it could not be used for sensing studies in human serum due to its tendency to aggregate (discussed in detail later on). The bilirubin sensing studies in human serum was conducted with the copolymers PF-Ph-GlcA and PF-Ph-Glu. 0.1 ml of human serum was mixed with free bilirubin in the concentration range of 1×10^{-6} M to 1×10^{-4} M and this mixture was added to 1 µM solution of the polymers. A blank experiment was performed by recording the emission of bilirubin in water as well as in serum at pH = 10 in the absence of polymer. Figure 3.8 compares the emission intensity from

bilirubin upon excitation at 325 nm (the polymer absorption wavelength which was used to excite the polymer in the actual bilirubin sensing experiments) as well as at 455 nm (the bilirubin absorption maximum). Bilirubin in water at pH=10 did not exhibit any fluorescence upon excitation at 325 nm or 455 nm. In serum at pH =10, bilirubin exhibited a weak emission centered at 520 nm indicating that selective excitation of polymer at 325 nm was not possible due to the not so negligible absorption of bilirubin at 325 nm. Direct excitation at 455 nm resulted in sharp emission from bilirubin at 520 nm.
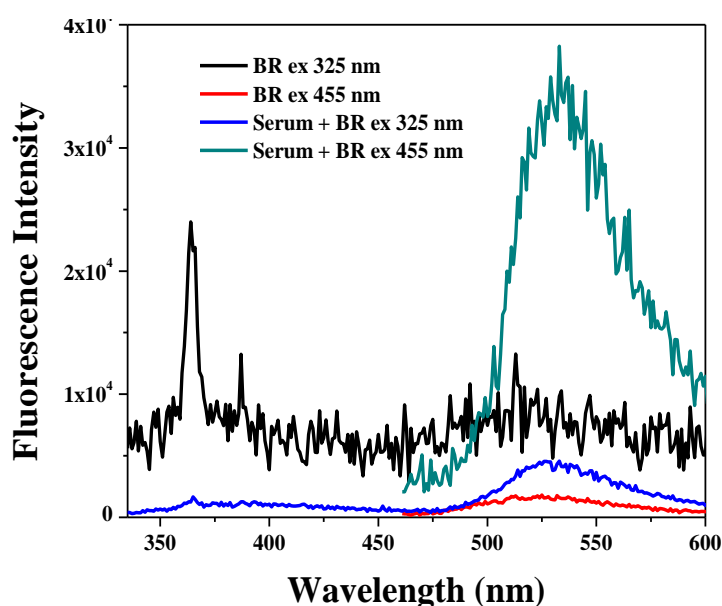
Figure 3.8 Emission spectra of bilirubin in water and in serum at pH = 10 (excitation λ= 325 nm and 455 nm) in the absence of polymer.

Figure 3.9.a-d demonstrates the changes in the photophysical properties of the probe for various concentrations of the analyte. In the absorption spectrum (Figure 3.9.a), human serum exhibited strong absorption of light below 300 nm indicating the presence of other analytes. In the emission spectrum of PF-Ph-GlcA (Figure 3.9.b), blue fluorescence of the polymer quenched upon addition of bilirubin with concurrent appearance of light green emission from bilirubin. The photograph of the visual color change from blue to green observed in the serum is given as inset in Figure 3.9.b highlighting the sensing ability of PF-Ph-GlcA in human serum. The

emission plot also shows the emission from bilirubin in serum at pH =10 which indicated that its intensity was negligible compared to the FRET induced emission from bilirubin in presence of polymer. From the Figure 3.9.d it could be seen that the quenching of fluorescence of polymer upon addition of bilirubin was much less for the reference glucose appended polymer PF-Ph-Glu and also the FRET induced bilirubin emission was almost negligible. Figure 3.10 compares the efficiency of FRET induced bilirubin emission for both polymers for increasing additions of bilirubin. The plot gives the ratio of the integrated areas of bilirubin emission (486-600 nm) to that of polymer emission (335 − 486 nm) as a function of increasing concentration of bilirubin.
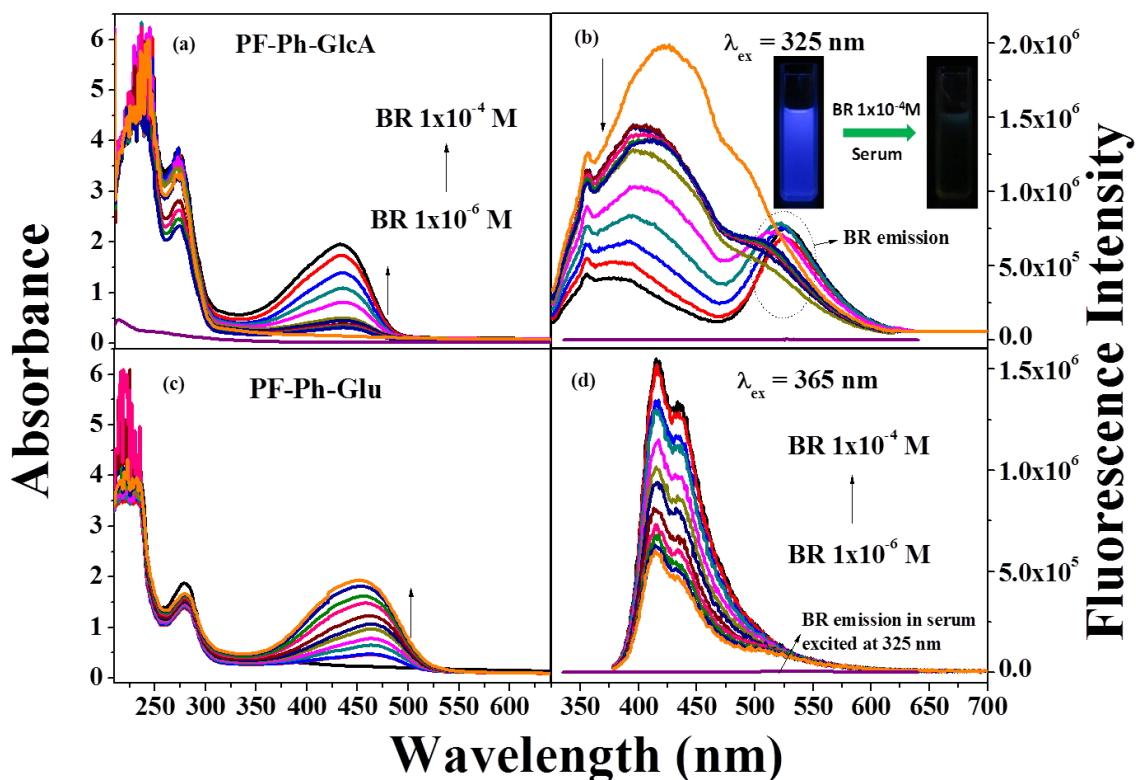

Figure 3.9 (a, c) Absorption and (b, d) emission spectra of PF-Ph-GlcA and PF-Ph-Glu respectively in human serum upon addition of various concentrations of Bilirubin from $1x10^{-6}$ M to $1x10^{-4}$ M in phosphate buffered saline at pH=10. (The emission from $1x10^{-4}$ M bilirubin in serum upon excitation at the polymer absorption wavelength is also included in the emission spectra).

PF-Ph-GlcA exhibited more than five-fold increase in bilirubin emission compared to PF-Ph-Glu at the highest added bilirubin concentration of 10^{-4} moles. The reduction in fluorescence emission (area under the emission plot) as a function of increasing bilirubin concentration is compared between the polymers. The drop was much steeper for the glucuronic acid functionalized polymer thereby once again establishing its superiority as a bilirubin sensor. Although the photophysical criteria for FRET based energy transfer from polymer to bilirubin was favorable for both polymers PF-Ph-GlcA and PF-Ph-Glu, the higher tendency of the glucuronic acid-bilirubin interaction in the former compared to the low or non-interacting glucose-bilirubin combination in the latter acted in favor of PF-Ph-GlcA to behave as a better sensor for bilirubin in human serum. Additionally, the low solubility of PF-Ph-Glu also could have resulted in the poor performance of PF-Ph-Glu as an efficient bilirubin sensor. Thus, among the three polymers examined for sensing bilirubin, only the glucuronic acid appended copolymer i.e. PF-Ph-GlcA was found to be effective for sensing bilirubin in human serum. Therefore, only PF-Ph-GlcA was taken up for further detailed studies to better understand its biosensing characteristics.
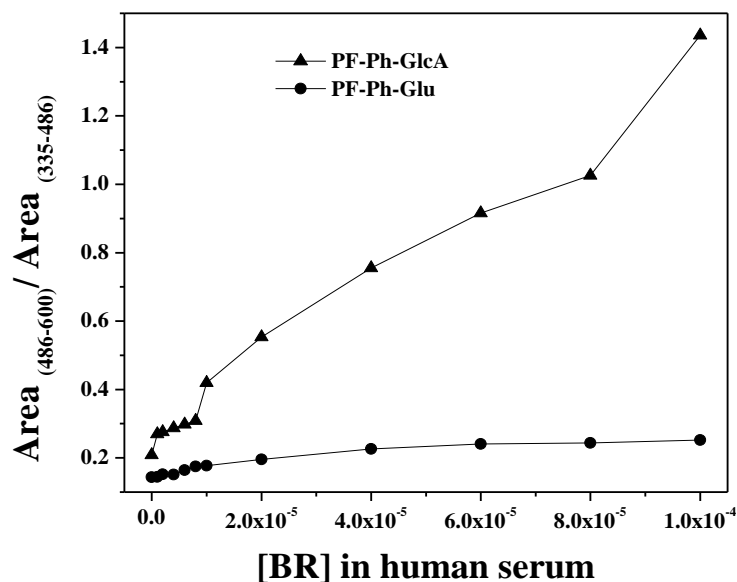
Figure 3.10 Ratio of integrated area of FRET induced bilirubin emission (486 − 600 nm) to that of the polymer emission (335 − 486 nm) for PF-Ph-GlcA and PF-Ph-Glu in serum as a function of bilirubin concentration.

Although the homopolymer PF-GlcA had exhibited better sensing efficiency for bilirubin in water compared to the copolymer, its employment for sensing studies in serum could not be carried out. This was due to the considerable quenching of fluorescence as well as aggregate emission at 550 nm, which hampered observation of the bilirubin emission beyond 520 nm in serum. Figure 3.11 shows the reduction in fluorescence intensity ~ 410 nm and aggregate emission at 550 nm exhibited by the homopolymer (PF-GlcA) in serum.
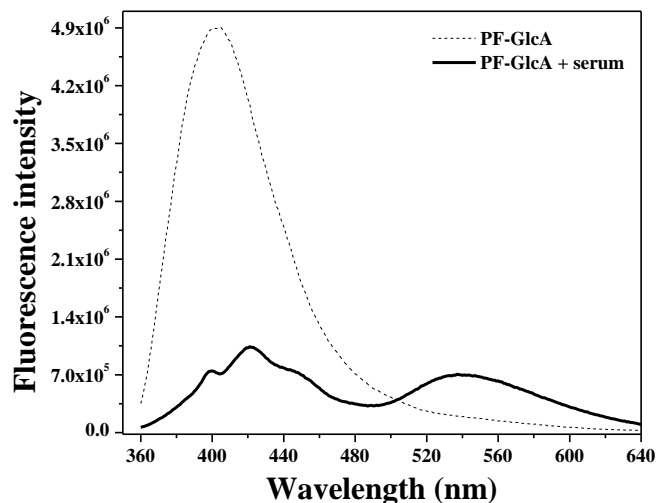
Figure 3.11 Emission spectrum of PF-GlcA polymer in PBS buffer at pH=10 upon addition of Serum and excited at 360 nm

Dynamic light scattering (DLS) studies conducted both in water as well as in serum also supported the tendency of the homopolymer to form large size aggregates in serum. In water, PF-GlcA exhibited particle size of 330 nm whereas PF-Ph-GlcA formed smaller particles with size of 110 nm (Figure 3.12.b). Figure 3.12.a-d compares the size versus intensity plot from the DLS studies for the three polymers in water and serum and the DLS spectrum of human serum is shown in Figure 3.12.a. The Figure 3.12.a shows that the serum itself exhibited multimodal distribution of particle size due to presence of proteins and other ingredients. From Figure 3.12.c and 3.12.d it could be seen that while the copolymer did not exhibit any changes in the inherent size of the particles upon addition of serum (Figure 3.12.c), the homopolymer exhibited both broadening of its inherent particle size as well as appearance of new broad peak at higher particle size (Figure 3.12.d). It could be

inferred from the above results that the homopolymer PF-GlcA with higher volume ratio of glucuronic acid tend to adhere to the hydrophilic patches of proteins[26] in serum resulting in polymer aggregation in serum. Therefore, it is essential to design a polymer with optimum content of glucuronic acid appendage so as to avoid adherence to proteins.
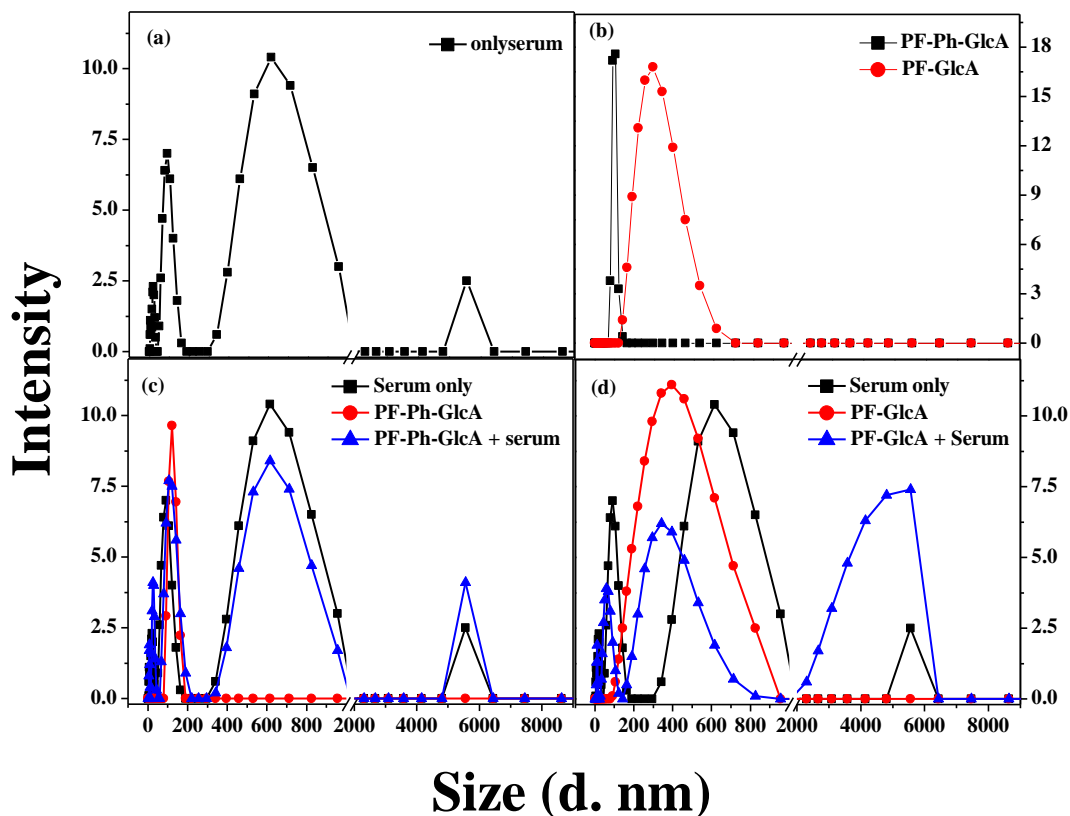

Figure 3.12 DLS plot of (a) serum, (b) polymers in water, (c) PF-Ph-GlcA and (d) PF-GlcA in PBS buffer at pH=10 upon addition of serum. The concentration of polymers was 1μM and serum of 100 μL was added to the polymer solution.

3.3.5 Identification of the Interactions Between Polymer and Bilirubin:

The nature of interaction existing between the new polymers appended with D-glucuronic acid and bilirubin in water medium was identified using ITC. ITC measures the heat changes produced in the course of the addition of bilirubin acting as ligand to the polymer acting as the macromolecule. High concentration of bilirubin (20 mM) was required to observe saturation of polymer-bilirubin interaction in the ITC experiment. Such high concentrations of bilirubin could be fully solubilized only

in PBS buffer at pH=12. Thus, 20 mM of bilirubin solution in PBS buffer at pH = 12 was added in injections of 2 μL volume to 200 μL polymer solution at a concentration of 2 mM. Corresponding results of heat changes during the course of addition for both the polymers PF-GlcA and PF-Ph-GlcA are given in Figure 3.13.a, b and 3.13.c, d. The outcome of the results revealed the exothermic nature of the interaction between polymer and bilirubin. To eliminate the solvent-solvent and solvent-bilirubin interactions, blank reactions without polymer was also carried out.
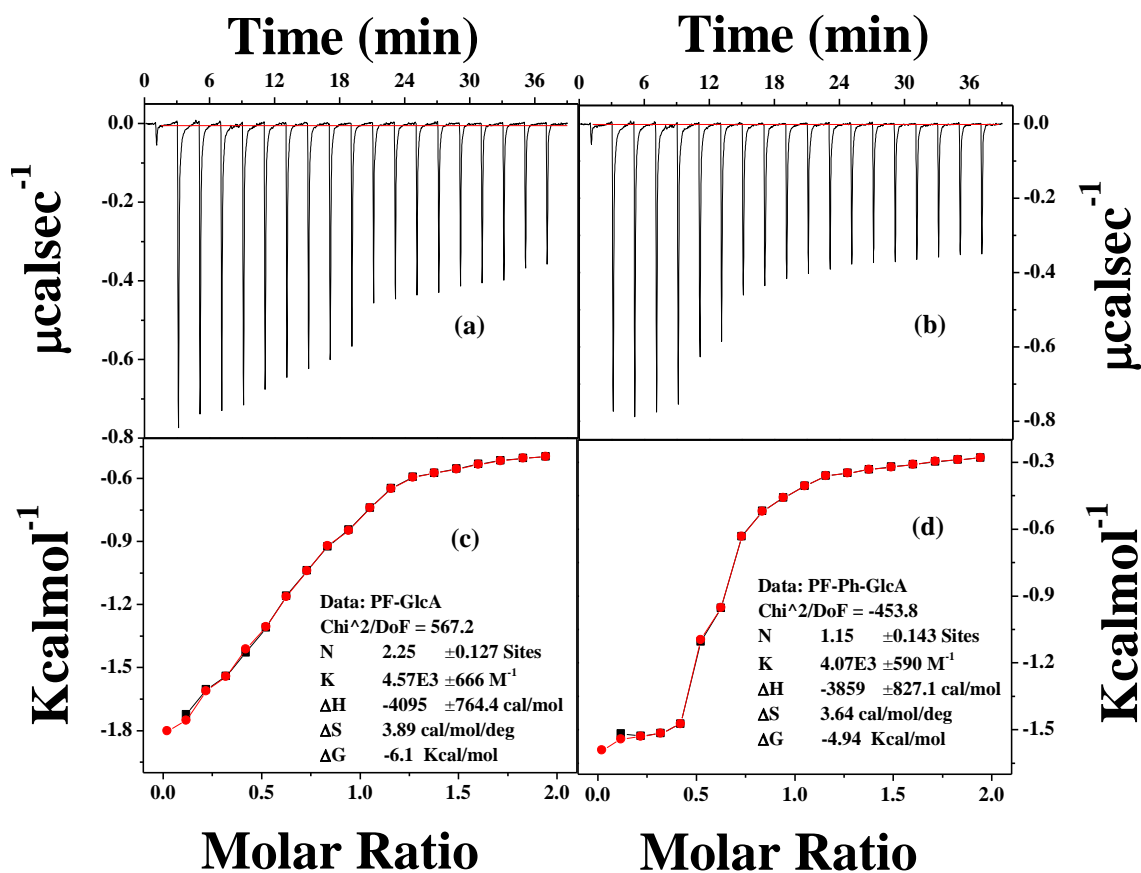
Figure 3.13 Isothermal calorimetric thermograms (a, c) for the injection of 2 μL of 20 mM bilirubin into 2 mM PF-GlcA and PF-Ph-GlcA at an interval of 3 minutes at pH=12 and (b, d) the respective sigmoidal fit.

The blank heat change value was subtracted from the heat change value for the polymer-bilirubin complex. The fitting in Figure 3.13.c and 3.13.d and calculation methods are given under the methods and materials section. The free energy change for the reactions obtained in the negative scale indicated the spontaneity of the

binding of bilirubin with the polymer. The free energy change ΔG for the binding of bilirubin with PF-GlcA was –6.1 Kcal/mol while that for binding with PF-Ph-GlcA polymer was –4.94 Kcal/mol. Generally, the Gibbs free energy change for electrostatic type of interactions and hydrogen bonding interactions falls in the range of –(15-30) kcal/mol and –(2-10) kcal/mol respectively.[27] From the values of ΔG of polymer-bilirubin complex, the type of interaction between the polymer and bilirubin was identified to be that of hydrogen bonding interactions. The OH and COOH groups of glucuronic acid appendage on the polyfluorene could be expected to play a key role in making hydrogen bond interactions with COOH and NH moieties present in the pyrrole ring of the bilirubin. The binding constants for the interaction between bilirubin and polyfluorenes were 4.57 x 10^3 M^{-1} for PF-GlcA polymer and 4.07 x 10^3 M^{-1} for PF-Ph-GlcA respectively. The stoichiometry of the interaction was obtained as 2.25 for homopolymer (PF-GlcA) and 1.13 for copolymer (PF-Ph-GlcA). As the homopolymer PF-GlcA contained relatively more glucuronic acid side chains per mole than the copolymer PF-Ph-GlcA, the PF-GlcA has higher possibility for non-covalent interactions resulting in higher binding constant. Therefore, the homopolymer showed relatively higher sensing activity in water compared to the copolymer. Unfortunately, the sensing activity of homopolymer in serum was hindered due to its severe aggregation in serum.

3.3.6 Fluorescence Lifetime:

For a better understanding of the energy transfer processes taking place between the polymer and bilirubin, time correlated single photon counting (TCSPC) analysis of the fluorescence lifetime was utilized. Time resolved fluorescence decays were collected for the polymers PF-Ph-GlcA and PF-GlcA at 420 and 410 nm with excitation from nano LED at 320 and 375 nm in PBS buffer at pH=10 at 25 ^{0}C. The decay curve for the polymer PF-Ph-GlcA is shown in Figure 3.14.a. The fluorescence decays were fitted to a biexponential fit and the lifetime values are given in Table 3.2. PF-Ph-GlcA exhibited a lifetime of τ_1= 457 ps and τ_2=2.42 ns with α_1=0.87 and α_2= 0.13. Upon addition of various concentrations of bilirubin, the lifetime of the polymer decreased drastically to a minimum value of τ_1=21 ps and τ_2=2.56 ns with α_1=1 and α_2= 0. Time resolved fluorescence decays were also collected at 520 nm (bilirubin

emission) for 320 nm excitation. Figure 3.14.c reveals the decay curve for excitation at 320 nm and collection at 520 nm upon various additions of bilirubin to PF-Ph-GlcA polymer. This graph confirmed the increase in the lifetime of bilirubin in the polymer-bilirubin complex giving evidence for the FRET process.
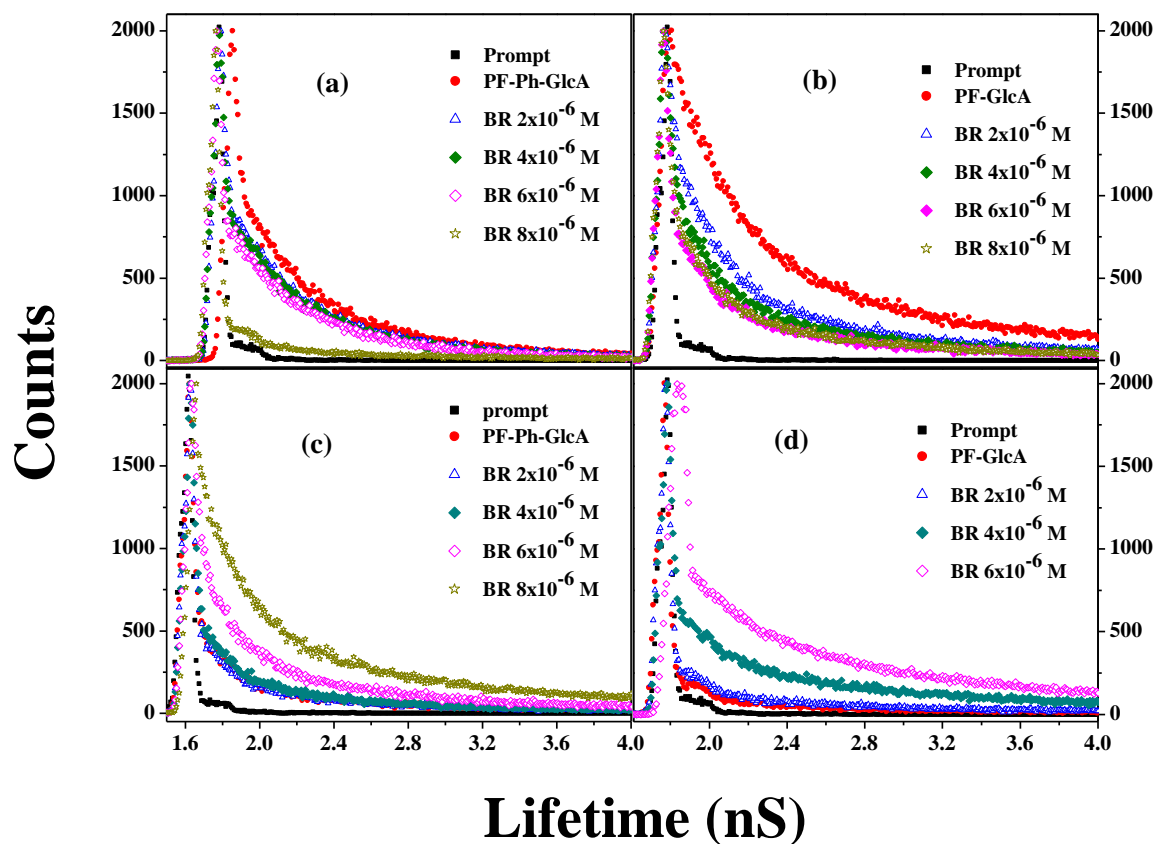
Figure 3.14 Picosecond time resolved lifetime measurements for (a, c) PF-Ph-GlcA polymer (1μM) (excitation at 320 nm and collection 420 nm; excitation at 320 nm and collection 520 nm respectively) and (b, d) PF-GlcA (excitation at 375 nm and collection at 410 nm; excitation at 375 nm and collection 520 nm respectively) at various concentration of bilirubin ranging from 1×10^{-6} M to 8×10^{-6} M in PBS buffer at pH=10.

The increase in the lifetime values of bilirubin are given in the Table 3.2. Similar behavior was observed for PF-GlcA homopolymer that showed lifetime of τ_1= 470 ps and τ_2=3.54 ns with α_1=0.89 and α_2= 0.11. The lifetime value of the polymer decreased continuously with the addition of bilirubin and on final addition of analyte the value reached τ_1=52 ps and τ_2=1.54 ns with α_1=0.97 and α_2= 0.03. The

corresponding decay curve for polymer (PF-GlcA) is shown in Figure 3.14.b and d. The decay curve for excitation at 375 nm and observation at 520 nm is given in Figure 3.14.d. The rise in the lifetime of the bilirubin values are tabulated in Table 3.3

Table 3.2 Lifetime fitting parameters (τ: decay time, α: pre-exponential factor, χ^2: chi-squared value) retrieved from the biexponential fit. The decay time was collected for PF-Ph-GlcA at 420 nm and PF-GlcA at 410 nm by using nano LED 320 and 375 nm for excitation for various additions of bilirubin.

| PF-Ph-GlcA lifetime; excited 320 nm; collected at 420 nm					
Sample	τ_1 **(ps)**	τ_2 **(ns)**	α_1	α_2	χ^2
PF-Ph-GlcA	457	2.42	0.87	0.13	1.24
BR 1×10^{-6}M	439	2.29	0.87	0.13	1.25
BR 2×10^{-6}M	247	1.12	0.89	0.11	1.003
BR 4×10^{-6}M	148	1.09	0.89	0.11	1.005
BR 6×10^{-6}M	37	1.14	0.92	0.08	1.008
BR 8×10^{-6}M	21	2.56	1	0	1.012
PF-GlcA lifetime; excited 375 nm; collected at 410 nm					
Sample	τ_1 **(ps)**	τ_2 **(ns)**	α_1	α_2	χ^2
PF-GlcA	470	3.54	0.89	0.11	1.14
BR 2×10^{-6}M	348	2.81	0.90	0.1	1.18
BR 4×10^{-6}M	267	2.21	0.91	0.09	1.15
BR 6×10^{-6}M	146	1.94	0.93	0.07	1.12
BR 8×10^{-6}M	52	1.54	0.97	0.03	1.09

Table 3.3 Lifetime values of polymers. Ex at λ=320, 375 nm; Collection at λ=520 nm.

Sample	τ_1 in ps (α1)	τ_2 in ns (α2)	χ^2	Sample	τ_1 in ps (α1)	τ_2 in ns (α2)	χ^2
PF-Ph-GlcA	97(0.93)	1.42(0.07)	1.14	PF-GlcA	87(0.91)	2.18(0.09)	1.17
BR (alone)	25 (1)	-	1.02	BR (alone)	25 (1)	-	1.03
BR 2x10^{-6}M	45(0.91)	1.12(0.09)	1.1	BR 2x10^{-6}M	50(0.91)	1.34(0.09)	1.09
BR 4x10^{-6}M	83(0.89)	1.69(0.11)	1.14	BR 4x10^{-6}M	93(0.90)	1.81(0.10)	1.19
BR 6x10^{-6}M	106(0.86)	1.94(0.14)	1.08	BR 6x10^{-6}M	128(0.89)	2.24(0.11)	1.12
BR 8x10^{-6}M	121(0.85)	2.56(0.15)	1.11	BR 8x10^{-6}M	139(0.87)	2.67(0.13)	1.16

Simultaneous decrement in fluorescence lifetime of the polymer and increase in the lifetime of the bilirubin strongly supported the occurrence of FRET from polymer to bilirubin.

3.3.7 Selectivity and Sensitivity of Bilirubin Sensing in Human Blood Serum:

Sensing of analyte in presence of crucial interferences is important in order to establish the potential of the sensor for real world biosensing applications. Human serum contains components such as hemoglobin, proteins, iron, cholesterol, glucose, sodium etc. The $_D$- glucuronic acid appended PF-Ph-GlcA polymer could selectively sense bilirubin in presence of these components of blood. The porphyrin unit of hemoglobin has structural similarity to bilirubin, but as demonstrated by a control experiment, where the polymer was added to human serum sample in the absence of added bilirubin, (Figure 3.15), the emission of polymer (PF-Ph-GlcA) did not quench in the serum. Despite the similarity in chemical structure, the closed ring structure of hemoglobin prevented hydrogen bonding interaction with the polymer.
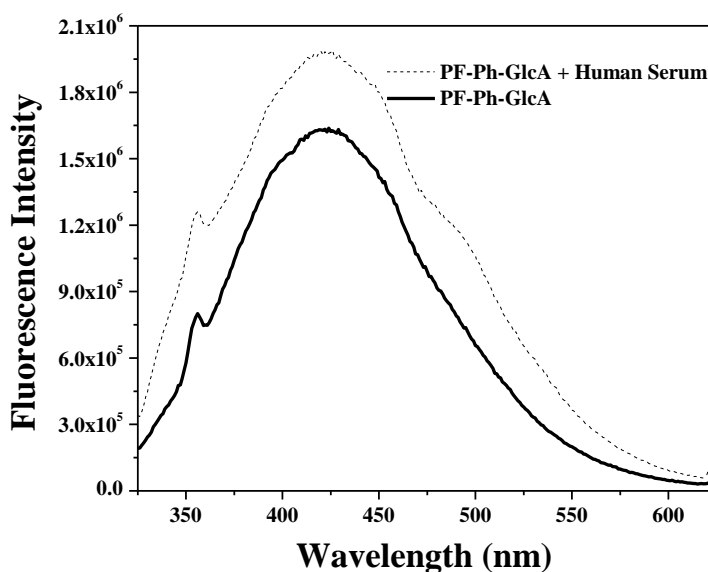
Figure 3.15 Polymer (PF-Ph-GlcA) emission spectrum in PBS buffer at pH=10 upon addition of Human blood serum (excited at 315 nm).

In fact, HSA is known to bind to free bilirubin with high affinity; however, the polymer exhibited competitive binding with free bilirubin in human serum sample via the hydrogen bonding interactions of its $_D$-glucuronic acid appendage. This was evident from the quenching of polymer emission in human serum samples containing bilirubin. Other notable interferences such as biliverdin which is the structural analogue of bilirubin, rhodamine, cholesterol, glucose, and sucrose were

supplemented in fixed concentration $(1 \times 10^{-4}$ M) to 100 µL serum in separate experiments. The polymer PF-Ph-GlcA concentration was fixed at 1µM and the total volume of the experimental solution was made up to 2.5 ml with PBS buffer. Each sensing experiment was performed four times and the average fluorescence response of the polymer was recorded and plotted against respective analytes in Figure 3.16a as a bar graph representation with error bars.
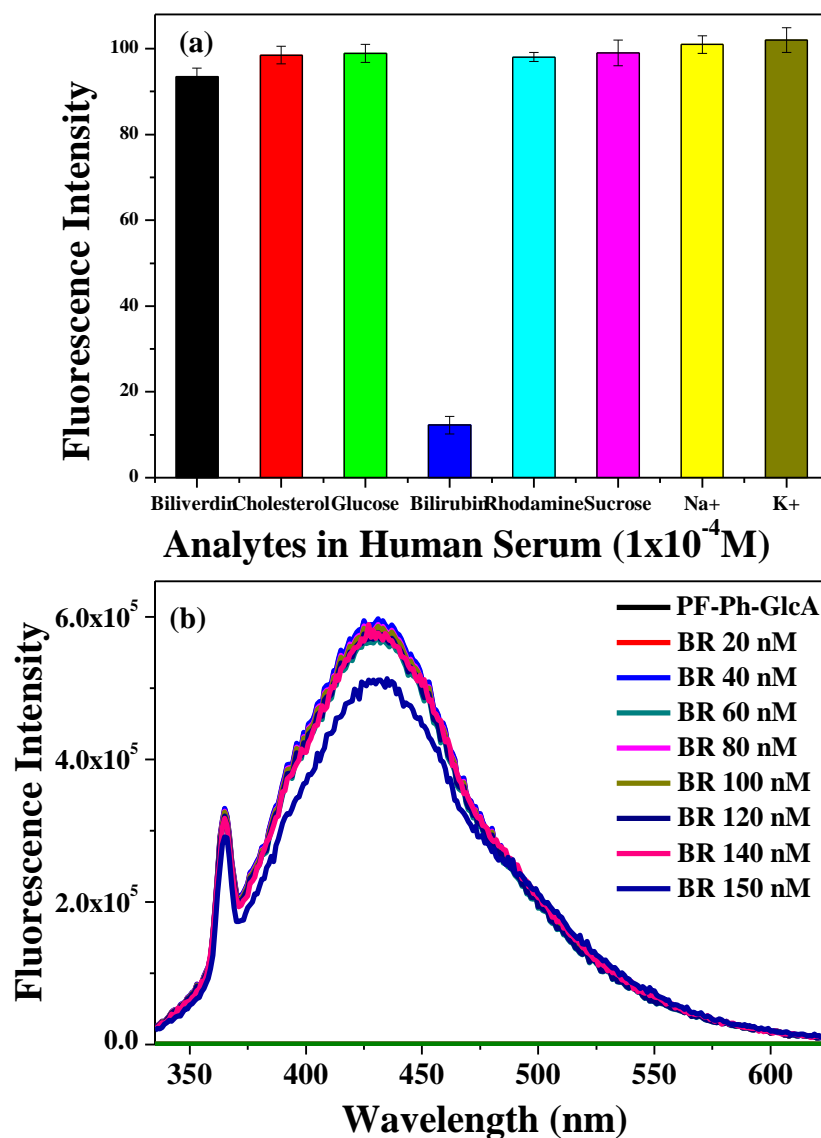

Figure 3.16 a) Bar diagram depicting the effect of various interfering analytes on the fluorescence intensity of PF-Ph-GlcA in human serum. The analyte concentration was kept constant at 1×10^{-4} M (b) Nanomolar sensing by PF-Ph-GlcA in human serum, [polymer] = 1×10^{-5} M.

Besides selective sensing, sensitivity of detecting nanomolar amounts of analyte is also an important requirement for an efficient sensor. Therefore, nanomolar amounts of bilirubin (1 − 150 nm) was added to a $2x10^{-5}$ M solution of PF–Ph–GlcA in human serum at pH =10. Figure 3.16b depicts the change in fluorescence emission from polymer upon addition of various nanomolar concentration of bilirubin. A 10 % reduction in total area of fluorescence emission was observed upon addition of 150 nm of bilirubin. This was well below the clinically relevant range of < 25 μmol/L to > 50 μmol/L bilirubin observed in the human blood serum. Thus, the selectivity and sensitivity experiments demonstrated the superior performance of the glucuronic acid appended polyfluorene – PF–Ph–GlcA as a biosensor for sensing bilirubin in human serum.

A huge decrement in fluorescence intensity of polymer was observed only with the addition of bilirubin highlighting the high selectivity of new polymer towards bilirubin in human blood serum samples. To differentiate the type of bilirubin, the fluorescence experiment under same conditions were conducted keeping conjugated bilirubin as the analyte. Conjugated bilirubin (B_c) was prepared following reported literature procedure and the details are given in the experimental section.[18] There was not much change observed for the emission intensity of the polymer in presence of conjugated bilirubin, indicating its poor interaction with the polymer (Figure 3.17).

Conjugated bilirubin was incapable of hydrogen bonding interactions with the glucuronic acid appendage; thereby disabling the polymer from binding the conjugated bilirubin. Biliverdin is a structural analogue of bilirubin, with an extra double bond in the C10 position, which makes the two dipyrromethene units conjugated.[28] Although this structural change is very small, it makes biliverdin more rigid compared to bilirubin. The probability of hydrogen bond interaction between biliverdin and glucuronic acid is good; however, a probable non-favorable conformation of the former could be the reason for the observed poor quenching of polymer fluorescence.
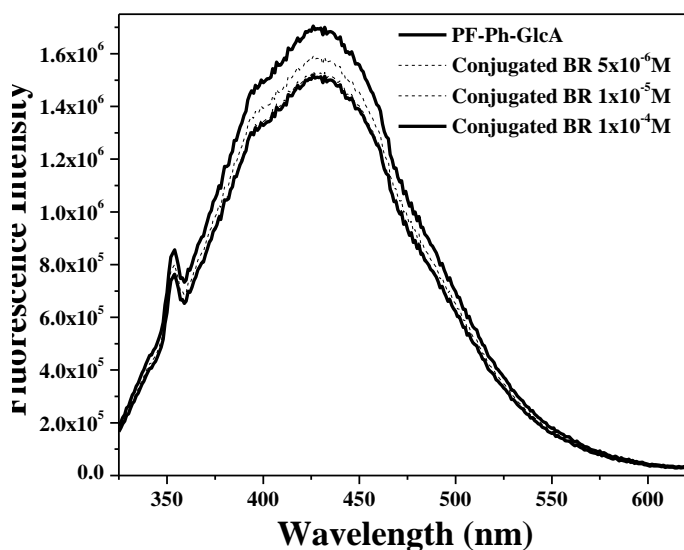
Figure 3.17 Emission spectra of PF-Ph-GlcA in presence of various concentrations of conjugated bilirubin in PBS buffer at pH=10 in serum

3.3.8 Mechanism of sensing:

The aforementioned experiments displayed the ability of the glucuronic acid appended polyfluorene to function as a highly selective and sensitive visual sensor for sensing bilirubin. The appendage of $_D$-glucuronic acid performed the dual role of imparting water solubility to the polymer and interacting with the analyte through hydrogen bonding. The polymer exhibited good extent of spectral overlap with bilirubin in water as well as in human serum, which was the necessary condition to facilitate energy transfer from polymer to bilirubin. When bilirubin was added to the polymer in aqueous medium or in serum, the appendage of $_D$-glucuronic acid interacted with bilirubin enabling the binding of bilirubin with the polymer (highlighted schematically in Figure 3.18)**.** The binding of bilirubin with polymer, in turn, facilitated energy transfer from polymer to bilirubin, which was manifested as a visual fluorescence color change from blue to light green. In contrast, a reference polymer designed with $_D$-Glucose as the appendage in place of $_D$-Glucuronic acid (PF-Ph-Glu) could not perform as effectively as PF-Ph-GlcA even though its photophysical properties were favorable for FRET based energy transfer.
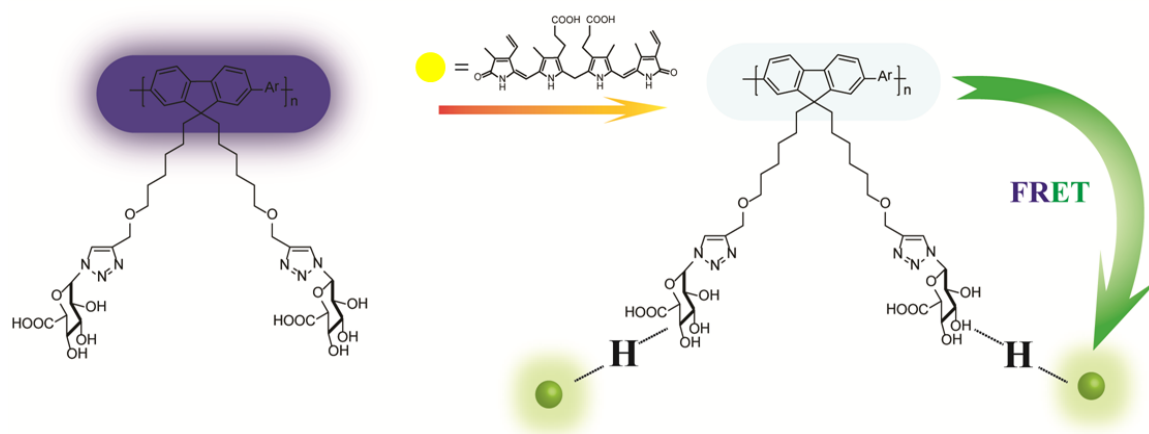
Figure 3.18 Schematic diagram showing mechanism of FRET induced sensing of bilirubin in human serum using PF-Ph-GlcA.

The glucose appendage was not successful in affording the high water solubility that was made feasible by the glucuronic acid appendage. PF-Ph-GlcA was highly selective towards free bilirubin compared to other interferences and biological substances present in the serum due to the feasible hydrogen bonded interactions and favorable spectral overlap existing only for the bilirubin-polymer pair. Though competition for binding sites could be expected to be present in the pool of interferences, binding of bilirubin in minimum sites was sufficient for FRET based energy transfer to occur due to the well-known molecular wire effect[29] that is inherent for the conjugated polymer backbone. It also successfully demonstrated its efficiency in sensing nanomolar amounts (~150 nm) of bilirubin in human serum. Consolidating all the observations, the combined role of spectral overlap and non-covalent interactions afforded high selectivity and nanomolar sensitivity for the sensing of free bilirubin in water as well as in human blood serum.

3.4 Summary

Novel water soluble polyfluorenes were designed and successfully synthesized by using click chemistry followed by Suzuki polymerization. The polymers were structurally characterized by NMR spectroscopy and size exclusion chromatography. The appendage of D-glucuronic acid to polyfluorene imparted water

solubility through hydrogen bonded interactions of polar -OH and -COOH groups with the aqueous medium. In analogy to the key role of enabling easy excretion of free bilirubin from the body played by $_D$-glucuronic acid in the body metabolism, the appendage of $_D$-glucuronic acid to polyfluorene afforded the added advantage of interactive site for the analyte bilirubin. Taking advantage of the water solubility and spectral overlap of the polymer emission with bilirubin absorption, the sensing of free bilirubin in water was targeted. A complete quenching of the blue polymer fluorescence was observed at 20 µM concentration of bilirubin addition for PF-GlcA and 40 µM for PF-Ph-GlcA. Energy transfer from polymer to bilirubin was proved by the decrease in polymer fluorescence lifetime with concurrent increase in the emission as well as the lifetime of bilirubin. Isothermal titration calorimetric (ITC) experiments revealed hydrogen bonding interaction between the polymers and bilirubin with a strong binding constant of $\sim 4.5 \times 10^3$ M^{-1}. Although both polymers exhibited similar sensing activity towards bilirubin in water, their sensing activity in human serum was entirely different. The homopolymer PF-GlcA aggregated in serum with aggregate emission observed at 550 nm, which was also supported by DLS experiments conducted both in water and serum media. DLS experiments showed that PF-GlcA formed particles with size of 330 nm in water, which increased considerably in serum.

The copolymer, PF-Ph-GlcA was successful as an efficient sensor for bilirubin in human serum with visual change of emission color from blue to green for FRET induced bilirubin emission at 520 nm. The sensing of bilirubin in human blood serum was found to be sensitive even in presence of crucial interferences such as hemoglobin, biliverdin, proteins, triglyceride, cholesterol, metal ions, and sugars. Nanomolar sensing of bilirubin could also be demonstrated successfully in human serum using PF-Ph-GlcA as the conjugated polymer sensor. Thus, we have demonstrated for the first time the successful application of water soluble conjugated polymer based on polyfluorenes in the selective and sensitive (sensing ~ 150 nm bilirubin in human serum) sensing of free bilirubin in the clinically relevant range of < 25 µmol/L to > 50 µmol/L in the human blood serum. These novel polyfluorenes appended with glucuronic acid could thus function as a highly selective and sensitive

material for the visual sensing of free bilirubin in human blood serum via the combined operation of energy transfer and non-covalent interactions.

3.5 References

1. Zhu, C.; Liu, L.; Yang, Q.; Lv, F.; Wang, S. *Chem. Rev*. **2012**, *112*, 4687−4735.

2. Jiang, H.; Taranekar, P.; Reynolds, J. R.; Schanze, K. S. *Angew. Chem. Int. Ed.* **2009**, *48*, 4300 – 4316.

3. Liu, B.; Yu, Wang-L.; Lai, Yee-H.; Huang, W. *Macromolecules* **2002**, *35*, 4975 – 4982.

4. Huang, F.; Hou, L.; Wu, H.; Wang, X.; Shen, H.; Cao, W.; Yang, W.; Cao, Y. *J. Am. Chem. Soc*. **2004**, *126*, 9845 – 9853.

5. Jose, M.; Tome, M.; Esquembre, R.; Mallavia, R.; Mateo. C. R. *Biomacromolecules* **2010**, *11*, 1494-1501.

6. Gaylord, B. S.; Heeger, A. J.; Bazan, G. C. *J. Am. Chem. Soc*. **2003**, *125*, 896-900.

7. Kim, I. B.; Dunkhorst, A.; Bunz, U. H. F. *Langmuir* **2005**, *21*, 7985–7989.

8. Miranda, O. R.; You, C. C.; Phillips, R.; Kim, I. K.; Ghosh, P. S.; Bunz, U. H. F.; Rotello, V. *J. Am. Chem. Soc*. **2007**, *129*, 9856-9857.

9. Xue, C.; Donuru, V. R. R.; Liu, H. *Macromolecules* **2006**, *39*, 5747-5752.

10. Takasu, A.; Iso, K.; Dohmae, T.; Hirabayashi, T. *Biomacromolecules* **2006**, *7*, 411-414.

11. Boyer, T. D.; Manns, P. P.; Sanyal, A. J.; *Hepatology: a textbook of liver disease.* Elsevier, Saunders, London, 6th edition, **2011**, pp.1079.

12. Silbernagl, S.; Despopoulos, A. *Color atlas of physiology.* Thieme**,** 6th edition, **2009,** pp.252.

13. Hansen, T. W. R. *J. Perinatol*. **2001**, *21*, S48 – S51.

14. Rand, R. N.; di Pasqua, A. *Clin. Chem*. **1962**, *8,* 570-578.

15. Senthilkumar, T.; Asha, S. K. *Macromolecules* **2013**, *46*, 2159-2171.

16. Zheng, Z.; Fang, J. L.; Lazarus, P. *Drug Metab. Disp*.**2002**, *30*, 397–403.

17. Fevery, J. *Liver Int.* **2008**, 592-605.

18. Wu, T. W.; Zumbulyadis, N.; Gross, S.; Gohlke, R. S. *Clin. Chem*. **1980**, *26*, 1323-1335.

19. Tosin, M.; Murphy, P. V. *Org. Lett.* **2002**, *4*, 3675-3678.

20. Pu, K. Y.; Shi, J.; Wang, L.; Cai, L.; Wang, G.; Liu, B. *Macromolecules* **2010**, *43*, 9690–9697.

21. Lakowicz, J. *Principles of fluorescence spectroscopy*. Springer, 3rd edition, **2006.**

22. Sindbert, S.; Kalinin, S.; Nguyen, H.; Kienzler, A.; Clima, L.; Bannwarth, W.; Appel, B.; Muller, S.; Seidel, C. A. M. *J. Am. Chem. Soc*. **2011**, *133*, 2463-2480.

23. Bonnett, R.; Davies, J. E.; Hursthouse, M. B.; *Nature* **1976**, *262*, 326-328.

24. Brodersen, R. *J. Biol. Chem.* **1979**, *254*, 2364-2369.

25. Lamola, A. A. *Effects of Environment of Photophysical Processes of Bilirubin. In Optical Properties and Structure of Tetrapyrroles*. Blauer, G., Sund, H., Eds.; Walter de Gruyter & Co.: Berlin. **1985**; p 311.

26. Dutton, G. J. *Glucuronic acid Free and Combined Chemistry, Biochemistry, Pharmacology, and Medicine.* Academic press, **1966**.

27. Moreno-Pirajan, J. C. Thermodynamics - Interaction studies, solids, liquids and gases. InTech publisher, **2011**.

28. Blauer, G.; Wagnière, G. *J. Am. Chem. Soc*. **1975**, *97*, 1949-1954.

29. Zhou, Q.; Swager, T. M. *J. Am. Chem. Soc*. **1995**, *117*, 7017-7018.

CHAPTER - 4

Orientation Effect Induced Selective Chelation of Fe^{2+} to Glutamic acid appended Conjugated Polymer for Sensing and Live Cell Imaging

Intracellular detection and imaging of labile iron(II) pools is very important in tracking physiological processes that demands new and rapid sensing probes. In this chapter, we present a water soluble polymer based fluorescence probe for sensing and live cell imaging of labile Fe^{2+} ions with high selectivity and cell viability. The polymer probe was based on conjugated polyfluorene which was appended with L-glutamic acid. Simple glutamic acid did not show selectivity towards any of the divalent ions. However, glutamic acid appended polyfluorene exhibited selective chelation to Fe^{2+} ion resulting in immediate sensing activity for Fe^{2+} ion in water and living cells with fluorescence turn-off response. The probe was successfully applied for the fluorescence imaging of intracellular and supplemented labile iron(II) pools in living HeLa cells.

4.1 Introduction

Iron is a vital element participating in various biological processes such as oxygen transport,[1-3] electron transport,[4,5] enzymatic conversions[6,7] and DNA/RNA repair[7] taking advantage of the spin states of Fe^{2+} and redox potential that flexibly shuttles between Fe^{2+}/Fe^{3+} oxidation states. It is very important that the levels of iron and the balance in the oxidation states are maintained as overloading of iron causes variety of disorders such as cell damage, abnormal production of reactive oxygen species, hepatitis, organ dysfunction, Alzheimer's and Parkinson's diseases.[8-10] Owing to the pivotal role of iron in biological functions, detection of iron pools in labile and exchangeable forms is important to monitor cell metabolism and in addition it facilitates an access for understanding the mechanisms of biological reactions.

Ferrous state of iron is predominantly favored inside the cell by inherent factors such as reductive environment, higher water solubility and presence of ferric reductase enzyme.[11] Thus detection of ferrous ion is desirable for monitoring of labile iron pools. Since the ferrous state is prone to oxidation under aerobic conditions, selectivity for intracellular ferrous state in presence of other metal ions including Fe^{3+} ion poses challenges for the sensing probe. There are plenty of literature reports available for sensing of Fe^{3+} and most of them have been applied to cells.[12-19] A few probes designed using small molecules are reported for detection and imaging of Fe(II),[20-22] however the emission response of the probes in water could be obtained only after a delayed period of 1 hour limiting the applicability in understanding the course of rapid physiological transport reactions. The strategies based on reaction demand stoichiometric amounts of Fe^{2+} ions and also require pretreatment of cells with $Fe^{3+/2+}$ equilibrium shifting reagents (ascorbic acid) that imposes a constraint on sensitivity.[20] In 2011, there was a report on carboxyl functionalized semiconducting polymer nanoparticles, which was used to sense both Cu^{2+} and Fe^{2+} in water based on the principle of aggregation induced fluorescence quenching.[23] However there was no selectivity and the quenching efficiency was low. Low levels of iron or copper ions (<10 μM) could not be detected using this polymer probe. The selectivity for Fe^{2+} over bio-available transition metal ions such as Cu^{2+}, Zn^{2+} and Co^{2+} also remains an

issue in some of the probes.[20,23] In view of the aforementioned context, development of rapid working new probes with high sensitivity, selectivity, water solubility and biocompatibility for imaging labile Fe^{2+} pools in living cells is very challenging and important.[20]

Conjugated polymers are acclaimed for amplified fluorescence sensitivity even with trace amount of analyte.[24-26] Cell penetrability is a prerequisite to find applicability in the field of intracellular imaging. So far, small molecule based probes are dominating in this area since they can meet the challenge of cell penetrability.[27-29] A polymer based probe for selective detection and imaging of intracellular Fe^{2+} pool is unprecedented. In this work, we report water soluble conjugated polyfluorene appended with glutamic acid (PF-Ph-GA) as a selective and sensitive fluorescent probe for sensing iron(II) in water as well as in living cells for the first time.

Glutamic acid shows propensity for coordinating with Fe^{2+} in most of the monocluear non-heme proteins, cupin and in stacking of Fe^{2+} with keratin.[30] Inspired by the bio-coordination features and other advantages, glutamic acid was appended to polyfluorene to develop an assay that was based on the selective chelation of amino acid moiety to Fe^{2+} resulting in quenching of polymer fluorescence. Additionally, the amino acid appendage was expected to facilitate entry of the polymer into the cells. Although 'turn-on' probes are preferentially adopted in place of 'turn-off' probes in the literature, in cases of cell systems with high background interference and noise fluorescence, a turn-on probe is not expected to have sensitive advantage. Swager et. al.,[31] had demonstrated that turn-off probe would be a more reliable sensor in such cases. The selectivity of the probe for Fe^{2+} ion was verified by conducting the same experiment with various metal ions including bioavailable alkali metal ion, transition metal ions particularly Fe^{3+}, Cu^{2+}, Zn^{2+}, Co^{2+}, Hg^{2+} and s-block elements. The amino acid appendage provided excellent biocompatibility to the polymer facilitating fluorescence imaging of intracellular Fe^{2+} in living HeLa cells.

4.2 Experimental Section

Materials: 2, 7-dibromofluorene, 6-bromo-1-hexanol, 4-dimethyl amino pyridine, boc-L-glutamic acid-1-tert butyl ester, dicyclohexyl carbo diimide (DCC), Tetrabutyl

ammonium chloride, Pd(PPh$_3$)$_4$, Ferrous(II) sulphate and 1, 4-benzene diboronic bis(pinacolatoester) were purchased from sigma Aldrich. NaOH, Na$_2$CO$_3$, HCl, DMSO and K$_2$CO$_3$, were purchased from Merck chemicals. THF, methanol, toluene, DCM, ethylacetate and pet ether were purchased locally and dried by the standard drying procedures. Dulbecco's Modified Eagle Medium (DMEM), Fetal bovine serum (FBS), (3-(4, 5-Dimethylthiazol-2-yl)-2, 5-diphenyltetrazolium bromide (MTT), and phosphate buffer saline (PBS) - biological grade were purchased from Invitrogen, India. Cell line HeLa required for biological experiments were purchased from National Centre for Cell Science (NCCS), Pune, Maharashtra, India.

Methods: ^{1}H and ^{13}C NMR spectra were analyzed using Bruker-AVENS 200 MHz spectrometer. Chemical shifts are reported in ppm at 25°C using CDCl$_3$ and MeOH-d$_4$ as solvents containing trace quantity of tetramethylsilane (TMS) as internal standard. MALDI-TOF analysis was done on Voyager-De-STR MALDI-TOF (Applied Biosystems, Framingham, MA, USA) equipped with 337-nm pulsed Nitrogen laser used for desorption and ionization. 1 μM solution of sample was premixed with DHB (2, 5 dihydroxy benzoic acid) matrix in THF and mixed well before spotting on 96-well stainless steel MALDI plate by dried droplet method for MALDI analysis. The molecular weights of the polymer was determined by gel permeation chromatography (GPC), which was performed using a Viscotek VE 1122 pump, Viscotek VE 3580 RI detector and Viscotek VE 3210 UV/vis detector in tetrahydrofuran (THF) using polystyrene as standards.

Photophysical measurements:

Absorption spectra were measured using Perkin-Elmer Lambda 35 UV-spectrophotometer. Steady-state fluorescence studies were recorded using Horiba Jobin Yvon Fluorolog 3 spectrophotometer having a 450 W xenon lamp for steady-state fluorescence. The emission and excitation slit width was maintained at 1 nm throughout the experiments, and the data was obtained in "S1/R1" mode.

Isothermal titration calorimeter experiment:

ITC experiments were carried out in Micro cal iTC-200 instrument. ITC titration was carried out in water using an isothermal titration calorimeter (Microcal iTC-200) with

standard conditions (1000 rpm, pH=7, 25 ^{0}C). The sample cell was filled with 200 µL of polymer (PF-Ph-GA) at a concentration of 2mM and Fe(II) sulphate (20 mM) was taken in syringe. 2 µl of Fe(II) sulphate was introduced in the duration of 20 s in 19 consecutive injections at intervals of 180 s in a titration experiment. A blank titration was performed by injecting the analyte solution into the solvent to obtain the heat of dilution. The heat of binding between polymer and Fe^{2+} was obtained by subtracting the value of heat of dilution from the total value of heat of binding. A single set of binding model was fitted with the binding isotherm which was used to extract binding constant (K), binding stoichiometry (N), change of enthalpy (ΔH) and the change of entropy (ΔS) for the binding

Determination of stoichiometry using Job plot:

A series of solutions containing PF-Ph-GA polymer and iron(II) were prepared where the total concentration of both components was kept constant (100 µM). The mole fraction of the iron(II) was varied from 0, 0.05, 0.1 etc to 1. The emission of the polymer was collected and plotted against the mole fraction of the iron(II) ions in water.

Cell viability assay (MTT Assay):

The cell viability assay was analyzed using colorimetric method which is based on MTT (3-(4, 5-Dimethylthiazol-2-yl)-2, 5-diphenyltetrazolium bromide). HeLa cells were seeded in a flat bottomed 96-well plate at a density of 1 x10^4 cells/well in DMEM containing 10 % FBS. The plate was incubated at 37 °C with 5 % CO_2 atmosphere for 24 hours. After incubation, media was replaced with PF-Glu (1 mg/mL in DMEM containing 10 % FBS). The different concentration of sample (0, 2, 4, 6, 8, 10, 20, 40, 60, 80, 100, 150, 200, 300, 400 µg/mL) were added to make final volume 100 µL/well and incubated for 40 hrs at 37 °C with 5 % CO_2 atmosphere. After incubation media, was replaced with filter sterilized MTT (0.45 mg/mL) prepared in DMEM containing 10 % FBS and further incubated for 4 hrs at 37 °C with 5 % CO_2 atmosphere. After incubation the MTT reagent was replaced with 100 µL/well DMSO solvent. Addition of DMSO dissolves the formazan crystals formed by reaction of sample with MTT and developed color was measured at 550 nm using

a microtitre plate reader (Veroscan, Thermo Scientific). The cell viability was calculated as a percentage relative to untreated control cells.

Live cell imaging:

Live cell images were acquired using epifluorescence microscope by Carl Zeiss (Model: Axio Observer.Z1, Oil emersion objective, 63X). (Filters set 49 DAPI shift free EX G 365, BS FT 395, EM BP 445/50). In a 24 well flat bottom plate HeLa cells were seeded on glass cover slips at a density of 1×10^5 cells per well (1 mL) in DMEM containing 10 % FBS and incubated for 16 h at 37 °C with 5 % CO_2 atmosphere. To evaluate selective sensitivity of PF-Ph-GA for intracellular labile Fe^{2+} pool, a series of four experiments from set A to set D were set up. In the live cell experiments the incubation time was fixed for bpy as 1 h, polymer as 4 h,[32] and iron(II) as 1 h respectively.

Synthesis procedures for monomers and polymers:

Synthesis of 6, 6'-(2, 7-dibromo-9H-fluorene-9, 9-diyl)bis(hexan-1-ol) (1):

2, 7-dibromofluorene (6 g, 18.52 mmol), 6-bromohexan-1-ol (8.3 g, 46.3 mmol) and tetrabutyl ammonium bromide (3 g, 9.26 mmol) were taken in two neck round bottom (RB) flask and dissolved in toluene (120 ml). Then 60 g of 50 wt% of aqueous NaOH solution was added to the reaction mixture and heated to 120 ^{0}C under Argon atmosphere for 18 h. After cooling to room temperature, water was added and the aqueous layer was extracted with diethyl ether. The toluene layer was extracted with water until the color of the solution turned yellow. The aqueous layer was again extracted with diethyl ether. The ether layer was dried over sodium sulphate and evaporated under reduced pressure. The crude product was purified by column chromatography with hexane:ethyl acetate (97:3) with yield-92 %. ^{1}H NMR spectrum: (200 MHz, $CDCl_3$) δ 7.6-7.3 (m, 6H), δ 3.50 (t, 4H), δ 1.93-1.87 (m, 4H), δ 1.66-1.56 (m, 4H), δ 1.35 (m, 4H), δ1.08 (m, 4H), 0.56 (m, 4H). MALDI (calculated (M+Na) = 524.075; observed (M+Na) = 524.069).

Synthesis of (S)-1-tert-butyl 5-(6-(2,7-dibromo-9-(6-(((R)-5-(tert-butoxy)-4-((tert-butoxycarbonyl)amino)-5-oxopentanoyl)oxy)hexyl)-9H-fluoren-9-yl)hexyl) 2-((tert-butoxycarbonyl)amino)pentanedioate (2):

4-dimethyl amino pyridine (2.56 g, 21 mmol) and boc-L-glutamic acid-1-tert butyl ester (7.24 g, 23.85 mmol) were taken in two neck round bottom flask under Argon atmosphere. Dry DCM was added to the reaction mixture and the RB was cooled to 0 ^{0}C. After 5 minutes dicyclohexyl carbo diimide (DCC) was added and the whole mixture was stirred for 1 h at the same temperature. 2, 7-dibromo-9, 9-di-n-hexanol fluorene was added to reaction mixture at 0 ^{0}C and RB was warmed to room temperature and stirred for 16 h. The reaction mixture was diluted with DCM and the organic layer was extracted twice with 0.02 M NaOH followed by extraction with saturated $NaHCO_3$. The organic layer was then washed with brine, water and finally evaporated under reduced pressure. The product was purified by column chromatography using pet ether: ethyl acetate (55:45). ^{1}H NMR spectrum: (200 MHz, $CDCl_3$) δ 7.6-7.3 (m, 6H), δ 5.02 (d, 2H), δ 3.94 (t, 2H), δ 3.28 (q, 2H), δ 2.34 (q, 4H), δ 2.13 (m, 4H), δ 1.93-1.87 (m, 4H), δ 1.43 (s, 18H), δ 1.41 (s, 18H), δ1.08 (m, 8H), 0.55 (m, 4H). Yield (85 %). MALDI (calculated (M+K) = 1131.472; observed (M+K) = 1131.469). FT-IR stretching frequency (υ) in cm^{-1}: 3362, 2977, 2931, 2859, 1716, 1505, 1450, 1365, 1250, 1149, 1058 and 752.

Polymerization of (2):

Monomer (**2**) (1 g, 0.91 mmol), 1, 4-bis(4, 4, 5, 5-tetramethyl-1, 3, 2-dioxaborolan-2-yl)benzene (0.3 g, 0.91mmol) and Pd(PPh$_3$)$_4$ (40 mg, 12 µmol) were taken in a two neck round bottom flask fitted with reflux condenser and connected with Argon atmosphere. Dry THF (12 ml) was added to the reaction mixture which was then subjected to a sequence of three freeze-pump-thaw cylces. Degassed aqueous K_2CO_3 (0.503 g, 3.64 mmol) was then added to the reaction mixture and the contents refluxed at 65 ^{0}C for 48 h. The polymerization solution was evaporated under reduced pressure and dissolved in THF and filtered through whatmann filter paper to remove the Pd catalyst. The solvent was concentrated to 1 ml and the polymer was precipitated in methanol. The methanol precipitation was repeated 3 times. Finally, the polymer powder was dried under vacuum. The crude yield of the polymer (PF-Ph-GA(Boc)) was 1.15 g (82 %). ^{1}H NMR spectrum: (200 MHz, $CDCl_3$) δ 7.9-7.3 (m, 6H), δ 5.08 (b, 2H), δ 3.94 (b, 4H), δ 3.30 (b, 2H), δ 2.32 (b, 4H), δ 2.06 (m, 4H), δ 1.93-1.86 (m, 4H), δ 1.41 (bs, 18H), δ 1.40 (b, 18H), δ1.12 (b, 8H), 0.74 (b, 4H).

^{13}CNMR spectrum (400 MHz, CDCl$_3$) δ 172.76, 171.23, 155.25, 152.11, 138.95, 130.18, 125.95, 121.42, 121.42, 81.96, 79.57, 70.7, 67.82, 64.51, 55.46, 53.3, 40, 29.38, 28.34, 28.19, 27.86, 25.47, 23.43. Mn=25400; Mw=42800; PDI=1.7.
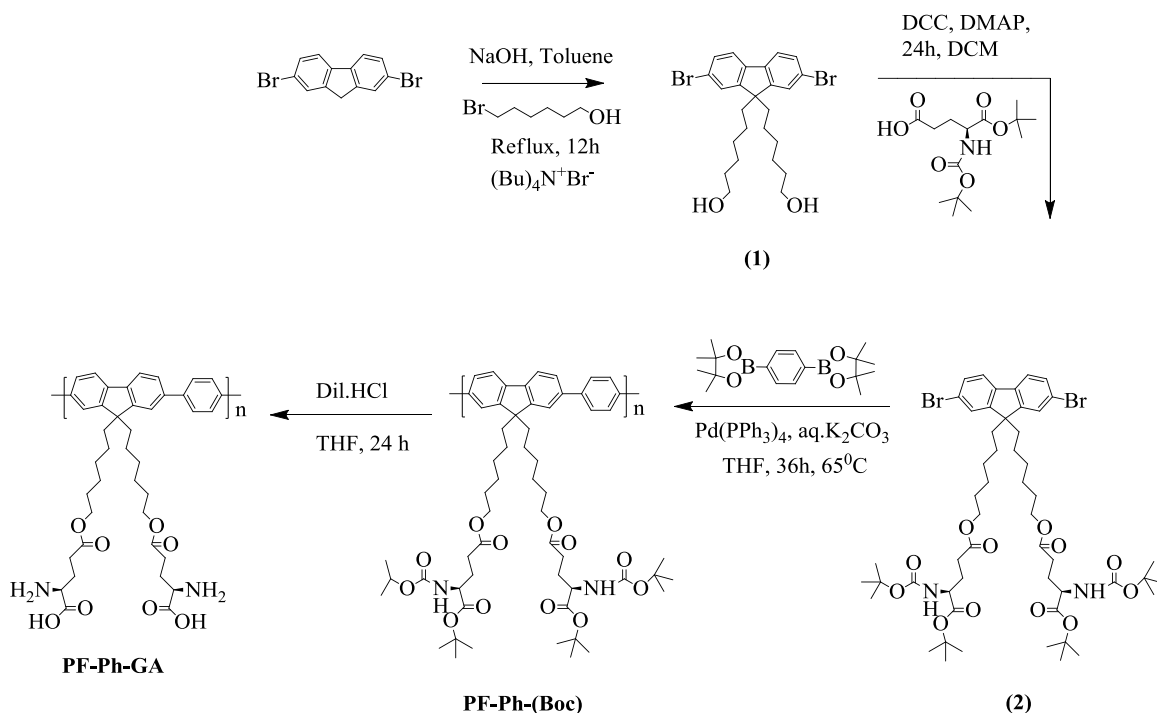
Deprotection of polymer (PF-Ph-GA(Boc)):

The polymer (40 mg) was dissolved in THF under Argon atmosphere. Dilute HCl was added to deprotect the boc groups in polymer. Reaction mixture was stirred for 24 h at room temperature to complete the deprotection. Solvent was evaporated under reduced vacuum and the polymer was washed with DCM to remove protected polymer. The polymer was further purified by dialyzing the polymer powder against Mill-Q water with 2KDa molecular weight cut-off dialysis membrane for 24 h. The aqueous solution was freeze dried to remove the water to obtain water soluble polymer (PF-Ph-GA). The yield of deprotection reaction was (70 %). ^{1}H NMR (MeOH-d$_4$, 400 MHz). δ 7.8-7.5 (dd, 10H), δ 5.05 (b, 2H), δ 4.16-3.94 (dd, 4H), δ 3.28 (b, 2H), δ 2.29 (b, 4H), δ 2.06 (b, 4H), δ 1.12 (b, 6H), δ 0.74 (b, 4H).

4.3 Results and Discussion

4.3.1 Synthesis and characterization of the polymer:

The polymer probe for selective sensing of iron(II) ions in living cells was designed with conjugated polyfluorene (PF) appended with glutamic acid moiety. Conjugated polyfluorenes are well known for their amplified sensitivity with brilliant blue fluorescence and therefore they have been used for visual sensing of biomolecules.[33] However, in order to find sensing applications in water and to extent the studies to living cells, the polymer should be water soluble and biocompatible. In order to make polyfluorene water soluble as well as biocompatible, amino acid appendage was selected and the selection was also bioinspired due to the inherent propensity of glutamic acid to participate in the coordination sphere of bioavailable mononuclear Fe^{2+} non-heme proteins.[30] The side chain carboxylate of glutamic acid was used for linking to PF, while the α-amine and carboxylate groups were freely available for expected coordination. The amino acid appendage was expected to bring water solubility along with biocompatibility.

The novel water soluble CP, poly((S)-2-ammonio-5-((6-(9-(6-(((R)-4-ammonio-4-carboxylatobutanoyl)oxy)hexyl)-9H-fluoren-9-yl)hexyl)oxy)-5-oxopentanoate)-alt-1, 4-phenylene sodium salt was named as PF-Ph-GA. The Scheme 4.1 depicts the synthesis of L-glutamic acid functionalized water soluble polyfluorene (PF-Ph-GA) by a four step process. 2, 7-dibromofluorene was reacted with 6-bromo-1-hexanol to obtain 6, 6'-(2, 7-dibromo-9H-fluorene-9, 9-diyl)bis(hexan-1-ol). This compound was further esterified with boc-L-glutamic acid-1-tert butyl ester to get monomer (2). Monomer (2) was polymerized via Suzuki coupling to produce PF-Ph-GA(boc). The PF-Ph-GA(boc) was deprotected using dil.HCl to form the desired glutamic acid functionalized water soluble polyfluorene (PF-Ph-GA). The polymer was purified by dialyzing against water for 2 days using dialysis cut-off membrane (2000 KDa) followed by freeze drying to obtain the water soluble polyfluorene. PF-Ph-GA was highly soluble in water, methanol, DMSO, and DMF.

Scheme 4.1 Synthesis of water soluble polyfluorene (PF-Ph-GA)

Figure 4.1a denotes the ^{1}H NMR spectrum of deprotected polymer (PF-Ph-GA). The molecular weight of the polymer (PF-Ph-GA(boc)) was analyzed using size exclusion chromatography (SEC) using THF as eluent and is shown in Figure 4.1b. The

molecular weights of the polymer obtained from SEC were Mn = 25,400; Mw = 43,200; Polydispersity (Đ) = 1.7 using polystyrene standard.
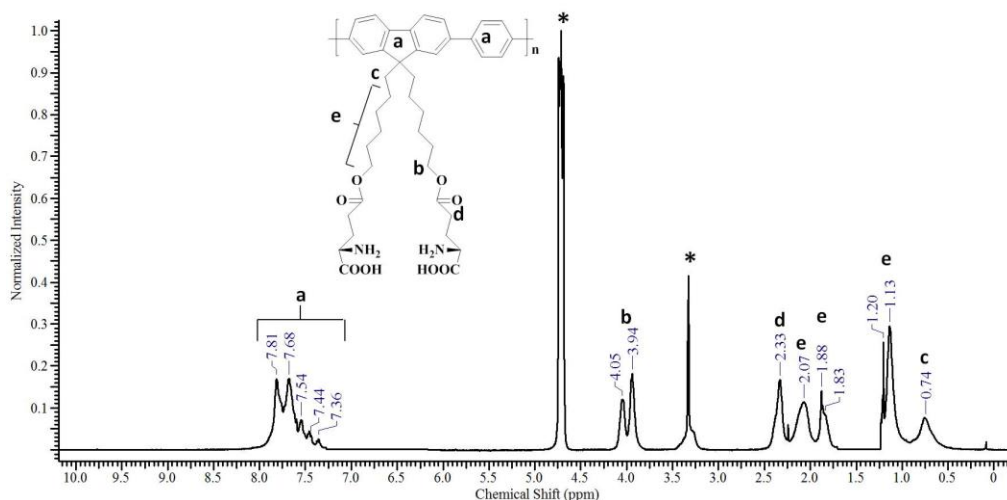

Figure 4.1a ^{1}H NMR spectrum of PF-Ph-GA recorded in MeOH-d$_4$.
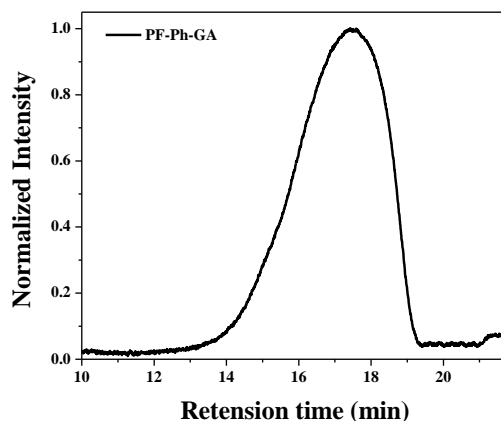
Figure 4.1b Size exclusion chromatogram (SEC) of PF-Ph-GA(boc) in THF as eluent and polystryrene as standard.

The absorption and emission spectra of PF-Ph-GA are shown in the Figure 4.2. The absorption maximum of PF-Ph-GA polymer was centered at 350 nm. The emission spectrum showed vibronic fine structure of polyfluorene with emission maximum at 430 nm. The fluorescence quantum yield of the polymer in water was determined as 0.58 using quinine sulphate as reference (Φ_{fl}= 0.546 in 0.1 M H$_2$SO$_4$).
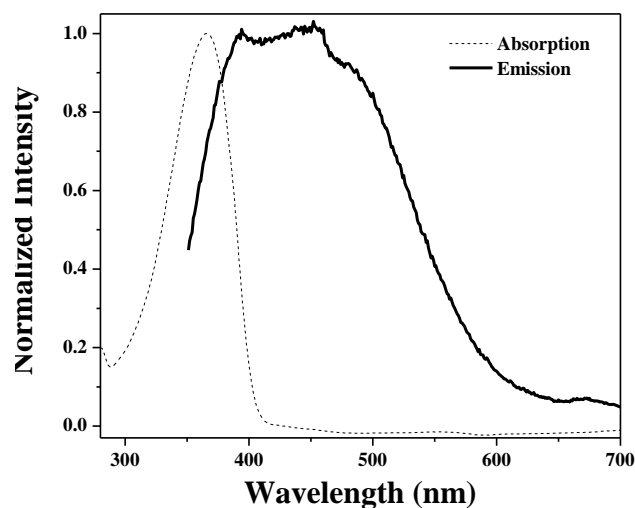
Figure 4.2 Absorption and emission spectra of the polymer (PF-Ph-GA) in water.

4.3.2 Fluorescence sensing of Iron(II) in water:

The sensing of Fe^{2+} by the polymer (PF-Ph-GA) is based on the coordinating ability of the α-amino acid appendage as described later on. The sensing experiments were conducted in water at pH=7 using various concentration of Fe^{2+} ranging from 0.1 μM to 10 μM that was added to polymer maintained at a constant concentration of 5 μM. The changes in the absorption and emission spectra of the polymer upon addition of Fe^{2+} ion are presented in Figure 4.3a and b. The addition of Fe^{2+} to the polymer resulted in the quenching of the polymer fluorescence accompanied with visual change in color from blue to colorless. The fluorescence quenching of PF-Ph-GA upon addition of Fe(II) was further studied using stern-volmer plot. Figure 4.3c depicts the stern-volmer plot (I_0/I *vs* concentration of the quencher [Q]) where I_0 denoted the initial fluorescence intensity of PF-Ph-GA polymer and I indicated the fluorescence intensity of the polymer after each addition of Fe^{2+} concentration. There was a reduction of >10 % in fluorescence intensity of the polymer for 0.1 μM addition and a maximum of ~91 % for 10 μM addition of Fe^{2+} that was indicative of interaction with Fe^{2+} ion. Such amplified quenching of polymer fluorescence was realized by the phenomenon of 'Molecular wire effect',[35,36] which is caused by inherent efficient energy migration across the conjugated polymer backbone.

The nice fitting of the plot in a straight line indicated the high fluorescence quenching and the corresponding value of quenching constant (K_{sv}) obtained was 0.927×10^6 M^{-1}.
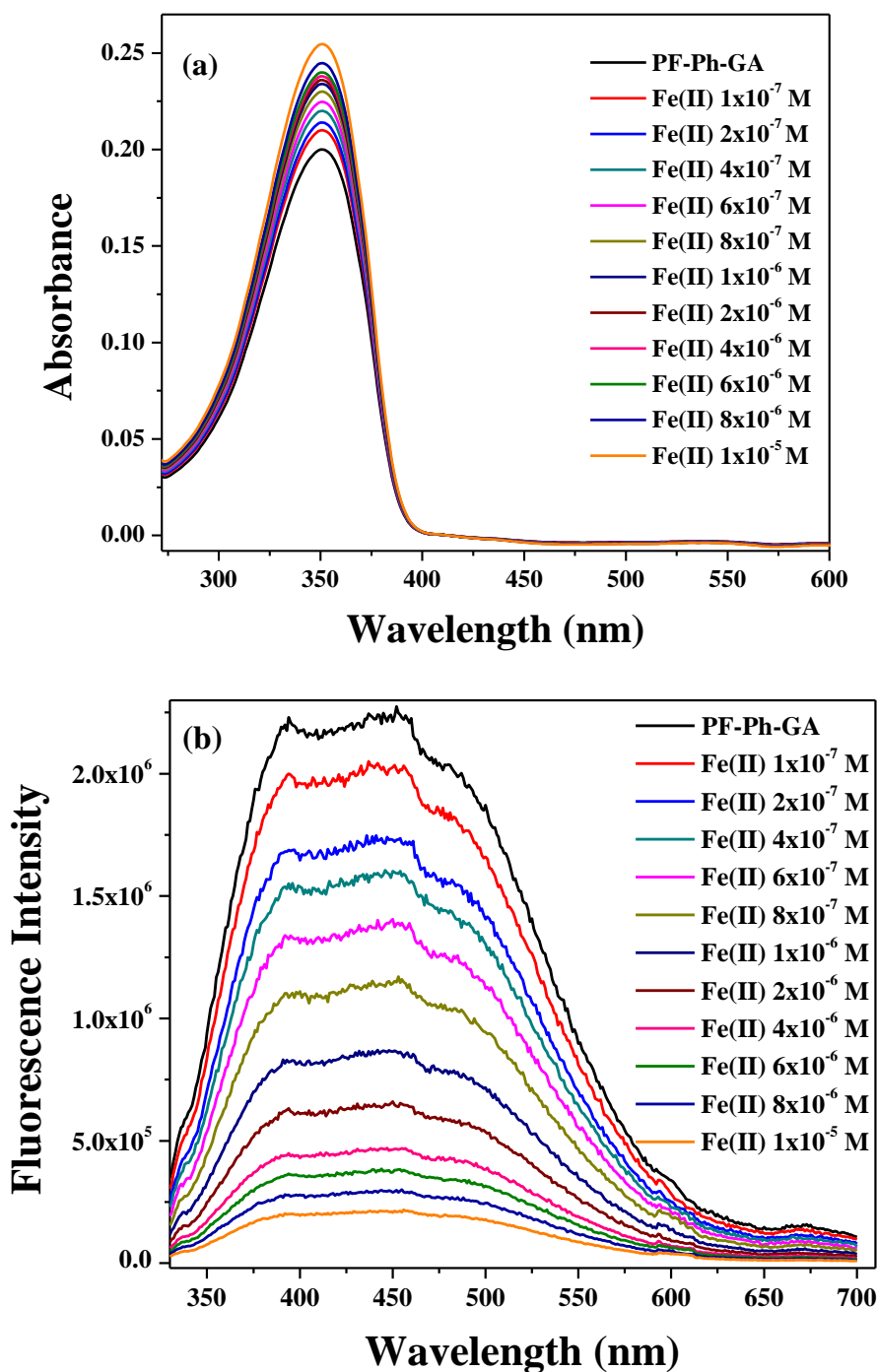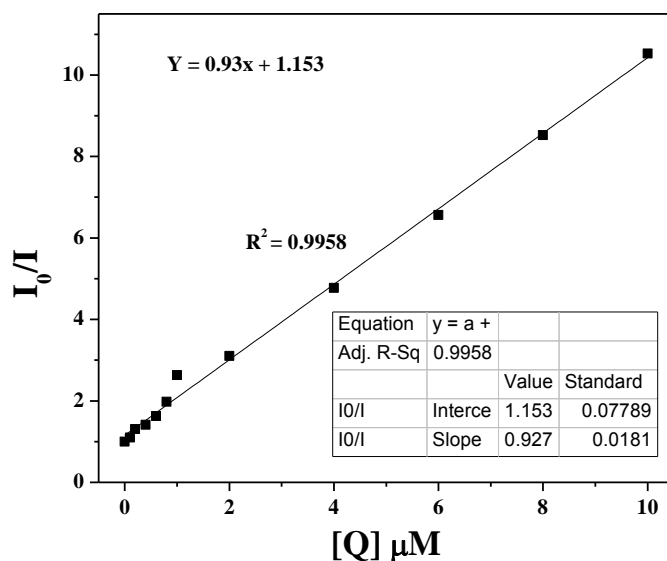
Figure 4.3 (a) Absorption spectra, (b) Emission spectra of PF-Ph-GA polymer with various concentration of Fe^{2+} ranging from 1×10^{-7} M to 1×10^{-5} M and (c) Stern-Volmer quenching plot for emission spectra given in (b).

4.3.3 Effect of pH in the sensing of Iron(II):

The intracellular pH plays an influential role over the endogenous changes and therefore it is essential to explore the pH stability and sensing activity of the intracellular probes. The sensing studies were performed at different pH (3, 5, 7 and 9) conditions covering acidic, neutral and basic pH regimes. Figure 4.4 shows the changes in the fluorescence intensity of the polymer upon addition of Fe(II) at various pH. From the plot it could be seen that sharp drop in the polyfluorene emission was observed at pH 5 and above, which happen to fall in the intracellular pH range (5.5-8). In the present design, the coordinating site constitutes amine and acid groups which have reversible protonated forms with respect to pH changes. The possible forms of amino acid in the respective pH range are given in Figure 4.5. As the amino acid groups are protonated in the condition of acidic pH=3, the lone pair of electrons of Nitrogen and bond pair electrons of oxygen becomes less available for coordinating with metal ion, which in turn decreases the quenching efficiency. When the pH was increased to 5, 7 and 9, the quenching efficiency also improved significantly.
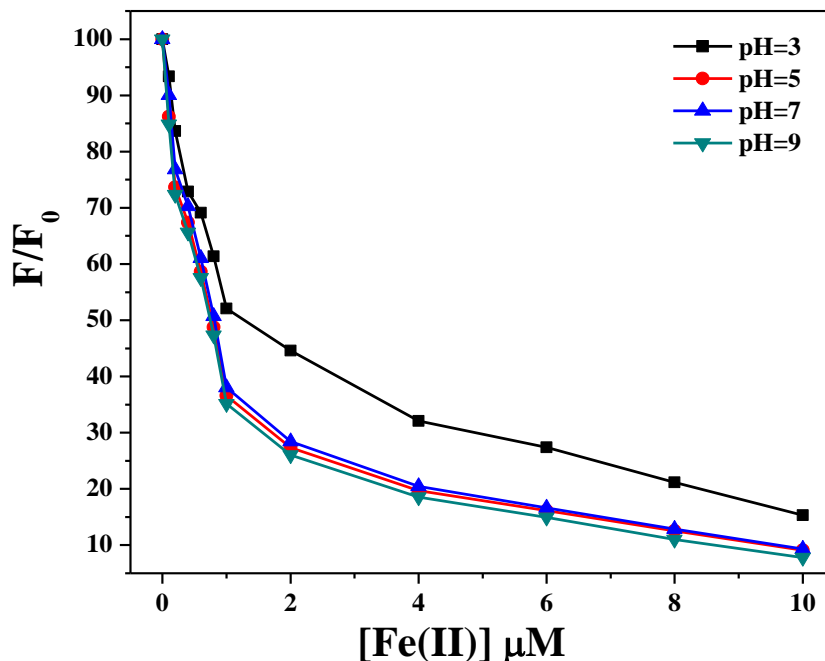
Figure 4.4 Ratio between area of polymer fluorescence observed (F) to that of the initial emission area (F_0) at different pH (3-9) as a function of Fe(II) concentration.
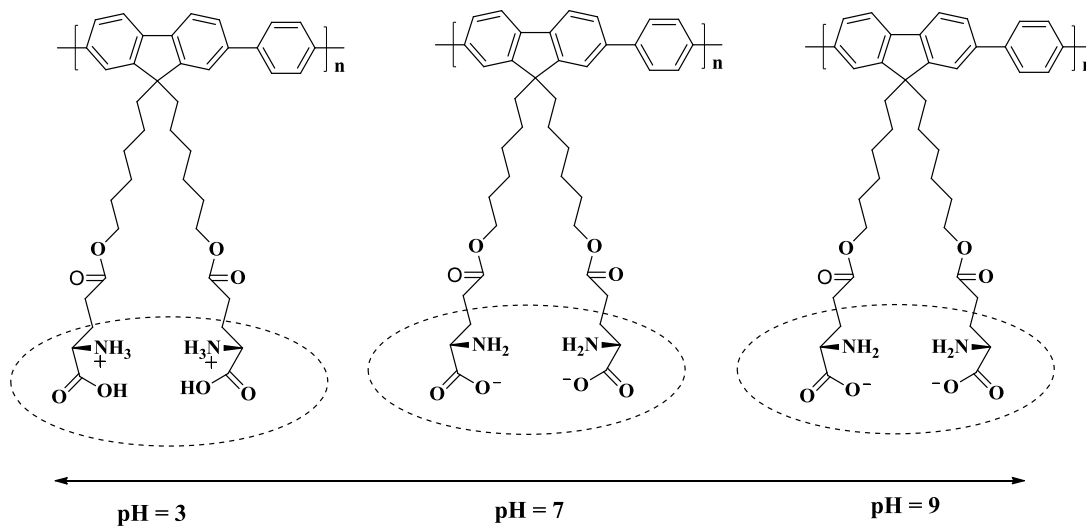
Figure 4.5 Effect of pH on the charged states of the polymer.

The amino acid groups were freely available for strong binding to Fe^{2+} ion at higher pH resulting in almost complete quenching (~ 95 %) of polymer fluorescence. It is to be emphasized that the improved sensing activity in the intracellular pH range is advantageous for identifying labile iron pools.

4.3.4 Selectivity and limit of detection for Iron(II):

To explore the selectivity of the polymer towards Fe^{2+} ions, similar fluorescence experiments were conducted with the addition of Cu^+, Cu^{2+}, Co^{2+}, Fe^{3+}, Na^+, K^+, Zn^{2+}, Cr^{3+}, Ag^+, Hg^{2+}, Cd^{2+}, Ni^{2+}, Pb^{2+} and Ca^{2+} ions at 10 μM concentration. This analysis covers almost all the competing bioavailable transition metal ions. The plot of reduction in fluorescence intensity versus various added metal ions is given in Figure 4.6a. This demonstrated the supreme selectivity of the polymer probe only towards Fe^{2+} with the highest quenching observed for Fe^{2+} probe whereas other metal ions particularly Cu^{2+}, Fe^{3+}, Co^{2+} and Zn^{2+} did not quench the polymer fluorescence appreciably. The limit of detection (LOD) of Fe^{2+} was determined using various nanomolar quantities of Fe^{2+} added to the polymer. The polymer was sensitive to 46 ($\pm$ 2) nM concentration of Fe^{2+} with 8 % fluorescence quenching as shown in Figure 4.6b. This result on LOD of Fe^{2+} in nanomolar concentration clearly indicated the high sensitivity of the polymer towards iron(II) ions.

4.3.5 Isothermal titration calorimetry and job plot:

The binding interaction between the polymer (PF-Ph-GA) and iron(II) was probed with the help of isothermal titration calorimetric (ITC) experiment. Figure 4.7 shows the typical ITC titration experiment with polymer (PF-Ph-GA) and Fe^{2+} in water at pH=7. In a typical experiment the concentration of polymer was taken as 2 mM and Fe^{2+} was taken as 20 mM. Addition of Fe^{2+} into the polymer resulted in endothermic heat changes which were monitored. The completion of reaction was identified from the saturation in the heat changes. ITC graph was fitted to a sigmodial plot from which the heat parameters such as change in enthalpy [(ΔH) = 3.5×10^4 cal/mol], change in entropy [(ΔS) = 146 cal/mol/deg], binding constant [(K) = 4.39×10^5 M^{-1}] and stoichiometry [N = 1.01] were extracted. Using the standard equation ΔG=ΔH-TΔS, the obtained value of Gibbs free energy (ΔG) was −8.5 Kcal/mol. The Gibbs free energy for the electrostatic interactions fall in the range of 1-20 Kcal/mol.[37,38] The Gibbs free energy value indicated the electrostatic interaction between the polymer and iron(II) ions.
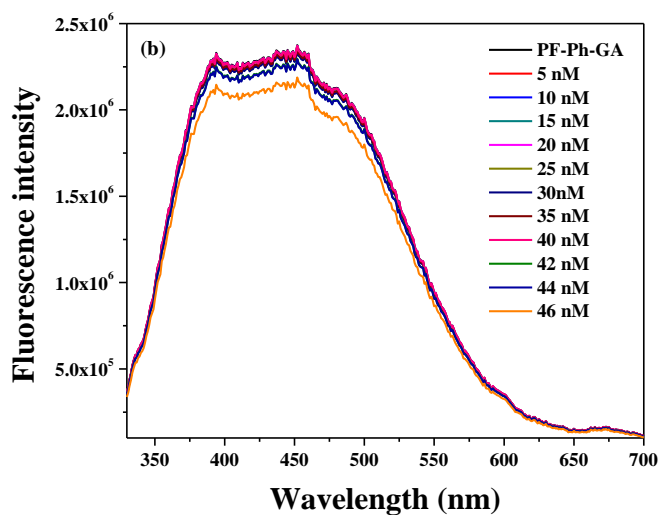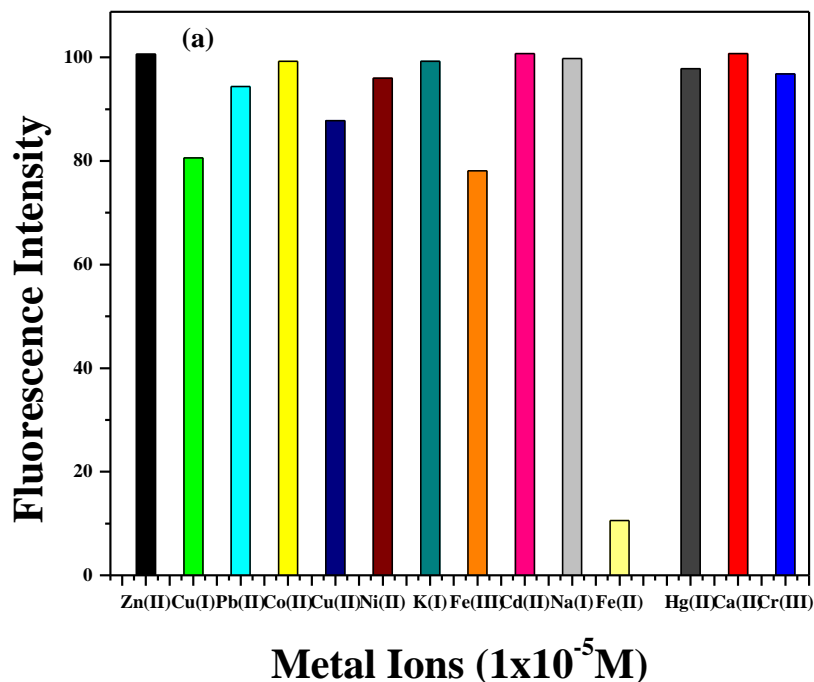
Figure 4.6 (a) Selectivity of PF-Ph-GA polymer towards Fe^{2+}: The concentration of the analytes was $1x10^{-5}$ M and the polymer was $5x10^{-6}$ M and (b) Limit of detection of iron(II) by the polymer probe.

The stoichiometry could also be verified from job plot experiments by varying the mole fraction of iron(II) from 0 to 1 and observing the corresponding emission of PF-Ph-GA.
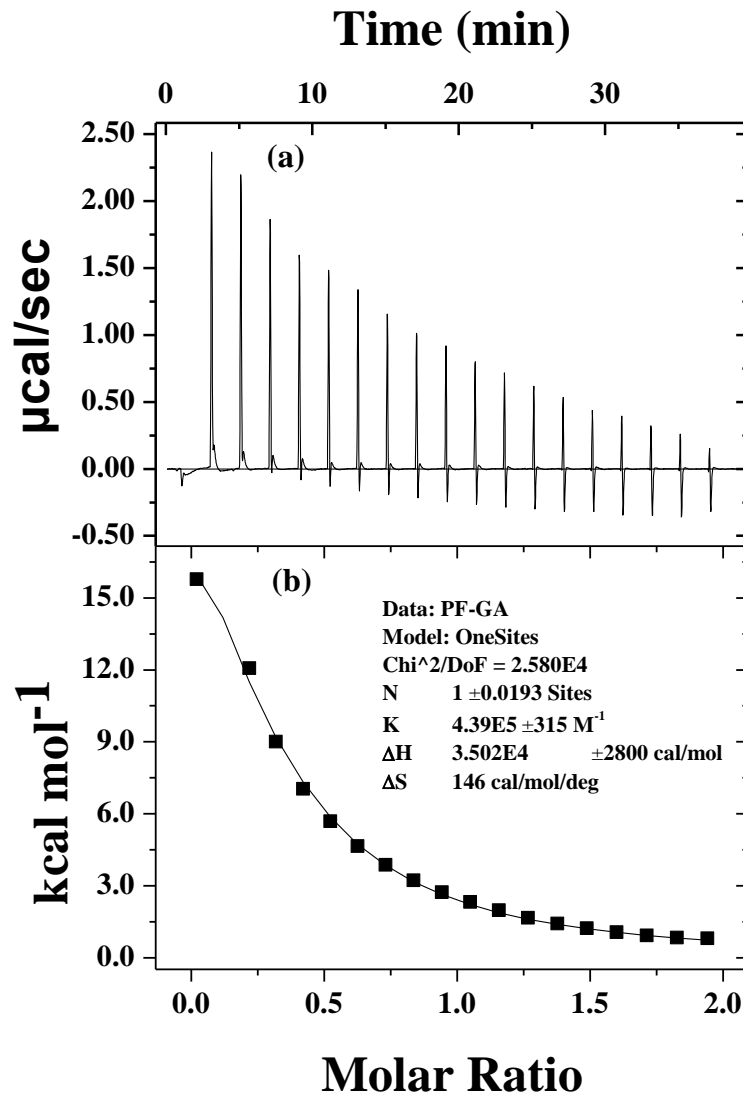
Figure 4.7 Isothermal calorimetric thermogram (a) for the injection of 2 µL of 20 mM Fe(II) perchlorate into 2 mM PF-Ph-GA polymer at an interval of 3 minutes at pH=7. The respective sigmoidal fit (b) for PF-Ph-GA polymer-Fe^{2+} interactions.

The details of the fluorescence experiment are given in the experimental section and the job plot is given in Figure 4.8. The fluorescence intensity of the polymer versus the mole fraction of Fe(II) was plotted and the stoichiometry was determined as PF-Ph-GA:Fe(II) = 1:1.
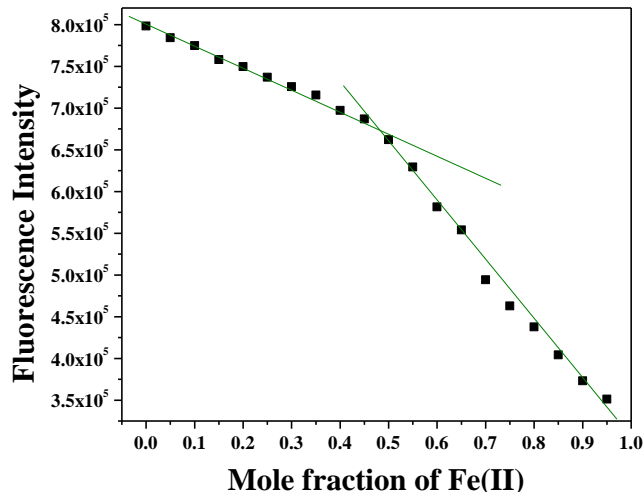
Figure 4.8 Job plot for the sensing of Fe^{2+} ion using polymer (PF-Ph-GA). Concentration of polymer was 50 µM at pH=7.

4.3.6 Determination of cell viability using MTT assay:

The selective sensing of iron(II) in water was made use of to extent the application of the polymer PF-Ph-GA to intracellular imaging of labile Fe^{2+} pools in HeLa cells (HeLa cell line was chosen for *invitro* live cell imaging which will be discussed later on). The cell viability of the polymer (PF-Ph-GA) was determined from MTT (3-(4, 5-Dimethylthiazol-2-yl)-2, 5-diphenyltetrazolium bromide) assay in HeLa cells. The plot of % cell viability against the concentration of polymer supplementation in HeLa cells obtained from MTT assay is shown in the Figure 4.9.
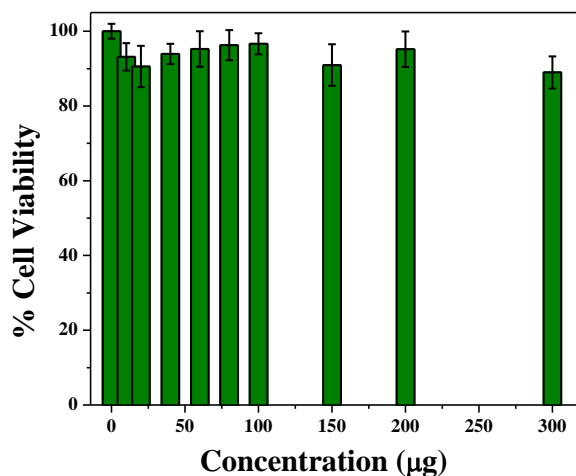

Figure 4.9 In vitro cell viability of HeLa cells incubated with polymer (PF-Ph-GA) at different concentrations for 4 hrs.

The direct method of determination of cell viability is described in detail in the experimental section. The relative cell viability of polymer treated cells was calculated by considering viability of the untreated HeLa cells as 100 %. MTT assay results showed that the polymer had >90 % viability upto the concentration of 300 µg/ml of polymer supplementation. This gave compelling evidence for significant biocompatibility of the polymer. The amino acid appendage thus conferred biocompatibility to the polymer.

4.3.7 Live cell imaging of labile Iron(II):

The successful selective sensing of iron(II) by the polymer probe (PF-Ph-GA) was further extended to explore the imaging of the intracellular labile Fe^{2+} in live cells. A series of systematic experiments were designed to establish the selective detection of Fe^{2+} in live HeLa cells. Complete details of experimental conditions are given in experimental section. Set A was the control experiment that was performed for the purpose of complete chelation of available labile Fe^{2+} pool using bipyridine (bpy) ligand. The ligand bpy is a well known selective chelator for complexing iron(II)[39,40] without any change in the morpholology of the cells as shown in set A (Figure 4.10 a-c). Set B experiment was carried out with only polymer supplementation in HeLa cells for 4 h and the images are given in Figure 4.10 d-f. There was complete quenching of fluorescence of the polymer inside the cells that is ascribed to complexation of labile Fe^{2+} to the polymer as per the demonstration of sensing experiments carried out in water. To confirm this claim, set C experiment was conducted by first treatment of bpy ligand in HeLa cells followed by same amount and time of polymer supplementation. Since the bpy ligand complexes with Fe^{2+} in the previous stage, labile Fe^{2+} would not be available to complex with polymer and as expected, the retention of polymer fluorescence was observed. Set C in Figure 4.10g-i shows the visual observation of blue fluorescence of the polymer indicative of selective complexing to Fe^{2+} in set B experiment. The region in which polymer fluorescence was quenched can be identified as labile Fe^{2+} pools.
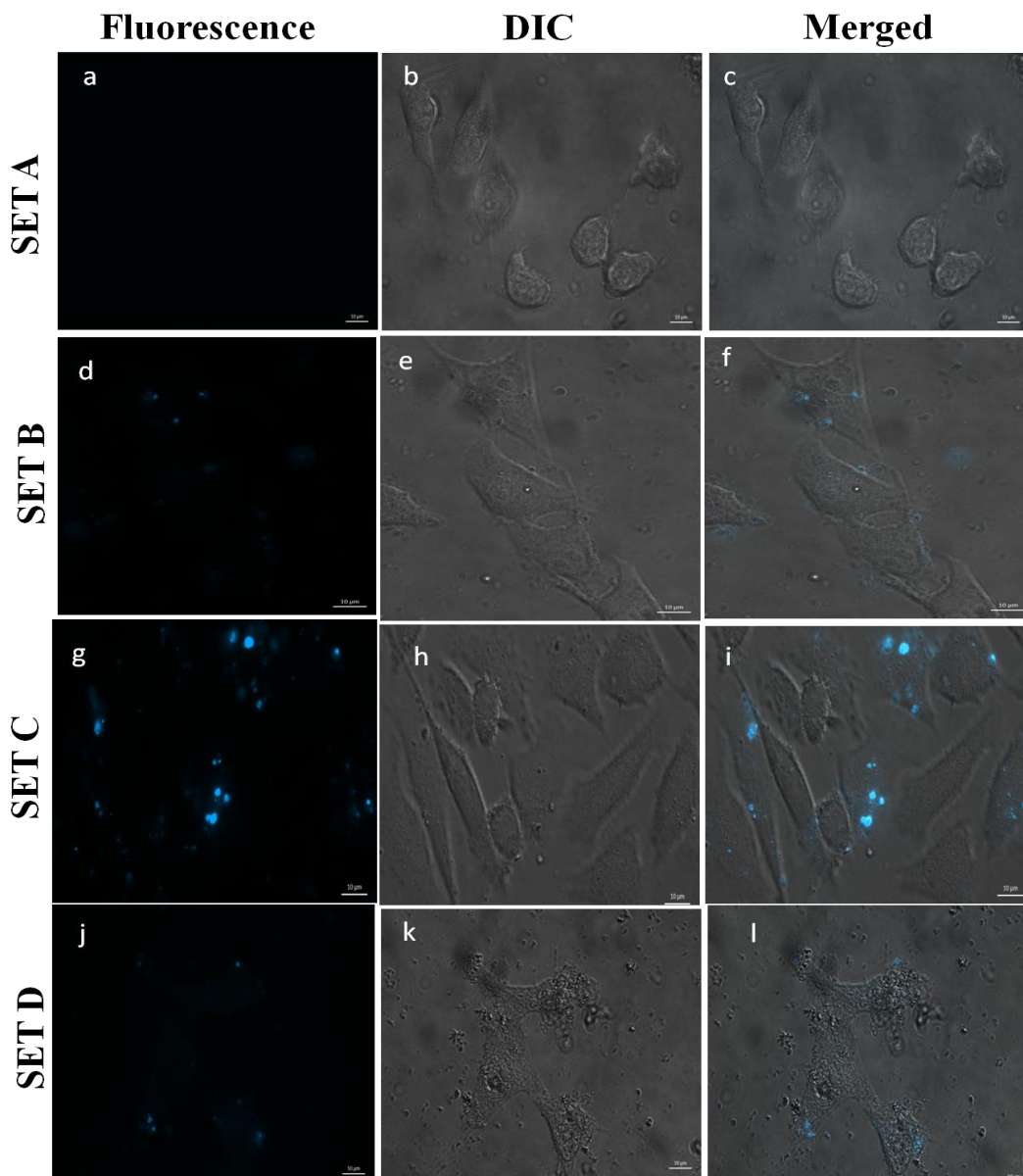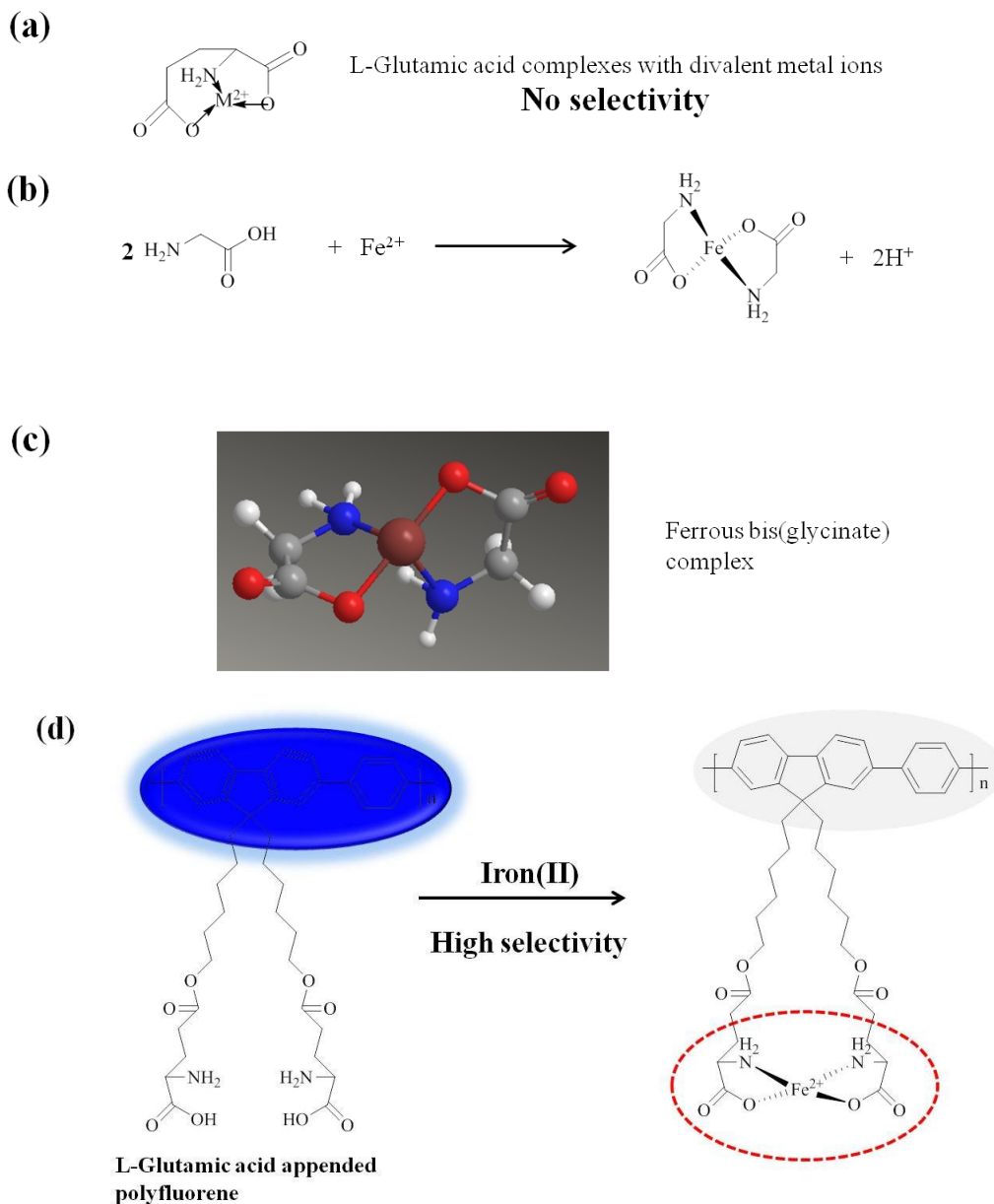
Figure 4.10 Epifluorescence and DIC images of HeLa cells. In SET A, (a-c) HeLa cells incubated with bpy (100 µM) for 1 hr. In SET B, (d-f) HeLa cells incubated for 4 hrs with 50 µg/mL polymer. In SET C, (g-i) HeLa cells incubated with bpy (100 µM) for 1 hr followed by the addition of 50 µg/mL polymer and incubated for 4 hrs. In SET D, (**j-l**) HeLa cells incubated with bpy for 1 hr followed by the addition of 50 µg/mL polymer and incubated for 4 hrs and then supplemented with ferrous sulfate (50 µM) (prepared in growth media) and incubated for 1 hr. In all experimental sets incubation at 37 ^{0}C with 5% CO_2 atmosphere was maintained. Before live cell imaging cells were washed with PBS.

As already discussed in fluorescent sensing in water, other cellular metal ions did not present any interference highlighting the selectivity of polymer towards Fe^{2+} ion. It is also important to examine the ability of the polymer to differentiate the changes in the endogenous levels of labile iron. Therefore, external supplementation of iron was done in set D experiment using ferrous sulphate (50 μg/ml) that induced changes in the endogenous levels of labile Fe^{2+} pools. The same sequence of two stages in set C was followed in set D and completed with external supplementation of iron at the final stage. The first stage treatment of HeLa cells by bpy ligand was to complex already available labile Fe^{2+} pool. The polymer that was treated in the second stage exhibited visual blue fluorescence because of the non-availability of labile Fe^{2+} ions. When iron was supplemented into the cells, the fluorescence of the polymer was quenched due to the complexation of polymer with the supplemented labile iron. Corresponding images are given in set D (Figure 4.10j-l). This demonstration highlighted the applicability of the new polymer probe for extremely selective detection and imaging of labile Fe^{2+} pools in HeLa cells and also to determine the changes in the endogenous levels of labile Fe^{2+} by stimulants.

4.3.8 Probable mechanism of Fe^{2+} sensing:

Glutamic acid is known to complex in a tridentate fashion forming 8 membered chelate ring and 5 membered chelate ring with most of the divalent ions as shown in Figure 4.11a, without any appreciable selectivity.[41] When the glutamic acid was appended to fluorene unit through side chain carboxylate, only one amine and one carboxyl moiety remained accessible for coordination. In this aspect it resembled simple amino acids like glycine, which is known to form stable ferrous bis-glycinate chelate complexes[42-44] in water at pH between 3 and 8, as shown in Figure 4.11b. In the ferrous bis-glycinate complex, a covalent bond is formed between the oxygen from the carboxyl COO- group and the Fe(II). A second coordinate covalent bond is formed by the donation of both electrons from the amino group on glycine to the metal ion in a Lewis acid-Lewis base interaction. The interaction of the ligand and metal in the ferrous bis-glycinate complex also follows the least sterically hindered orientation by assuming uniform tetrahedral bond angles between the covalent and

(a)

L-Glutamic acid complexes with divalent metal ions
No selectivity

(b)

$2\ H_2N$ ... OH $+$ Fe^{2+} $\longrightarrow$ ... $+$ $2H^+$

(c)

Ferrous bis(glycinate) complex

(d)

Iron(II)

High selectivity

L-Glutamic acid appended polyfluorene

Figure 4.11 (a-d) Schematic representation of the sensing of iron(II)

coordinate bonds and the metal ion as confirmed with the single crystal data in Figure 4.11c.[42] The charge on the ferrous ion also makes it energetically feasible to form bonding interaction with two glycine ligands. The appendage of two units of glutamic acid per repeating unit of fluorene is expected to bring into play favorable orientation effects for selectivity towards ferrous ions. With the side chain carboxyl unit covalently linked to the side chain of polyfluorene, the glycine-like unit from two side

chains on the same repeat unit is favorably oriented to engage in ferrous-bis-glycinate type chelate complexes.

In the case of the actual ferrous bis-glycinate chelate, the charges on the ion and ligand are balanced at a 1:2 molar ratio. In PF-Ph-GA, since one repeat unit accounts for two glycine-like units, a stoichiometry of 1:1 (polymer: metal ion) was observed in the ITC as well as fluorimetric titration experiments. Figure 4.11d shows the schematic representation of the tetrahedral ferrous complex formed between the polymer and the metal ion which results in the quenching of polymer fluorescence.

4.4 Summary

The levels of intracellular labile Fe^{2+} pools are necessary to be monitored in the biological system to understand the physiological processes. To meet this purpose, development of rapid sensing probes with cell viability is strongly suggested by recent reports in literature. For the first time, we have introduced polymer based probe for rapid selective detection of Fe^{2+} in water as well as imaging labile Fe^{2+} pools in living cells. The polymer has pronounced, fast nanomolar sensitivity for Fe^{2+} in water with quenching of blue fluorescence. A 'turn-off' probe is a more reliable sensor in the systems like cells having high background interference. Though simple glutamic acid does not show selectivity for any of the divalent ion, interestingly the appended glutamic acid exhibited supreme selectivity for Fe^{2+} over various metal ions particularly competing bioavailable metal ions such as Fe^{3+}, Zn^{2+}, Co^{2+}, Cu^{2+}, Mn^{2+} and Ni^{2+} etc in water. The polymer design with two glutamic acid appendage from each repeat unit allowed for a glycine like structure which is known to form stable tetrahedral ferrous bis-glycinate chelate complexes, accounting for the selectivity of the polymer towards Fe^{2+} ions. The amino acid appendage also facilitated the easy entry of the polymer into cells affording cell viability. MTT assay performed in HeLa cells highlighted the >90 % cell viability of the polymer even at 300 µg/ml of supplementation. Intracellular imaging of labile Fe^{2+} ion pools in living cells could be successfully carried out using the polymer PF-Ph-GA. This contribution is expected to stimulate the development of biocompatible selective intracellular imaging probes for identifying the endogenous changes in living cells.

4.5 References

1) Wilson, M. T.; Reeder, B. J. *Exp. Physiol*. **2008**, *93*, 128–132.

2) Terwilliger, N. B. *J. Exp. Biol*. **1998**, *201*, 1085–1098.

3) Maton, A; Hopkins, J; Johnson, S; Maryanna Quon Warner; McLaughlin, D. L. C. W.; Warner, M. Q.; Wright, J. D. *Human Biology and Health*. Englewood Cliffs, New Jersey, USA: Prentice Hall, **1994**.

4) Rouault, T. A.; Tong, W.-H. *Nat. Rev. Mol. Cell. Biol*. **2005**, *6*, 345–351.

5) Brzóska, K.; Męczyńska, S.; Kruszewski, M. *Acta. Biochimica. Polonica*. **2006**, *53*, 685-691

6) Aisen, P.; Wessling-Resnick, M.; Leibold, E. A. *Curr. Opin. Chem. Biol*. **1999**, *3*, 200–206.

7) Costas, M.; Mehn, M. P.; Jensen, M. P.; Que, L. J. *Chem. Rev*. **2004**, *104*, 939–986.

8) Barton, J. C.; Edwards, C. Q.; Phatak, P. D.; Britton, R. S.; Bacon, B. R. *Handbook of Iron overload and disorders*. Cambridge University Press, New York, **2010**.

9) Molina-Holgado, F.; Hider, R. C.; Gaeta, A.; Williams, R.; Francis, P. *BioMetals* **2007**, *20*, 639-654.

10) Huang, X. *Mutat. Res., Fundam. Mol. Mech. Mutagen*. **2003**, *533*, 153–171.

11) McKie, A. T.; Barrow, D.; Latunde-Dada, G. O.; Rolfs, A.; Sager, G.; Mudaly, E.; Mudaly, M.; Richardson, C.; Barlow, D.; Bomford, A.; Peters, T. J.; Raja, K. B.; Shirali, S.; Hediger, M. A.; Farzaneh, F.; Simpson, R. J. *Science* **2001**, *291*, 1755-1759.

12) Qin, C.; Cheng, Y.; Wang, L.; Jing, X.; Wang, F. *Macromolecules* **2008**, *41*, 7798–7804.

13) Wang, B.; Hai, J.; Liu, Z.; Wang, Q.; Yang, Z.; Sun, S. *Angew. Chem. Int. Ed.* **2010**, *49*, 4576–4579.

14) Bricks, J. L.; Kovalchuk, A.; Trieinger, C.; Nofz, M.; Buschel, M.; Tolmachev, A. I.; Daub, J.; Rurack, K. *J. Am. Chem. Soc*. **2005**, *127*, 13522–13529.

15) Wu, X.; Xu, B.; Tong, H.; Wang, L. *Macromolecules* **2010**, *43*, 8917–8923.

16) Kennedy, D. P.; Kormos, C. M.; Burdette, S. C. *J. Am. Chem. Soc*. **2009**, *131*, 8578–8586.

17) Sui, B.; Tang, S.; Liu, T.; Kim, B.; Belfield, K. D. *ACS Appl. Mater. Interfaces* **2014**, *6*, 18408−18412.

18) Ho, J. A.; Chang, H.-C.; Su, W.-T. *Anal. Chem*. **2012**, *84*, 3246−3253.

19) Dwivedi, A. K.; Saikia, G.; Iyer, P. K. *J. Mater. Chem*. **2011**, *21*, 2502-2507.

20) Au-Yeung, H. U.; Chan, J.; Chantarojsiri, T.; Chang, C. J. *J. Am. Chem. Soc*. **2013**, *135*, 15165–15173.

21) Hirayama, T.; Okuda, K.; Nagasawa, H. *Chem. Sci*. **2013**, *4*, 1250-1256.

22) Li, P.; Fang, L.; Zhou, H.; Zhang, W.; Wang, X.; Li, N.; Zhong, H.; Tang. B. *Chem. -Eur. J*. **2011**, *17*, 10520 – 10523.

23) Chan, Y.-H.; Jin, Y.; Wu, C.; Chiu, D. T. *Chem. Commun*. **2011**, *47*, 2820–2822.

24) McQuade, D. T.; Pullen, A. E.; Swager. T. M. *Chem. Rev*. **2000**, *100*, 2537−2574.

25) Liu, B.; Bazan, G. C. *Chem. Mater*. **2004**, *16*, 4467–4476.

26) Senthilkumar, T.; Asha, S. K. *Macromolecules* **2013**, *46*, 2159-2171.

27) Manhat, B. A.; Brown, A. L.; Black, L.A.; Ross, J. B. A.; Fichter, K.; Vu, T.; Richman, E.; Goforth, A. M. *Chem. Mater.* **2011**, *23,* 2407–2418.

28) Bang, J. H.; Suh, W. H.; Suslick, K. S. *Chem. Mater.* **2008**, *20,* 4033–4038.

29) Kumar, R.; Ding, H.; Hu, R.; Yong, K.-T.; Roy, I.; Bergey, E. J.; Prasad, P. N. *Chem. Mater.* **2010**, *22,* 2261–2267.

30) Cunzhi, H.; Jiexian, J.; Xianwen, Z.; Jingang, G.; Shumin, Z.; Lili, D. *Biol. Trace Elem. Res.* **2003**, *94*, 113-122.

31) Thomas III, S. W.; Joly, G. D.; Swager. T. M. *Chem. Rev.* **2007**, *107*, 1339−1386.

32) McRae, R. L.; Phillips, R. L.; Kim, I.-B.; Bunz, U. H. F.; Fahrni, C. J. *J. Am. Chem. Soc.* **2008**, *130*, 7851.

33) Senthilkumar, T.; Asha, S. K. *Macromolecules* **2015**, *48,* 3449–3461.

34) Senthilkumar, T.; Asha, S. K. *Chem. Comm.* **2015**, *51*, 8931-8934.

35) Swager, T. M. *Acc. Chem. Res.* **1998**, *31*, 201-207.

36) Zhou, Q.; Swager, T. M. *J. Am. Chem. Soc.* **1995**, *117*, 12593–12602.

37) a) Moreno-Pirajan, J. C. Thermodynamics - Interaction studies, solids, liquids and gases. InTech publisher, **2011**;

38) http://www.chimica.unipd.it/fabrizio.mancin/pubblica/Suprachem/IIIezione Mancin.pdf

39) Breuer, W.; Epsztejn, S.; Cabantchik, Z. I. *J. Biol. Chem.* **1995**, *270*, 24209–24215.

40) Romeo, A. M.; Christen, L.; Niles, E. G.; Kosman, D. J. *J. Biol. Chem.* **2001**, *276*, 24301–24308.

41) Sajadi, S. A. A. *Natural Science* **2010**, *2*, 85-90.

42) Ashmead, S. D. *Arch Latinoam Nutr*. **2001**, *51*, 7-12.

43) Pineda, O.; Ashmead, H. D. *Nutrition* **2001**, *17*, 381-384.

44) Olivares, M.; Pizarro, F. *Arch Latinoam Nutr.* **2001**, 51, 22-25.

CHAPTER - 5

Homochiral Biomimetic Polyfluorene for Enantioselective Separation and Chiral Sensing

Chiral sensing and enantioselective separation of biomolecules remains a significant challenge since the biological and chemical activities are highly specific for particular chiral form. A polyfluorene appended with protected $_L$-glutamic acid is presented that exhibited α-helix/β-sheet conformation and helical porous morphology. The new homochiral polymer probe enabled efficient heterogeneous enantioselective separation and chiral sensing of a wide variety of substrates from their aqueous racemic mixture in an easy 'Filter-and-Separate' method.

5.1 Introduction

Chirality plays an indispensible role in the molecular design of naturally occurring biomolecules like amino acids, sugars, proteins and DNA.[1] Most of the biologically active drugs, food additives, perfume bases, herbal products are optically active. Since the biological and chemical activities are highly specific for particular chiral form,[2] chiral sensing and enantioselective separation of desired biologically active enantiomers remains a significant challenge.

Chromogenic receptors with inbuilt chirality can act as chiral sensing probes via non-covalent interactions with chiral analytes, thereby enabling the analysis of multiple components in a less time consuming manner. For example, supramolecular ensembles, 'indicative displacement assays', stereodynamic probes etc have been reported for chiral sensing based on coordinative complexation with chiral analytes.[3-7] Recently, an achiral supramolecular-dye ensemble probe was reported for chiral sensing of amino acids, which could be extended to proteins also.[8] Although there are several reports on chiral sensing probes, the main drawback of a majority of these probes is their specificity to particular chemical group of analytes due to inherent specific binding nature. Besides, they require chiral isomer at high levels of enantiopurity to realize sensing activity and also for building homochiral structure. They are thus unable to separate racemic mixture because the introduction of racemic mixture would diminish their activity. Enantiomeric excess determination and enantioselective separation of racemic mixtures are important aspects that still rely on tedious asymmetric synthesis involving costly chiral catalysts and time consuming chromatographic techniques. Homochiral metal organic frameworks (MOF) have been demonstrated for enantioselective separation[9,10] due to their inherent molecular adsorption property. However, the low certainty in crystal growth of the homochiral MOF and narrow range of analyte window are prevailing limitations. To the best of our knowledge, a single homochiral probe for combined operations of enantioselective separation and chiral sensing for wide range of biomolecular analytes is unprecedented so far.

In this chapter, a homochiral polyfluorene (PF-GAP) with protected $_L$-glutamic acid appendage is presented for demonstrating enantioselective separation and chiral

sensing of biomolecules in a wide range of chemical classes namely amino acids, sugars, ascorbic acid, hydroxy acid, amino alcohol and aromatic drug for the first time. Synthesis of homochiral conjugated polymers can be achieved by polymerizing chiral monomers, doping or blending a chiral moiety to the conjugated backbone.[11,12] Polyfluorenes are known to induce helical conformation with preferred handedness.[13,14] Chiral amino acids are very interesting molecules to be incorporated either into the backbone or side chain to induce chirality in polymers. Appending chiral amino acid to polyfluorene is expected to confer homochirality to the conjugated polymer, thereby combining the photophysical characteristics of the polymer with specific conformations creating an attractive route for biomimetic design. The new homochiral polyfluorene exhibited biomimetic helical conformation and porous 3D morphology. The porous wall could be expected to allow passage of biomolecules into the polymer scaffold and the homochirality could be expected to play a role in the selective uptake of particular enantiomer.

5.2 Experimental Section

Materials: 2, 7-dibromofluorene, 6-bromo-1-hexanol, 4-dimethyl amino pyridine, dicyclohexyl carbo diimide (DCC), Tetrabutyl ammonium bromide, o-phthaldialdehyde, Borate buffer, Trifluoro acetic acid, Phosphate buffered saline (PBS), Pd(PPh$_3$)$_4$, and 1, 4-benzene diboronic bis(pinacolatoester) were purchased from sigma Aldrich. Boc-**L**-glutamic acid-1-tert butyl ester was purchased from Alfa Aesar chemical Ltd & co. NaOH, Na$_2$CO$_3$, K$_2$CO$_3$ and 2-mercaptoethanol were purchased from Merck chemicals. Toluene, Tetrahydrofuran (THF), methanol, DCM, ethylacetate and pet ether were purchased locally and dried by the standard drying procedures. HPLC grade acetonitrile, hexane, 2-propanol and methanol were purchased from Merck chemicals.

Methods: NMR spectrum was analyzed using Bruker-AVENS 400 MHz spectrometer. Chemical shifts are reported in ppm at 25 ^{0}C using CDCl$_3$ and DMSO-d$_6$ solvents containing trace quantity of tetramethylsilane (TMS) as internal standard. The MALDI-TOF analysis was done on Voyager-De-STR MALDI-TOF (Applied Biosystems, Framingham, MA, USA) equipped with 337-nm pulsed Nitrogen laser

used for desorption and ionization. 1 μM solution of sample was premixed with DHB (2, 5- dihydroxy benzoic acid) matrix in THF and mixed well before spotting on 96-well stainless steel MALDI plate by dried droplet method for MALDI analysis. The molecular weights of the polymer was determined by Gel Permeation Chromatography (GPC), equipped with a Viscotek VE 1122 pump, Viscotek VE 3580 RI detector and Viscotek VE 3210 UV/vis detector in THF using polystyrene as standards. Scanning Electron Microscopy (SEM) images were recorded using a FEI, QUANTA 200 3D scanning electron microscope with tungsten filament as electron source. Polymer powder was directly mounted on the carbon tape. Before recording the morphology, films were coated with a 5 nm thick gold film by spluttering method. The thermal stability and uptake of enantiomers by the polymer was analyzed using a PerkinElmer:STA 6000 thermogravimetric analyzer (TGA) under Nitrogen atmosphere from 50 to 800 °C at 10 °C/min. Differential scanning calorimetric (DSC) analysis was performed using a TA Q10 model. 2−3 mg of the sample was taken in aluminum pan, sealed and scanned at 10 °C/min. The instrument was calibrated with indium standards before measurements.

Circular Dichroism (CD) studies:

Solution state CD measurements were recorded using JASCO-815 CD spectrometer equipped with a Jasco PTC-424S/15 peltier system. 2 mm path-length quartz cuvettes were used for a sample volume of 1 mL in distilled water at 25 ^{0}C. Three scans were averaged for each sample. The polymer powder was ground with KBr and made into a thin transparent pellet and used for the solid state CD measurement.

HPLC Measurements:

Chiral HPLC measurements were performed in an Agilent technology (1200 infinity series USA) instrument using CHIRALCEL OJ-H columns (150 x 4.6 mm, particle size 5 μm) maintained at 35 ^{0}C using UV detector (λ at 257 nm). The mobile phase used was 2-propanol:*n*-hexane = 10:90 with 0.1 % TFA. The flow rate of the mobile phase was 0.8 ml/min and the injected volume was 10 μl. Analytical quantification was performed using 2 different columns. The method followed for amino acids was as follows: HPLC − Agilent technologies (1200 infinity series USA) equipped with

Eclipse Plus-C18, (4.6 x 100 mm) column maintained at 35 ^{o}C, with UV detector (λ at 334 & 350 nm). Mobile phase-A (PBS buffer), B (acetonitrile/methanol/water-45/40/15). Composition A and B were varied for each amino acids. For glutamic acid the composition was A (90 %) and B (10 %), for tyrosine A (60 %) and B (40 %) and for phenylalanine A (40 %) and B (60 %). For leucine and proline the mobile phase was changed to A (25 %) and B (75 %). The flow rate of the mobile phase was 0.5 ml/min. The quantification of mannitol sugar was performed using Agilent technologies HPLC (1200 infinity series USA) equipped with HC – 75 Pb^{2+} Hamiltaon, 7.8 mm x 300 mm) column maintained at 80 ^{o}C, detector – refractive index detector. During analysis the temperature was maintained at 40 ^{o}C. Mobile phase: H$_2$O; Flow rate: 0.5 ml/min and the injected volume was 10 μl.

Heterogeneous enantioselective separation (HES):

HES experiments were carried out in water. Racemic mixture (10 mg of (D):10 mg of (L)) of enantiomers was dissolved in 10 ml of distilled water. The Fine powdered (5 mg) polymer particles were suspended in water and stirred for 48 hours. At the end of 48 hours the mixture was filtered using whatmann filter paper to separate out the polymer. The polymer powder was used to measure the solid state CD measurement. The decanted aqueous solution was used for quantifying the enantiomer uptake of the polymer. The enhancement of solid state CD of polymers was calculated from the area under the curve of the CD spectra of the polymer before and after HES process. The ratio between the areas gave the % enhancement of chiral amplification. The percentage enantiomer uptake of polymer was determined using solution state CD spectra of filtered solutions and pure enantiomers (10 mg/10 ml) in water. The area under the curve was calculated for each reference enantiomer and filtered solutions. The ratio between the areas gave the % uptake of enantiomer by the polymer.

Sample preparation for HPLC: The amino acids were quantified in HPLC using a derivatization procedure. o-Phthalaldehyde (OPA) reacts with primary amines in the presence of 2-mercaptothiol to form highly fluorescent isoindole products (D. Fekkes, *J. Chromatogr. B: Bomed. Sci. Appl.* **1996**, *682,* 3-22). In a typical experiment, o-phthaldialdehyde (OPA) (1.34 g), 2-mercaptoethanol (6 ml) was dissolved in borate buffer. The pH of the borate buffer was maintained at 6.9. This derivatizing reagent

was kept overnight at 4 ^{0}C and filtered through 0.45 μm PTFE filter. The amino acid was dissolved in water. The derivatizing reagent (OPA+thiol) was added to free amino acids to form isoindole products. This fluorescent isoindole product is characteristic of each amino acid and has different characteristic retention times. The concentration of the isoindole derivative directly indicates the concentration of amino acids in solution. To calculate enantiomeric excess (ee) of amino acids adsorbed on polymer, the amino acids were separated from the polymer and quantified using HPLC. Known concentrations (10, 7, 5, 3 mg/ml) of the derivatized amino acids were injected in HPLC to quantify the unknown amount of adsorbed enantiomer in the PF-GAP polymer. The area under the peak in HPLC was measured using the software for all the enantiomers from which the amount of unknown enantiomer was calculated.

5.3 Results and Discussion

5.3.1 Synthesis and Characterization:

The synthesis of protected ₗ–glutamic acid appended polyfluorene (PF-Ph-GA(boc) denoted as PF-GAP is discussed in previous chapter. The structure of the polymer (PF-GAP) was shown in scheme 5.1.
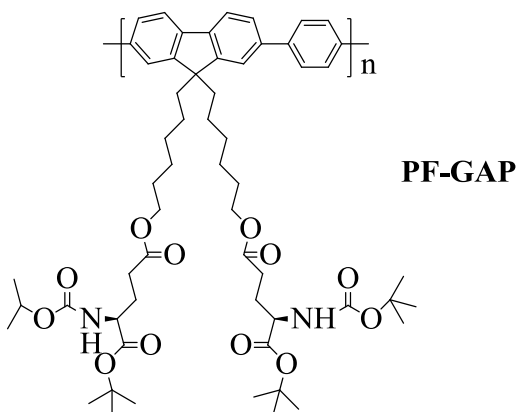
Scheme 5.1 Structure of the polymer PF-GAP.

PF-GAP was structurally characterized using ^{1}H NMR and ^{13}C NMR (Figure 5.1)**.** The molecular weights of the polymer obtained from SEC were Mn = 25,400; Mw = 43,200; Polydispersity (Ð) = 1.7 using polystyrene standard.
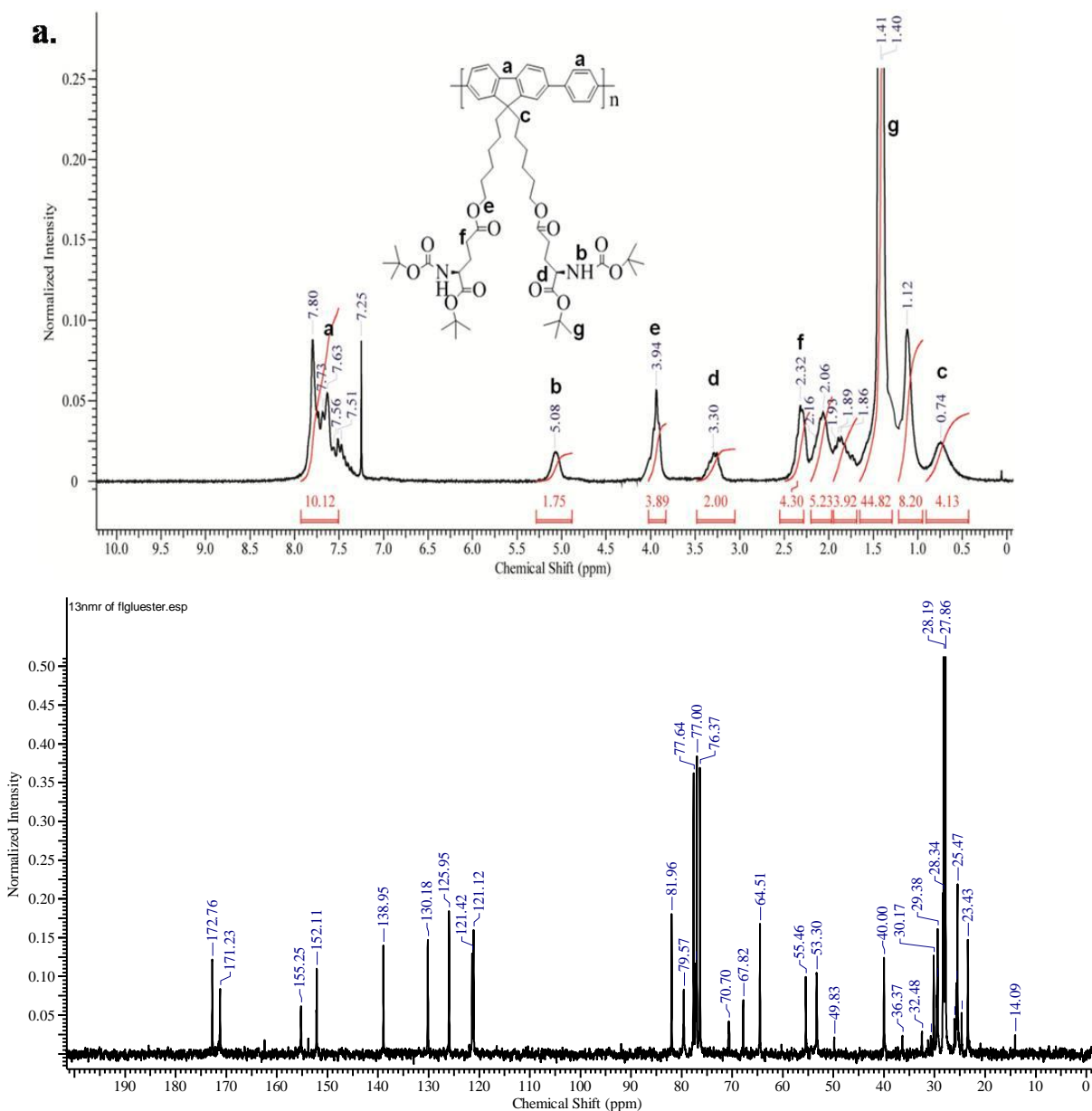
Figure 5.1 (a) ^{1}H NMR and (b) ^{13}C NMR spectra of PF-GAP in CDCl$_3$.

5.3.2 Conformation studies of the polymer:

The absorption and CD effects of PF-GAP were probed in THF as solvent. Figure 5.2a compares the normalized CD spectra of the protected L-glutamic acid (GAP) with that of the PF-GAP in THF. The absorption spectrum of the polymer (Figure 5.2b) is also included in the plot for comparison. L-GAP showed positive dichroic maxima at 215 and 228 nm with well defined negative maxima at 247 nm in its CD spectrum. The CD spectrum of the polymer was similar in shape to that of GAP with

positive dichroic maxima at 215 and 228 nm, but the negative extreme had double inflection points at 244 and 250 nm. More importantly, CD effects were observed covering the entire absorption range of polyfluorene (300-400 nm), where GAP did not have any dichroic activity. The CD spectrum of PF-GAP in the 300-400 nm region consisted of positive bands at 325 and 375 nm with a sharp negative band at 343 nm. The absorption maximum of the polymer was at 368 nm. The observation of the CD signal in the absorption range of the polymer confirmed the transfer of chirality from the side chain appended amino acid to the polymer backbone.
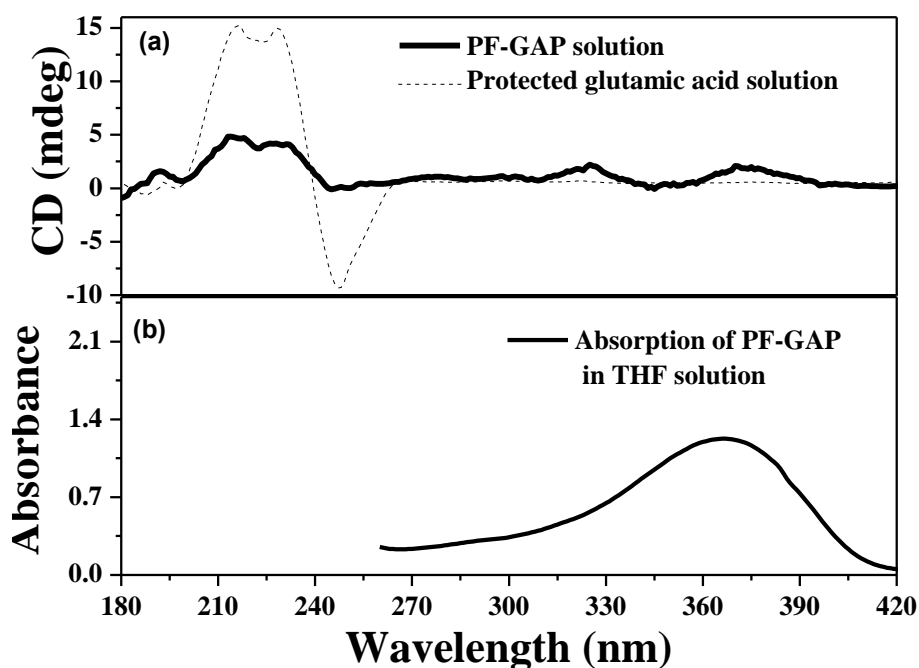
Figure 5.2 Solution state CD spectra (a) of PF-GAP and protected glutamic acid in THF and absorption spectrum (b) of PF-GAP in THF.

For the projected application of enantioselective separation, the chiral properties of the polymer in the powder form would be more relevant. Therefore, the solid state CD spectrum of the PF-GAP in dry powder form was analyzed (Figure 5.3). The spectra were recorded by grinding the polymer powder with KBR to form a thin transparent pellet, which was used for the solid state CD measurement. The CD spectrum of the powder sample was characterized by an intense positive cotton effect with peak maximum around 210 nm along with negative cotton effects around 230 nm and 245 nm. These features of the CD spectrum are characteristic of α-helix

conformation.[15] Compared to the CD spectrum in THF (Figure 5.2), the intensity of the signal in the < 275 nm region was high in the powder form. However, the CD signal beyond 300 nm in the range of the polymer absorption was not very significant.
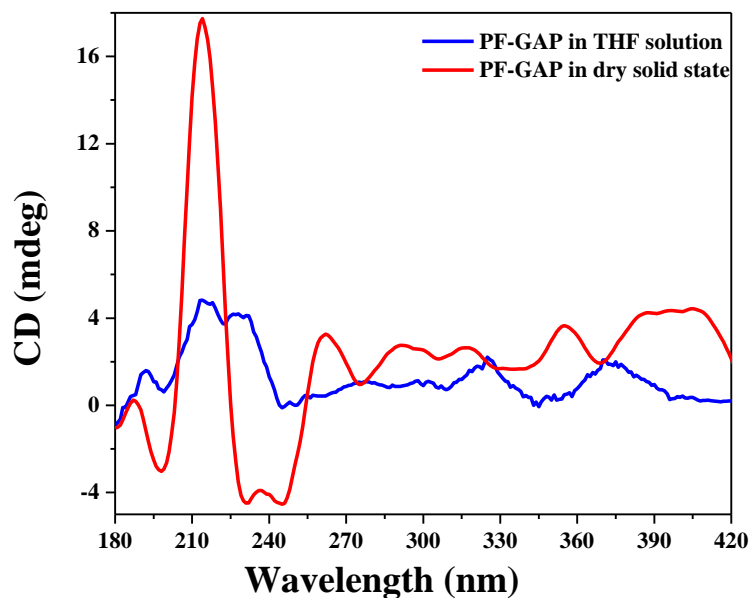

Figure 5.3 Comparison of the CD spectra of PF-GAP in solution and solid state.

The dry polymer powder was suspended in water for prolonged periods of time (48 h) and subsequently dried and the CD spectrum was recorded again. Figure 5.4.a, b compares the CD spectra of the polymer powder before and after treatment with water. It could be seen that after treatment with water the polymer conformation was altered; the typical double inflected negative band of the α-helix had disappeared. In its place a broad negative band was observed which was more characteristic of the β-sheet-like conformation. It is believed in protein unfolding studies that in presence of water, the hydrophobic moieties would collapse inside while the polar residues would remain on the surface to engage in intermolecular hydrogen bonding interaction with water molecules. In a similar way, the intermolecular hydrogen bonding interaction between the N-H groups of glutamic acid and water molecules formed the driving force for the observed change in conformation of PF-GAP upon being suspended in water.
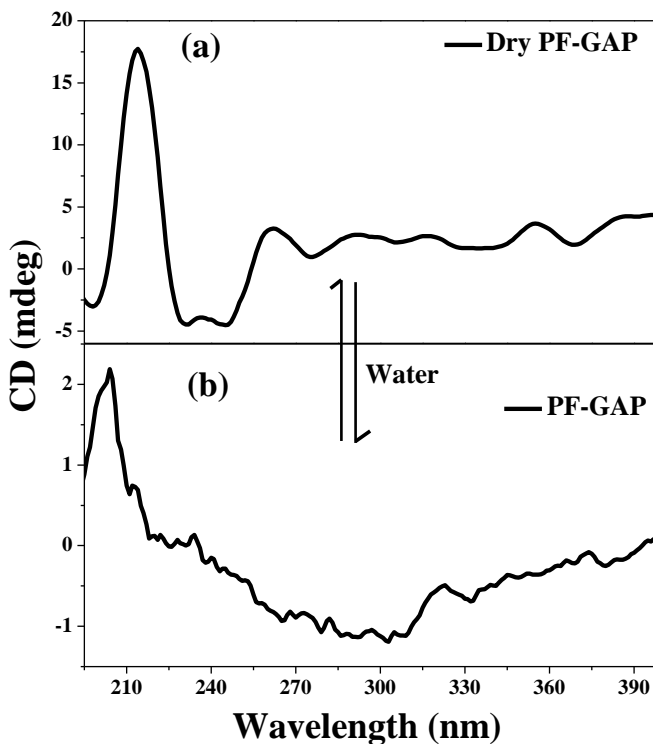
Figure 5.4 Solid-state CD of dry (a) and 2 days water treated (b) spectra of polymer (PF-GAP).

FT-IR spectroscopy has been used as a reliable tool to characterize the various secondary structures of proteins and polypeptides. This is based on the fact that the secondary structure of proteins like the α-helix, β-sheet and random conformations are associated with characteristic hydrogen bonding pattern between the amide >C=O and N-H groups. Therefore, each type of secondary structure will give rise to characteristic amide I absorption in the range 1600 -1700 cm^{-1}.[16] For instance, the vibration band at 1648 cm^{-1} is characteristic for α-helix conformation, while the β-sheet exhibits vibration at lower frequencies.[17] Figure 5.5 compares the expanded region in the FTIR spectra of PF-GAP before and after treatment with water, highlighting the characteristic vibrations. The band at 1648 cm^{-1} characteristic of α-helix conformation disappeared upon treatment with water. However, the α-helix conformation could be regained upon drying (Figure 5.6). The reversible change in conformation from α-helix to β-sheet and eventually to a random one in aqueous medium is known to occur in proteins due to variation in extent of hydration.[18]
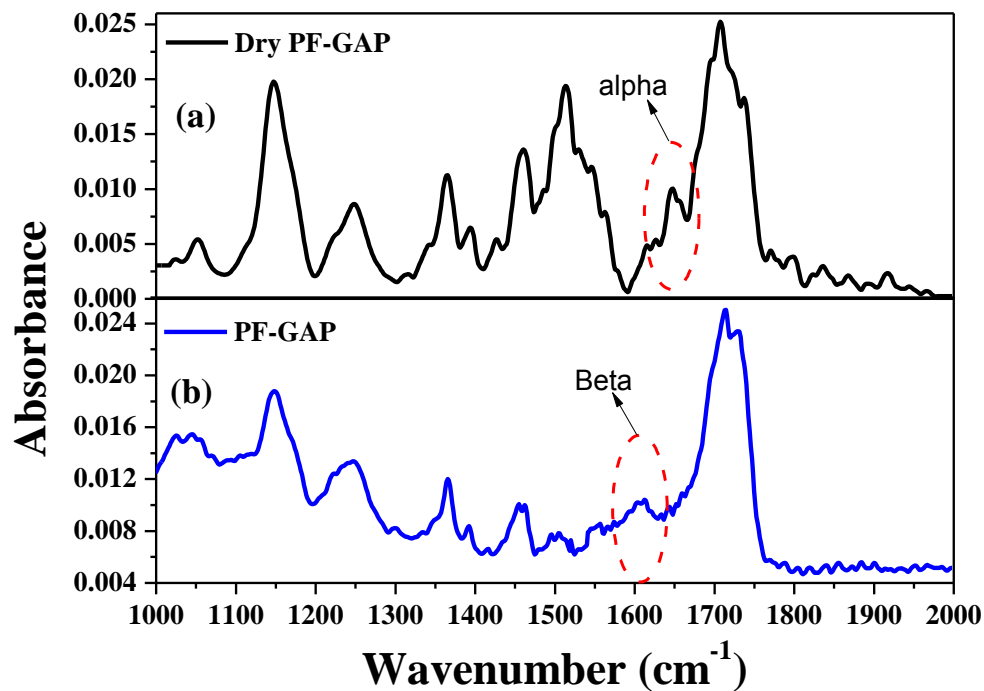
Figure 5.5 FT-IR spectra of the polymer PF-GAP in (a) dry and (b) after two days of treatment with water.
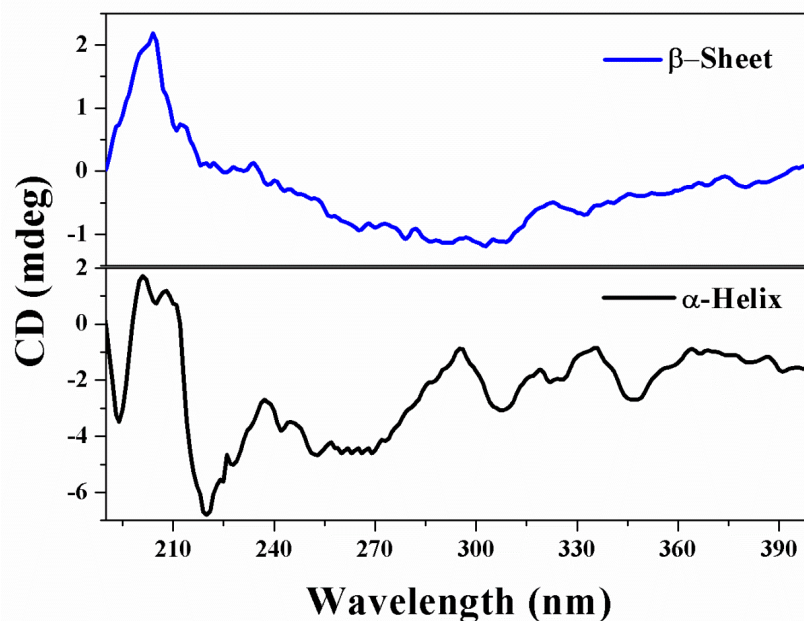
Figure 5.6 CD spectra of PF-GAP confirming reversibility between α-helix and β-sheet conformations.

5.3.3 Contact Angle and Morphology Studies:

The scanning electron microscopy (SEM) images of the dry PF-GAP are given in Figure 5.7.a-d**.** Dry PF-GAP revealed fibrous 3D filaments with pores on the surface and in Figure 5.7.d, the helical twisting of the filaments is well observed. The three dimensional helical fibrous morphology with pores on the surface mimicked the protein superstructure. Though the polymer was insoluble in water, the water treatment can influence noncovalent interactions with the polar amide moieties in the polymer structure. The changes in the hydrophillicity in PF- GAP polymer due to water treatment was traced by water contact angle measurements. THF solutions (10 µM) of the as-dried polymer and water-treated-and-dried polymer were drop cast on cover slip for the contact angle measurement (Figure 5.7.e and 5.7.f). A drop in contact angle was observed from an obtuse angle of 105° for the as-dried polymer with α–helix structure to <90° for the water treated-and-dried polymer with β-sheet-like structure.
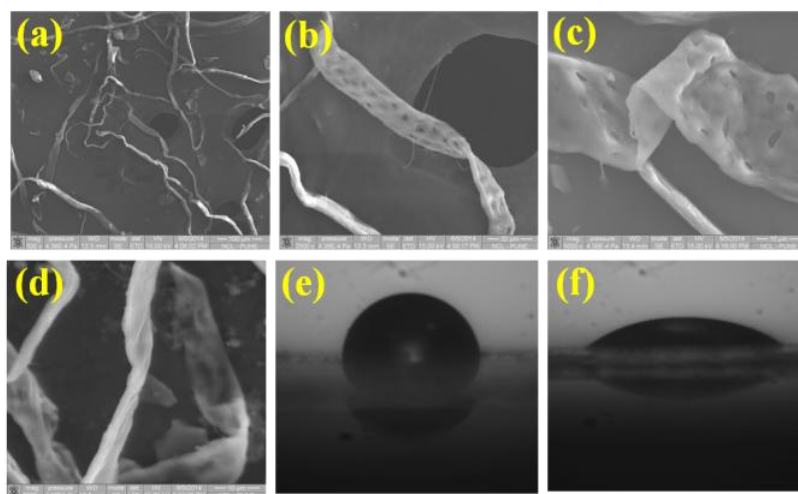

Figure 5.7 (a-d) Scanning electron microscopy (SEM) images of PF-GAP polymer particles on carbon tape. Contact angle of dry (e) and water treated (f) polymer (PF-GAP) drop cast from THF solutions on cover slip. [polymer]=10 µM.

As the enantioselective separation studies are planned to be demonstrated in water medium, the probe is expected to be insoluble in water in order to serve as solid

adsorbent of substrates in water. PF-GAP was not soluble in water; however the surface of the polymer became hydrated upon prolonged treatment with water. In fact, the hydration is expected to assist the polymer in interacting with the dissolved substrates in water by facilitating easy contact between water and the surface of the polymer. The morphology of the polymer also assists in the process of adsorption of the substrates. The pores on the polymer surface allowed the easy entry of the substrates into the polymer scaffold.

5.3.4 Heterogeneous Enantioselective Separation and Sensing:

The design of the polymer, the biomimetic conformations, influence of water on the conformations and the performance in enantioselective separation and sensing are schematically illustrated in Figure 5.8.
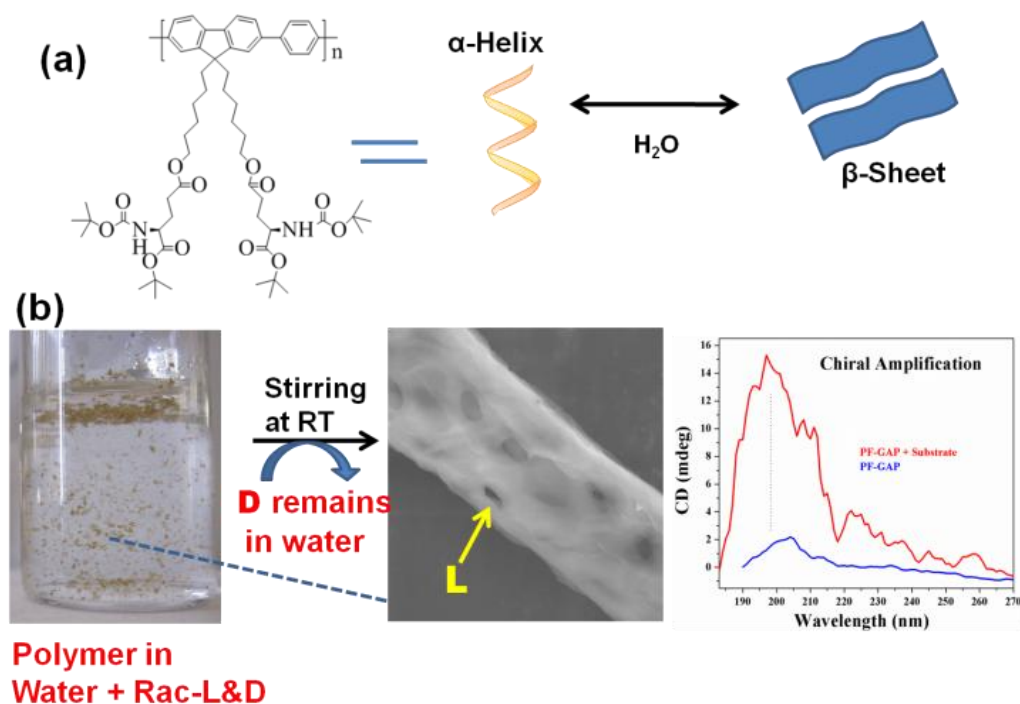
Figure 5.8 Schematic representations of the enantioselective separation and sensing using suspended polymer probe.

The homochirality with biomimetic helical conformation and porous morphology was exploited for enantioselective separation and sensing in water. The suspension of the polymer powder in water for prolonged periods with concurrent conformational change did not seem to bring about solubility in water, which was advantageous since

the polymer powder could be simply filtered and removed after the enantioselective separation. The chemical structure of the various classes of racemic mixtures of D- and L- substrates screened in the present study, which included various amino acids including glutamic acid, sugars such as mannitol, amino alcohol, hydroxy acids, Camptothecin and ascorbic acid is given in Figure 5.9. A typical heterogeneous enantioselective separation experiment involved dissolving 10 mg each of the D- and L- enantiomer in 10 ml of distilled water, into which 5 mg of fine powdered polymer was suspended. After 48 hours of stirring at room temperature the polymer powder was filtered, dried at ambient condition and analyzed.
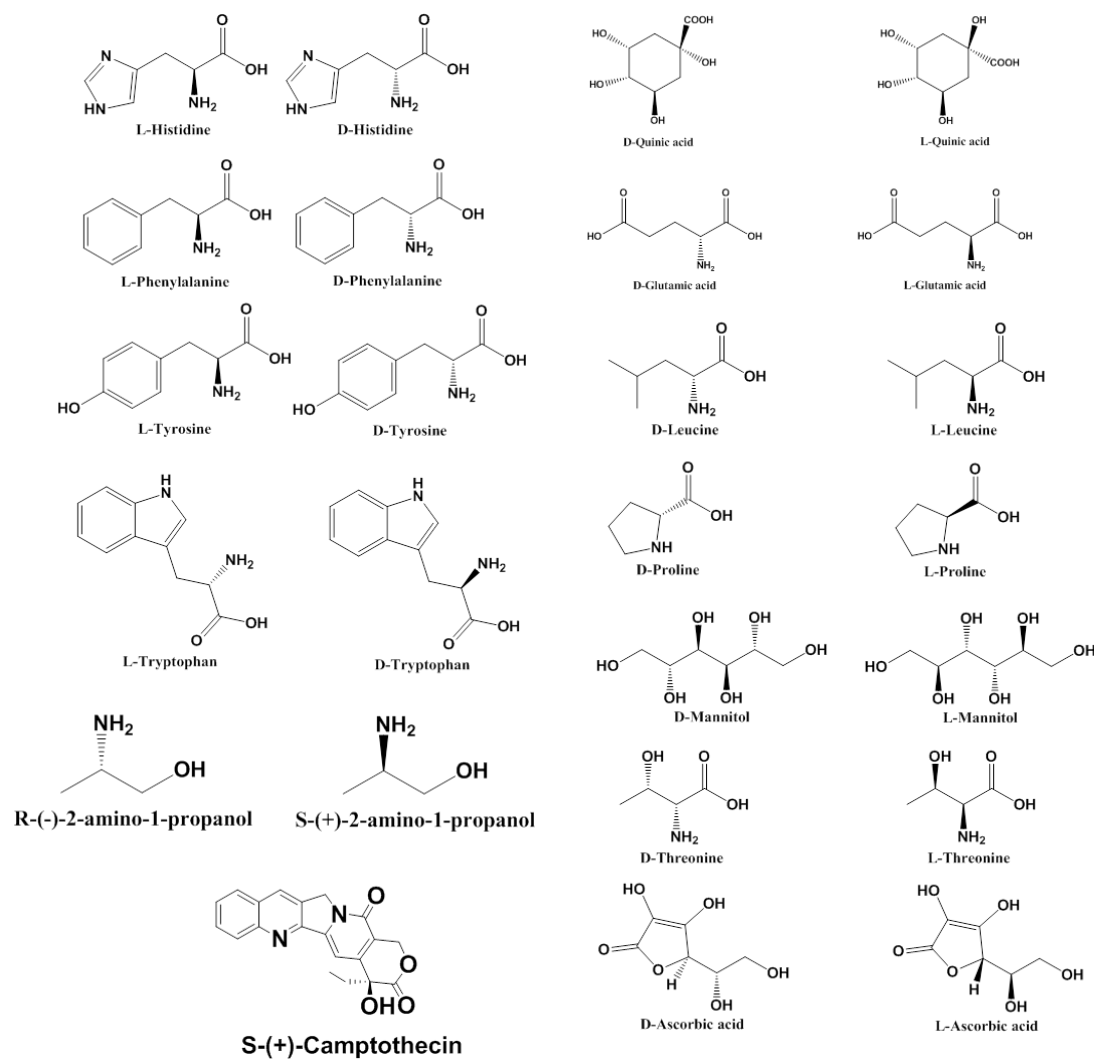

Figure 5.9 The chemical structure of all substrates screened in the present study.

Figure 5.10 shows three important substrates; a) Glutamic acid which has similar structure as that of the appendage b) Camptothecin which is a well known cancer drug and c) 2-amino propanol which is an important intermediate for several chiral drugs. The rest of the results corresponding to other substrates are grouped in Figure 5.11. The solid state CD spectra of the polymer powder collected after filtration from racemic mixtures of various substrates along with the CD spectrum of the β-sheet-like structure of the polymer is included in each plot for comparison.
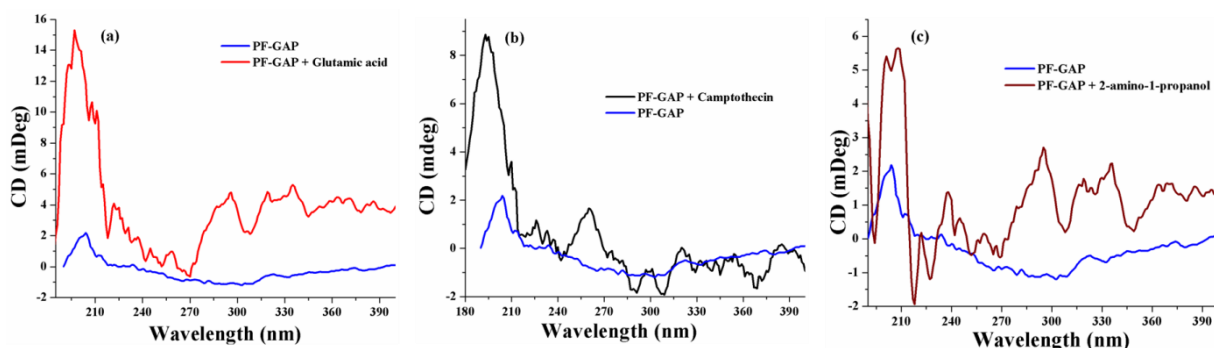
Figure 5.10 Circular dichroism sold state (CD) spectra of PF-GAP upon treatment with aqueous solutions of (a) Glutamic acid, (b) Camptothecin and (c) 2-amino-1-
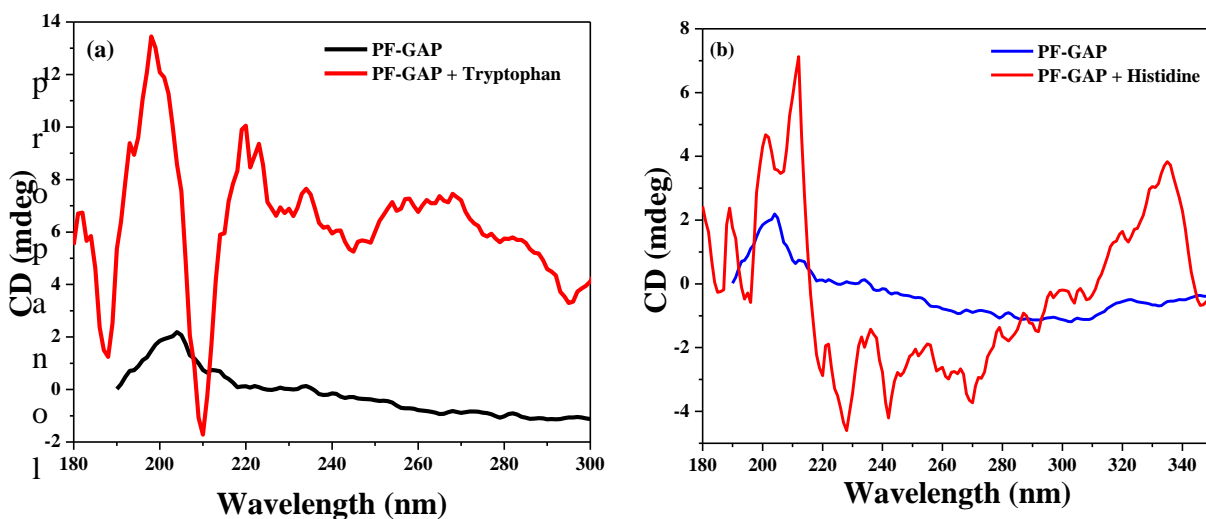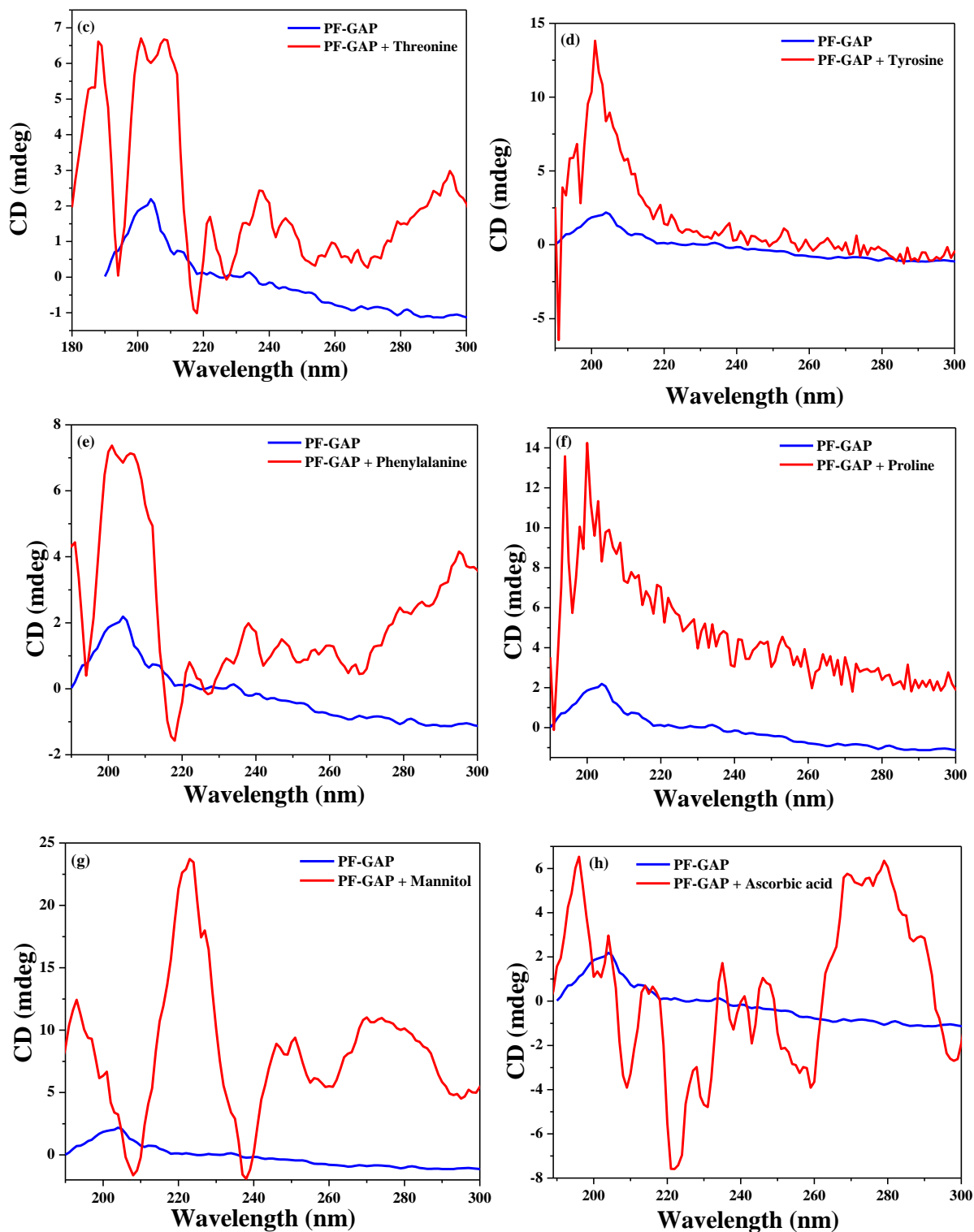
Figure 5.11 Solid state CD spectra of PF-GAP polymer treated with racemic mixtures.

It was observed that in all cases the chirality of the polymer PF-GAP was significantly amplified. The amplification of the CD signal was obtained from the area under the corresponding CD peak maxima (spectra in Figure 5.10 and 5.11). The enhancement was highest for glutamic acid which exhibited 11 fold increment in the intensity of the CD signal. Table 5.1 summarizes the percentage enhancement in the CD intensity of the polymer upon interaction with various racemic mixtures. The filtered solution remaining after removal of the polymer powder was also analyzed for the chiral signature.

**Table 5.1** Enatioselective separation, chiral sensing and % L-Enantiomeric excess determined from CD and HPLC data.

| Entry	± Substrate	Enhancement of Solid state CD of polymer (PF-GAP)	% L-Enantiomeric excess [a]	
			From CD	From HPLC
1	Glutamic acid	11.08	83.4	84.34
2	Threonine	5.3	58.12	
3	Histidine	2.37	49.55	
4	Quinnic acid	10.73	24.2	
5	Ascorbic acid	1.14	53.4	
6	2- Amino-1-propanol	3.43	94.5	
7	Phenylalanine	4.4	85.59	81.27
8	Leucine	8.34	38.2	39.16
9	Tyrosine	5.5	32.1	33.2
10	Proline	4.86	36.0	34.89
11	Mannitol	11.1	53.1	58.66
12	Tryptophan[b]	7.84	75.2	
13	Camptothecin[b]	8.45	75.62	

[a] Areas under the CD spectra shown in Figure 5.10 & 5.11 and HPLC chromatogram were used to determine the ee. [b] Only S or L - type of the isomer was used.

Figure 5.12 compares the solution state CD signal of the filtered solution along with the corresponding reference D- and L-enantiomers. In almost all examples, the filtered solution showed the signature of D-enantiomer confirming the fact that the polymer had selectively separated the L-enantiomer from the racemic mixture. The uptake of the L-enantiomer by the polymer was quantified based on the ratio between the area under the CD curve for the pure reference enantiomer (10 mg/10 ml) and filtered solution and is listed in Table 5.1.

It can be seen from Table-5.1 that PF-GAP exhibited the highest % uptake of 95 % for 2-amino-1-propanol. Enantiomeric excess (ee) of more than 80 % was observed for the amino acids – glutamic acid (83 %) and phenylalanine (86 %). Although amino alcohol exhibited the highest ee, other alcohol substrates like mannitol and ascorbic acid exhibited ee of around 50 % only. This value of the % enantiomeric excess obtained from the CD data was verified for a couple of samples by quantification using HPLC. In order to perform the HPLC experiment, the polymer with the adsorbed sample was filtered and removed from water, dried and then dissolved in toluene. The PF-GAP polymer remained soluble in toluene whereas the adsorbed substrates which were insoluble in toluene were precipitated out. The precipitated substrate was washed repeatedly with toluene to remove all traces of polymer, dried and used for the quantification experiments using HPLC.
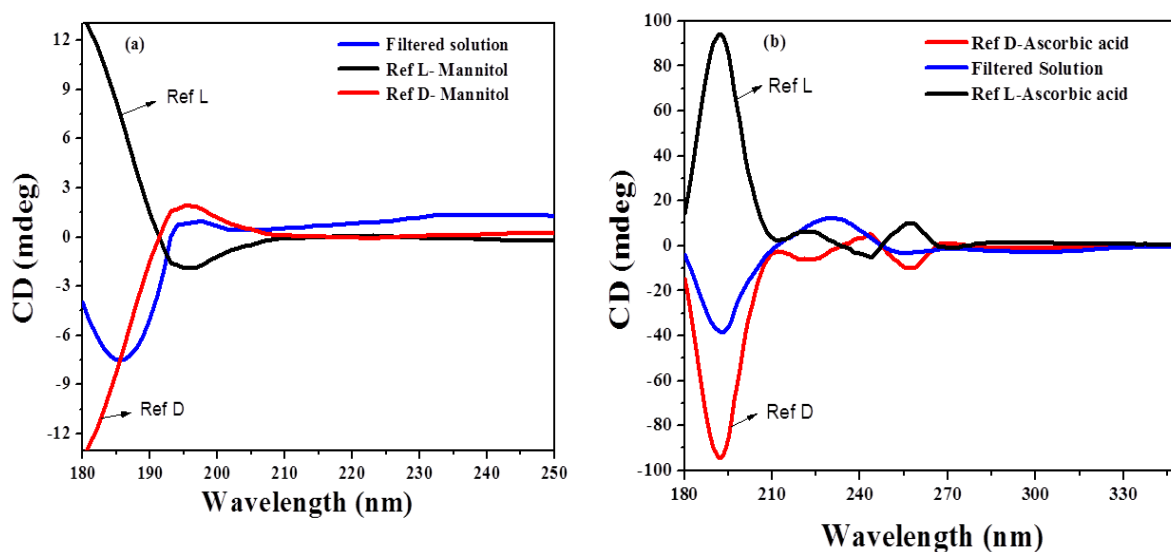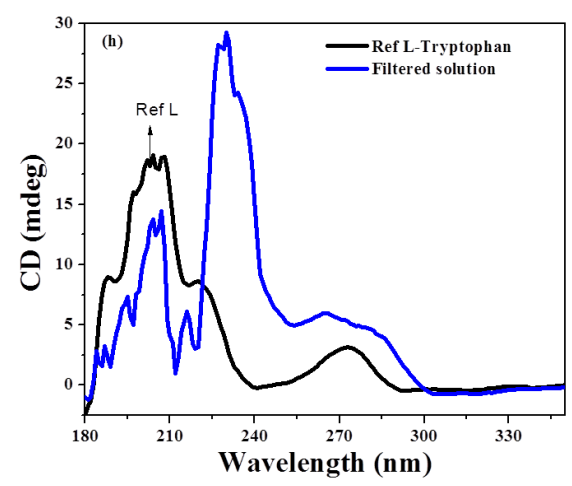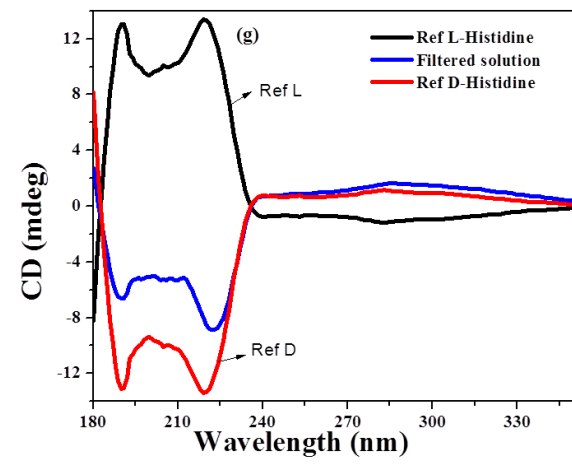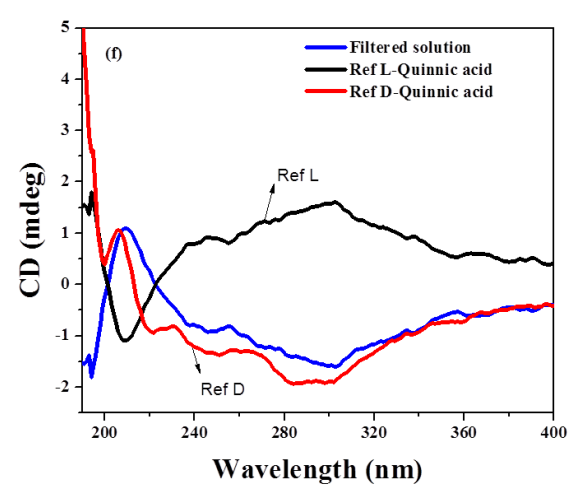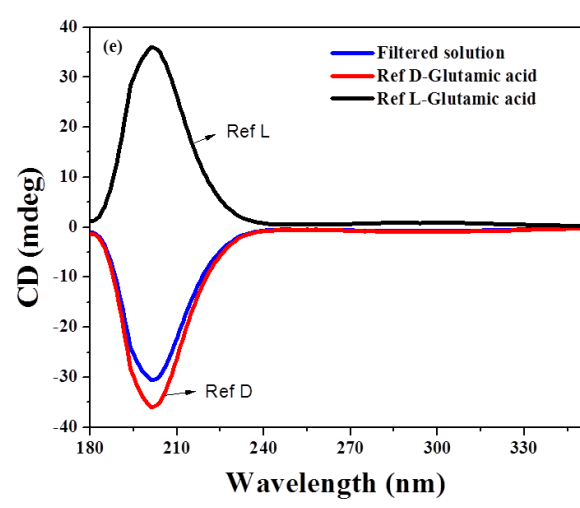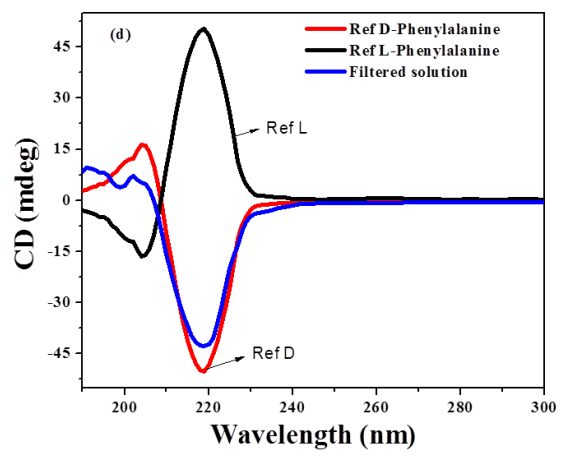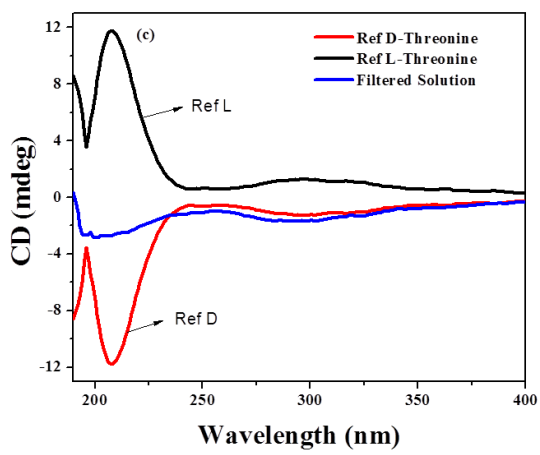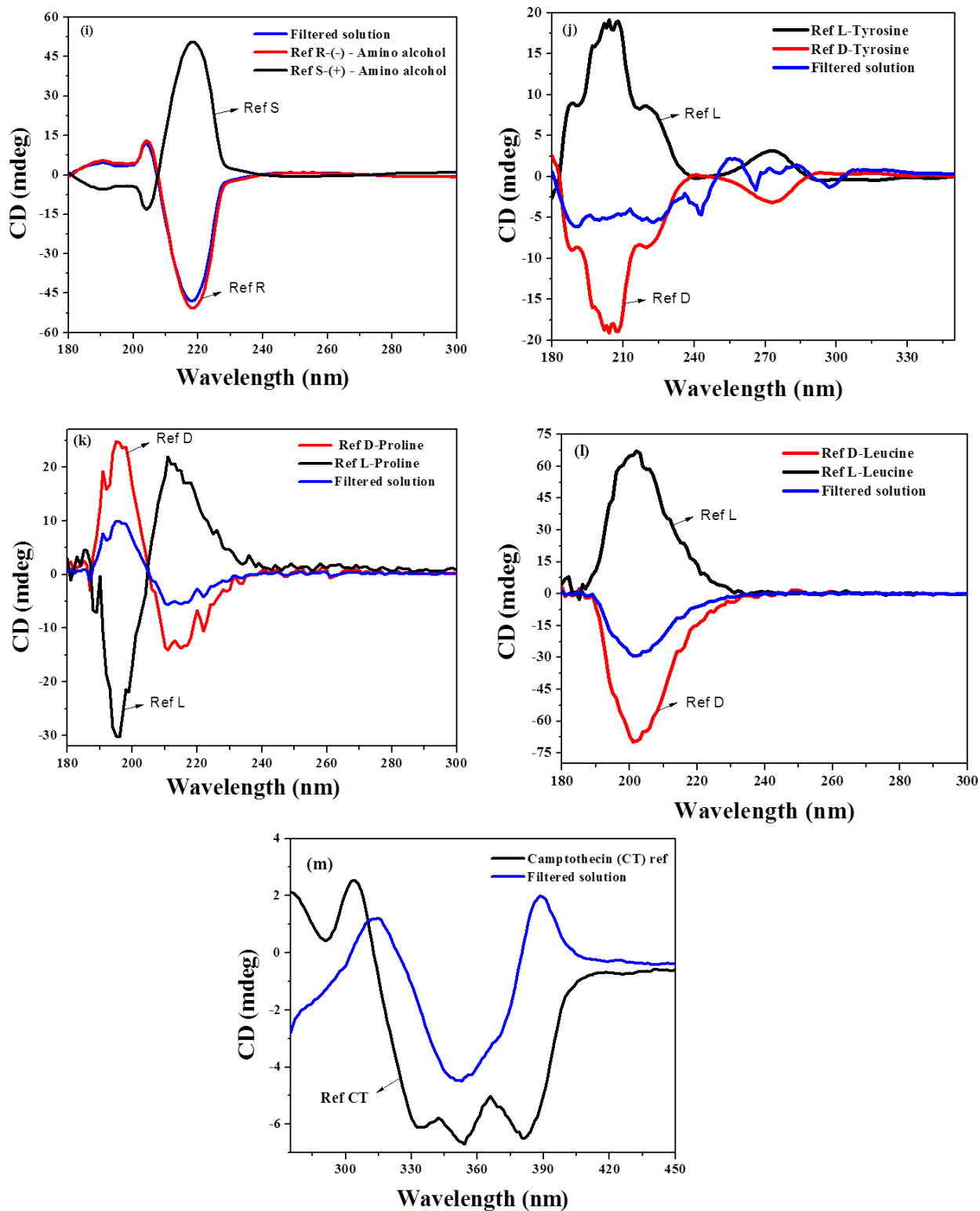
Figure 5.12 Circular dichroism spectra of the water solution obtained from heterogeneous enatioselective separation for various racemic mixtures.

Prior to the quantification experiments, pure D- and L- enantiomers of one of the samples – phenylalanine was injected into a chiral HPLC column (CHIRALCEL OJ-H, mobile phase: isopropanol/pet ether = 10:90 with 0.1 % TFA) and analyzed for their retention times. It was observed that the pure D-enantiomer had a retention time of 4.575 minutes, while the pure L-enantiomer had a retention time of 5.033 minutes. The adsorbed phenylalanine from the polymer sample exhibited a retention time of 5.025 minutes clearly demonstrating that it was the L-enantiomer, with complete absence of any trace of the D-enantiomer (Figure 5.13).
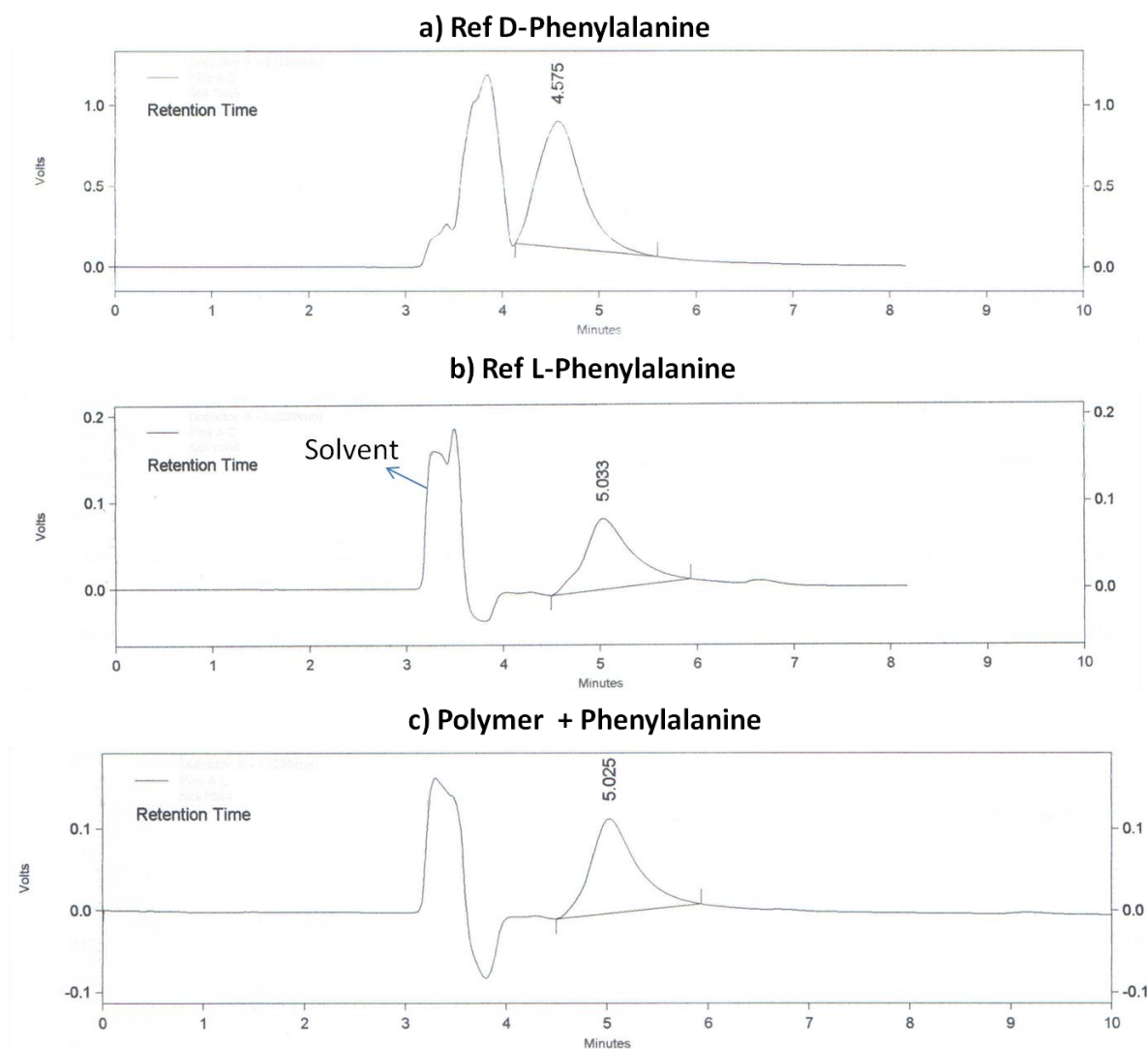
Figure 5.13 Chiral HPLC chromatogram of D- & L- Phenylalanine and adsorbed Phenylalanine.

Having demonstrated the absence of the D-enantiomer in the adsorbed sample, the quantification of the L-enantiomer adsorbed on the polymer was carried out in the analytical HPLC instrument after derivatization of the amino acids following standard literature procedure as explained in experimental section.[19] The details of the derivatization as well as the various columns used for the samples glutamic acid, phenylalanine, leucine, tyrosine and mannitol are provided in the experimental section. Table 5.1 compares the % enantiomeric excess obtained from the HPLC data. The values were in good agreement with that calculated using CD measurements.

The enantioselective uptake by the polymer could also be confirmed by analyzing dry polymer containing adsorbed substrate that was filtered from the separation process. The absorption spectra (in DMSO) had peaks of the substrate along with the polymer indicating the uptake of the substrates. Figure 5.14 shows the absorption spectra of few adsorbed samples.
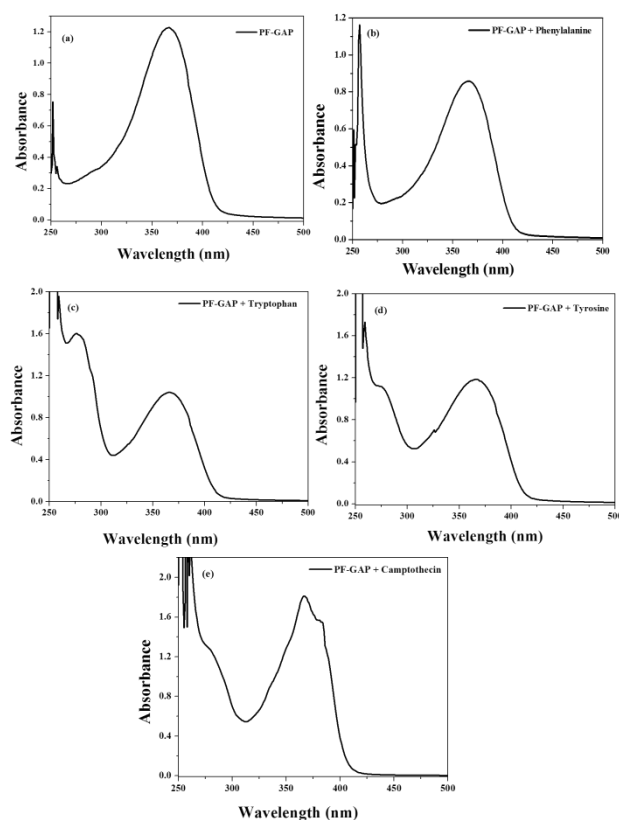
Figure 5.14 Absorption spectra recorded in DMSO for (a) PF-GAP, PF-GAP treated with (b) phenylalanine, (c) tryptophan, (d) tyrosine and (e) camptothecin.

One of the adsorbed polymer; PF-GAP + Phenylalanine was taken as a representative example and its proton NMR spectrum was recorded in DMSO-d_6. Figure 5.15 compares the proton NMR spectra of PF-GAP and PF-GAP + Phenylalanine in DMSO-d_6 and for comparison purpose, the proton NMR spectrum of phenylalanine was recorded in D_2O. The aromatic protons of phenylalanine appeared in the range 7.2 – 7.3 ppm, which merged with that of the aromatic protons of the polymer resulting in broadening of the entire aromatic region. The aliphatic proton signals of phenylalanine were also broadened which indicated the interaction between the polymer and substrate. The thermal characteristics of the substrate loaded polymer were also investigated using theromogravimetric analysis (TGA). Figure 5.16 compares the percentage weight loss data for PF-GAP + Phenylalanine along with that for dry PF-GAP and PF-GAP powder after stirring in water for 48 hours and drying. Although the decomposition pattern was the same, PF-GAP + Phenylalanine showed a higher (> 5 wt %) weight loss indicating loss of adsorbed material. In fact, PF-GAP stirred in water without any substrates also showed slightly different % weight loss indicating adsorption of water. The DSC thermogram exhibited a lowering of the glass transition temperature upon uptake of substrate (Figure 5.17).

All these evidences indicated adsorption of substrate in an enatioselective manner into the polymer matrix during the stirring process in water. The amplification of the chiral signal of the polymer upon enantioselective adsorption suggested a 'Sergeants and Soldiers' principle,[20] involving organization of the adsorbed enantiomer in the homochiral confines of the porous polymer fiber. Although both enantiomers entered the porous fibrous channels of the polymer along with water, the homochiral channels retained only the L-enantiomer following a 'like-dissolves-like' rule. Unlike a membrane based separation where only selective materials are allowed to pass through, the porous fibers of the polymer resembled 'cellular' uptake. The specific folding of the homochiral polymer could be expected to stabilize only the enantiomers with similar chiral identity through non-covalent interactions, just like the polypeptide folds which are able to perform specific biological function solely due to the specific sequence of amino acids having one type of chirality.
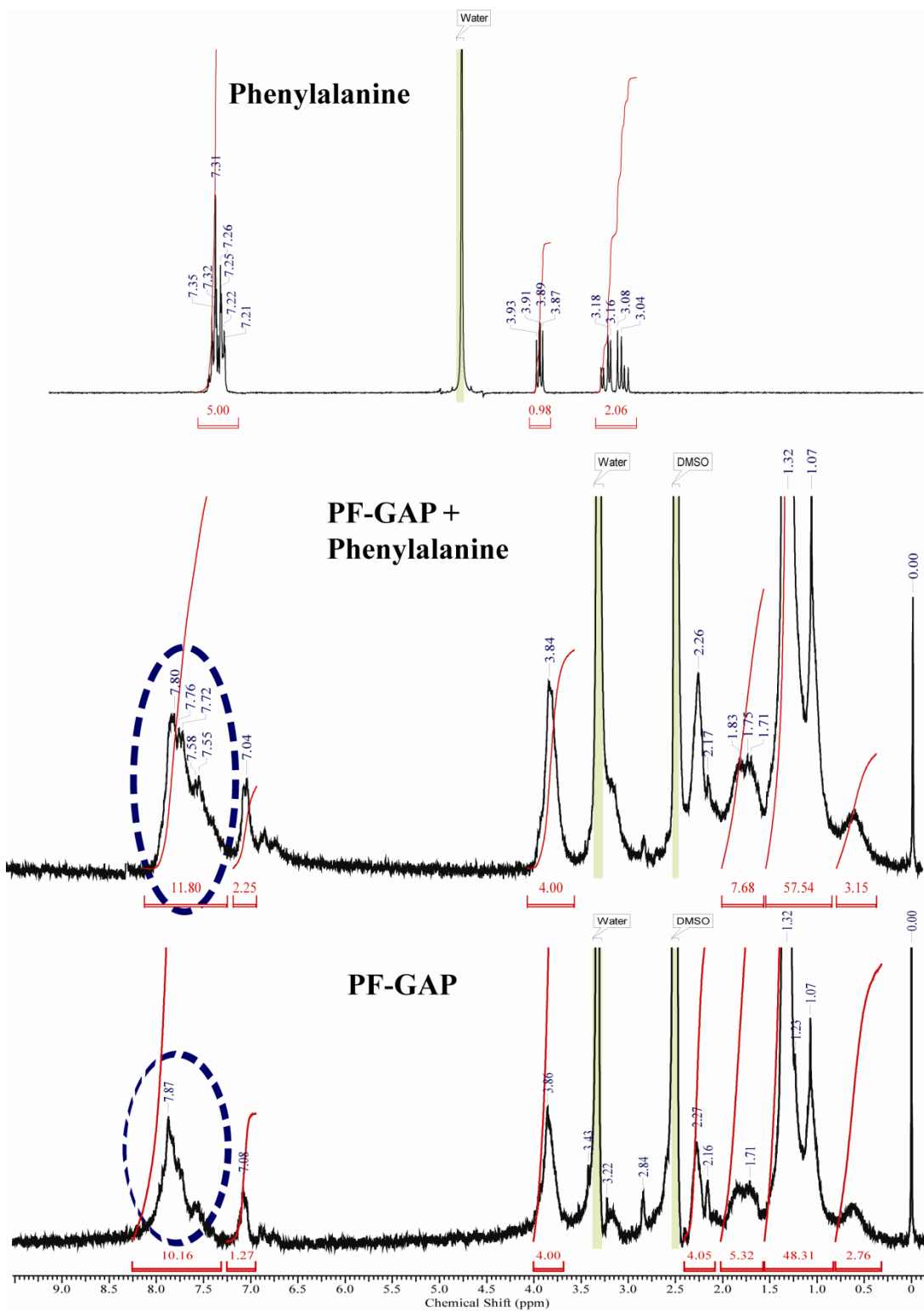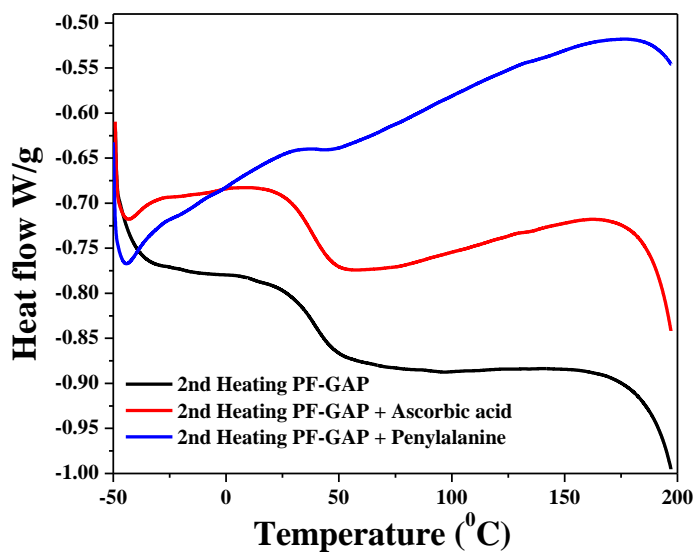
Figure 5.15 ^{1}H NMR spectra of Phenylalanine recorded in D_2O and PF-GAP, PF-GAP+Phenylalanine recorded in DMSO-d_6.
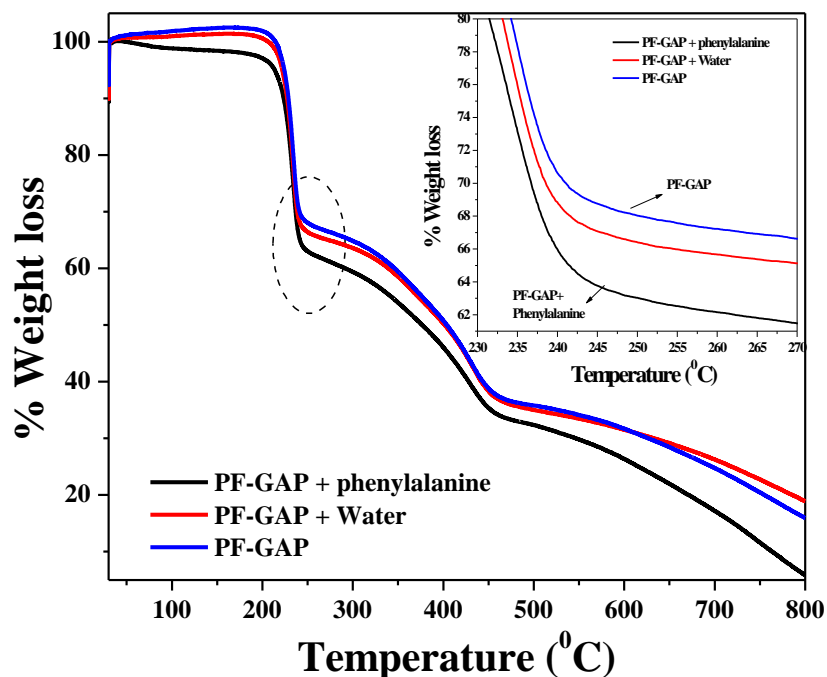
Figure 5.16 TGA analysis of PF-GAP in dry form, 2 days water treated, 2 days stirred in aqueous solution containing racemic mixture of phenylalanine. The inset shows the enlarged portion of the circle.

Figure 5.17 DSC thermograms showing 2nd heating cycles of PF-GAP, PF-GAP treated with racemic mixtures of ascorbic acid and phenylalanine.

Among the various substrates, glutamic acid exhibited the highest enhancement of CD signal due to structural similarity between the substrate and the appendage unit. The

degree of enhancement of the CD signals varied from substrate to substrate depending on the extent of non-covalent interactions with the homochiral polymer channels. The amplification of chirality demonstrated here proved the potential of PF-GAP polymer as an effective enantioselective separation media for racemic mixtures.

5.4 Summary

In summary, we have developed homochiral biomimetic helical polyfluorene by appending protected $_L$-glutamic acid. The polymer (PF-GAP) depicted the characteristic α-helix conformation of the proteins that changed reversibly from α-helix to β-sheet-like conformation upon treatment with water. The polymer exhibited helical fibrous morphology with pores on the walls that mimicked the protein super-structure. Heterogeneous enantioselective separation of a wide range of racemic mixtures of amino acids, sugar, amino alcohol, hydroxy acid, ascorbic acid and aromatic drug in water was successfully accomplished using PF-GAP as probe. The chiral recognition ability of the polymer resulted in the enantioselective uptake of the $_L$-form of enantiomer from their racemic mixture in water. Enantioselectively adsorbed substrates lead to an amplification of chirality with the highest value of 11-fold enhancement based on the 'Sergeant Soldier principle'. This work demonstrates a very efficient design of a biomimetic polymer probe for the combined operation of enantioselective separation and sensing with wide applicability.

5.5 References

1) Avalos, M.; Babiano, R.; Cintas, P.; Jimenez, J. L.; Palacios, J. C. *Chem. Commun*. **2000**, *11,* 887-892.

2) Gawronski, J.; Kazmierczak, F.; Gawronska, K.; Rychlewska, U.; Norden, B.; Holmen, A. *J. Am. Chem. Soc*. **1998**, *120*, 12083-12091.

3) Folmer-Andersen, J. F.; Lynch, V. M.; Anslyn, E. V. *J. Am. Chem. Soc*. **2005**, *127*, 7986-7987.

4) Gopalaih, K. *Chem. Rev.* **2013**, *113*, 3248-3296.

5) Zhao, J.; Fyles, T. M. James, T. D. *Angew. Chem. Int. Ed*. **2004**, *43*, 3461-3464.

6) Mei, X.; Wolf, C. *J. Am. Chem. Soc.* **2006**, *128*, 13326–13327.

7) Wolf, C.; Liu S.; Reinhardt, B. C. *Chem. Commun.* **2006**, *24*, 4242–4244.

8) Biedermann, F.; Nau, W. M. *Angew. Chem. Int. Ed.* **2014**, *53*, 5694-5699.

9) Seo, J. S.; Whang, D.; Lee, H.; Jun, S. I.; Oh, J.; Jeon Y. J.; Kim, K. *Nature* **2000**, *404*, 982-986.

10) Wang, W.; Dong, X.; Nan, J.; Jin, W.; Hu, Z.; Chen Y.; Jiang, J. *Chem. Commun.* **2012**, *48*, 7022–7024.

11) Yan, Y.; Yu, Z.; Huang, Y.; Yuan W.; Wei, Z. *Adv. Mater.* **2007**, *19*, 3353-3357.

12) Oh, H. S.; Liu, S.; Jee, H.; Baev, A.; Swihart, M. T.; Prasad, P. N. *J. Am. Chem. Soc.* **2010**, *132*, 17346–17348.

13) Oda, M.; Nothofer, H.-G.; Scherf, U.; Sÿunjic, V.; Richter, D.; Regenstein, W.; Neher, D. *Macromolecules* **2002**, *35*, 6792-6798.

14) Abbel, R.; Schenning, A. P. H. J.; Meijer, E. W. *Macromolecules* **2008**, *41*, 7497-7504.

15) Beychok, S. *Science* **1966**, *154*, 1288-1299.

16) Jackson, M.; Mantsch, H. H. *Crit Rev. Biochem. Mol. Biol.* **1995**, *30*, 95-120.

17) Hu, X.; Kaplan, D.; Cebe, P. *Macromolecules* **2006**, *39*, 6161-6170.

18) Griebenow, K.; Klibanov, A. M. *Proc. Natl. Acad. Sci. USA* **1995**, *92*, 10969-10976.

19) Fekkes, D. *J. Chromatogr. B: Biomed. Sci. Appl.* **1996**, *682*, 3-22.

20) Prins, J.; Timmerman, P.; Reinhoudt, D. N. *J. Am. Chem. Soc.* **2001**, *123*, 10153-10163.
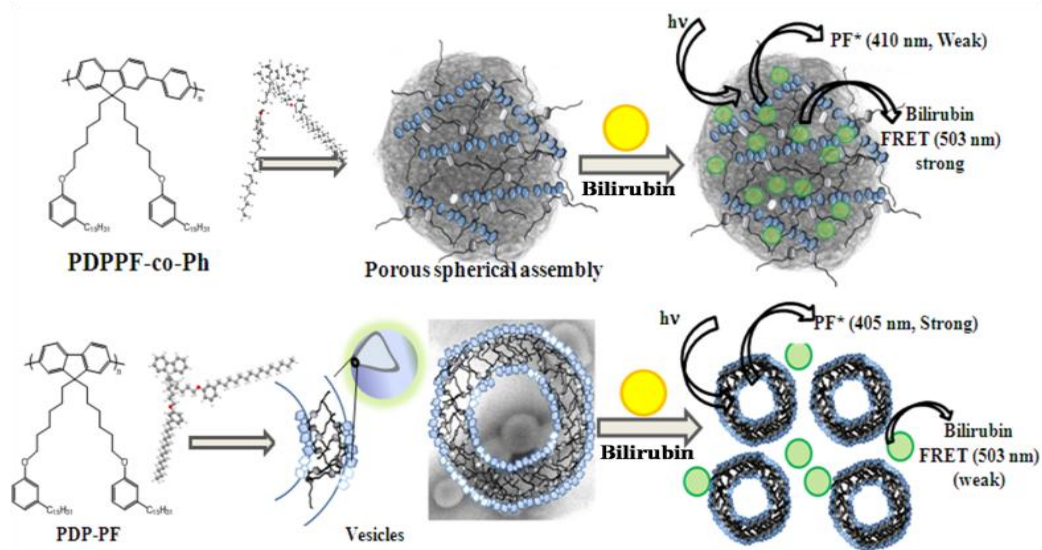
CHAPTER - 6

Conclusion

6. Conclusion

This section compiles the conclusion derived from each chapter.

The **chapter 1** presented the principles and types of sensors highlighting the applicability in day-to-day life. Among various sensors, fluorimetric sensors for chemo and biosensing applications were majorly elaborated. Conjugated polymers based fluorimetric probes were discussed with relevant literature reports. The properties of polyfluorene class of conjugated polymer was described in detail as the conjugated polymer of our choice and the effect of appendages on tuning structure property relationship was also explained. This chapter presented the overview on the appendages, synthetic methods, characterization methods and biosensing applications that were demonstrated in the thesis. In the end, motivation of the work, objectives and outline of the thesis was enumerated.

The second chapter described new tailor made polyfluorenes for sensing of bilirubin. Two new polyfluorene based homo (PDP-PF) and copolymers (PDPPF-co-Ph) appended with bulky 3-pentadecylphenoxy group were synthesized using Suzuki coupling polymerization. Investigation on the morphology of the polymers indicated the formation of self-assembled nanostructures like vesicles by PDP-PF and porous spheres by PDPPF-co-Ph respectively both in solution and as solvent evaporated film form. The favorable photophysical properties of the polyfluorenes were taken advantage of for the selective sensing of unbound bilirubin (BR) in THF. A high energy transfer efficiency of 86 % upon addition of bilirubin with color change from blue (polyfluorene emission) to green (FRET induced bilirubin emission) was observed with PDPPF-co-Ph. Time-resolved fluorescence decay measurements evidenced efficient energy transfer from polymer to bilirubin. The open porous spherical assembly of PDPPF-co-Ph enabled better adsorption of the analyte and closer proximal distance to the analyte, which along with the good spectral overlap resulted in greater efficiency for FRET induced energy transfer. Figure 6.1 displays the schematic presentation of visual sensing of bilirubin. Selectivity and sensitivity of the probe were verified. Enhancement of bilirubin emission coupled with quenching of polyfluorene emission made this approach adaptable for bilirubin sensing.

Figure 6.1 Schematic presentation of FRET based sensing using new tailor-made polyfluorenes.

The **third chapter** dealt with the real world application of sensing of bilirubin in complex biofluids namely human blood serum. The adherence of serum protein on conjugated polymer is a major bottleneck in the application of the latter for selective sensing of small biomolecules in blood serum. The third chapter presented two new polyfluorenes with ᴅ-glucuronic acid appendage that was a non-receptor for any serum protein, thereby providing a platform for selective sensing of free bilirubin in the clinically relevant range of < 25 µmol/L to > 50 µmol/L in human blood serum.
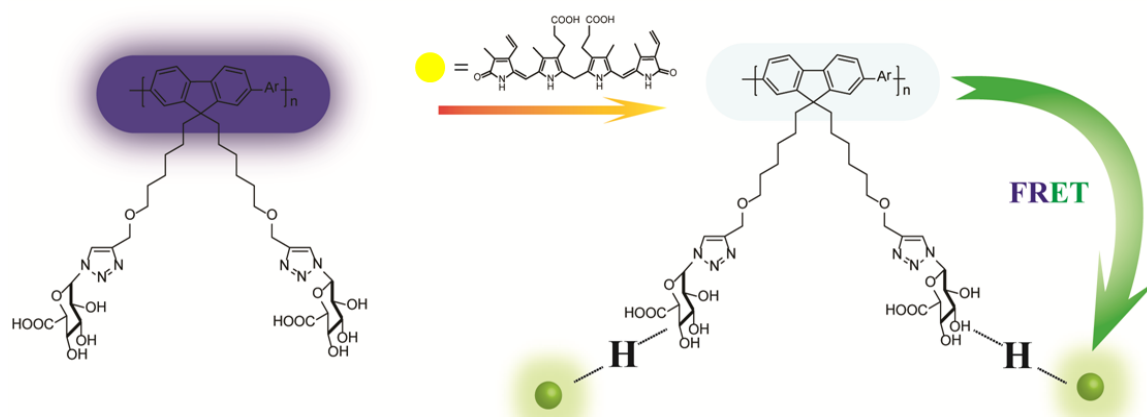
Figure 6.2 Schematic illustration of mechanism of FRET induced sensing of bilirubin in human blood serum using water-soluble PF-Ph-GlcA.

The appended D-Glucuronic acid formed non-covalent interactions with bilirubin, which in conjunction with favorable spectral overlap between the polymers and bilirubin facilitated efficient FRET process in aqueous solutions. Addition of bilirubin resulted in the quenching of the polyfluorene emission with simultaneous appearance of bilirubin emission exhibiting visual emission color change from blue to light green. Figure 6.2 shows the diagrammatic presentation of mechanism of FRET induced sensing of bilirubin in human blood serum using water-soluble glycopolymer, PF-Ph-GlcA. The polymer remained stable in serum even under severe basic conditions and exhibited high selectivity with visual sensitivity only towards free bilirubin in human serum in the presence of crucial interferences such as hemoglobin, proteins, biliverdin, glucose, cholesterol, and metal ions. The combined role of energy transfer and non-covalent interaction highlighted the potential of the new polymer design for highly selective sensing activity in complex biofluids. In future, it is anticipated that it would become possible to generate home kit using this conjugated polymer probe for FRET based sensing of free bilirubin.

The **fourth Chapter** described the idea of intracellular metal ion detection and sensing in living cells using amino acid appended polyfluorene (PF-Ph-GA). Inspired by the bio-coordination systems, glutamic acid was appended to the polyfluorene to develop an assay that worked on selective chelation of glutamic acid moiety to Fe^{2+} resulting in quenching of polymer fluorescence. Polymer based probe in selective detection and imaging intracellular Fe^{2+} pool is unprecedented till date. Figure 6.3 shows the chemical structure of the polymer probe and the fluorescent imaging of labile iron pools in living cells. The polymer shows immediate sensitive response and supreme selectivity for Fe^{2+} ion over various metal ions including bioavailable alkali metal ion, transition metal ions particularly Fe^{3+}, Zn^{2+}, Co^{2+}, Hg^{2+} metal ions. The polymer was demonstrated as fluorescent probe for imaging labile Fe(II) pools in living cells. This work is expected to stimulate the development of cell viable probes for selective, sensitive detection and imaging of labile metal ion pools.
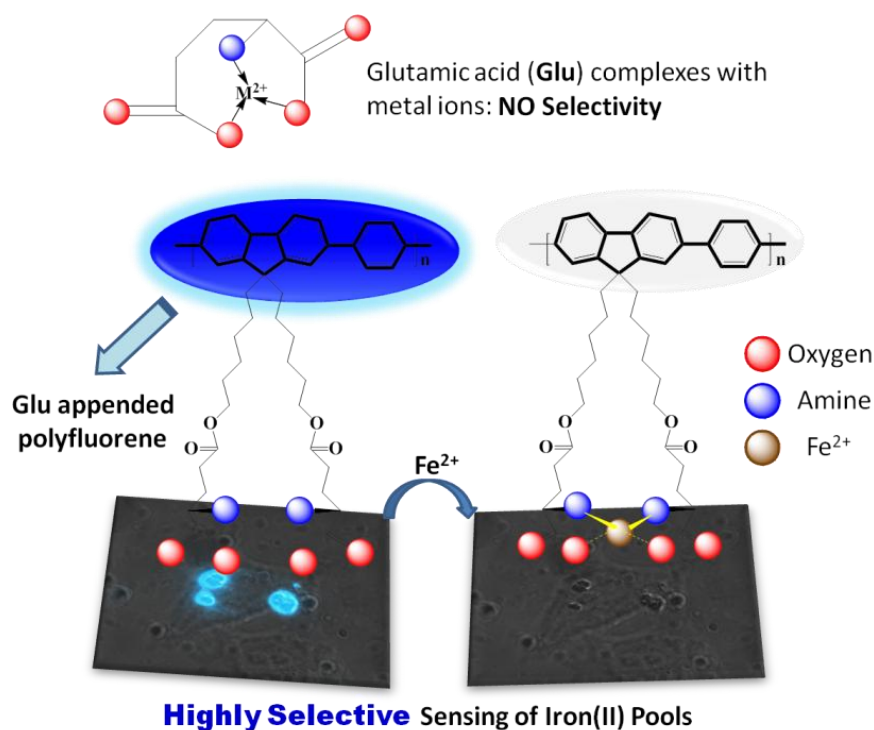
Figure 6.3 Selective sensing and fluorescent imaging of labile iron pools in living cells using water-soluble amino acid polyfluorene.

In the **fifth chapter**, homochiral polymer was designed by appending protected L-glutamic acid to conjugated polyfluorene. Chiral amino acids are very interesting molecules to be incorporated either into the backbone or side chain to induce chirality in polymers. The chiral polymer was demonstrated for enantioselective separation and sensing for wide variety of racemic mixtures such as amino acids, amino alcohols, hydroxyl acids, sugars and aromatic drug in water for the first time. The conformation and morphology of the polyfluorene is presented in Figure 6.4 and the schematic presentation of enatioselective separation and sensing of biomolecules from the aqueous racemic mixtures is also given. The polymer exhibited biomimetic helical porous morphology and conformations such as α helix, β sheet that were evidenced from SEM and solid state CD studies. Chiral sensing and separation were evidenced from relevant techniques like HPLC. The approach of designing homochiral biomimetic polymer with protected amino acid can be extended to other

systems. The new polymer material can be developed into chiral columns for enantioselective separation of analytes in water.
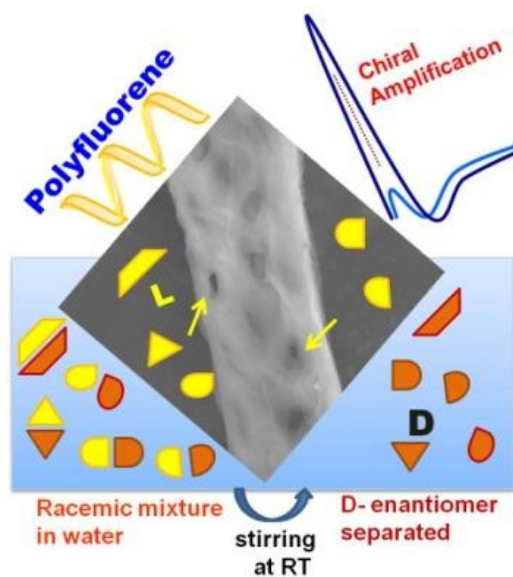
Figure 6.4 Schematic presentation of enantioselective separation and sensing of wide range of substrates using biomimetic homochiral polyfluorene.

List of Publications:

1. **T. Senthilkumar** and S. K. Asha* "Self-Assembly in Tailor-Made Polyfluorenes: Synergistic Effect of Porous Spherical Morphology and FRET for Visual Sensing of Bilirubin". *Macromolecules* **2013**, *46*, 2159-2171.

2. **T. Senthilkumar***and S. K. Asha* *"An Easy 'Filter-and-Separate' Method for Enantioselective Separation and Chiral Sensing of Substrates Using a Biomimetic Homochiral Polymer"*. *Chem. Comm.* **2015**, *51*, 8931-8934.*

3. **T. Senthilkumar** and S. K. Asha* **"**Selective and Sensitive Sensing of Free Bilirubin in Human Serum Using Water-Soluble Polyfluorene as Fluorescent Probe". *Macromolecules* **2015**, *48,* 3449–3461. **(Highlighted in *Macromolecules* main panel in June 2015)**.

4. **T. Senthilkumar**, Nimisha parekh and S. K. Asha* "Orientation Effects Induced Selective Chelation of Fe^{2+} to Glutamic acid Appended Conjugated Polymer for Sensing and Live Cell Imaging". ***Manuscript submitted for publication.***

5. **T. Senthilkumar** and S.K.Asha* "Macromolecular Light-up Probe for Free Biliruibin Sensing in Human Blood Serum". ***Manuscript Under Preparation***.

Patents:

1. S K Asha and **T. Senthilkumar**, *Water soluble polyfluorene functionalized with glucuronic acid useful in bilirubin sensing.* Application No - **WO2015015517-A1** *PCT/IN2014/000505*.

2. S K Asha and **T. Senthilkumar,** Patent Filed: *Easy filter-and-separate method using polymer for enatioselective separation.* **CSIR No- 2015-NF-0053.**

*Academic Awards***:**

1. CSIR-UGC National Eligibility Test for Ph.D Admission and eligibility for lectureship held in December **2008- Awarded Junior Research Fellowship.**

2. GATE (Graduate Aptitude Test For Eligibility) National Level Test − held in February **2009**, **Qualified with 90 percentile.**

3. CSIR **Senior Research Fellowship** Awarded in August **2011**.

4. **Best poster Award** "Nanomolar sensing of bilirubin using tailor made polyfluorenes" in National Science Day Celebration held at CSIR-NCL, **2013**.

5. **Selected for Oral Presentation** – **FAPS MACRO 2013** - International Conference on Polymers held at IISC, Bangalore.

6. **Best Poster Award**-"Selective sensing of free bilirubin in human blood serum using rationally designed macromolecular probe" in National Science Day Celebration held at CSIR-NCL, **2014**.

Papers Presented in Conference:

- **T. Senthilkumar** and S. K. Asha. "Synthesis, characterization and self -assembly of pentadecyl phenol functionalized polyfluorenes". PSNDS-11, National Conference on Advances in Polymer Science and Nanotechnology, Design and Structure, Vadodara, Gujarat, 2011.

- **T. Senthilkumar** and S. K. Asha. 3rd FAPS Conference and MACRO 2013 (FAPS-MACRO, 2013)- Oral presentation, International Conference on Polymers, Indian Institute of Science, Bangalore, 2013.

- **T. Senthilkumar** and S. K. Asha. "Selective and sensitive sensing of free bilirubin using water-soluble glycopolymers". MACRO-2015 International Conference on polymers, Indian Association of Cultivation Science, Kolkata.